CREATION OF A ^{22}Na AND ^{7}Be GLOBAL DATA SET FOR USE AS AN ATMOSPHERIC TRACER AND RADIOCHRONOMETER

CRÉATION D'UN ENSEMBLE DE DONNÉES GLOBALES DU ^{22}Na ET DU ^{7}Be POUR UTILISATION EN TANT QUE TRACEUR ATMOSPHÉRIQUE ET RADIOCHRONOMÈTRE

A Thesis Submitted to the Division of Graduate Studies
of the Royal Military College of Canada
by

Ian Hoffman

In Partial Fulfillment of the Requirements for the Degree of
Doctor of Philosophy

18th March 2016

Acknowledgements

I would like to express my gratitude to my two co-supervisors, Dr. Brent Lewis and Dr. Paul Chan, for their knowledge, time, effort, and support. Both supervisors demonstrated patience as I completed the programme requirements while working at Health Canada (HC). Our conversations and interactions throughout this project have made this experience valuable.

I would also like to express my gratitude to Dr. Kurt Ungar, for giving me the advice, guidance, and opportunity to complete this graduate degree while continuing to work full-time at HC. This project would not have been possible without the full support of Dr. Ungar.

I would like to thank Dr. Harri Toivonen of the Radiation and Nuclear Safety Authority, Finland (STUK) and Mr. Andreas Pelikan for sharing the Java MUltiplet FItting (JMUFI) spectroscopic computer code. This code was a key component in the efficient processing of the large amount of data that this project required.

I would also like to thank Dr. Hughes Bonin for his work on translating the abstract into French.

I would also like to acknowledge the Provisional Technical Secretariat (PTS) of the Comprehensive Nuclear-Test-Ban Treaty Organization (CTBTO) for their kind permission to publish the ^{7}Be and ^{22}Na International Monitoring System (IMS) data.

Finally, I would also like to thank my partner and spouse, Norah Lynn Paddock, for proof-reading this manuscript and for her support and patience during my programme of study.

Disclaimer

The views expressed here are those of the author. These views do not necessarily reflect those of HC, the PTS or the CTBTO.

Abstract

Cosmogenic radionuclides often serve as environmental tracers, tracking both the timing and pathway of pollutants and other materials in the environment. Radionuclides with significantly different half-lives ($t_{1/2}$), such as ^{7}Be ($t_{1/2}$ = 53.22 d) and ^{10}Be ($t_{1/2}$ = 1.51×10^{6} year), are commonly used as tracers, given their ability to function as a radiochronometer. Changes in the relative concentrations of these two radionuclides provide timing information on environmental processes, such as atmospheric circulation processes. However, the relatively high cost and specialized nature of equipment needed to measure ^{10}Be, due to its long half-life, are significant barriers to its widespread use.

This thesis investigates the use of ^{22}Na ($t_{1/2}$ = 2.6027 year) as an alternative to a ^{10}Be based radiochronometer. Given its low production rate, ^{22}Na, is seldom measured with ground-level aerosol samplers, except under special atmospheric conditions. Spectral summation, the process of summing spectra from consecutive aerosol samples, was developed through this work as a new technique to quantify ^{22}Na and allow for its use as a tracer. Furthermore, quantification was improved over several previous studies of ^{22}Na by incorporating True Coincidence Summing (TCS) correction factors in the calculations of activity concentration.

The new spectral summation technique was evaluated using 7 d and 30 d intervals. The 30 d interval performed better and was used to generate the first TCS-corrected multi-year global data set of ^{22}Na and ^{7}Be activity concentrations. Validation of the ^{22}Na data set was performed by statistical comparisons between data derived from the summation technique and that from previous non-summation analyses for ^{7}Be. The data were examined in the context of a semi-empirical model that incorporated both production and atmospheric transport components, leading to the conclusion that atmospheric transport was the dominant factor in ground-level ^{22}Na concentrations. It is anticipated that this spectral summation technique will be useful in other studies involving low-activity radionuclides and that the ^{22}Na data set will be valuable for future studies involving atmospheric circulation, both within and beyond the domains of meteorology and climatology.

Résumé

Les radionucléides cosmogéniques servent souvent de traceurs environnementaux, traçant le moment ainsi que la trajectoire de matières polluantes et d'autres matériaux dans l'environnement. Les radionucléides dont les demi-vies diffèrent de façon significative, tels que le ^{7}Be ($t_{1/2}$ = 53.22 d) et le ^{10}Be ($t_{1/2} = 1.51 \times 10^{6}$ année), sont communément utilisés comme traceurs à cause de leur capacité de fonctionner comme radiochronomètres. Les changements des concentrations relatives de ces deux radionucléides procurent de l'information temporelle sur les processus environnementaux tels que les processus de circulation dans l'atmosphère. Cependant, le coût relativement élevé et la nature spécialisée de l'équipement nécessaire pour la mesure du ^{10}Be, à cause de sa longue demi-vie, représentent des obstacles importants pour son application répandue.

Cette thèse étudie l'emploi du ^{22}Na comme alternative pour un radiochronomètre basé sur le ^{10}Be. Le ^{22}Na, à cause de son faible taux de production, est rarement mesuré par des échantillonneurs d'aérosols au niveau du sol, sauf dans des conditions atmosphériques spéciales. Une méthode de sommation spectrale qui est un procédé d'addition de spectres obtenus d'échantillons d'aérosols consécutifs, mise au point pour ce travail est une nouvelle technique pour quantifier le ^{22}Na et permettre son utilisation comme traceur. De plus, la quantification a été améliorée par rapport à plusieurs études précédentes du ^{22}Na par l'incorporation de facteurs de corrections dits de Sommation de Vraies Coïncidences (SVC) dans les calculs des concentrations d'activité.

La nouvelle technique de sommation spectrale est évaluée pour des intervalles de 7 d et de 30 d. La technique basée sur des intervalles de 30 d a donné de meilleurs résultats et a été utilisée pour générer la première base de données globale multi-années avec la correction SVC pour les concentrations d'activité de ^{22}Na et de ^{7}Be. La validation de la base de données du ^{22}Na a été effectuée par des comparaisons statistiques entre les données obtenues par la technique de sommation et celles obtenues d'analyses précédentes du ^{7}Be non-basées sur la sommation. Les données ont été examinées dans le contexte d'un modèle semi-empirique qui incorpore les composantes de la production et du transport atmosphérique, menant à la conclusion

que le transport atmosphérique était le facteur dominant des concentrations de ^{22}Na au niveau du sol. À ce que cette technique de sommation spectrale va devenir utile pour d'autres études impliquant des radionucléides de faibles activités et la base de données du ^{22}Na pourra servir à des études futures sur la circulation atmosphérique, domaines de la météorologie et de la climatologie, et au-delà.

Contents

List of Tables

List of Figures

List of Acronyms

AATAMI Advanced Analysis Tool for the Assessment of Monitoring Information
AMS Accelerator Mass Spectrometry
ANOVA ANalysis Of VAriance
ASCII American Standard Code for Information Interchange
ATM Atmospheric Transport Models
CTBT Comprehensive Nuclear-Test-Ban Treaty
CTBTO Comprehensive Nuclear-Test-Ban Treaty Organization
ECMWF European Centre for Medium Range Weather Forecasts
EML Environmental Measurements Laboratory
GCM General Circulation Model
GCR Galactic Cosmic Rays
GEANT GEometry ANd Tracking
GMI Global Modelling Initiative
HC Health Canada
HPGe High-Purity Germanium
ICRP International Commission on Radiological Protection
IDC International Data Centre
IGRF International Geomagnetic Reference Field
IMS International Monitoring System
IQR Interquartile Range
JMUFI Java MUltiplet FItting
LINSSI LINux System for Spectral Information
LOWESS Locally Weighted Regression Scatter Plot Smoothing
MC Monte Carlo
MCA Multi-Channel Analyser
MCNP Monte Carlo N-Particle
MDA Minimum Detectable Activity
MDC Minimum Detectable Concentration
MLE Maximum Likelihood Estimation
NAO North Atlantic Oscillator

NDC National Data Centre
NM Neutron Monitor
PDF Probability Density Function
PTS Provisional Technical Secretariat
QA Quality Assurance
R_c Geomagnetic Vertical Cut-off Rigidity
SEP Solar Energetic Particles
STE Stratosphere-Troposphere Exchange
STUK Radiation and Nuclear Safety Authority, Finland
SN Sunspot Number
SPHDF Sample Pulse Height Data File
SQL Structured Query Language
TCS True Coincidence Summing
USA United States of America

1 Introduction

Studies of the circulation of air masses and the exchange of air between the stratosphere and troposphere have several important scientific applications. Atmospheric chemistry, aerosol deposition, pollutant transport and models of the Earth's climate and weather are examples of the many domains that require some level of understanding of these dynamic processes. Until relatively recently, knowledge of these phenomena were largely a mystery; it was not until the completion of several environmental radioactivity studies and measurement campaigns that these processes could be modelled with some detail and accuracy. Most previous studies of environmental radioactivity were conducted over a limited geographic area and over short durations. The scope of these studies was often limited because many researchers only had access to national monitoring data and, in some cases, some additional data from a small number of international collaborators. As a result, it has been difficult to understand the global and mesoscale behaviour of the atmosphere using radionuclide techniques.

Many radionuclides with a variety of half-lives ($t_{1/2}$) are produced through cosmic interactions, such as: ^{7}Be ($t_{1/2}$ = 53.22 d), ^{32}P ($t_{1/2}$ = 14.26 d), ^{33}P ($t_{1/2}$ = 25.34 d), ^{35}S ($t_{1/2}$ = 87.51 d), and ^{22}Na ($t_{1/2}$ = 2.6027 year). These radionuclides have long been of interest for use as tracers of environmental processes[1–6]. With an accurate radionuclide production model, environmental measurements of these radionuclides can provide both valuable timing information on environmental transport of pollutants and a better understanding of atmosphere dynamics.

^{10}Be ($t_{1/2}$ = 1.51×10^{6} year), another product of cosmogenic interactions, has also been used in the study of environmental processes. Due to its long half-life, it is particularly useful for the examination of environmental processes that occur over extended timeframes such as climate studies that use ice cores[7]. In these types of studies, ^{10}Be is often used as a time reference or clock for studying domains where the environment is relatively undisturbed over long periods of time, such as in soil and ice cores. For example, atoms of ^{10}Be are trapped in glacial ice at its formation and, if production and deposition rates are well understood, activity concentration measurements of this radionuclide can be used to date the formation of the ice sample.

The difficulty with ^{10}Be measurement is that, due to its long half-life, it cannot be measured with traditional spectroscopic techniques. Instead, it requires an expensive and consequently rare laboratory technique, Accelerator Mass Spectrometry (AMS), to measure the radioactivity in samples. The AMS requirement has meant that data on ^{10}Be is relatively scarce and limited in both temporal density and geographic location.

Beyond ease of measurement, radionuclides that are ideal as tracers for atmospheric studies generally possess several desirable characteristics such as:

- reasonably short half-lives, scaled appropriately to the nature of the study;
- a chemically nonreactive state from source to measurement;
- a unique, yet well understood production process, free from anthropogenic interferences; and
- sufficient activity concentrations for consistent measurement.

Given these requirements, ^{10}Be is not very practical for atmospheric studies. In contrast, two other nuclides, ^{22}Na and ^{7}Be, do meet the described criteria. Together, these two nuclides could be used as a radiochronometer, a clock based upon radioactive decay. By examining the behaviour of the relative amounts of these nuclides present in the sample it is possible to determine the duration of a process of interest. By examining changes in their relative concentrations, it is possible to extract additional information related to their transport time and environmental pathway.

Given ^{7}Be has been studied frequently in the past, its production process is well understood and is easily measured. Access to a broad historical data set also allows for the validation of new analysis techniques. The use of ^{22}Na as a tracer has been quite limited, in comparison, since it requires very large air volumes to obtain the required sensitivity. Furthermore, since ^{22}Na is rarely measured, observations by ground-based systems can be significant in terms of atmospheric dynamics, while those of ^{7}Be, are generally less informative as they are observed daily.

The principal difficulty with using ^{22}Na as an atmospheric tracer is that, by the time it can be sampled, the combination of limited detector sensitivity and low activity concentration (roughly 4 orders of magnitude lower than ^{7}Be[8]) restricts observations to sites with very specific atmospheric conditions. The typical observation scenario occurs when the sampling site experiences strong vertical down-mixing in the atmosphere, carrying the stratospheric ^{22}Na to the air sampler. This down-mixing process that leads to surface observations of stratospheric radionuclides, such as ^{22}Na is called Stratosphere-Troposphere Exchange (STE). In essence, stratospheric and tropospheric air is much more efficiently mixed than under normal conditions[9]. However, this mechanism is not well understood[2] and appropriate tracers may assist in understanding the STE mechanism and process.

A new technique is required to overcome this limitation and facilitate the use of ^{22}Na as a tracer within a broader range of atmospheric conditions. The technique

used to develop this data set involves performing spectral summation on sequential sample measurements to obtain sufficient measurement sensitivity. Once the necessary sensitivity has been obtained, the spectra can be analysed using traditional gamma spectroscopy software to find ^{22}Na signals. The results of the spectral summation procedure can then be analysed to produce a global data set on a synoptic timescale, which can be useful for two principal applications. First, these environmental radioactivity measurements can be used to increase the understanding and accuracy of global air circulation models. Second, this technique may provide a means to obtain additional information on individual samples of interest. More specifically, it may be possible to infer the history of an airmass by looking at ratios of ^{22}Na and ^{7}Be. By examining the relative ^{22}Na and ^{7}Be concentrations, the global circulation of air masses could be better understood. Since the stratosphere and troposphere are normally isolated from one another, the phenomenon of radioactive decay depletes (or ages) the ^{7}Be activity faster than ^{22}Na. In other words, if the concentration of ^{22}Na increases relative to ^{7}Be, it indicates the stratospheric (older) air has undergone more efficient mixing with the tropospheric (younger) air. A more thorough discussion of the interpretation of variations in the relative concentration of these radionuclides is included in Chapter 2.

The primary data source for this study is the global Comprehensive Nuclear-Test-Ban Treaty (CTBT) International Monitoring System (IMS) network. Although the primary purpose of this network is to detect clandestine nuclear tests, it also provides valuable environmental monitoring data since the samples collected can be analysed for civil applications. The generation and analysis of ^{22}Na and ^{7}Be data is relevant not only for the study of environmental radioactivity, as described above, but also for the CTBT. Normally, seismic signals are interpreted to identify the location and time of a nuclear test. However, if those seismic signals are absent or ambiguous, atmospheric radiochronometer information may assist with source attribution or characterization. Although ^{22}Na and ^{7}Be are not relevant fission products for detecting a nuclear test, the presence of these radionuclides in a sample can provide useful auxiliary information. For example, if the history of an air mass can be inferred by the relative amounts of ^{22}Na and ^{7}Be present in a sample, it may help to geographically or temporally limit the possible source (or emission) location. It must be stated that application of radionuclide tracer techniques to CTBT monitoring is outside the scope of this project.

Another key component that is necessary to fully understand cosmogenic radionuclides and their environmental behaviour is a model that helps explain the key factors in how these radionuclides behave from their genesis to their detection with surface-based aerosol samplers. This work will introduce a semi-empirical model that examines the production and atmospheric transport components of these radionuclides as they transit through the environment.

This work begins in Chapter 2 with a literature review that provides a description of the production process of cosmogenic radionuclides and a survey of previous ^{7}Be and ^{22}Na monitoring results. ^{22}Na may be able to serve as a surrogate for ^{10}Be aerosol concentrations for some applications in the airborne environment, so a review of atmospheric ^{10}Be monitoring will also be presented. Given the central role of the atmosphere as a link between production and observation, there will be a brief discussion on relevant atmospheric phenomena that influence observations of these radionuclides. The goals of the work are presented in Chapter 3. Following an overview of spectroscopic analysis terminology in Chapter 4, a discussion of the measurement equipment used is described in Chapter 5. The analysis methodology and the results of the spectral summation technique are discussed in Chapter 6, including a description of relevant analytical tools developed and used in this work. In Chapter 7, a semi-empirical model is proposed and the components and factors of this model are described. The summation results and examination of these results in the context of the semi-empirical model proposed is the focus of Chapter 8. The final two Chapters, 9 and 10, will present the conclusions of this work and recommendations for future work, respectively.

2 Literature Review

2.1 Introduction to Cosmogenic Radionuclides

The discovery of cosmogenic radionuclides in rain water during the 1950s allowed connections to be made between various environmental radiation measurements and environmental processes, including large-scale atmospheric transport[10]. At that time, monitoring programmes were being established in many countries to study the radioactive products of atmospheric nuclear testing and their health impacts. These monitoring programmes began to generate data and knowledge that were also relevant to other fields. For example, Lal et al. attempted to use the relative beryllium concentrations in precipitation, combined with knowledge of the original concentrations at the site of production, to trace precipitation and provide a history of the contributing air masses[10]. The use of these tracers was further expanded to provide information on numerous other environmental processes, such as: precipitation, washout, resuspension, atmospheric particle deposition, movement of other airborne contaminants, aerosol deposition and aerosol trapping by above-ground vegetation[4, 11], and terrestrial in-situ production[12–14].

More recently, measurements of ^{22}Na have been used to determine the residence time, or age, of bodies of fresh water[3] and the residence time of aerosols in the atmosphere[15]. Previous work suggests that it should also be possible to apply similar techniques to study the movement of air masses from the ^{22}Na measured in aerosol filters. The generation of such a data set could then be useful in atmospheric circulation studies to determine air mass age and composition (relative amounts of young and old air) and to develop a better understanding of STE mechanisms and events.

Both ^{7}Be (γ = 477.6 keV) and ^{10}Be (β^{-} = 202.56 keV) are formed in the atmosphere through spallation with N, O, Ar and C[1, 8, 10, 16–19]. These radionuclides are predominantly produced in the stratosphere (67 %), with the remaining production (33 %) occurring in the upper troposphere[20, 21]. Similarly, ^{22}Na (γ = 1274.54 keV) is also formed in the atmosphere with the same production characteristics as cosmogenic beryllium, but through ^{40}Ar spallation [8, 17]. The decay scheme, including the

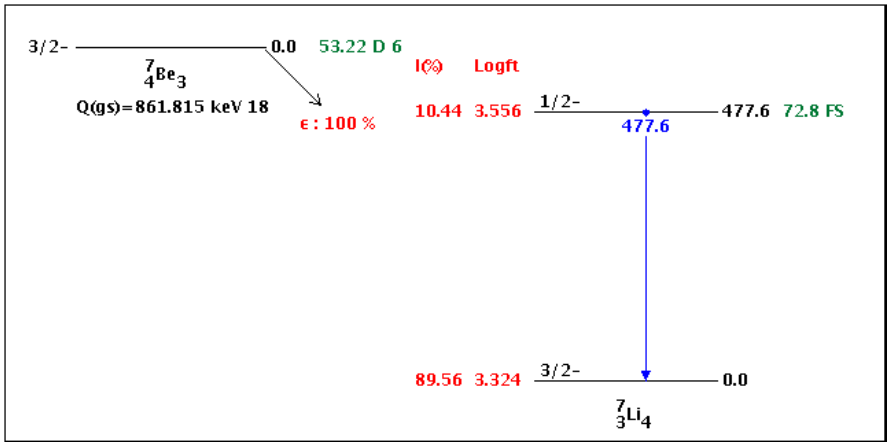

Figure 2.1 – Decay scheme of ^{7}Be[22]. Starting from left to right, this scheme shows that the ground state of ^{7}Be has a 3/2 spin with negative (-) parity. The total energy released, Q, of the decay process is 861.815(18) keV. Decay from the ground state (energy is 0.0) is by electron capture (ϵ=100 %); the half-life is 53.22(6) d. The intensity (I=10.44 %) indicates the fraction of decays that end at the excited state (spin 1/2) and the beta transition has a log ft value of either 3.556 or 3.324. The photon emitted from the excited state has an energy of 477.6 keV and a lifetime of 72.8 fs.

decay energies of ^{7}Be, ^{10}Be, and ^{22}Na are shown in Figures 2.1, 2.2 and 2.3, respectively. The similarities between the production processes of ^{22}Na and ^{10}Be are part of the motivation for the hypothesis that these two radionuclides can be interchanged, depending on the time scale of the environmental processes one wishes to investigate. For shorter processes, such as atmospheric transport, ^{22}Na can be used for a temporal reference. In comparison, ^{10}Be or other long-lived species must be used for lengthier processes, such as ice core deposition in glaciers, as it has an extremely long half-life.

In order to take full advantage of these cosmogenic radionuclides, it is necessary to understand the main factors that influence their production rates. The first factor is the intensity of incoming Galactic Cosmic Rays (GCR) and Solar Energetic Particles (SEP), while the second is the strength of the geomagnetic field where the nuclides are formed. The Earth's geomagnetic field deflects the GCR and SEP toward the poles so that production is higher near the poles and much weaker at tropical and mid-latitudes[23]. A schematic of the magnetic field is shown in Figure 2.4. Particles that travel parallel to the magnetic field lines experience little deflection, as is the case near the Earth's poles. Particles entering the atmosphere at the geomagnetic equator are travelling perpendicular to the field lines and experience a poleward deflection if their rigidity is less than the Geomagnetic Vertical Cut-off Rigidity (R_c)[24].

It is important to note that there are two different axes shown for the Earth

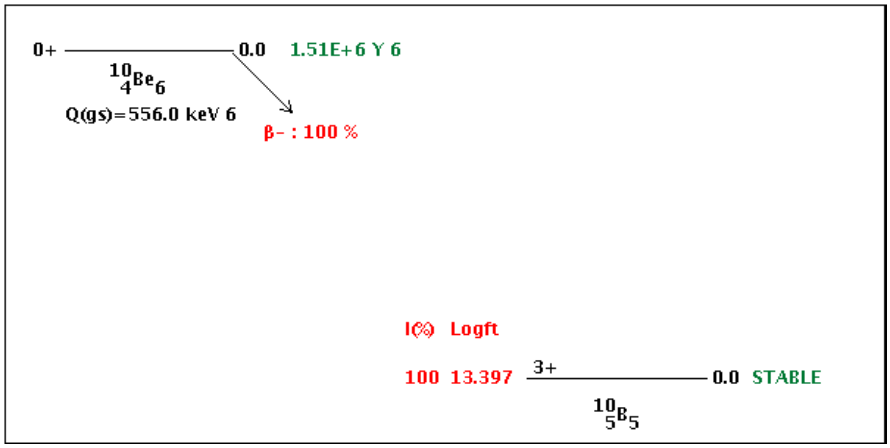

Figure 2.2 – Decay scheme of ^{10}Be[22] through β^- emission. See Figure 2.1 for more details on how to interpret this diagram.

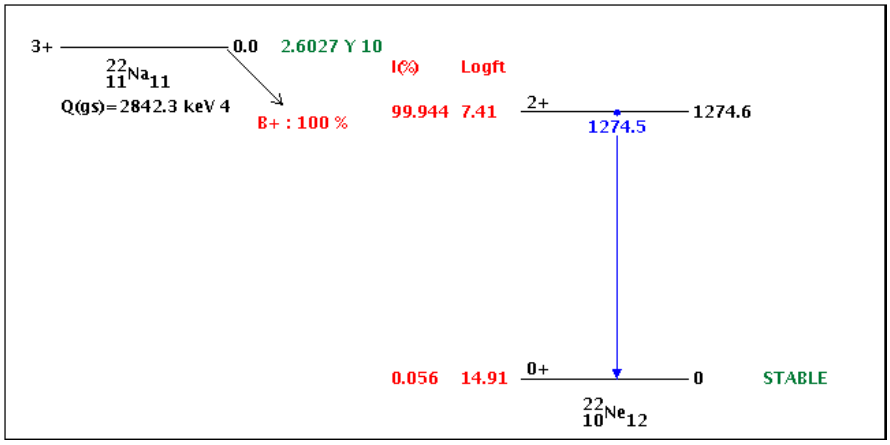

Figure 2.3 – Decay scheme ^{22}Na[22] through β^+ emission. There is a small branching component (not shown) where the ^{22}Na β^+ is followed by a γ emission at 511 keV. See Figure 2.1 for more details on how to interpret this diagram.

in Figure 2.4. The geomagnetic axis is offset from the Earth's rotational axis by approximately 11°, meaning that equivalent geographic latitudes in the Southern and Northern hemispheres experience slightly different magnetic shielding. A contour mapping of the International Geomagnetic Reference Field (IGRF) R_c values used is shown in Figure 2.5. Production is highest where the balance of cosmic radiation and density of atmosphere gases is optimized, which occurs in the lower stratosphere and near the poles[20, 21, 26, 27].

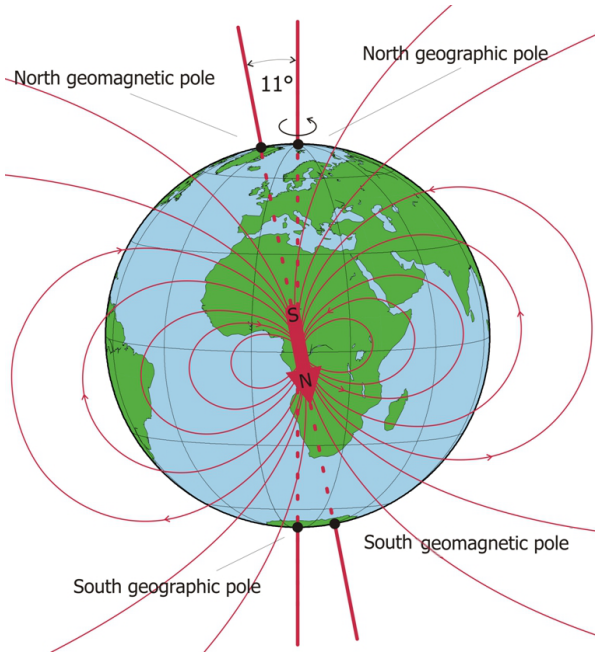

Figure 2.4 – The geomagnetic field. The magnetic dipole axis is offset from the Earth's axis by approximately 11°. The magnetic field lines are more aligned with the rotational axes at the poles to the incoming GCR and SEP. Particles entering the atmosphere near the equator are perpendicular to the magnetic field lines and require much higher potentials than at the poles to interact with the atmosphere. Spallation is therefore much more likely to occur near the poles than the equator. Image from Istitituto Nazionale di Geofisica e Vulcanologia[25].

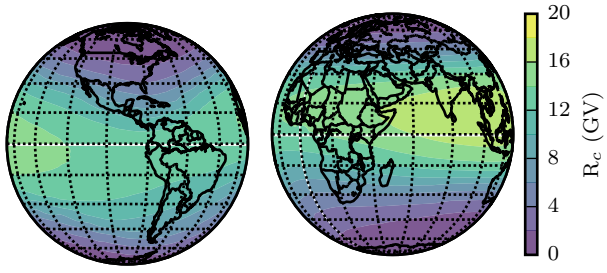

(a) West **(b)** East

Figure 2.5 – A two hemisphere contour map of the Geomagnetic Vertical Cut-off Rigidity (R_c) (GV) at 20 km altitude derived from IGRF 1995. The equatorial region is particularly difficult for GCR to interact with the atmosphere due to the high rigidity present. At the poles, GCR interactions with the atmosphere are much more likely to occur.

2.2 A Brief Introduction to Atmospheric Transport

The atmosphere is divided into separate layers as shown in Figure 2.6. As stated previously, the bulk of cosmogenic radionuclide production occurs in the lower stratosphere, with the stratosphere and troposphere being fairly isolated from each other[28]. One or several atmospheric phenomena must therefore occur to transport the radionuclides to ground-level, where they can be captured by collection instruments.

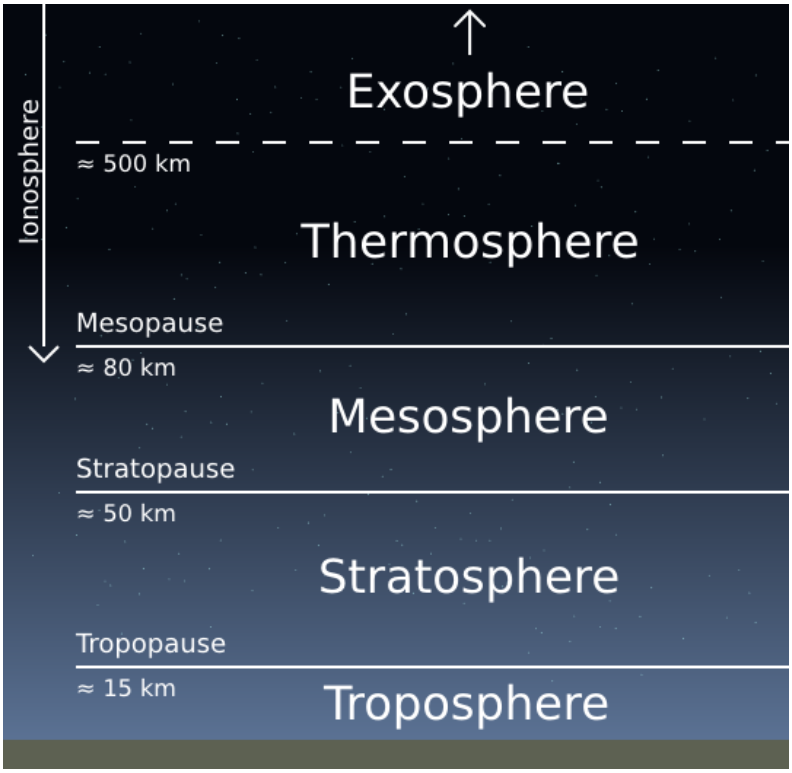

Figure 2.6 – Vertical Structure of the Atmosphere. This figure shows the structure of the atmosphere. Weather is primarily confined to the troposphere, while the stratosphere is the principle site of cosmogenic radionuclide production. The remaining layers of the atmosphere are not relevant to this study. Image courtesy of [29].

A generalized picture of the movement of the atmosphere helps to illustrate the processes that affect concentrations of cosmogenic radionuclides. Over broad continental scales, depending on the region involved, the bulk movement of air follows either the Hadley, Ferrell (mid-latitude) or Polar cells shown in Figure 2.7. The greatest mixing of tropospheric air masses with stratospheric air in the tropopause

occurs in winter at polar latitudes. Conversely, minimal mixing occurs in the summer at equatorial latitudes[26]. A corresponding amount of stratospheric air is then displaced to the troposphere in the polar and mid-latitudes, which gives rise to a maxima in the $^{10}Be/^{7}Be$ ratio (which should also be true for $^{22}Na/^{7}Be$) in the spring[23] as the tropopause rises. The rising of the tropopause increases the mixing of stratospheric and tropospheric air, as does the seasonal shifting of the jet stream[8, 23]. The boundaries between the three cells are the locations where troposphere folding occurs, thus the study of $^{22}Na/^{7}Be$ ratios may provide interesting results at sites near these boundary regions.

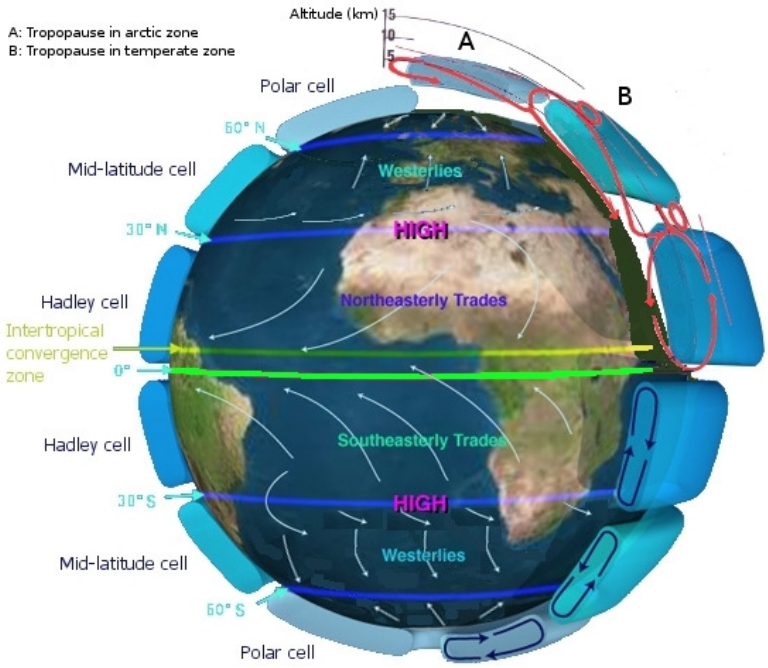

Figure 2.7 – Generalized major atmospheric circulation cells. From the equator poleward, the circulation of the Hadley, Ferrell (Mid-latitude) and Polar cells are shown with red arrows (northern) and blue arrows (southern)[30]. Note that each cell operates at different altitudes — lowest in the polar cell and increasing towards the Hadley cells.

Feely et al. proposed four phenomena that affect the atmospheric concentrations of cosmogenic beryllium and sodium:

1. The vertical transport of stratospheric air, for example, during STE events;
2. A decrease in tropospheric stability during summer, when beryllium is transported from the upper troposphere to the middle and lower troposphere (ground-level air);

3. The movement of tropospheric air masses from middle latitudes to high latitudes (>60°), following the generalized Hadley cell movement, as shown in Figure 2.7; and
4. The effect of washout, which transports aerosolised beryllium and sodium to the ground[20, 21, 26].

As the general production and transport processes of cosmogenic radionuclides have been described, a review of previous measurements of cosmogenic beryllium and sodium is needed. Studies of both ^{7}Be and ^{22}Na will be reviewed before moving on to measurements of ^{10}Be. Both ^{7}Be and ^{22}Na have been measured either jointly or individually at many sites around the world. In the case of ^{7}Be, data are often available from many sources over extended time intervals. In contrast, the data for ^{22}Na are much sparser. A review of previous studies focused on the measurement results of these radionuclides will allow comparisons to the spectral summation results.

2.3 ^{22}Na and ^{7}Be Measurements and Studies

There are only a few studies referring to both ^{7}Be and ^{22}Na[5, 8, 20, 21, 26, 31–38], while there has not been a single study examining ^{22}Na globally. However, several measurements reported from various sites are worth noting for comparison and validation purposes.

The earliest reported measurements of ^{22}Na and ^{7}Be over an extended time period were from Lithuania in the 1960s[5] and the most recent reported results are from Northern Finland, with data from the 1990s and 2000s[35]. The following section provides a review of ^{22}Na aerosol monitoring results, from the earliest to most recent.

2.3.1 Lithuania

Luyanas et al. measured ^{22}Na and ^{7}Be atom ratios after processing approximately 50 air sampler filters with radiochemical techniques (i.e. ashing) during the 1960s[5]. The ^{7}Be/^{22}Na atom ratios were observed to depend on two factors — the air residence time in the stratosphere and the rate of removal of ^{22}Na to the troposphere. Theoretical calculations gave a typical ratio of 1.3×10^{-2} for old stratospheric air and this ratio was confirmed using aircraft measurements. During the measurements from 1965 to 1969, atom ratios observed ranged from 0.2×10^{3} to 33.4×10^{3}. However, Luyanas et al. was unable to identify factors to correlate the observations with meteorological conditions. Due to the limits of available technology of the era and analytical tools of that era, it is not surprising that the minimum ratio observed was fairly high in comparison to all later studies that follow in this section.

2.3.2 Poland

A single study was conducted in Poland over several years. In this study, weekly sampled air volumes ranging from 30 000 m^3 to 80 000 m^3 were collected from 1996 to 2002[31]. The collected aerosol samples were divided into summer and winter populations, and spectra from each season were summed by channel to achieve the quantities of air needed to detect a ^{22}Na signal (each sample had >1 000 000 m^3 of air collected, representing half a year of data). Seasonal variability was observed in the Kraków data, as the mean concentration of ^{22}Na in the summer was 0.333(95) μBq m^{-3}, while in the winter the mean concentration observed dropped to 0.137(45) μBq m^{-3}, resulting in an overall mean value of 0.242 μBq m^{-3}. ^{22}Na/^{7}Be values were also tabulated for the observation period. The mean summer ratio was $1.18(30) \times 10^{-4}$, while the mean winter ratio was $0.67(10) \times 10^{-4}$, with the overall mean ratio of 0.95×10^{-4}.

2.3.3 Czech Republic

The Czech studies used an air sampler with a nominal flow rate of 900 m^3/h[32]. The filters were dried and counted for 500 000 s, or 5.8 d, using a High-Purity Germanium (HPGe) detector with 150 % relative efficiency. The mean activity concentration values observed in Prague over 21 year of monitoring were 2.8×10^{-3} Bq m^{-3} for ^{7}Be and 2.3×10^{-7} Bq m^{-3} for ^{22}Na. The Minimum Detectable Activity (MDA) reported for ^{22}Na was approximately 2×10^{-7} Bq m^{-3}. Data from the summer and winter seasons were tested using the Kruskal-Wallis nonparametric ANalysis Of VAriance (ANOVA) test and were found to be significantly different ($p < 0.05$) between seasons. ^{7}Be and ^{22}Na had the strongest seasonal variations of the cosmogenic nuclides tested. Rulík et al. found concentrations of ^{7}Be and ^{22}Na were correlated at a significance level of 0.01 on a weekly basis.

2.3.4 Spain

Baeza et al. investigated the temporal pathway of ^{7}Be through the environment at Cáceres, Spain[37]. Using weekly samples, several important observations were made. For example, snow was found to be more effective than rain for removing ^{7}Be from the atmosphere. Periodicity of precipitation affected observations, meaning that sites with high amounts of precipitation had limited observable ground-level concentrations. Precipitation can have even more impact on ^{22}Na observations, as wash-out may prevent sufficient activity build-up in the atmosphere before sampling can occur by ground-level monitoring equipment. Considering these factors, a model was proposed for ^{7}Be concentration in the atmosphere that could apply to any

radionuclide with the same production and transport mechanisms (e.g. ^{22}Na):

$$\frac{dA(t)}{dt} = k_1 R(t) - k_2 P(t) A(t) - \lambda_d A(t) - \lambda_f A(t) \tag{2.1}$$

where $A(t)_{\mathrm{R_c}}$ is the activity of the radionuclide at time t, $k_1 R(t)$ is the ground-level concentration proportional to the time-dependent solar activity. In other words, $k_1 R(t)$ is the term that accounts for the change in production rate also due to $\mathrm{R_c}$, which was briefly mentioned in Section 2.1. Together, $R(t)$ and $k_2 P(t) A(t)$ represents the washout of the radionuclide by the rain rate, $P(t)$. The final two terms, $\lambda_d A(t) - \lambda_f A(t)$, represent radioactive decay and dry fallout, respectively. Performing multiple regression on a finite difference version of Equation 2.1 resulted in a ^{7}Be atmospheric residence time of 10.3 d with a standard error interval of (9.0, 12.1) d. However, if radioactive decay is neglected, then the residence time is 12.8 d, with a standard error interval of (10.8, 15.7) d.

2.3.5 Finland

Leppänen and Grinsted reported on measurements of ^{22}Na and ^{7}Be from Rovaniemi, Finland. Measurement results for ^{7}Be were available from 1998 to 2007 on a continual basis, with frequent observations of ^{22}Na. Cyclical behaviour was observed, with lower ^{7}Be and ^{22}Na activity concentrations in winter than in summer. Over the time period of the study, the ^{7}Be activity concentrations ranged from around 0.5 mBq m^{-3} to 6 mBq m^{-3}, and the ^{22}Na activity concentrations ranged from around 0.1 µBq m^{-3} to 1.3 µBq m^{-3} over the time period of study. The ^{7}Be/^{22}Na ratios obtained ranged from 2500 to 30 000, with typical values of around 7500. Good agreement was also found by comparing the annual GCR intensity with annualized ^{7}Be activity concentrations.

2.4 A Selection of Relevant ^{7}Be Measurements and Studies

Many published results of ^{7}Be studies can be found in the literature. A review of the most relevant ones will provide a more comprehensive and global perspective than solely looking at studies of both ^{7}Be and ^{22}Na. This is particularly important since observations of ^{22}Na may only occur during strong STE events and may not represent the typical state of the atmosphere. To conclude this section, an important study of the cross-tropopause movement of ^{7}Be is examined as it is relevant to the behaviour of both ^{7}Be and ^{22}Na in the atmosphere.

2.4.1 Germany

In a series of measurements taken at Shauinsland, Germany, Zähringer et al. reported average concentrations of ^{7}Be for the period from July 2003 to June 2006[34]. The entire period's average was 4000 µBq m^{-3}, with a summer (June through August) average of approximately 4500 µBq m^{-3} and a winter (December through February) average of 3100 µBq m^{-3}[34]. The authors noted that ^{7}Be and relative humidity seemed to be anti-correlated, and that periods of rain and fog resulted in dramatically lower ^{7}Be concentrations, which was similar to the observations of Baeza et al.[37].

2.4.2 United States of America (USA) with Global Data

The most geographically diverse measurements of ^{7}Be were reported in two different studies by the Environmental Measurements Laboratory (EML) of the USA, conducted predominantly in the Northern and Western hemispheres[26, 39]. Viezee and Singh found that beryllium concentrations became elevated at sites where tropospheric low-pressure troughs occurred. These low-pressure troughs were assumed to be a sign of a tropopause folding event, indicating a time during which STE was active, and were strongly latitude-dependent. Examining the same data, Feely et al. reported the theoretical equilibrium concentrations at various altitudes and latitudes, assuming the only processes were production and decay. Of interest are the ground-level concentrations ^{7}Be quoted for both the theoretical and typical measured values, which have been reproduced in Table 2.1.

2.4.3 Europe

Kulan et al. also examined ^{7}Be concentrations at five different sites in Europe to study latitudinal effects[20, 21]. The sites compared were Kiruna (67.84° N); Grindsjön (59.07° N); and Ljungbyhed (56.08° N) in Sweden; Prague (50.05° N) in the Czech Republic; and Dijon (47.20° N) in France. The measurements in Sweden covered the time period from 1972 to 2000, while the remaining stations were active from 1984 to 2003. The minimum ^{7}Be activity concentration, observed in Kiruna, was 42 µBq m^{-3} and the maximum activity concentration, observed in Prague, was 9870 µBq m^{-3}. The average activity concentrations of ^{7}Be roughly doubled from the southern-most station (Dijon), 1888 µBq m^{-3}, to the northern-most station (Kiruna), 3775 µBq m^{-3}, indicating a latitude correlation in ^{7}Be concentrations. A plot of the mean annual beryllium activity versus latitude, with data from this study and several other sources, showed a Gaussian curve with a peak at roughly 38° N, indicating the latitude of maximum ground-level concentration.

Using a Hamming Fourier transform power spectral analysis, the data sets showed both a short-term annual cycle and a long-term nine- to ten-year cycle

Table 2.1 – Equilibrium ^{7}Be concentrations and some typical measured concentrations within the stratosphere and troposphere (adapted from [26]).

Latitude	**Equilibrium Concentration** mBq m^{-3}	**Measured Concentration** mBq m^{-3}
60° to 70° N:		
Stratosphere at 18 km	740	459
Stratosphere at 12 km	296	296
Ground level air	<7.4	2.8
20° to 40° N:		
Stratosphere at 18 km	<370	259
Stratosphere at 12 km	<111	18.5
Ground level air	<5.6	5.2
0° to 20° N:		
Stratosphere at 18 km	<148 to 222	178
Stratosphere at 12 km	<74 to 111	7.4
Ground level air	<3.7	2.4

roughly comparable to the solar cycle. The observations, with the exception of Prague, showed a high correlation in cyclical behaviour after being smoothed using the Locally Weighted Regression Scatter Plot Smoothing (LOWESS) technique.

Figure 2.8 of the ^{7}Be concentration, Sunspot Number (SN) and GCR intensity shows the correlation between ^{7}Be concentration and GCR (r^2=0.71), the anti-correlation between ^{7}Be concentration and SN ($r^2 = -0.70$), and the anti-correlation between GCR and SN ($r^2 = -0.84$). SN and ^{7}Be concentrations were found to have the longest lag, ≤6 months, at Grindsjön. Kulan et al. gave several factors for the slight mismatch in correlation time. First, there may have been a time lag between GCR and SN due to a variable perturbation of the heliosphere and a diffusive or drift propagation of cosmic-ray particles (also described by Usoskin et al.[40]). Secondly, the long residence time of ^{7}Be in the stratosphere imparts a delay to ground-based observations. Thirdly, STE and latitudinal mixing of air masses of differing ages or sources may create a mismatch. The authors acknowledged that there may be some measurement error present in the data, although no reason was given as to whether or why this was a particular concern for the data presented.

2.4.4 ^{7}Be Cross-Tropopause Studies

Liu et al. as part of the Global Modelling Initiative (GMI) used ^{7}Be to investigate its use

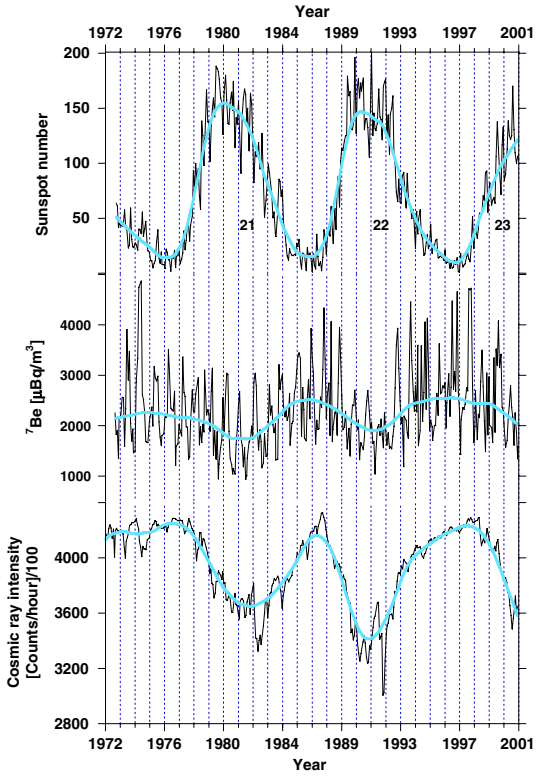

Figure 2.8 – Monthly ^{7}Be activity at Grindsjön monitoring station (middle) versus solar activity (top) and cosmic-ray intensity variation (bottom). Smoothed fit to the monthly data is shown by the turquoise line in each set. Numbers refer to the solar cycle. During periods of high solar activity (high sunspot number) the Earth experiences more shielding and thus the ground-level cosmic ray intensity drops as well as the production of stratospheric radionuclides such as ^{7}Be. Figure and caption adapted from [20].

as a tracer for cross-tropopause transport and STE events[41]. A further goal of this work was to determine if ^{7}Be could be used as a tracer for ozone transport studies. The transport time from stratosphere to troposphere was reported to be between 1 and 2 years. Simulations were performed using four different models to examine the behaviour of ^{7}Be as a function of pressure and latitude. At ground-level in the four models considered, the concentration of ^{7}Be was approximately between 2 mBq m^{-3} to 10 mBq m^{-3}, with the peak values occurring around the 30° latitude on an annual basis. Each of the four models had different characteristics in terms of how much stratospheric air was present at ground-level, but, being an atmospheric simulation, Liu et al. could not provide a full assessment about which model performed better.

The latitudinal variation in ^{7}Be from this study is reproduced in Figure 2.9. In the conclusion to this work, the author noted that the ratio of ^{10}Be to ^{7}Be is a sensitive indicator of STE.

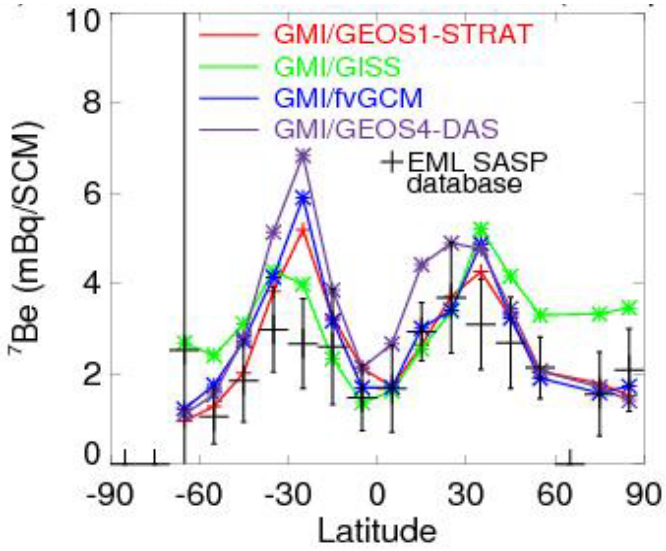

Figure 2.9 – Observed and simulated latitudinal distributions of ^{7}Be near the surface. Four different meteorological models were used as part of the GMI modelling framework with the observed data shown in the black cross series. Liu et al. noted that the *fvGCM* model is much better at representing STE than the *GEOS1-STRAT* model. Figure is from [41].

2.5 ^{10}Be Measurements and Studies

As a constant reference or baseline radionuclide in a radiochronometer, ^{10}Be has been used successfully for studies in many different environmental domains including: marine and alluvial sediments, ice cores and soils[7, 19, 42], and air masses[28, 43]. It is particularly suited for this role given its extremely long half-life relative to many other cosmogenic radionuclides. However, as mentioned previously, ^{10}Be measurement requires expensive laboratory facilities, including an AMS system[19, 28, 43], which has limited its study and application. An examination of some of the results from studies using ^{10}Be is important, since ^{22}Na is expected to play a similar role as ^{10}Be, but with a half-life suited to the circulation of air masses.

Raisbeck et al. began the very first studies of ^{10}Be aerosol samples in the 1970s. Samples were collected from both ground-level air and from the stratosphere[43]. This first study was quite limited, with four samples taken in July 1978 at 65° N, a

single sample taken in July 1976 from 9° N, and two samples taken in January and July 1976 from the South Pole region. Excluding one outlier in the northernmost samples, the mean ^{10}Be/^{7}Be ratio was found to be 2.3. These were all stratospheric samples collected at 13.7 km, 16.8 km and 19.2 km altitudes. Comparison of the 65° N sample at 13.7 km to the stratospheric sample from 9° N at 16.8 km (similar temperature surface) found agreement on the ratio, but the ^{10}Be concentration at the northern site was approximately four times greater. Although there were very few measurements from which to draw conclusions, the proposed explanation was the Hadley cell bringing fresh (^{7}Be enriched) air up from the troposphere. Lastly, the ground-level data from the South Pole was used to investigate STE. Using the measured concentrations in the two samples, STE only needed to provide an injection of approximately 5 % stratospheric air before a large increase was observable as a perturbation in the ratio of ^{10}Be/^{7}Be[43].

Aldahan et al. examined the connection between solar activity and atmospheric concentrations of ^{10}Be and ^{7}Be[44]. The motivation was to help understand climate change impacts by examining past solar modulations for changes in total solar radiation (UV), particularly as CO_2 concentrations increased in the atmosphere. The data presented showed that average ^{10}Be concentration was approximately double that of ^{7}Be at 56° N and 68° N, and that concentrations of both isotopes were between 20 and 30 % higher at the lower latitude. The data examined showed an enhancement of beryllium concentrations in the spring to summer months of up to 70 % due to the previously discussed phenomena of tropopause folding[26] and temperature-enhancing aerosol abundance[45].

The measurements presented by Aldahan et al. showed production modulations consistent with the 11 year solar cycle[44]. All ratios presented for ^{10}Be/^{7}Be were less than four, but nearly all data points were above the theoretical ratio of 0.5 at the time of production. Higher ratio values indicated the presence of older air, which is reasonable, given these were ground-based measurements. Both beryllium isotopes showed a seasonal delay when moving from lower to higher latitudes, but, as this trend has only been observed at two geographic locations, it merits further investigation. The North Atlantic Oscillator (NAO)[1] was examined as a possible explanation for low beryllium concentrations from 1989 to 1992 at a time when average temperatures were below normal, resulting in fewer stratosphere-troposphere inversion events.

Masarik et al. attempted to model cosmic-ray-induced thermal and fast fluxes. One of the goals of the work was to examine ^{10}Be and ^{26}Al concentrations in boulders and determine if a GCR model could replicate the depth profile concentrations. Both the Monte Carlo N-Particle (MCNP) and GEometry ANd Tracking (GEANT) codes were

[1] The NAO is a meteorological phenomenon that controls the strength and direction of the westerly winds and is most active from November to April[44].

used to simulate fast and thermal neutron cosmic ray fluxes at the air/soil boundary layer. When the presence of snow cover or water was added at the boundary layer (concentrations of up to 5 %), the water was found to act as both a moderator and reflector, increasing the thermal neutron flux by a factor of approximately 10, while decreasing the overall or total (fast and thermal) flux[42].

Another modelling exercise examined the production of ^{10}Be and ^{7}Be during the Maunder Minimum[2] where the production rate was determined to be anti-correlated with solar activity and geomagnetic field intensity[47]. Ice cores were extracted and examined from Greenland and Antarctica, and the cosmogenic production process was found to be well-correlated with ^{14}C production (which is also cosmogenic in origin, but behaves differently geochemically). The tree ring ^{14}C samples were from temperate and tropical latitudes, while the ice cores (^{10}Be and ^{7}Be) were from polar regions. Heikkilä et al. also found that the ^{10}Be concentrations were mixed well enough in each hemisphere to be considered symmetric and uniform in concentration[48]. However, deposition of most of the ^{10}Be occurred in the subtropics.

The ^{10}Be/^{7}Be ratio can be used to find evidence of STE. The maximum ratios were obtained during winter and spring, with a stronger signal at high-altitude measurement sites. As mentioned before, this is the time period when the NAO is most active. The ratio at production, 0.5, grows exponentially as ^{7}Be decays. In the stratosphere, high ratios are observed due to the long residence time and short half-life of ^{7}Be. For production in the troposphere, the ratio should be close to 0.5, as the residence time is short relative to the ^{7}Be half-life[47]. Time intervals where the ratio exceeds 0.5 could possibly be good evidence of an STE event.

In the Canadian Arctic, at Alert, Nunavut, this ratio was observed to be nearly constant, with values ranging from 2.0 to 3.0 with an average of 2.2(3)[49]. Data from this study is of limited use as the measurements were only taken for a single year (1990-1991), and the impact of solar cycles on production was not examined.

Field et al. examined ^{10}Be from a long-term climatological perspective using a General Circulation Model (GCM)[7]. Model validation was performed using measurements and predictions of ^{7}Be concentrations at 91 different locations worldwide. The GCM was able to replicate the general trends for ^{7}Be in the data over the period of a single year, with the model often predicting concentrations either within or just outside 1σ. The model was then applied to predict the deposition of ^{10}Be in ice cores under several scenarios and historical time periods.The transport time between stratosphere and troposphere was given as approximately 2 years.

With the potential to be used as a more convenient reference isotope than ^{10}Be, ^{22}Na could be used to date air masses and study their movements. It is clear that many

[2]The Maunder Minimum, or Prolonged Sunspot Minimum, was a period of time between 1645 and 1715 when sunspots became extremley rare[46].

factors influence observations and that cosmogenic nuclides may provide useful information on these atmospheric phenomena. Both Jordan et al. and Rehfeld and Heimann recognised that the ratio of ^{10}Be to ^{7}Be was an ideal tool to examine processes in the atmosphere because both isotopes are equally impacted by phenomena that create, remove, or affect their concentrations in the atmosphere[23, 50]. Furthermore, beryllium is not subject to chemical reactions like ozone, so atmospheric chemistry is not a consideration[23]. Although the chemical properties of ^{22}Na and ^{7}Be are different, their behaviour in the troposphere and stratosphere should not differ (i.e. they are subject to the same processes such as deposition, precipitation, etc.)[51]. With a similar behaviour, ^{22}Na could be used as an alternative to ^{10}Be for studying the circulation of global air masses if a sufficient rich data set was made available.

2.6 Theoretical Models and Simulation Studies

The study of ^{7}Be, ^{22}Na and their ratio will hopefully provide a new and more efficient means to identify STE events. The data generated may also be useful in understanding broad-scale trends through the study of seasonal fluctuations in observed concentrations. With a sufficient density of data, the influence of local conditions (e.g. precipitation) may be potentially observed in the data set. Additionally, it is helpful to look at other theoretical models already existing in the literature that were created to examine the environmental behaviour of cosmogenic radionuclides. Before the full potential of using ^{22}Na and ^{7}Be as an environmental tracer, a theoretical model must be developed as a tool for comparing and understanding the output generated.

Jasiulionis and Wershofen studied the vertical turbulent air movement of air masses using both ^{7}Be and ^{22}Na[8]. Concentrations of ^{7}Be in ground-level air were modelled by a log-normal distribution, as expressed in Equation 2.2.

$$y = y_0 + A \exp\left[-\frac{\ln^2(x/x_c)}{2w^2}\right] \tag{2.2}$$

Here, y is the probability for the radionuclide activity concentration, x, to occur, y_0 and A are parameters of the exponential distribution, x_c is the weighted average activity concentration and w is the dispersion of the distribution. This model was fit to measurement data from the Ignalina nuclear power plant in Lithuania (^{7}Be) from 1978 to 1983, and from a monitoring site in Braunschweig, Germany (^{22}Na) from 1985 to 1995, as shown in Figure 2.10.

Jasiulionis and Wershofen then modelled the behaviour of these nuclides using what is called the Standard Atmospheric Model. This model is a 1D, or vertical, steady state (stationary) system that incorporates the turbulent diffusion of air masses on

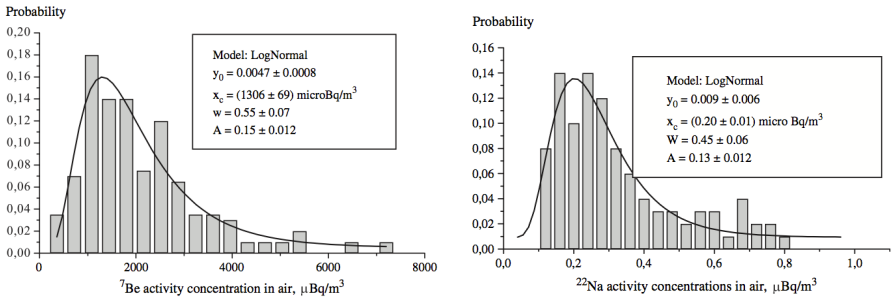

(a) ^{7}Be **(b)** ^{22}Na

Figure 2.10 – Probability distribution of the ^{7}Be activity concentration in air near Ignalina Nuclear Power Plant between 1978 and 1983 (592 measurements) and probability distribution of the ^{22}Na activity concentration in Braunschweig between 1985 and 1995 (112 measurements). Figures and captions adapted from [8].

an average monthly basis, including a washout component. The equation for activity concentration, C, is reproduced in Equation 2.3[8].

$$\frac{\partial}{\partial z} k_z \frac{\partial C}{\partial z} + \left(v_z + \frac{k_z}{H} \right) \frac{\partial C}{\partial z} - \left[(\lambda + \sigma) - \frac{\partial v_z}{\partial z} - \frac{1}{H} \frac{\partial k_z}{\partial z} + \frac{\partial H}{\partial z} \frac{k_z}{H^2} \right] C + qS = 0 \tag{2.3}$$

Here, $(\lambda + \sigma)C$ is the cosmogenic radionuclide quantity lost to decay, λ, and washout, σ, in a unit volume per unit time. qS is the source, or the production per unit volume of the cosmogenic radionuclide per unit time at an altitude z, $k_z(z)$ is the vertical turbulent diffusion coefficient, $v_z(z)$ is the vertical velocity of orderly movement, and H is function of air density, (ρ), expressed as $(1/\rho)(\partial\rho)/(\partial z)$.

Its use allowed for the derivation of a model of ^{7}Be and ^{22}Na concentration versus altitude at mid-latitudes, as shown in Figure 2.11. According to this theoretical model, the ground-level concentrations predicted for ^{22}Na are approximately 0.2 to 1.1 μBq m^{-3}.

Rehfeld and Heimann examined the transport of both ^{10}Be and ^{7}Be in 3D using Atmospheric Transport Models (ATM) from the European Centre for Medium Range Weather Forecasts (ECMWF)[23]. The goal was to predict global concentration ratios and examine the seasonality of these cosmogenic radionuclides. The model developed predicts a much higher ^{10}Be/^{7}Be ratio in spring than in autumn and was reasonably successful in accounting for rainfall scavenging using both a grid model (7.83° latitude, 10° longitude, 19 layers) and the scavenging model reproduced in Equation 2.4.

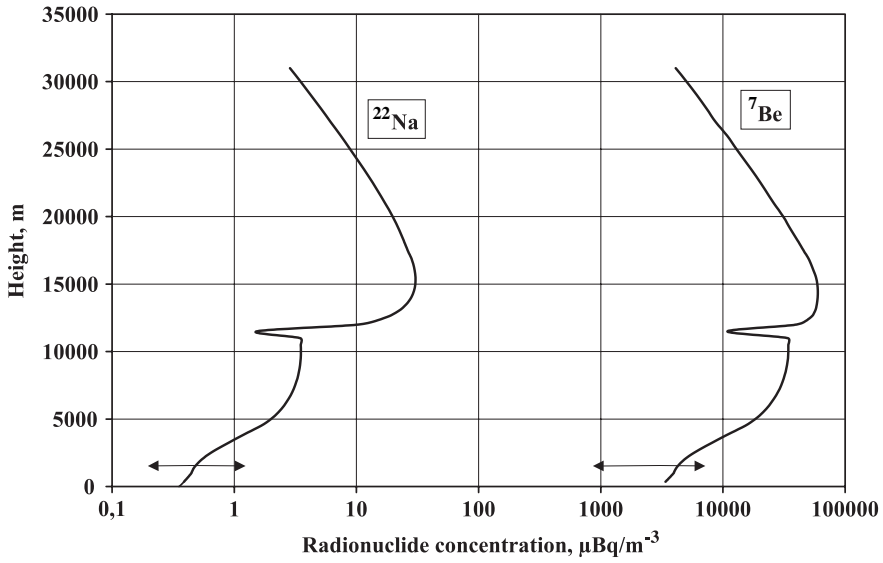

Figure 2.11 – Distribution of the mean activity concentrations of ^{7}Be and ^{22}Na. The range of the concentration variation in the ground-level layer are indicated by ↔. Figure and caption from [8].

The ATM provided by the ECMWF that was used to simulate the ratio of beryllium isotopes shows reasonably strong latitude banding in both the spring and autumn seasons. However, the simulation of the individual ^{7}Be concentration did not exhibit strong banding, a distinction that is possibly related to its short half-life. An inverse relationship was found between the 11 year solar cycle and the concentration of ^{7}Be. ^{7}Be production varied by as much as 70 % in polar regions and 7 % in equatorial regions. Both these results agree with the measurement results discussed above. The model derived for the scavenging efficiency, λ, was as follows:

$$\lambda = R\rho_w / LH \tag{2.4}$$

where R is the precipitation rate out of a grid column (m s^{-1}), ρ_w is the density of water (kg m^{-3}), L is the cloud liquid water content (kg m^{-3}) and H is the vertical extent of precipitation (m).

To explain the concentrations of cosmogenic radionuclides observed at ground-level, it is necessary to understand both the dominant mechanism by which the radionuclides arrive in the troposphere from the stratosphere, STE, and other phenomena which influence the observed concentrations of cosmogenic radionuclides[50]. Understanding STE has been a goal of meteorology and climatology for decades, and

the study of cosmogenic radionuclides has been a key to increasing the understanding of this mechanism[52]. A global data set of ^{22}Na activity concentrations would be useful in models to validate results and perform further studies on this phenomenon.

2.7 Summary

Existing studies using ^{7}Be and ^{10}Be have greatly improved the understanding of atmospheric processes. Using radioisotope production and ATM, knowledge of atmospheric dynamics has increased dramatically. Increased insight has been gained throughout the entire lifespan of these radioisotopes — from production in the upper atmosphere, to ground deposition and observations that occur at ground-level. The behaviour and characteristics of ^{22}Na in the atmosphere are very similar to ^{7}Be and ^{10}Be. Like these isotopes of beryllium, ^{22}Na also experiences cyclical patterns associated with solar cycles. Ground-level measurements have shown that both ^{7}Be and ^{22}Na follow a log-normal distribution, as was shown in Figure 2.10.

Although ^{22}Na has been used in some environmental studies, its use in understanding atmospheric dynamics has been limited due to a number of factors. It is difficult to measure due to low activity concentrations at ground-level. This difficulty has led to an insufficient density of measurements over extended time intervals and geographic areas. Several atmospheric phenomena, such as the NAO and STE, have been understood fairly well, but additional data could help improve the models and the understanding of these effects. Since, the solar cycle also plays a strong role in the production process, ^{22}Na data may provide insight into solar processes. Precipitation, or scavenging, also impacts ground-level ^{7}Be observations, but no study has examined scavenging impacts on ^{22}Na.

The results of previous studies have been summarized in Table 2.2, providing a useful reference for comparison purposes when examining the results in Chapter 8.

[3]Original atom/atom values were converted to activity ratios

Table 2.2 – Summary of ^{7}Be and ^{22}Na activity concentrations and ratios previously reported.

^{7}Be mBq m^{-3}	**^{22}Na** µBq m^{-3}	**^{22}Na/^{7}Be** 10^{-4}	**Location**	**Source**
-	-	0.11–19	Lithuania	Luyanas et al.[3]
-	0.242	0.95	Poland	Grabowska et al.
2.8	0.23	0.082	Czech Rep.	Rulík et al.
0.5–6	0.1–1.3	1.3	Finland	Leppänen and Grinsted
4.00	-	-	Germany	Zähringer et al.
2.4–5.2	-	-	Worldwide	Feely et al.
1.888–3.775	-	-	Europe	Kulan et al.

3 Thesis Goals

The purpose of this work is to create, analyse, and examine the first high-quality, coincidence summation corrected multi-year global data set of ^{22}Na that could be used as an atmospheric tracer and radiochronometer. As noted previously, ^{10}Be has been used in similar roles, but is not practical for an atmospheric tracer due to its long half-life. The relationship between ^{22}Na and the commonly observed, yet much shorter-lived radioisotope, ^{7}Be will also be examined. Following the literature review of previous ^{7}Be and ^{22}Na studies, it is clear that insufficient ^{22}Na data, due to a lack of appropriate samples for analysis, have prevented the full use of this radionuclide as a tool to better understand atmospheric dynamics. In all previous studies, ^{22}Na was studied over a very limited timeframe and, perhaps more importantly, with sparse geographic coverage. No previous study has examined ^{22}Na on a global, continental or even regional scale, as prior research has included results from only a few different monitoring sites. Consequently, there is insufficient information to gain a truly global perspective on the temporal trends of ^{22}Na. Most reported ^{22}Na measurements have been from developed countries, typically at northern mid-latitudes, and therefore a large portion of the Earth has never been studied. Furthermore, coincidence summation corrections were not mentioned in any of the reviewed studies; therefore, it can be reasonably assumed they were not performed. As ^{22}Na coincidence summation for short sample-detector distances can lead to significant underestimations of activity concentrations, this is a significant weakness in the quantifications presented in prior work.

The second goal of this work is to relate the ^{22}Na data set to the generalized atmospheric transport cells, as discussed in Section 2.2. This requires an understanding of the production process, the bulk motion of the atmosphere, and the detection equipment located on the surface. Rather than performing a full 3D simulation, which can be quite complicated and computationally expensive, the approach used here will be semi-empirical. A semi-empirical approach still represents the first step in demonstrating that GCM can apply to the motion of ^{22}Na in the atmosphere (see [7] for an excellent example of the application of a GCM applied to ^{10}Be).

The study of ^{22}Na is important because it is produced primarily in the strato-

sphere with a small production component in the high troposphere. A thorough understanding of its production, combined with ATM and ground-based measurements, can contribute to the understanding of the movement of atmospheric air parcels. The presence of ^{22}Na is often an indicator of a phenomena called STE, which is an area of atmospheric dynamics that is not well understood. With actual measurement data for ^{22}Na, it may be possible to provide more of an assessment about which meteorological models simulate STE better. A complete set of ^{22}Na data can help increase ATM accuracy. Furthermore, by looking at the behaviour of ^{22}Na relative to another cosmogenic radionuclide, ^{7}Be, it is possible to infer transit time information for the movement of air masses. In effect, the two nuclides can serve as a radiochronometer, providing a clock or time reference to an observer, and allowing the relative amounts of stratospheric air to tropospheric air in an aerosol sample to be inferred. The cosmogenic signature provided by quantification of both of these isotopes can also be used in CTBT applications to detect sample tampering. If an aerosol sample contains unrealistic activity concentrations of these radionuclides, it may indicate that the sample was not properly representative of the environment.

To improve the understanding of atmospheric processes, measurements of both ^{22}Na and ^{7}Be must be performed together over a sufficiently long time period, as solar processes greatly affect cosmogenic isotope production. This work will examine under what conditions (geographically and seasonally) ^{7}Be and ^{22}Na differ from their general trends, and provide a comparison of the new results obtained with those from previous studies.

4 Spectroscopic Theory

4.1 Spectrum analysis terminology

This section will briefly outline several key concepts and definitions used in the analysis of gamma-ray spectra. There are many excellent textbooks and articles on the analysis of spectra[53–56]. The material presented in the following sections uses several of these sources extensively. Section 4.1.1 is based principally on the work of Currie with a single channel analyser, extended to a modern Multi-Channel Analyser (MCA) by De Geer[56]. Section 4.2 on activity calculation was adapted from Gilmore and Hemingway[53].

Two of the more basic terms that are often encountered in spectroscopy are the concepts of a peak and line. A peak is a Gaussian feature that is usually above the baseline or radioactive background that is identified by the chosen analysis software. A line refers to the library or reference location of the centroid for a decay process. In other words, an analyst measures a peak, then consults a library for lines to aid in nuclide identification. The mathematical formulations presented in this chapter assume a single line decay process and the discussion relates solely to peaks.

4.1.1 Critical Limit, Detection Limit and Significance

There are several fundamental definitions used in the analysis of spectra. The first is the concept of critical or decision limit, L_C, and the second is a related parameter, the detection limit, L_D. The critical limit is the value at which a signal is said to be reliably detected. L_C is established after measurement (an *a posteriori* value). For Gaussian signals, L_C is given by Equation 4.1.

$$L_C = k\sqrt{\mu_B\left(1+\frac{1}{m}\right)} \tag{4.1}$$

where k is the risk level (k=1.65, or a 95 % confidence level for the spectra analysed here), μ_B is the true mean of the background signal, and m is the number of times the background signal was measured. Setting the Type I (false positive) and Type II (false

negative) errors to have equivalent risks, as is standard practice for environmental monitoring, gives a detection limit as expressed in Equation 4.2. The detection limit represents the threshold at which a signal is detectable and is determined before measurement (an *a priori* value).

$$L_D = k^2 + 2L_C \tag{4.2}$$

Peak significance is defined as the peak size, in multiples of the detection limit, L_D. Peaks with a significance of <1.0 are not normally considered during spectroscopic analysis, as they are less than the detection limit. For this work, however, peaks >0.7 will be considered real peaks; therefore, the risk level is no longer based upon the 95 % confidence level previously mentioned. This aggressive limit was chosen over a more conservative value based on the assumption that ^{22}Na is always present at some level in the sample. Choosing a less conservative significance threshold will also capture more of the underlying statistical distribution. The risk of making a Type II error is minimal if it is assumed that there is always some concentration of ^{22}Na present in the tropospheric air sampled. Furthermore, any anomalies and outliers in activity concentrations will be investigated and removed if there are any issues with the peak fitting process and resulting data.

4.2 Activity Calculation

Once signal detection has been defined, the next topic of interest is how to calculate the activity concentration of radionuclides. There are two important factors to consider in performing spectral analysis to arrive at an activity concentration of a radionuclide. The first is how to translate the net peak area (Gaussian peak fit minus the baseline in peak vicinity) in the spectra into an activity, and the second is a series of several parameters related to the timing of various events during the entire measurement and analysis process. Figure 4.1 shows an example of a gamma spectra acquired in Resolute Bay, Canada with typical sampling, measurement, and cool down periods of one day per process.

In order to have an accurate assessment of peak area or the contribution that the activity of the radionuclide of interest has made to the spectra, it is necessary to subtract the contribution of the natural radiation background. The Java MUltiplet FItting (JMUFI) software uses a linear baseline spectral fitting technique to estimate the background. This technique works very well, assuming the baseline is relatively featureless. In contrast, a poor peak fit can be caused by the presence of either higher energy emitters in the sample that create a strong Compton shelf underneath the peak of interest, or multiplets in the vicinity of the peak of interest. For typical aerosol

environmental radionuclides, it is not expected that the baseline fitting requires anything more sophisticated than a linear model.

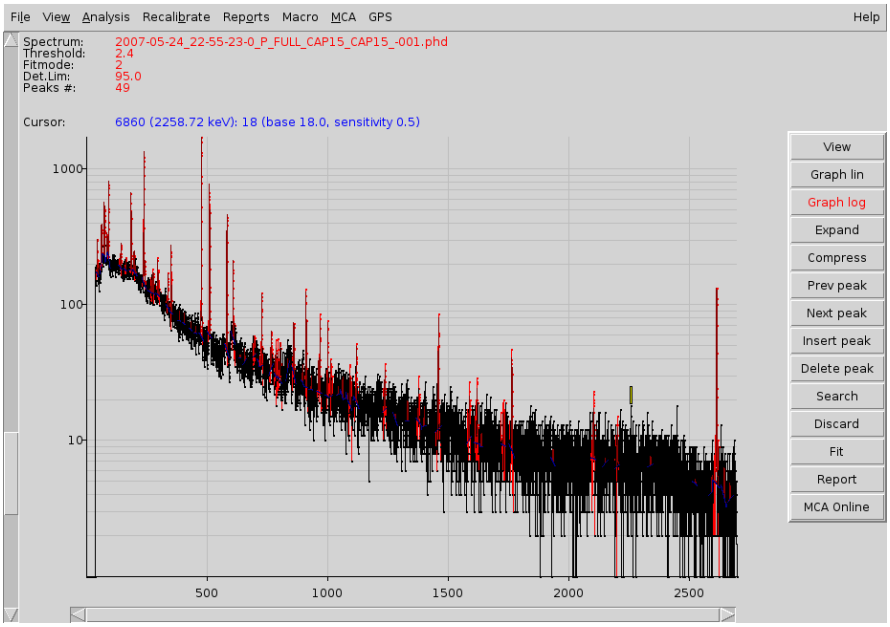

Figure 4.1 – A typical daily aerosol spectra obtained from the CTBT monitoring site in Resolute Bay, NU, Canada. The ordinate axes shows the counts recorded by the HPGe detector while the abscissa shows energy in keV. The only radionuclides present are naturally occurring and include isotopes of Pb, Bi, Be, K and Tl.

Once a signal is present, the next analytical step is the calculation of the actual activity present in the sample. To calculate the activity, the peak area, detector efficiency, live time and emission probability are generally required. It is also necessary to specify a common time basis. For this analysis, the reference time of all reported activities is the total activity collected during sampling, or collection stop. Two correction factors are needed given this reference time. The first correction is for decays during spectral acquisition or measurement. The second correction accounts for the waiting time or cool-down period after sample collection and before spectral acquisition and is more difficult to assess accurately.

The challenges associated with the latter correction factor are particularly acute due to the spectral summation technique used for this research (see Section 6.1). Normally, the exact waiting or cooling time is known and a correction factor can be applied directly. In this case, the information on the waiting time becomes lost during the process of creating the summation Sample Pulse Height Data File (SPHDF) file. Since the entire operational schedule of the samplers is relatively fixed (24 hours of

sampling or aerosol collection, 24 hours of cool-down, and 24 hours of measurement), the activity calculations will use a simple correction based on the product of the number of samples being summed and the typical 24-hour collection interval). This should give reasonably accurate results and, as discussed above, any outliers or anomalies will be investigated and removed for the data population, if necessary.

For certain nuclides (in particular ^{22}Na), coincidence correction factors also need to be determined to correct the activity for coincidence counts. This correction process is more complex and will be discussed in detail later on.

In order to calculate the peak area, the peak centroid is located (by minimizing the χ^2 of the Gaussian fit to the signal), then the signal and background are calculated. The signal is simply the sum of the counts in the peak region, or

$$G = \sum_{i=L}^{U} C_i \tag{4.3}$$

where G is the area of the peak region (including background), C_i are the counts in the i^{th} channel, and L and U are the indices of the lower and upper channels of the peak region, respectively. To calculate the background, several channels adjacent to the fitted peak are used. Mathematically, this can be expressed as:

$$B = n \left[\sum_{i=L-m}^{L+1} C_i + \sum_{i=U+1}^{U+m} C_i \right] /2m \tag{4.4}$$

where B is the background, n is the number of channels in the peak region of G, and m is the number of adjacent channels to the peak used for the background estimation. Note that this formulation assumes that the same number of channels were used on each side of the peak.

The net peak area is then the difference between G and B. Once the net peak area is known, the peak activity can be calculated by:

$$A = \frac{G - B}{e t_c p} \tag{4.5}$$

where A is the net peak area, e is the detector efficiency at the peak centroid, t_c is the detector live time, and p is the emission probability of the nuclide. The result of this calculation is the activity at the end of acquisition.

To change the reference time to the time period of sample collection, three correction factors must be applied. Two of the correction factors are for radioactive decay that occurs after collection stop and one is for decay before collection stop.

The first correction factor is the acquisition time correction for the radioactive decay during counting. Defining the acquisition time correction factor as C_c, its

associated uncertainty as σ_{C_c}, and assuming the uncertainties in both the half-life, $\sigma_{t_{1/2}}$, and the live time, σ_{t_c}, are negligible gives Equations 4.6 and 4.7. The assumption that the half-life and live time are negligible is reasonable considering that the relative uncertainties in both half lives are very small (^{7}Be — 0.11 % and ^{22}Na — 0.038 %). The low activities present in the environmental samples means that the live time of the detector system approaches the measurement time.

$$C_c = \ln 2 \frac{t_c}{t_{1/2}(1 - 2^{-t_c/t_{1/2}})} \tag{4.6}$$

$$\frac{\sigma_{C_c}}{C_c} = \frac{\sigma_{t_{1/2}}}{t_{1/2}} \frac{1 - 2^{t_c/t_{1/2}} - \ln 2\,(t_c/t_{1/2})(2^{-t_c/t_{1/2}})}{1 - 2^{-t_c/t_{1/2}}} \tag{4.7}$$

Here t_c is the live time and $t_{1/2}$ is the half-life of the radionuclide. Once this factor is applied to the previously calculated activity, the new reference time becomes the start of the spectrum measurement.

The second correction factor is used to correct for the cool-down period of the collected sample. The wait time correction factor, C_w, with its associated uncertainty, σ_{C_w}, is given in Equations 4.8 and 4.9:

$$C_w = 2^{t_w/t_{1/2}} \tag{4.8}$$

$$\frac{\sigma_{C_w}}{C_w} = \frac{\sigma_{t_{1/2}}}{t_{1/2}} \frac{\ln 2\, t_w}{t_{1/2}} \tag{4.9}$$

where t_w is the wait time between sample collection and spectrum measurement. The formulation in Equation 4.8 is appropriate for a single sampling and analysis process. Since the spectra used in this work are the summation of many individual measurements, it is necessary to modify the calculation to account for the waiting time of all the summed spectra. An assumption is made that all cool-down periods were exactly 24 h and that the total acquisition time indicates how many spectra were involved in the summation process. In most cases, this assumption is reasonable, as only samples that meet the operating specifications in Appendix A are sent from the Comprehensive Nuclear-Test-Ban Treaty Organization (CTBTO) in Vienna to Health Canada (HC). However, this assumption is not valid for data from Canada which are sent directly from the sampling station to HC, bypassing the CTBTO quality assurance process. The Canadian data would only present a problem if there were two periods of sample collection less than 12 h during the integration period. As this is not a likely occurrence, it is neglected in the analysis. In any event, the correction factor is small relative to the half-lives of the nuclides, therefore any deviation from the normal length of the cool-down period is negligible in the overall calculation of activities.

The final correction factor needed is for the decay that occurred during the sample collection process, C_s, with associated uncertainty σ_{C_s}. It is identical to the one in Equation 4.6, but with the sampling time, t_s, replacing the counting time. This leads to the final calculation for activity concentration[1], A, and its relative uncertainty, which are given in Equations 4.10 and 4.11:

$$a = \frac{C_c C_w C_s A}{V} \tag{4.10}$$

$$\frac{\sigma_a}{a} = \sqrt{\left(\frac{\sigma_A}{A}\right)^2 + \left(\frac{\sigma_V}{V}\right)^2 + \left(\frac{\sigma_{C_c}}{C_c} + \frac{\sigma_{C_w}}{C_w} + \frac{\sigma_{C_s}}{C_s}\right)^2} \tag{4.11}$$

where A and σ_A are the raw activity concentration and associated uncertainty, respectively. V and σ_V are the volume of air sampled and the uncertainty in the volume of air sampled, respectively.

Since the error in the volume sampled is very small, it can be neglected, and the final form of Equation 4.11 used to calculate the relative uncertainty becomes:

$$\frac{\sigma_a}{a} = \sqrt{\left(\frac{\sigma_A}{A}\right)^2 + \left(\frac{\sigma_{C_c}}{C_c} + \frac{\sigma_{C_w}}{C_w} + \frac{\sigma_{C_s}}{C_s}\right)^2} \tag{4.12}$$

4.2.1 True Coincidence Summing (TCS)

There is one other phenomena that can occur in spectroscopy and affect the quantification of activities — a coincidence phenomena called either TCS or Cascade Coincidence Summing. This phenomena occurs if a sample contains radionuclides with complex decay schemes. If a decay scheme has either cascades of gamma rays or emissions of positrons, it is possible for TCS to occur[53]. The near simultaneous emission of photons or x-rays from a source causes what would normally be separate signals (with different centroids) to be registered together at the sum of the energies of the individual photons. For this correction, detector geometry is the key factor rather than count rates. The key parameters are the solid angle subtended by the detector and the sample-detector distance. TCS increases as the sample approaches the detector. There are several detector geometries used in the IMS, those being most prone to TCS are samples measured in Marinelli beakers, where the sample-detector geometry is optimized for low-activity environmental samples. A schematic of a Marinelli beaker is shown in Figure 4.2. For this work, only ^{22}Na suffers from TCS, where decay signals from the line at 511 keV are summed with the 1274.5 keV and

[1]There is one further correction for coincidence summation, but this is a specialized case and is discussed further in Section 4.2.1.

appear at approximately 1784.5 keV. Although there are several methods to calculate the magnitude of this effect, the model proposed by Andreev et al. is a common approach[57].

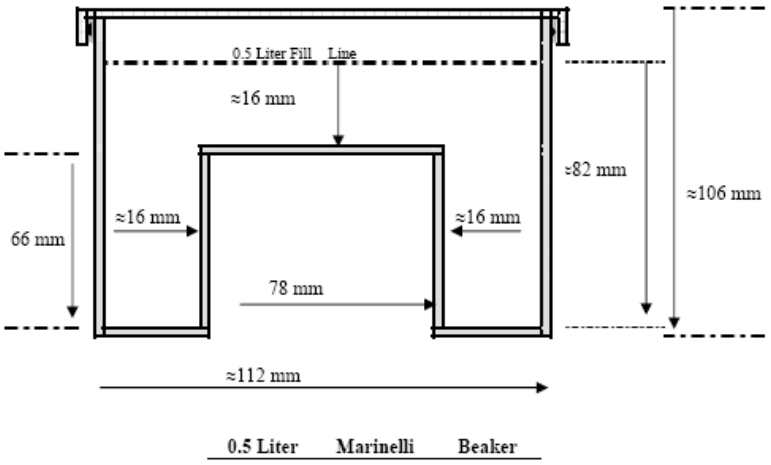

Figure 4.2 – Cross-section of a 0.5 l Marinelli beaker[58]. The detector sits in the middle of the inverted "U" shape. In this configuration, the source completely surrounds the detector. This is a common container used to measure environmental samples due to the high efficiency provided by the source-detector geometry.

There are two distinct TCS problems with the CTBTO data. The first problem is related to the detector efficiency calibrations. Generally speaking, calibration sources are comprised of a mixture of radionuclides that have a wide range of decay energies to cover the full range of gamma rays to be measured. For the CTBT detectors, two of the calibration nuclides used, ^{88}Y and ^{60}Co, experience significant coincidence summing when they are measured. The impact of TCS is often calculated by performing a Monte Carlo (MC) simulation, using software such as MCNP or GEANT to calculate a correction factor that can be applied to the original efficiency data point. As a MC simulation has never been performed on almost all of the CTBT monitoring equipment, corrected calculation points are not available. As a result, the log-polynomial function that is used to provide efficiency values at arbitrary decay energies can deviate significantly from its true behaviour. This is problematic particularly in the energy domain around ^{22}Na, since the 1274 keV gamma is between the 898 keV gamma of ^{88}Y and the 1332 keV gamma of ^{60}Co. An example of an uncorrected efficiency calibration is shown in Figure 4.3.

Corrections for TCS during the measurement process are usually provided by a

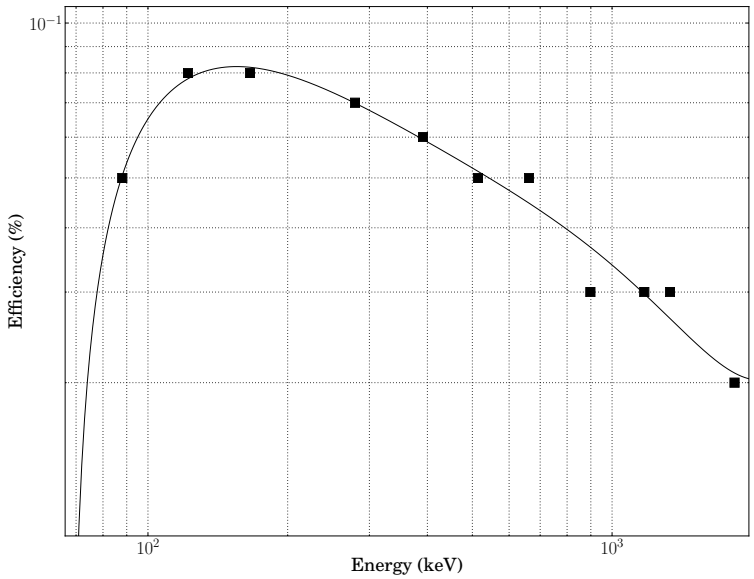

Figure 4.3 – An example of an efficiency calibration and 5^{th} order log polynomial fit which has not been corrected for TCS. If coincidence summation corrections had been properly applied, the residual of the fit to the data points would have been much smaller. The correction would adjust four points (898 keV, 1173 keV, 1332 keV and 1836 keV) so that they become almost colinear above 300 keV on a log-log plot.

total efficiency calibration. Unfortunately, total efficiency calibrations are not yet available for IMS facilities. Normally, it would be possible to model the source-detector geometries at each site to create specific calibrations that could be used during the creation of each summation spectra. However, the geometry of each IMS site has not been verified. In some cases, the design of the detector environment has been modified from the original plan as operating experience was gained. Therefore, sites with the same type of monitoring system may have small but significant differences in their actual geometry. As a simulation cannot be performed due to an incomplete knowledge of the detector geometries, a modified approach was chosen to correct for summation.

The Shaman software can generate approximate correction factors to improve the ^{22}Na activity concentration values for most IMS stations. Shaman uses a parametrization of the total-to-peak efficiency ratio to estimate the summation correction for a specified relative efficiency. The characterization of a detector system using three different relative efficiencies allows for an estimate of the summation effects.

The characterization of the detector system is shown in Figure 4.4.

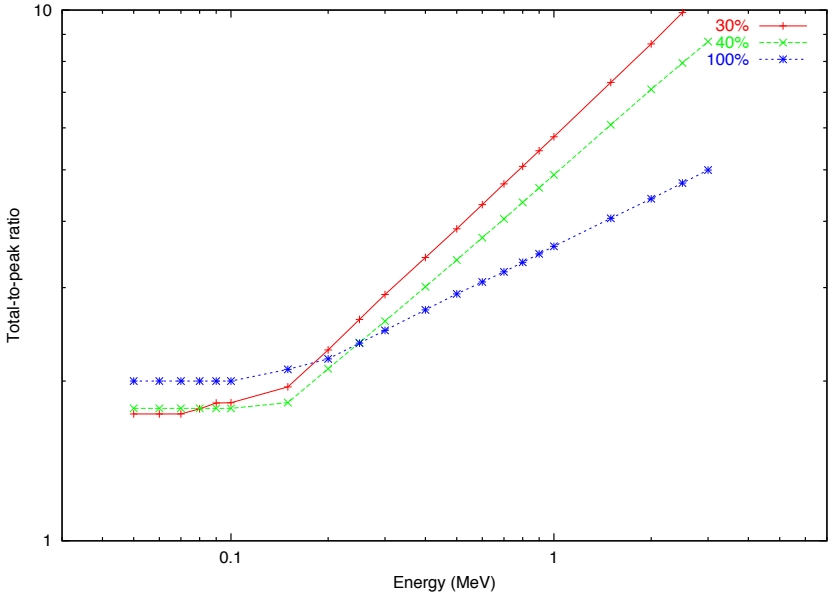

Figure 4.4 – The total-to-peak efficiency ratio is shown for three different relative efficiencies (30 %, 40 % and 100 %)[59]. A parametrized approximation based upon relative efficiency is used to estimate coincidence summation effects. The software assumes a p-type semiconductor detector with 40 % relative efficiency as the default configuration.

Once the parametrized correction factors were determined, a better estimate of the true activity was obtained by the product of the TCS factor and the activity concentration from Equation 4.10. Further details on the method that Shaman uses are provided in Section 6.2.1.3.

4.2.2 MDA and Minimum Detectable Concentration (MDC)

Definitions of MDA often vary depending on the source and context of the measurement. In this work, the definition given by Gilmore and Hemingway[53] will be followed, who define MDA as being equal to the detection limit (L_D). This use implies that the peak significance is equal to unity. In this context, it is important to note that the MDA has been averaged over the counting time rather than at a specific time period, as it is for some other definitions. However, given that the term MDA makes no reference to the amount of material (or airflow) sampled, MDC is a much more important concept in environmental aerosol sampling.

As MDC has an explicit reference to concentration, it is a measure of the activity needed in a given volume of air to register a measurable signal. In this work, the MDC is simply the MDA as defined above, corrected according to the factors described in the preceding section (i.e. waiting, counting, etc.) and divided by the air volume that passed through the filter medium. This definition of MDC assumes the sampling of aerosols is constant in terms of radioactivity during the sampling process for each nuclide present.

5 Experimental

The principal data sources used in this study are the daily aerosol samples collected by the CTBTO IMS. This network is quite sensitive as it is designed to detect clandestine nuclear tests in any environment. However, the high sensitivity and daily collection schedule is also useful for environmental studies. One major problem with measuring ^{22}Na is that almost all daily aerosol samples collected do not have sufficient ^{22}Na activity for detection using conventional spectroscopic software. For the CTBT IMS air samplers, typical ^{7}Be MDC values are approximately 0.8 µBq m^{-3} and, for ^{22}Na, they are approximately 0.2 µBq m^{-3}. With this MDC, ^{7}Be is easily detected in the daily IMS samples. With typical ^{22}Na activity concentrations below the critical limit, L_c, it is detected only on rare occasions. To study ^{22}Na effectively, a method was needed to improve the number of samples available for study. A spectral summation technique was therefore applied.

Spectral summation is very useful in situations when radionuclides are distributed around the critical limit. Since the spectral summation process essentially adds both signal (^{22}Na peak) and noise (broad Compton baseline) together, the question is the degree to which spectral summation can increase the detectability of the ^{22}Na signal. The answer lies in looking at signal processing and statistics. Under the assumption of a constant signal or aerosol concentration (which is more reasonable for shorter integration periods) with random noise, the noise should decrease by the square root of the number of averaged signals. If the integration period is 7 d, then the noise is decreased by approximately 2.6, while for a 30 d averaging the noise should go down by a factor of roughly 5.5. While the assumption of a constant signal is debatable, the random noise analogy is very accurate in its description of signals around the spectroscopic baseline. A spectral summation technique should therefore still allow for some improvement in the ratio of observations to non-observations. To generate a greater temporal density of data, consecutive samples are summed on a channel-by-channel basis over an integration period. This process artificially increases the airflow, but reduces temporal resolution.

Spectral summation only generates raw data files. These raw data files need further processing and analysis to determine the ^{22}Na signal. Fortunately, several very

good tools are available to assist with this task. There are many high-quality gamma spectroscopic software packages available. This work used two packages: Advanced Analysis Tool for the Assessment of Monitoring Information (AATAMI), developed for the CTBTO by the Radiation and Nuclear Safety Authority, Finland (STUK); and JMUFI, developed for internal use at STUK. Although JMUFI and AATAMI were useful, they could not perform the entire task — the reasons why and details on both software packages are discussed in detail in Section 6.2.1. Several new software codes were also needed to handle various aspects of the spectral summation process. The codes that were designed and created specifically for this work are: *Pysum*, for spectral summation; *Calupdate*, for database calibration management; and *Globalplot*, for activity calculation and graphical display. All of these codes were developed by the author in the Python computer language and are discussed in detail in Section 6.2.2.

Further details on the complete mechanics of how the spectral summation was performed, the use of new and existing codes for analysis, and the operation and interaction of the codes with one another and the LINux System for Spectral Information (LINSSI) database are described in detail in Chapter 6.

5.1 Radionuclide Monitoring Facilities of the IMS

As stated previously, the goal is to collect historical ^{22}Na aerosol concentrations from as broad a geographic distribution as possible in order to generate data useful to investigate atmospheric processes. One data source in particular has a combination of broad geographic coverage and high sample volume, and can provide several years of historical data on ^{22}Na activity concentrations. This global source is the network of CTBT samplers.

The CTBT is an international treaty that prohibits signatories from testing nuclear devices in any environment (underground, underwater, etc.). For the verification component of the treaty, the CTBT is supported by a treaty-defined global network of IMS monitoring sites. Each site is equipped with one or more different types of monitoring equipment. The monitoring technologies currently used include: hydrophones, seismometers, infrasound arrays, noble gas samplers and particulate aerosol samplers. The relevant technology for this work is the network of 80 particulate aerosol samplers. This network is the only one that can provide information on ^{7}Be and ^{22}Na atmospheric concentrations, and is discussed further below.

There are several different sampler designs used for particulates, but they generally operate in a similar fashion. A vacuum pump draws air through an orifice into the main body of the air sampler. A mass-flow meter records the volume of air entering the sampler, while the pump controller maintains a constant flow rate by adjusting the pumping speed according to the flow rate measured. The air then passes

through a polypropylene filter, depositing dust particles on the filter surface before leaving the sampler via an exhaust port. The sampler operational schedule requires a 24 h collection period, during which >20 000 m^3 d^{-1} of air is drawn through the filter. This collection period is followed by a 24 h cool down period to let the radon and other short-lived progeny decay before measurement. This cool down period reduces the impact on the analysis of these irrelevant (from a CTBT perspective) radionuclides. An image of a manual station in Sidney, Canada is shown in Figure 5.1.

Figure 5.1 – A photograph of the manual CTBT monitoring site (CAP14) in Sidney, Canada. Aerosols enter the sampler through the long tube, drawn in by a pump in the main body. The main body contains state-of-health monitoring equipment and controls the pumping rate to ensure constant airflow. The filter is located inside the dome and the air leaves the air sampler through the flange at the midpoint of the dome.

Once the cool down period is over, the filter is compressed into a small disc using a die press. The sample is then placed on a sample holder inside a lead shield, or castle, for a 24 h measurement period (or spectral acquisition process), during which the sample is counted using a germanium detector. Once counted, the raw data is sent via a private network to the International Data Centre (IDC) at the CTBTO headquarters in Vienna, Austria. The IDC provides State Signatories of the CTBT with both raw data and expert-analysed data products from the entire monitoring network. For the spectral summation technique, only raw data is suitable for use. A map of the CTBT radionuclide network is shown in Figure 5.2, with Table 5.1 giving the station code and location of the particulate samplers.

Table 5.1 – Location and station codes of CTBT monitoring sites. The location of site number 35 has yet to be determined. The 54 sites in *italics* had at least one observation of ^{22}Na during the period of 2005 to 2011.

Code	Location	Code	Location
ARP01	*Buenos Aires, Argentina*	LYP41	Misratah, Libya
ARP02	Salta, Argentina	*MYP42*	*Kuala Lumpur, Malaysia*
ARP03	*Bariloche, Argentina*	*MRP43*	*Nouakchott, Mauritania*
AUP04	*Melbourne, Australia*	MEP44	Baja California, Mexico
AUP05	Mawson, Antarctica	*MNP45*	*Ulaanbaatar, Mongolia*
AUP06	*Townsville, Australia*	*NZP46*	*Chatham Island*
AUP07	Macquarie Island	*NZP47*	*Kaitaia*
AUP08	*Cocos Islands*	NEP48	Bilma, Niger
AUP09	*Darwin, Australia*	*NOP49*	*Spitsbergen, Norway*
AUP10	*Perth, Australia*	*PAP50*	*Panama City, Panama*
BRP11	Rio de Janeiro, Brazil	*PGP51*	*New Hanover, Papua New Guinea*
BRP12	Recife, Brazil	*PHP52*	*Quezon City, Philippines*
CMP13	*Douala, Cameroon*	PTP53	Ponta Delgada, São Miguel, Azores
CAP14	*Sidney, Canada*	*RUP54*	*Kirov, Russian Federation*
CAP15	*Resolute, Canada*	RUP55	Norilsk, Russia Federation
CAP16	*Yellowknife, Canada*	*RUP56*	*Peleduy, Russian Federation*
CAP17	*St. John's, Canada*	RUP57	Bilibino, Russian Federation
CLP18	*Punta Arenas, Chile*	*RUP58*	*Ussuriysk, Russian Federation*
CLP19	*Hanga Roa, Easter Island*	*RUP59*	*Zalesovo, Russian Federation*
CNP20	Beijing, China	*RUP60*	*Petropavlovsk-Kamchatskiy, Russian Federation*
CNP21	Lanzhou, China	*RUP61*	*Dubna, Russian Federation*
CNP22	Guangzhou, China	ZAP62	Marion Island
CKP23	*Rarotonga, Cook Islands*	*SEP63*	*Stockholm, Sweden*
ECP24	Isla San Cristóbal, Galápagos Islands	*TZP64*	*Dar es Salaam, Tanzania*
ETP25	Filtu, Ethiopia	THP65	Bangkok, Thailand
FJP26	*Nadi, Fiji*	*GBP66*	*Chagos Archipelago*
FRP27	*Papeete, Tahiti*	*GBP67*	*St. Helena*
FRP28	*Pointe-à-Pitre, Guadeloupe*	*GBP68*	*Tristan da Cunha*
FRP29	*Réunion*	GBP69	Halley, Antartica
FRP30	*Port-aux-Français, Kerguelen*	*USP70*	*Sacramento, USA*
FRP31	*Cayenne, French Guiana*	*USP71*	*Sand Point USA*
FRP32	Dumont d'Urville, Antarctica	*USP72*	*Melbourne, USA*
DEP33	*Schauinsland, Germany*	USP73	Palmer Station, Antarctica
ISP34	*Reykjavik, Iceland*	*USP74*	*Ashland, USA*
XXX35	TBD	*USP75*	*Charlottesville, USA*
IRP36	Tehran, Iran	*USP76*	*Salchaket, USA*
JPP37	*Okinawa, Japan*	*USP77*	*Wake Island*
JPP38	*Takasaki, Japan*	USP78	Midway Islands
KIP39	*Kiritimati, Kiribati*	USP79	Oahu, USA
KWP40	*Kuwait City, Kuwait*	USP80	Upi, Guam

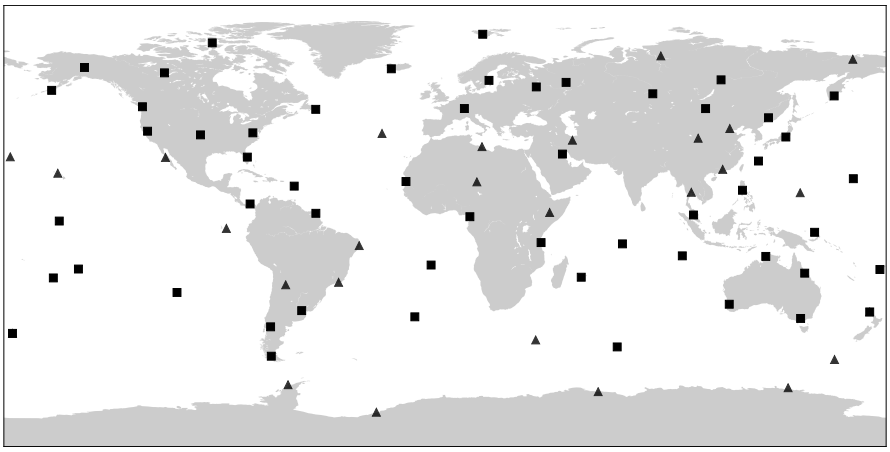

Figure 5.2 – Locations of IMS particulate monitoring samplers of the CTBTO IMS. An increasing number of sites became available during the period of study, however some sites are still awaiting completion. Sites that contributed data to the study are shown with a square, while sites that did not contribute or were not built are shown with a triangle.

5.2 Detection System

Although HPGe-type detectors are the only type of detector used at every CTBT monitoring site, they are not uniform in terms of model or supplier and therefore it is impossible to describe them consistently. However, they must all meet the specifications detailed in Appendix A. Cooling for the detectors is typically done through electro-mechanical means (e.g. Stirling cycle cooling) rather than using liquid N_2. Since there are no requirements for the detectors to be of p-type or n-type, the network contains a mix of the two different types of semiconductors. The MCA used typically have 8k channels, but a few detection systems are using 16k channels. The energy calibration of each detector is verified daily by using a mixed calibration standard that is counted for a brief period. A full calibration is normally done twice a year. Monitoring of the detection and sampling system (overall station operation) is done by the CTBTO. When necessary, the CTBTO will issue any necessary corrective actions to the station operator to ensure proper operation of the system and assists with troubleshooting in the event of a failure.

5.3 Data Formats and Protocols

Samples are measured on-site at each monitoring facility and the raw data is sent to the CTBTO in Vienna, Austria in a prescribed American Standard Code for Information

Interchange (ASCII) message format called SPHDF. SPHDF files contain a header block, calibration blocks for energy, resolution and efficiency, and the MCA output of the spectrometry system. The header contains the sampling, acquisition, and various logistical information associated with the sample. The calibration blocks contain channel-value pairs that can be mathematically fit to an equation to generate the appropriate calibration curve that describes the characteristics of the detector over the entire energy range. Finally, the MCA output is encoded as a series of channel indices, followed by a series of counts in five channel increments. The complete specification of the SPHDF format is given in [60], but the key features are reproduced in Appendix B.

5.4 The National Data Centre (NDC) at HC

Part of the mandate of HC is to provide scientific and technical analyses to assess radiation risks from both natural and anthropogenic sources to the Canadian public. HC also serves as the Canadian NDC for the radionuclide monitoring component of the CTBT. Using both national and international data, department analysts search for evidence of nuclear weapons testing in contravention of the CTBT. To fulfil both mandates, HC must be capable of: performing measurements and analyses on environmental samples (CTBT or otherwise), receiving and analysing raw data from remote monitoring stations, and maintaining the scientific tools and technical expertise necessary to perform such analyses. A further aim is perform full source reconstruction with the goal of determining the release amount and location of any observed radionuclides using advanced mathematical techniques.

The NDC at HC has access to several different analytical engines for performing gamma spectroscopy, with a database being the primary repository of all raw information and processed analytical results. During routine operations, the IMS SPHDF files are sent via email on a private network to HC from the CTBTO. The mailbox is monitored by a process daemon that checks for new messages and initiates the analysis pipeline. When any messages are detected, the Unisampo/Shaman software package performs an automated analysis. Unisampo performs the peak finding using a Mariscotti second derivative method and Shaman performs both the activity calculation and peak identification using a series of expert rules tailored to aerosol monitoring. Shaman is also the source of the coincidence summation corrections, as described in Section 4.2.1. Both the raw data and analysis results are stored in a MySQL database using a schema called LINSSI.[1] The LINSSI database schema was jointly developed by: the Radiation Physics Group of the Helsinki University of

[1] Complete manuals for LINSSI and associated database management scripts are available at `http://linssi.hut.fi/`.

Technology, STUK, and the Radiation Protection Bureau of HC. There are two major versions of the LINSSI database schema available — version 1.1 [61], which contains the Canadian NDC data from 2005 to 2011 and version 2.2 [62], which was used after the old format was retired in 2011.

6 Methodology

6.1 Spectral Summation

Papastefanou gives a ^{7}Be production rate of 8.1×10^{-2} atoms^2 cm^{-1} s^{-1} in the atmosphere, with an average tropospheric concentration of 12.5 mBq m^{-3}[11]. This typical concentration of ^{7}Be is easily measurable on a daily basis by the IMS and does not require any special processing, such as spectral summation. However, Papastefanou gives a ^{22}Na production rate of 8.6×10^{-5} atoms^2 cm^{-1} s^{-1}, with an average troposphere concentration of 0.0021 mBq m^{-3}. As discussed in Chapter 5, it is not normally possible to measure ^{22}Na at these concentrations, except under rare circumstances. For example, Leppänen and Grinsted occasionally observed ^{22}Na using a high-volume air sampler that is very similar to those at CTBT stations. Samples had to be collected over one week and ^{22}Na was believed to be observed only during times of strong vertical air currents[35]. These air currents rapidly bring ^{22}Na-rich air from the upper parts of the troposphere to the ground-based sampler, which allows them to be measured on rare occasion.

A typical CTBT IMS aerosol spectra, such as the one shown in Figure 4.1, contains very little ^{22}Na signal. Most spectroscopic analysis packages would be unable to find the ^{22}Na peak at 1274 keV. A signal processing analogy was used in Chapter 5 to briefly describe the benefits of spectral summation for finding small peaks. While the analogy was useful to get a sense of the possible benefits of summation, it did not describe the actual process.

One way to visualize spectral summation in a qualitative sense is shown in Figure 6.1. This figure is a 2D colour map. Each spectrum is stacked along the vertical axis. Several features of the resulting image are noteworthy and require further discussion. First, there is a general consistency of colour along the vertical axis, particularly at higher energies. The colour in each vertical row represents counts in the same channel of the 30 summed spectra. The colour is more consistent at higher energies, as there is very little variation in the number of counts between different spectra.

Second, many bright lines are visible at various energies. The bright vertical

lines indicate a high number of counts, or strong signals. For example, ^{7}Be (477 keV) can be seen near the left side of the figure. Many other natural radionuclides and other spectral features, such as single and double escape peaks, can also be seen. Each bright line does not deviate from being perpendicular to the horizontal axis, which indicates that the calibration of the detector remained stable throughout the measurement of all 30 spectra. Had the calibration changed or shifted, it would have been easy to see the misalignment in the vertical line.

The last thing to note is the approximate location of the ^{22}Na peak marked in the figure. This particular period of 30 spectra were chosen since they have the largest peak area observed throughout the entire study. ^{22}Na is clearly hard to find, even using visual techniques that tend to highlight relevant features. The location of the ^{22}Na peak lacks any obvious line characteristic and the colour of the approximate region varies, indicating that there is a fluctuating amount of ^{22}Na signal.

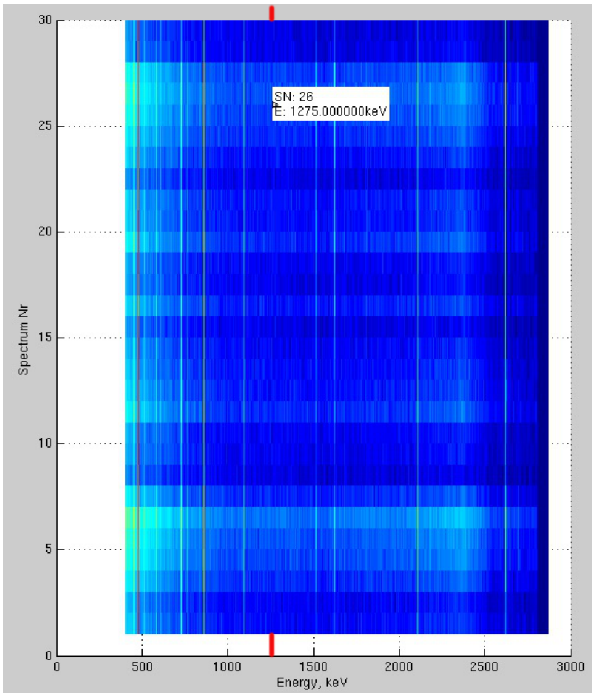

Figure 6.1 – A sequence of 30 gamma spectra lined up by channel and viewed in a two dimensional colour map. The colour gradient indicates the counts in each channel. The approximate location of ^{22}Na is in a line joined by the two red marks, just to the left of the inset box.

This 2D picture of spectral summation is only really useful qualitatively. To obtain actual activity concentrations (through the use of standard gamma spectroscopy

software), the summation process must work on sequences of raw data files. In this case, a new spectrum is generated by adding up the counts in each channel from all the daily spectra. The end result is that the summed spectrum will have effectively increased the air volume sampled (at a cost of decreased temporal resolution), thereby lowering the limits of detection. The spectra were added together on a channel basis under the assumption that the energy calibration remains constant over the summation period.

6.2 Process Map

Spectral summation is a technique that will be used to generate an additive spectra that should have a more consistent and observable ^{22}Na signal. These summation spectra are then processed by several pre-existing automated tools and the peak areas are inserted into a database. Once in the database, further processing is required to calculate activity concentrations and display the results in a useful graphical form. This process is described in the following three steps:

1. Retrieve daily spectra from the database (sorted by monitoring site) and generate a new raw summation data file.
2. Process the summation data files, fitting the peaks of interest and storing the results (peak area values) in a new database.
3. Perform the calculation of activity concentration and generate results in an interpretable manner.

Many individual software packages must interact in sequence before the ^{22}Na data can be generated, analysed and presented. The flow chart shown in Figure 6.2 describes the general interactions between the various software components that generate final results using data from HC's LINSSI 1.1 database.

The interactions between the software components shown in Figure 6.2 are quite complex.. *Pysum* is the first component, which retrieves, by station, the daily spectra over the integration period in an existing LINSSI 1.1 database and writes a new raw summation spectral file to the filesystem. Along with the summation spectra, the raw summation file contains the calibration information for the station. This file is then read by AATAMI and is inserted into a LINSSI 2.2 database.

The next program to be executed is *Calupdate*. *Calupdate* recommends the calibration (for use) that has been inserted into the database by AATAMI through the update of a calibration field in the new database.

Once the calibration is recommended, JMUFI is able to use the calibration to analyse the summation spectra. It writes the peak fitting results to the database so that they are associated with the correct sample and measurement. Note that JMUFI

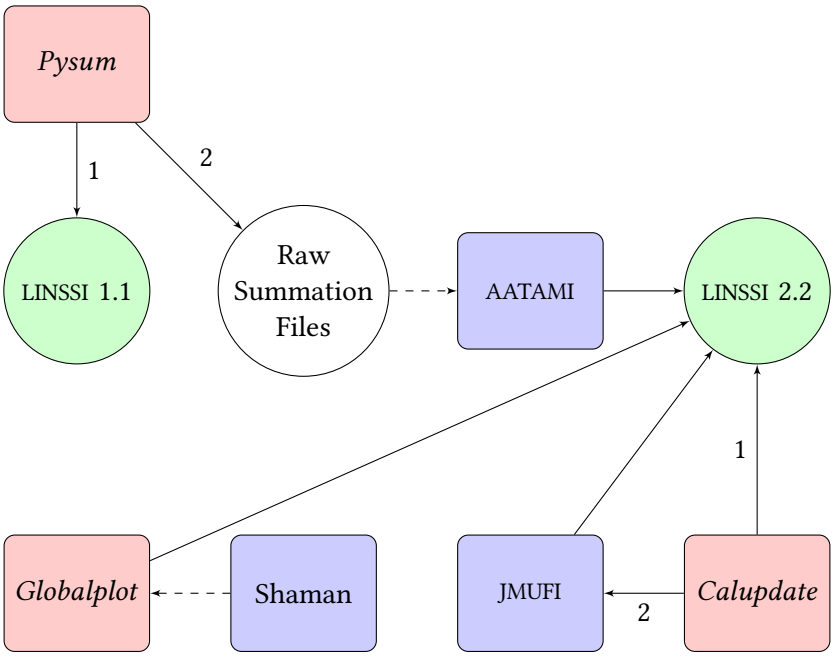

Figure 6.2 – Flow chart of spectral summation analysis process. The two databases are shown with green fill, while the pre-existing components have a blue fill and the new components have a red fill. The arrows indicate the direction of interaction and the dashed line indicates a prerequisite. The numbers on nodes indicate the order in which interactions take place. The sequence of execution is clockwise, beginning from top left.

writes peak area values to the database and not actual concentrations. This is the end of the second step in the analysis; however, there are actually two important tasks remaining to identify possible relationships between ^{7}Be and ^{22}Na radionuclides.

The first task is to verify the results of the analysis. JMUFI is very simplistic in how it fits peaks and it is possible to have spurious results. Figure 6.3 shows an example of a poorly fitted ^{7}Be peak that required special treatment. Problems such as this one are identified by examining the results of both the peak area and peak centroid of the natural radioisotopes present in the sample. Once identified, these problem cases can sometimes be fixed manually. However, if the spectra has more serious issues that cannot be fixed with human intervention, the analysis results are added to the blacklist of spectra to be excluded from further analysis. The final task is to visualize and analyse the resulting data to make conclusions about the individual isotopes and any relationships that may be present between these radionuclides. *Globalplot* is the routine created to display the data and it can process and apply optional summation correction factors in a text file to correct for TCS when it plots the results.

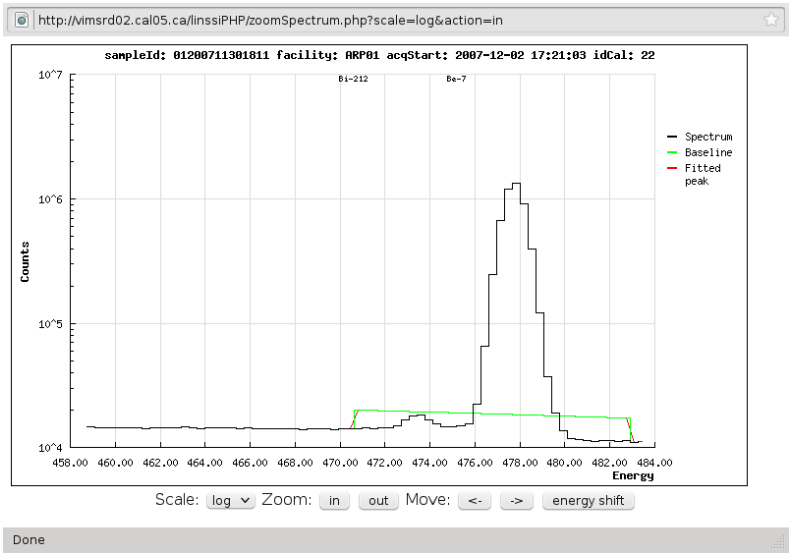

Figure 6.3 – An example of a poor JMUFI analysis. The energy fitting range and allowed deviation from the true peak centroid was set too large, and the ^{7}Be peak was not fit properly, as shown by the lack of red Gaussian curves above the baseline for both the 477.6 keV ^{7}Be peak and the 473.0 keV ^{212}Bi peak. The height of the baseline also reveals the poor fit — it is high due to the use of counts from the neighbouring peak in the background assessment. After fine tuning the allowed peak deviation, the peak was fit properly.

6.2.1 Pre-existing Software

Three pre-existing software packages (shown in the blue squares in Figure 6.2) are used to aid in the analysis of the data: AATAMI[63], JMUFI[64] and Unisampo/Shaman. AATAMI is only used in a limited fashion to insert the summed spectra into a database and provide the required calibration information that JMUFI requires to perform spectral analysis. These two software packages have unique characteristics that complement one other. A brief description highlighting the unique features of each software package is provided below.

6.2.1.1 Advanced Analysis Tool for the Assessment of Monitoring Information (AATAMI)

AATAMI is an advanced spectroscopic analysis tool with a comprehensive nuclide library, strong multiplet deconvolution capability and a sophisticated baseline fitting algorithm. The software package executes in a Matlab® environment. The key feature of this package is how it handles the fitting of the baseline under peaks, using a cubic spline fit. The display of fitting residuals, or the difference from the fitting function

and actual data, combined with the advanced baseline fitting, are ideal for finding small peaks. Figure 6.4 shows a typical view of the AATAMI software package, with the residual display shown above the spectra. However, it has a major drawback in that the algorithm is slow, even on modern hardware. Thus, it is not practical to use in the analysis of a large number of samples. It is sufficiently rapid if used only to perform the insertion of records into the LINSSI database, as it can operate in batch mode by inserting the raw spectra and calibration information without human intervention. AATAMI also supports writing analytical results to both major versions of the LINSSI database. These capabilities allow the transfer of the historical archive from the LINSSI 1.1 format to a LINSSI 2.2 database before final processing is performed with JMUFI.

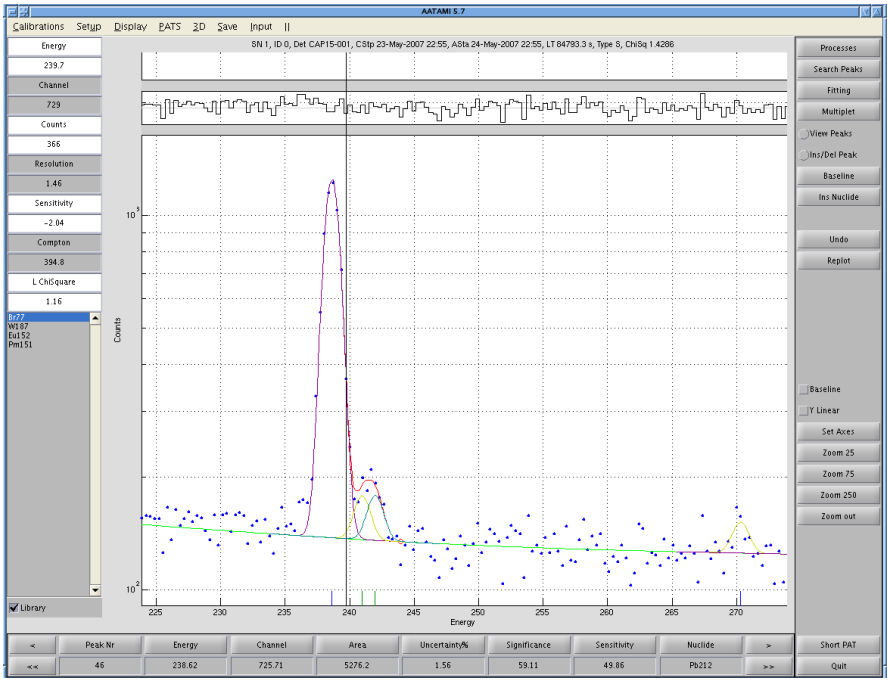

Figure 6.4 – The display of the AATAMI software package after automated processing. The abscissa is in energy (keV) and the ordinate shows the counts recorded by the MCA. The individual counts recorded are the blue points, with the baseline shown in green and the overall gaussian fit of the multiplet near 240 keV is shown in red. Individual peaks are shown in various other colours.

In addition to requiring the spectra to be transferred from the LINSSI 1.1 version to version 2.2, JMUFI also requires AATAMI calibration information to perform its analysis. To calculate the activities of the radionuclides observed, the detector ef-

ficiency needs to be known. AATAMI fits the energy/efficiency pairs using a special function, called HAE1-2 (named after the initials of its creators)[65]. This function is made up of two terms, as shown in Equation 6.1.

$$y(x) = S f_1(x) f_2(x) \tag{6.1}$$

where

$$f_1(x) = e^{-\left(\frac{E_1}{x}\right)^k} \tag{6.2}$$

$$f_2(x) = \begin{cases} 1 - e^{-b\left(\frac{-E_2}{x}\right)^m} & \text{if } x > E_2 \\ 1 & \text{if } x \leq E_2 \end{cases} \tag{6.3}$$

Here, $y(x)$ is the efficiency at energy, x. S, E_1, E_2, b, m, k are all parameters to be optimized during the fitting process.

In the rare event that the HAE1-2 function is unstable and generates an incorrect efficiency value, the software will revert to a more standard 5^{th} order (n=5) logarithm polynomial, given in Equation 6.4. This minor change in the calculated efficiency has only a slight impact on the final efficiency value.

$$\ln y(x) = \sum_{i=1}^{n} a_i x^{i-1} \tag{6.4}$$

The detector efficiency is now used to calculate the peak area. Normally, a calibration source containing several isotopes with certified activities covering a broad range of decay energies would be used to evaluate the response of the detector and derive an efficiency function. The calibration source specifically serves to evaluate the intrinsic, or detector construction material efficiency, and the geometric efficiency of both the sample and detector as a system.

AATAMI was used to verify the presence of the small ^{22}Na peaks in the summation spectra and to evaluate the quality of the calibration after JMUFI analysis. Unfortunately, AATAMI is only available to CTBT NDCs, as the software package was created for the CTBTO, which holds the commercial rights.

6.2.1.2 Java MUltiplet FItting (JMUFI)

JMUFI is a Java code that performs Gaussian multiplet peak fitting on gamma spectra that reside in a LINSSI 2.x database. JMUFI uses the spectra stored in the database, combined with the AATAMI shape calibration and a template file defining the nuclides, to perform automated spectra analysis. The template file specifies the isotopes to be searched for by the software. This is accomplished in the template file by providing an

acceptable tolerance in the peak centroid energy for the fitting process. The template for fitting was tuned iteratively so that optimal results could be obtained from the analysis. For example, the primary line of ^{7}Be was found to create an optimal data set using a 1.2 keV tolerance, or allowable deviation from the line reference value, in the peak centroid, while ^{22}Na was fit allowing for a 3.0 keV tolerance.

JMUFI fits the background using a linear baseline with the same width as the specified peak centroid tolerance. It then fits the largest area Gaussian peak possible using a Levenberg-Marquardt algorithm with adaptive-step reduction and box constraints. One drawback to JMUFI is that it lacks a full isotope library. For example, it can only determine peak areas, but it is not able to calculate activity concentrations directly. The peak area results of the JMUFI analysis are written to the LINSSI database, but further analysis and processing, as described in Section 6.2, is required before activity concentrations can be calculated. As mentioned previously, the software package *Globalplot* was developed to calculate activity concentrations and to visualize these results, as described in Section 6.2.2.3.

JMUFI was created under contract for use at STUK and is still in active development. STUK has graciously allowed HC access to the software for testing purposes and also for this work.

6.2.1.3 Unisampo/Shaman

One of the parameters missing for accurate quantification of ^{22}Na activities are the summation correction (TCS) factors for each station detector geometry. Since ^{22}Na emits positrons (and can experience pair production in the detector), it is possible for a 511 keV annihilation gamma-ray to sum with the 1274.5 keV gamma-ray. When summation occurs, counts that were supposed to appear at 1274.5 keV are now at 1785.5 keV. This leads to an underestimation of activity concentrations when using the 1274.5 keV peak to evaluate the ^{22}Na activity. As this work solely uses the 1274.5 keV peak, a correction factor is needed for accurate activity concentration values.

As mentioned in Chapter 4, one of two approaches is typically used to determine the correction factors. The first is to perform a MC simulation using software such as MCNP or GEANT to characterize the system and the summation effect. The second is to perform empirical measurements of the detector system to fully understand its response characteristics. In both cases, the goal is to derive what is called the total efficiency of the detector system.

This raises the question of how the total efficiency is defined, particularly in comparison to the efficiency previously discussed. Total efficiency is defined as the probability that a gamma-ray of a given energy will be recorded by the detector[54]. The key component of this definition is that the gamma must be recorded — there

is no expectation or requirement placed upon the energy at which the gamma-ray must be recorded at during the spectroscopic measurement (i.e. the energy is not required to be recorded at a decay energy). The ratio of total efficiency to peak efficiency can then be used as a correction factor for TCS. However, although total efficiency calibrations are permitted in the SPHDF data format, they are optional rather than required. Since they are optional, total efficiency calibrations are not available for all of the IMS sites. With the exact dimensions of each detector system unverified, a Monte Carlo simulation is not feasible. An alternative approach is needed and fortunately the archival databases of daily samples previously analysed by the *Shaman* software package can provide a solution.

Stored in the NDC LINSSI database are correction factors for the previous analyses of ^{22}Na from the expert identification software package *Shaman*. While *Shaman* prefers to use a given total efficiency calibration to calculate the TCS correction factors when it identifies and quantifies a nuclide, it is also capable of performing a very good estimate of the necessary correction factor. *Shaman* estimates the correction factor by using a parameterization of the total-to-peak-efficiency ratio for each nuclide in the spectrum. This parameterization is done on the basis of detector size and type. The size, or relative detector efficiency, is assumed to be 40 % and the detector is assumed to be a p-type semiconductor. The TCS correction factors estimated by *Shaman* are stored in the LINSSI database, and assuming the detector has not been changed, the previously calculated factors can be used to correct the activity concentration values (by simple multiplication) from the values calculated by Equation 4.10. The resulting ^{22}Na activity concentration data will be the first set of TCS corrected data available.

The library of coincidence correction factors from previously identified cases of ^{22}Na (stored in the LINSSI 1.1 database) were collected by station to determine appropriate correction factors. When multiple values were available, typical values were chosen to correct the activity results. When no value was available (four cases), other values from stations operated by the country were averaged and used as the correction factor. The reasoning behind this decision was that each country probably used the same vendor for each monitoring station. However, because there can be a significant length of time between different site installations, this assumption may not be true. It is also possible that revisions in the detection system design may occur between procurement intervals.

The magnitude of the correction factors from the LINSSI 1.1 database are shown in Figure 6.5. Looking at the figure, there are two distinct regions of corrections. The sites that require larger correction factors are predominantly manually operated. In these types of stations, the station operator compresses the filter into a puck and places the puck inside the detector shield. Such IMS systems generally have very close source-to-detector distances, leading to a larger correction factor. The sites

with smaller correction factors are predominantly fully-automatic systems. In these systems, there is no operator and the source-to-detector distance tends to be larger.

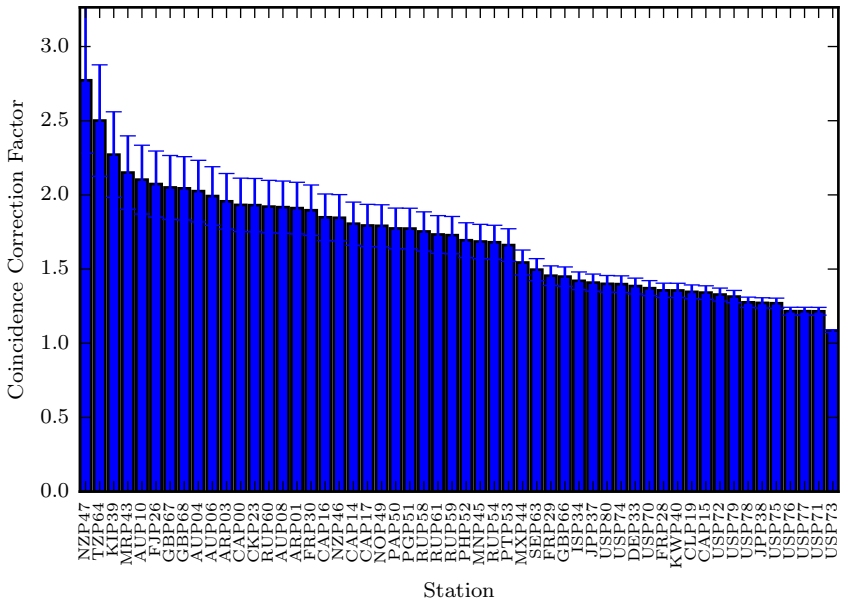

Figure 6.5 – Coincidence correction factors for the IMS monitoring sites. Only the factors generated by Shaman and stored in the LINSSI database are shown here. The error bars are symmetric and two-tailed.

6.2.2 New Software Specifically Developed for the ^{22}Na and ^{7}Be Analysis

Three computer codes (shown in the red squares in Figure 6.2) were developed to perform tasks required to find ^{22}Na at the CTBT monitoring sites. Each of these codes is discussed in detail in the following sections.

6.2.2.1 The Computer Code *Pysum*

The large amount of data that required processing presented a few challenges. First, nearly all of the processing needed to be as automated as possible. The generation of high quality results depends on having intelligent, automated data analysis routines able to screen and manage the raw spectral input data carefully and separate good data from bad. A computer code, called *Pysum*, was written in Python to interrogate the LINSSI 1.1 database by IMS radionuclide station, given a user-defined time

period and integration time. *Pysum* requires the Python modules Numpy, Scipy, Matplotlib[66], MySQLdb and Datetime. Below is a general description of the steps performed by *Pysum*:

1. Retrieve the list of stations for processing.
2. Retrieve collection start and stop, air volume sampled, acquisition start and stop, live time, real time, and MCA output for each station, within the integration period.
3. Perform Quality Assurance (QA) verification of all data retrieved and reject poor quality data.
4. For acceptable data, retrieve the initial calibrations (efficiency, energy, resolution) at the integration start period for each station and summation interval.
5. Perform channel by channel summation and write a new SPHDF with modified header and calibration blocks as detailed below.

The requirements of the SPHDF format, as specified in Appendix B, presented particular challenges for generating a file that could function properly in the analysis software, yet contain all the necessary information for spectral summation. Decisions had to be made on the best approach to handle the collection and acquisition periods, as well as the information in the calibration data blocks.

The SPHDF file created by *Pysum* was designed to have a collection start and stop that reflected the duration of the summation period. The acquisition time needed more careful handling as the analytical software did not accept acquisition times that occurred during the collection interval. The solution was to set the acquisition start period as the start of the final spectra being summed and to end the acquisition phase once the total acquisition time of all samples had elapsed. The problem with this approach is that there may be missing data between the integration start and stop, for both the collection and acquisition periods, which affects the activity calculation in several ways.

To give an example, suppose there is a one-day gap in the collection period. The collection interval remains the same, but the missing data will result in an underestimation of the nuclide activity. The underestimation occurs during the calculation of the sampling collection factor, since the formulation assumes a continual sampling interval. The total acquisition time is correct, however, as it is the sum of the individual spectra acquisition times.

There is a much more fundamental assumption behind the equations used to calculate activity. All the equations previously described in Section 4.2 assume that radioactivity in the air is constant during the sampling process. For environmental radionuclide monitoring using short sampling periods, this is a reasonable assumption. However, over a 30 d or seasonal integration period, this assumption may break down, particularly during integration periods that have volatile weather. The

activities calculated will still represent the average airborne concentration over the integration period, but specific incidences of STE may be difficult to discern in the results. The sample air volume in the SPHDF file was set according to the sum of all sample air volumes collected and the calibration information was set according to the calibration information present in the first sample. As the remaining fields in the header were not essential to the analytical process, they were all set either to the value in the first sample or filled with dummy values as appropriate.

6.2.2.2 The Computer Code *Calupdate*

JMUFI requires an AATAMI energy and resolution calibration in the LINSSI database before it is able to fit peaks in a spectra. An additional complication is that, in order for JMUFI to use the calibration in the database, the calibration must be recommended by updating the idCal field in the calsRecommended table of the LINSSI database. In normal operations, a recommended calibration is verified by an analyst and used repeatedly, since the calibration is expected to remain relatively stable and the analysis software is robust enough to adjust for small corrections to the calibration as required. Calibration issues are monitored by the analyst and can be corrected with a new recommended calibration when necessary. With the long spectral integration periods contained in each raw file and, due to the automated nature of the processing, this was not a practical approach for this project.

With the large number of spectra to be analysed, it was not possible to inspect all calibrations throughly for quality. AATAMI does a very good job of automatically making corrections to the calibrations supplied by the SPHDF file, assuming they are reasonably accurate. The strategy implemented to provide the best results without thorough review was to have AATAMI perform a calibration update based upon the natural radionuclides present for each spectra (which are reasonably rapid). The *Calupdate* code would then iteratively recommend the matching calibration for each spectra before each analysis with JMUFI. The last minor task that was incorporated into the *Calupdate* code was to scan each raw spectral summation files for the total volume of air filtered and insert the integration summed value into the database so that activity concentrations could be calculated.

6.2.2.3 The Computer Code *Globalplot*

The last computer code, *Globalplot*, also written in Python, was created to query the LINSSI 2.x database for the JMUFI-processed results and to perform data analysis and plotting. The code relies upon several Python modules: NumPy, SciPy, Matplotlib[66], Datetime, MySQLdb, Mpl_toolkits and also makes use of the Pandas dataframe toolbox for statistical analysis and time series resampling. This computer code is

a complete stand-alone tool that queries the peak area information and calculates activity concentrations and associated uncertainty. It is capable of plotting data with several different types of output. For example, it can generate a time series of isotopic data by station or plot the relative ^{22}Na and ^{7}Be behaviour by month. It also computes and plots the monthly slope coefficient to examine changes in the relationship between ^{22}Na and ^{7}Be. The code is relatively easy to extend to examine any other data characteristics of interest. For example, by changing a few lines of code, it is possible to look at other natural radionuclides and any relationships that may exist between them.

The first step in the program operation is for the user to set some initial parameters, such as the energy range to consider for retrieval of peak areas, the data to discard and the database connection parameters. Once this is completed, the code performs the following steps:

1. The LINSSI database is queried first, gathering the complete set of Be and Na peak areas.
2. Calculation of activity concentrations is then performed following the steps described in Section 4.2. A fifth order log polynomial fit is used for the channel-energy pairs in the database to calculate the detector efficiency at the energies of interest. This function provides a stable and accurate efficiency fit at the decay energies of ^{7}Be and ^{22}Na.
3. The program will then plot or save the resulting figures as follows:
   a) The yearly data for all stations for each nuclide, by hemisphere; or
   b) The data by month for both nuclides, by latitude or R_c, along with linear regression trends for Be and Na.

Additionally, the program has options to label data points in the charts with latitude, longitude, dates and station names. Any other desired database parameter can be easily added to the labelling code if the user wishes.

7 Model

7.1 Background

Any attempt to model the behaviour of cosmogenic radionuclides in the environment must incorporate several phenomena. In addition to the observations themselves, the production rate and a model for the motion of the atmosphere must be included to examine fully the environmental behaviour of cosmogenic aerosols. The approach used here will be to investigate the environmental behaviour using a semi-empirical model primarily because of the difficulties inherent in implementing a full model of the atmosphere. The reason for the selection of a semi-empirical model is entirely a practical one, since to perform a full GCM would essentially be a separate project in itself.

GCM simulations are extremely complex as they simulate the entire behaviour of the atmosphere and hydrosphere prior to and throughout the simulation interval. The simulation must be started sufficiently in advance of the period of interest to have the various simulated domains (hydrosphere, atmosphere, etc.) match the initial state of the simulation period studied as much as possible. GCM simulations have been successfully used in the study of several radionuclide tracers and chemical pollutants, such as atmospheric ozone[2, 6, 7, 28]. Accordingly, they require a large computational budget and typically involve supercomputing. Although not ideal, a semi-empirical approach allows for an examination of the data in an environmental context more rapidly before committing the necessary resources to performing a full GCM simulation.

Beyond the summation data generated by *Pysum*, there are two main components necessary to construct a semi-empirical model: cosmogenic production and the atmospheric transport. Furthermore, the cosmogenic production component of the model can be characterized by two components. The first is the incident GCR itself, and the second is the R_c, which is important when the GCR encounters the magnetic field of the the Earth. These components can be examined separately and in combination to help with the interpretation of the data. A schematic of the semi-empirical model is shown in Figure 7.1. The stratosphere is the dominant production location. The

deceleration potential, a measure of heliosphere shielding of the Earth from cosmic radiation, will be used to scale the production rate according to the Geomagnetic Vertical Cut-off Rigidity at each site. The heliospheric shielding is provided by the magnetic field created by the sun. Once the stratospheric air enters the troposphere (not shown in Figure 7.1, but represented by atmospheric transport), atmospheric transport becomes important. By separating the Earth into the major transport cells, it is hoped that the production can be related through the motion of the atmosphere in each cell to the ground-level observations generated by the spectral summation technique.

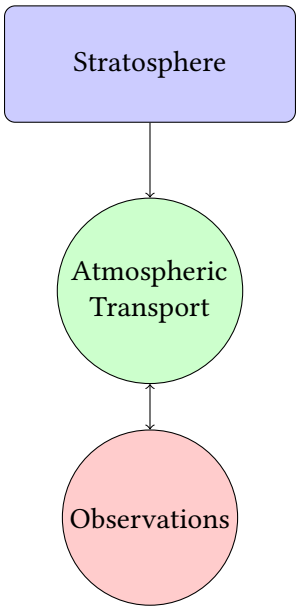

Figure 7.1 – The three major factors considered in the semi-empirical model. The production site of cosmogenic radionuclides is the stratosphere. The production rate is highly variable depending on solar activity as described in the following two sections. The atmospheric transport component is represented by the major circulation cells — Hadley, Ferrel, and Polar that were previously discussed in Section 2.2. Finally, there are the series of observations derived from the summation technique using sensors on the surface of the Earth.

7.2 Cosmogenic Production and Galactic Cosmic Rays (GCR)

Cosmic rays, with an origin typically beyond the solar system, encounter the heliosphere, a region that extends approximately 150 AU from the sun. This region

has powerful magnetic fields that strongly influence or modulate the cosmic rays observed on Earth[67]. While the general aspects of the production process are reasonably well understood, some of the specifics of the actual production for any cosmogenic radioisotope production process are difficult to model since there is a great deal of uncertainty around the incident particle fluxes and the cross-section of both radionuclides[17, 68].

To characterize the incident particle fluxes before their interaction with the gases in the atmosphere, a modulation parameter is used to account for the relative variation in GCR incidence caused by the variation in heliospheric shielding. However, a number of different modulation parameters are available to model this shielding of the incident GCR flux. There are only slight differences in how the modulation parameters are modelled and this work will use one of the more recent modulation parameters, the deceleration potential, ϕ, measured in MV and described by Badhwar and O'Neill[69, 70]. The key advantage in selecting this potential is that it does not suffer from delays in heliospheric response. This advantage comes from the use of satellite data in the model, rather than being based solely upon solar observations. If solar observations are used, the response lag of the heliosphere can range from 8 to 14 months[71]. With the data that was collected for this study, the deceleration potential varied as shown in Figure 7.2. The mean ϕ was 406 MV and it varied by a factor of approximately 2 from the mean during the study period.

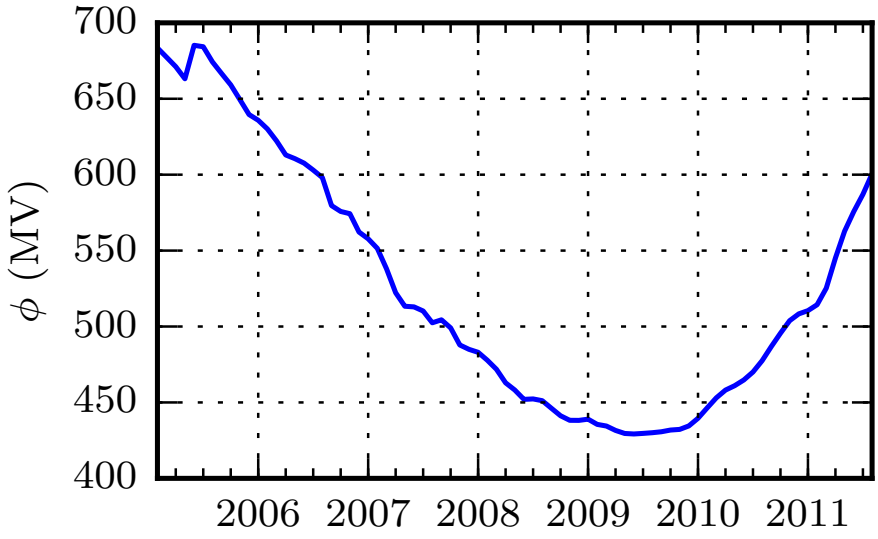

Figure 7.2 – Monthly deceleration modulation potential, ϕ, during the study period. Data from [72] (through personal communication).

Table 7.1 – Calculated production rates of ^{7}Be and ^{10}Be in the Earth's atmosphere (corrected and adapted from [68]).

	Production Rate (atoms cm^{-2} s^{-1})	
Source	^{7}Be	^{10}Be
Masarik and Reedy [1995]	0.0129	0.0201
Blinov [1988]	-	0.0260
O'Brien [1979]	0.005 78	0.009 63
Oeschger et al. [1970]	0.0185	0.0140
Lal and Peters [1967]	0.081	0.0450
Masarik and Beer [1999]	0.035	0.0184
Beer et al. [1994]	-	0.0160
Reyss et al. [1981]	-	0.021
Monaghan et al. [1986]	-	0.0380

7.3 Cosmogenic Production and Geomagnetic Vertical Cut-off Rigidity (R_c)

Recalling Figures 2.4 and 2.5, showing the magnetic dipole field of the Earth and the potential required for GCR to interact with the atmosphere, the difficulty is now to determine the actual production of cosmogenic radionuclides from the spallation of GCR gases in the atmosphere. Many studies have been performed to examine ^{7}Be and ^{10}Be production rates and Table 7.1 presents a brief summary of results from several studies.

These studies clearly show a great variability in production rate and presumably much uncertainty (which is seldom quoted). If you consider there is a factor of 14 and 5 between the minimum and maximum of the calculated global mean production rates for ^{7}Be and ^{10}Be respectively, ^{22}Na would have at least as much variation. As ^{22}Na has a much lower production rate than ^{7}Be, there would be considerably more uncertainty around its true production rate. It is therefore necessary to determine, which production rate, if any, should be used from those in the literature.

One possible approach to managing the variability is to create a model for each of the production rates, given in Table 7.1. However, that would only work for ^{7}Be and would require the development of evaluation criteria to select the best production rate that, when inserted into the model, gives the best agreement with the surface observations. While this is possible to do in practice, it is not very practical, as there is still the problem of whether the production rate is really accurate. Or

worse, the production rate may simply provide the best agreement with a limited set of observations while incorrectly modelling the actual process and its variability. Regardless, there remains the issue of how to handle the ^{22}Na production rate, which has not been well documented in the literature.

Instead, an alternate approach was chosen that uses an approximation to a simulated production rate. Using a radiation dosimetry study based upon International Commission on Radiological Protection (ICRP) weighting factors published in ICRP-92 for aircraft crews from Takada et al., the modelled ambient dose ($H^*(10)$) rate which is the energy imparted to matter per unit mass per unit time, is used as a relative scaling factor to adjust for variations in spallation production according to the R_c of the observing site. The variation in modulation and R_c is reproduced in Figure 7.3.

The essential components in Figure 7.3 are the deceleration potential, ϕ, and the equations given in Takada et al. for the solar modulation bounding curves. The equations for f_1 and f_2 are reproduced as Equations 7.1a and 7.1b while the equation for f_{2min} derived from the LUIN cosmic ray propagation code is reproduced as Equation 7.2[24].

$$f_1 = 1.70 + \frac{5.08}{1 + e^{(R_c - 5.11)/2.91}} \tag{7.1a}$$

$$f_2 = 1.59 + \frac{3.38}{1 + e^{(R_c - 5.60)/3.13}} \tag{7.1b}$$

$$f_{2min} = e^{1.2912 - 0.044807 R_c - 0.079977 e^{-R_c}} \tag{7.2}$$

Furthermore, this paper gives an equation to calculate the ambient dose equivalent ($H^*(10)$) rate as a function of ϕ and f_1, f_2, and f_{2min}. This equation is reproduced as Equation 7.3. Combining Equations 7.1a, 7.1b, 7.2 and 7.3 allows for computation of the ambient dose rate, $\dot{H}_o^{\phi}$ at any given R_c.

$$\dot{H}_o^{\phi} = \begin{cases} f_1 & \phi < 487\,\text{MV} \\ \frac{f_2 - f_1}{699}(\phi - 487) + f_1 & 487\,\text{MV} \le \phi \le 1186\,\text{MV} \\ \frac{f_{2min} - f_2}{1475}(\phi - 1186) + f_2 & 1186\,\text{MV} < \phi \le 2661\,\text{MV} \\ f_{2min} & \phi > 2661\,\text{MV} \end{cases} \tag{7.3}$$

The neutron energy spectra at the bottom of the stratosphere is dominated by neutrons with energy in excess of 20 MeV[67]. The corresponding weighting factor is a continuous function between 5 to 9 for neutrons in this domain and 2 for protons[73].[1] The combination of a neutron/proton ratio of between 1 to 1.6 at

[1]There are newer ICRP guidelines (ICRP-103) that modify the function describing the neutron weighting factor, w_R. However, for simplification, the older ICRP factors are used in this study.

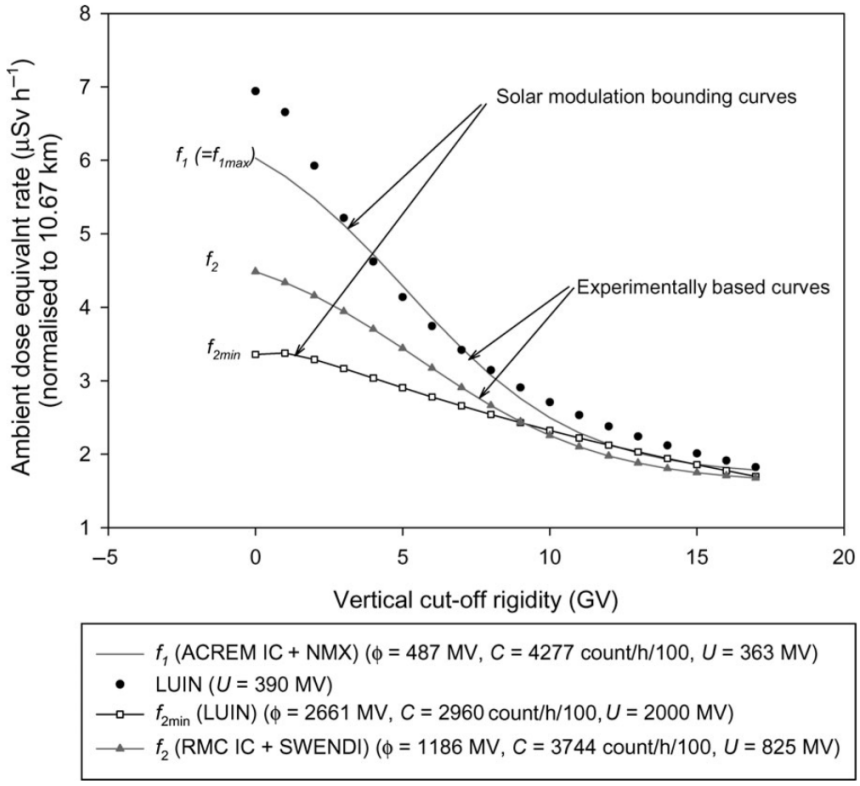

Figure 7.3 – Ambient dose equivalent rate, H*(10), as a function of the deceleration potential, ϕ, and R_c. f_1 is the bounding curve for the solar minimum and f_2 are the bounding curves for the solar maximum. f_2 is based upon actual NM measurements while f_{2min} and f_{1max} are based upon LUIN cosmic ray propagation models. The ground level count rate, C, from a NM located in Climax, Colorado is shown along with the heliocentric potential, U in the legend. SWENDI is an extended-range neutron rem meter, while NMX is a combined NM NE-NM2 with lead converter. Figure reproduced from [24]

.

the 10.67 km altitude (atmospheric depth of 243 g cm^{-2}) depending on geomagnetic latitude and the differences in weighting factors means the dose model is a reasonable proxy for a direct production rate value, even if it neglects other particles that are relevant to aircrew dose.

Now that the ambient dose rate as a function of R_c is available, the relative dose rate was used to scale the observed activity concentrations according to the ambient dose rate at the maximum R_c value from all observation sites. The information required to create a production scaling factor is the R_c of the observing sampler and a

modulation parameter (shown in Figure 7.2) for the GCR. Mathematically, this scaling factor, F, can be represented as shown in Equation 7.4.

$$F = \frac{H^*(10)_{R_c}}{H^*(10)_{R_{c\,\max}}} \tag{7.4}$$

Application of the scaling factor to the observed ground-level concentrations is used to compensate for the different production rates caused by R_c. In other words, the scaling factor allows for the removal of geomagnetic latitude-dependent production effects between different measurement locations, as well as observation times, assuming that the R_c at the ground receptor site is reasonably representative of the stratospheric R_c.

While the scaling factor approach is reasonable, there is a weakness with this approach. *H*(10)* used in the study is a conservative operational dosimetric concept for area monitoring that incorporates weighting factors for the various types of radiation. These weighting factors are designed to place different types of radiation on an equal risk basis[74]. This weighting of radiation effects is not necessary for this study, since the target is atmospheric gases rather than tissue.

There is one last item to note regarding the production model and the overall interpretation of results. If the production ratio of both cosmogenic radionuclides is used rather than individual species, the interpretation of the results becomes easier. The production ratio is much more constant in terms of atmospheric depth and latitude[67]. Figure 7.4 shows that at any given atmospheric depth, the production ratio is nearly constant across all latitudes. Although this figure shows the relationship between ^{7}Be and ^{10}Be, a very similar figure could be generated for ^{22}Na with an appropriate MC simulation. Outliers in the ratio of these radionuclides would be one indicator of important transient phenomena, such as STE.

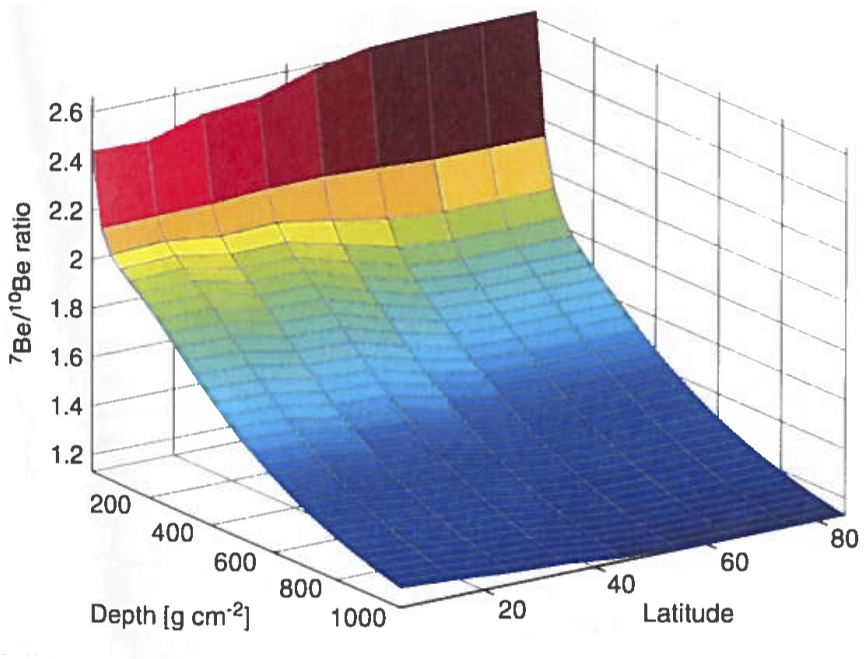

Figure 7.4 – $^{7}Be/^{10}Be$ production ratio for the present geomagnetic field and solar activity of Φ=550 MeV. Note that the modulation function, Φ, is related to the modulation potential by $\Phi = Ze\phi$, with Z being the charge of the cosmic ray particle. The proton, alpha particle and heavy components of cosmic ray flux are all included. Figure reproduced and caption modified from [67]

.

7.4 Atmospheric Transport

Recall Figure 2.7, which shows the general motion of the major atmospheric cells. The data generated by the spectral summation process will be examined geospatially using the three major cells. The process will be to collate the summation data into three domains: an equatorial band with latitudes between −30° to 30°; a mid-latitude domain of two regions with latitudes between −60° to −30° and 30° to 60°; and a polar domain of two regions with latitudes less than −60° or greater than 60°.

As environmental data can often be quite noisy (see Figure 2.8), a smoothing algorithm is usually necessary to observe general trends in data. The median values in each region were chosen for two very important reasons. First, the median assumes no underlying distribution (non-parametric). Second, unlike the mean, the median is robust to outliers present in the individual measurements. This is ideal since the data can be sparse in an individual month, where the presence of a single outlier can

dramatically affect the results and interpretation.

The atmospheric transport component will be examined with and without production scaling, as described in Section 7.3. By examining the global behaviour in this manner, it may be possible to draw further conclusions about the environmental behaviour of these cosmogenic radionuclides.

7.5 Integrated Model

The preceding sections must be combined to complete an overall integrated model. Following Figure 7.1, the semi-empirical model must incorporate the three domains for an overall assessment of the summation data and underlying model. Mathematically, the overall relationship is given in Equation 7.5.

$$C_{obs} \propto kPA \tag{7.5}$$

where C_{obs} is the observed concentration of ^{7}Be or ^{22}Na at ground-level, k represents the minor factors (e.g. influence of tropospheric production on overall data, the approximations made in coincidence correction factors, etc.) that are unaccounted for in the model, P is the component of C_{obs} due to variations in stratospheric production, and A is the component of C_{obs} accounting for variability created by atmospheric transport.

This formulation shows clearly how it is possible to examine the separate components that influence the ground-level observations. If the variable production rate is fully compensated and k can be neglected, an analysis of the data set and its behaviour would indicate features due to variability in the atmospheric transport.

8 Results and Discussion

To generate the final data set, all computer codes described in Section 6.2.2 were tested and developed gradually. This phased development approach allowed for corrections and improvements to be progressively implemented as the techniques and analysis matured. The first steps performed in the development of the computer codes were to generate a rough proof-of-concept to verify the techniques used.

First, a single year, 2006, was chosen to serve as a test data set to develop the new software codes. Another reason for working with a small subset of the data was to verify the methodology on a data set that could be quickly analysed and reanalysed as necessary. Even with modern computer hardware, the process of inserting approximately 4500 spectra into the database with the required AATAMI calibrations takes roughly one week. The calibration update and raw spectra insertion by AATAMI required the most time during the analysis process. The peak fitting analysis with JMUFI is quite rapid as analysing all spectra in the database required only a few hours. The *Globalplot* code, used in the visualisation of results, generated figures in approximately one minute. Lastly, using a small data set allowed the investigation of different integration periods to find an optimal integration period for the summation process.

The initial version of *Pysum* generated spectra that AATAMI could insert into the LINSSI database along with the calibration information. JMUFI was then run on all the AATAMI processed spectra using a template file with analysis parameters for ^{7}Be and ^{22}Na. Several problems immediately became apparent during these initial trials. The first issue was the quality of data in the database. Data from the CTBT stations is processed automatically and there is no indicator of the quality of the raw and logistical data. The first version of the spectral summation code needed refinement to ignore spectra with no MCA output during the summation process (i.e. spectra with 0 counts for all channels). The spectral summation code was further refined through several iterations by imposing sensible constraints on the data extracted by improving the Structured Query Language (SQL) queries used in the database interrogation. For example, limiting summation samples to those samples with reasonable air volumes, actual MCA output, and sound logistical data helped

to ensure good summation spectra. This was successful in screening poor quality data from the source database, ultimately resulting in an increased number of usable summation spectra.

Two stations, located in Shaunisland, Germany and St. John's, Canada, which had good operational records throughout 2006, were selected to illustrate the preliminary results obtained by spectral summation and to verify the operation of the code. Figure 8.1 shows the results of spectral summation for ^{22}Na and ^{7}Be. Since the *Globalplot* code was still in the process of being developed, only the peak areas were examined. Looking at the peak areas, the concentrations of beryllium and sodium appear to be largely correlated, which suggests that they follow the same pathway through the environment and that any differences observed in their ratio are potential indicators of atmospheric phenomenon acting to modify the normal environmental behaviour of the longer-lived ^{22}Na.

These preliminary results were encouraging, as the two radionuclides behave almost exactly as expected from the literature. At both sites, maximum peak area observations occurred in late spring and summer for both radionuclides, with St. John's having a more variable structure near the end of the year. The development of the *Globalplot* code would allow the use of the actual airborne activity concentrations for investigations and provide a means to look for data trends on a global scale.

Initial versions of the *Globalplot* code also highlighted problems with the data in the LINSSI 1.1 database records as some summation spectra had incorrect sampling and acquisition times, sample volumes, and calibration data. Any errors with the logistical data could cause incorrect summation spectra. These problems were corrected in *Pysum* either by improving the SQL queries used to retrieve data or through selective removal of bad spectra from the summation process. The analysis was also improved by refining the JMUFI analysis parameters empirically (e.g. size of the energy range in which to look for a peak).

A deeper look at the preliminary results found several other issues with the summation spectra created by *Pysum*, such as those involving calibrations and energy drift. An example of an energy calibration issue was demonstrated by attempting to fit the 2614 keV ^{208}Tl peak, as shown in Figure 8.2. What is normally a single peak has become a false doublet due to an energy calibration change during the summation interval. This type of problem required a more sophisticated solution. To solve this problem and improve the overall quality of the analysis, other natural radionuclides, spaced fairly evenly throughout the spectra, were fit using JMUFI. Extra nuclides such as ^{40}K, ^{212}Bi, and ^{208}Tl were incorporated into the JMUFI fitting template to provide an indication of the quality of the energy calibration and analysis. These nuclides have typical seasonal characteristics, or characteristic activity concentrations that can be verified by examining a time series of the activity concentrations. Unusual concentrations based on the individual and relative size of the extra nuclides

indicated problems with the analysis. A further refinement of the JMUFI template greatly improved the analytical quality by highlighting and reducing the quantity of erroneous analysis data.

Globalplot, which was now nearing completion, was run on a single year, 2006, using a 30 d integration period, as presented in Figures 8.3 and 8.4. At this point, the major capabilities missing from the code were the ability to handle coincidence correction factors, discussed in Section 4.2.1, and the calculation of uncertainties in the activity concentration values. The figures show a clear correlation between ^{7}Be and ^{22}Na activity concentrations, which was previously shown when the peak areas were examined. Again, higher concentrations are typically present during warmer weather, with a corresponding larger slope for the ^{22}Na/^{7}Be linear regression. Most observations of ^{22}Na occurred during the spring and winter — the increased frequency of observations during the spring and winter implies that either there were more monitoring sites operational during that timeframe or more likely that STE events were more frequent during these periods. The latter explanation would be more likely as the tropopause is known to break down with enhanced mixing in spring and early summer, as was discussed in Section 2.2.

The data trends become more apparent when the monthly slope coefficients for ^{22}Na and ^{22}Na/^{7}Be are collected and plotted, as done in Figure 8.5. In this figure, the greatest excess of ^{22}Na (relative to ^{7}Be) appears in the June to July timeframe. Since STE is strongest in the late spring and summer, the trend matches what was expected from the literature review. Older air appears to be making the transition from the stratosphere to the troposphere. The ^{22}Na/^{7}Be ratio trend is also very similar in shape to the ^{22}Na linear regression.

The trends shown in these figures were very promising, each showing clear correlations between the cosmogenic radioisotopes. However, the key result is that all the techniques to ensure data quality appear to be working. Highly correlated behaviour, no unusual outliers, and the presence of linear trends, with the overall data being fairly tightly distributed, are all indicators that the summation technique and subsequent analysis is discovering valuable features in the data. The last remaining tasks to generate the final results were to implement the use of coincidence correction factors and to calculate uncertainties for each data point. Coincidence correction of ^{22}Na activity concentrations is something that has not been reported before in the literature. Since the correction factor is relatively large, between 1.4 to 2.7 depending on the geometry configuration of the IMS detector involved, it had the potential to change the interpretation of the preceding results.

For the final results, the period of analysis was extended to cover the maximum amount of data available in the LINSSI 1.1 databases at the NDC. This required the generation of summation spectra from 2005 through to the end of 2011, which is approximately half of an 11 year solar cycle. All outliers were examined and

eliminated from the data set, if they were found to be spurious, following the process used in the preliminary analysis (looking at natural radionuclides, etc.). Finally, for consistency with the previous results, ^{22}Na was still considered detected if the 1274 keV peak significance, as defined in Section 4.1.1, was greater than 0.7.

The final results were stored in a new database specifically created for the analysis work. For the first time, the results obtained will be compared with previously reported values from the literature. For the remainder of this section, only figures that illustrate the key findings of this work are shown. However, Appendix C contains the complete set of figures and Appendix D contains the complete data set in tabular form.

The first component of the final analysis was to investigate the effect the integration period had on the results to see if any optimization was possible. Two improvements were sought — the first was to increase the temporal density of ^{22}Na data and the second was to improve the sensitivity of the ratio plots so that STE could be more easily observed. These two objectives involved a trade-off to some extent.

By integrating over longer periods, the relative frequency of ^{22}Na observations should increase. The improvement obtained will depend on how many of the integrated spectra contain a ^{22}Na signal. Recalling Figure 6.1, it is visually difficult to determine the optimal number of spectra for integration, as the ^{22}Na signal is quite small. It is also difficult to determine analytically the optimal number of spectra to sum as each sample contains an unknown amount of ^{22}Na. The cost of using long integration periods is that STE becomes harder to observe. As long integration periods are no longer sensitive to the meteorological changes that bring ^{22}Na to the ground, the STE indicator, the ^{22}Na/^{7}Be ratio, becomes ineffective.

To examine this trade-off, 7 d and 30 d integration periods were tested along with a seasonal, or three-month summation period. The use of seasonal data obscured the temporal details of the ratios and ^{22}Na activity concentrations. In these trials, both the slope evolution graph for ^{22}Na and the slope in ratio became rather scattered, losing the STE discrimination capability described earlier. The behaviour using seasonal integration periods is shown in Figure 8.6. The 7 d integration period was found to be too short, resulting in insufficient ^{22}Na data to draw meaningful conclusions. In summary, for the IMS data available, the optimal integration time appears to be some time period between 7 d and 30 d. It should be noted that the optimal summation period will vary somewhat depending on the sampler location and seasonal weather patterns. Since, the 30 d integration gave good preliminary results, it was chosen to be used for the generation of the final results.

The *Globalplot* code was then completed, incorporating the coincidence corrections and a proper treatment of uncertainty by adding error bars, calculated by Equation 4.11, to the activity concentrations. The linear regression fitting now used the uncertainty as a fitting weight for the activity concentrations and the ^{22}Na

activity in the ratio plots. The uncertainty was considered negligible for ^{7}Be (relative to ^{22}Na). Figures 8.3 and 8.4 were updated and regenerated as Figures 8.7 and 8.8. These figures show ^{22}Na and ^{7}Be to be highly correlated (generally r^2>0.8 for the entire year).

One interesting feature to note in Figures 8.7 and 8.8 is that some monitoring sites have unusual ratios that differ significantly from the linear regression line, such as the SEP63 (Stockholm, Sweden) observation in September and the CAP17 (St. John's, Canada) observation in December. These unusual observations, having an excess of ^{22}Na, are most likely to have been caused by a local STE event, as older air masses have higher proportions of ^{22}Na relative to ^{7}Be. Thus, the ratio analysis is a good technique to estimate the approximate time of STE events, but further work with an atmospheric model would be required to confirm these events. Monitoring sites below the regression line may be an indication of slower vertical transport as the air is older.

With the final activities calculated with coincidence corrections, the agreement between the spectral summation values was compared to literature values quoted in Chapter 2. Beginning with the ^{7}Be results, according to Table 2.1, ground-level air should have equilibrium activity concentrations of <3.7 mBq m^{-3} near the equator, <5.6 mBq m^{-3} in mid-latitudes, and <7.4 mBq m^{-3} in polar regions. The CTBT IMS stations have a mix of different geographical areas, but the ^{7}Be and ^{22}Na simultaneous observation requirement restricted the data to mostly temperate and polar latitudes. For the spectral summation technique, the mean ^{7}Be activity concentration observed over the same period was 5.83 mBq m^{-3}, while the median value was 4.82 mBq m^{-3}, which is in good agreement with the literature. The ^{7}Be activity concentration values when ^{22}Na was observed, ranged from 0.38 mBq m^{-3} to 32.18 mBq m^{-3}. It seems likely that a rapid STE event occurred at sites with activity concentrations significantly exceeding the equilibrium values.

With fewer measurements available from literature, the ^{22}Na summation results are harder to evaluate. By comparing with the few studies that are available, the summation ^{22}Na results were reasonable — that is, within the range given by Leppänen and Grinsted in Section 2.3.5 of 0.1 µBq m^{-3} to 1.3 µBq m^{-3}. Rovaniemi, being a polar station with a fairly long operational history (1998 through 2006), should have a broad measurement history spanning a majority of the ^{22}Na activity concentrations possible. Using the spectral summation technique, the ^{22}Na activity concentrations ranged from 0.036 µBq m^{-3} to 10.22 µBq m^{-3}, with a mean value of 0.46 µBq m^{-3} and a median value of 0.40 µBq m^{-3}.

Looking at the ratio of ^{22}Na to ^{7}Be, the best source of comparable data is again the Finland study. There was a sufficiently long operational history, and being a polar station, the monitoring data should span a wider range of possible ratios than other regions. Typical values reported from the Rovaniemi site were roughly

1.3×10^{-4}, with a range of 3.3×10^{-5} to 4×10^{-4}. The summation method gave ratios that ranged from approximately 2.8×10^{-5} to 2.9×10^{-3}, with an approximate mean of 1.5×10^{-4}. The range and mean of ^{22}Na/^{7}Be values agrees quite well with the results reported from the Finland study.

A major problem with examining nuclides with activities near the limit of detection is that only the uppermost part of the distribution is observed; in statistical terms, the data is said to be left censored. In such cases, it can be difficult to determine the actual population distribution function and correctly fit a model to the data. Jasiulionis and Wershofen believed that both ^{22}Na and ^{7}Be were log-normally distributed at ground-level[8]. However, their study relied on data from only two temperate locations that were geographically near to each other and may not be representative of the global behaviour. Furthermore, they did not mention or account for the limits of detection in the statistical analysis presented.

The spectral summation data provides a more representative sample with its global data. Of the 4396 JMUFI analyses performed (including bad data) only 749 had measurable ^{22}Na. Approximately 17 % of samples now had a quantifiable ^{22}Na signal. This far exceeds the normal rate of observation. Knowing that only the top 17^{th} percentile of the ^{22}Na data was measurable, a normalized histogram of the data and Maximum Likelihood Estimation (MLE) fit were performed for both the ^{22}Na and ^{7}Be data, as shown in Figure 8.9.

The MLE fit of the ^{22}Na data to a log-normal distribution worked quite well, with the mean and standard deviation being almost identical to the histogram. The model also indicated there was an insufficient number of low activity concentration values observed. Considering the data censoring problem linked to the fundamental detection limit of ^{22}Na, this was expected. To further validate the results, the same fitting was repeated using the entire database of ^{7}Be data. Since this is high-quality data, it should have a similar shape and fitting parameters as the smaller data set. Looking at Figure 8.10, it is clear that using the total ^{7}Be data set results in a histogram with similar shape and MLE fit, with slightly different mean and median values due to the presence of samples with small amounts of ^{7}Be that are likely not present in the summation data set.

The next step in the analysis was to investigate the role of R_c on the concentrations observed. Due to the Earth's magnetic field, there is a anisotropic or variable amount of cosmic ray shielding (recall Figure 2.5). By correcting for the shielding effect, which is related to the production rate, it is possible to compare the activity concentrations at different locations[24]. This correction functions well as long as two conditions are met. First, the transport time from stratosphere to observation point must be roughly the same for all measurement sites over the integration interval. Second, the overall transport must be zonal, with little meridional motion, to ensure that the air masses are confined to locations with similar R_c, so as not to confound the

interpretation.

The first condition is difficult to account for without having a full 3D transport model. Since, the processes involved in transport are somewhat characteristic, the use of summary statistics can provide a representative analysis. Consideration of the second condition was postponed until the final results could be examined in a broader context. Typical plots of the ^{22}Na and ^{7}Be activity concentrations versus the corresponding R_c value at the measurement site are shown in Figures 8.11 and 8.12.

A couple of interesting features appear in this analysis. First, one would expect negative slopes on both regression lines, due to lower production rates from the increased geomagnetic shielding as the monitoring sites become closer to the geomagnetic equator (larger R_c values). Second, in the December panel, the sign of the slope is different between the two nuclides, which is highly unusual. This may be a good indicator that a strong STE event has occurred in several locations, as the relative increase in ^{7}Be indicates a younger air mass as the decay rate for ^{7}Be is more rapid than ^{22}Na. This is also suggested when using the ratio plots of Figures 8.7 and 8.8 for comparison. The full set of R_c plots is given in Appendix C.1.

Finally, the previous analysis performed in Figures 8.5 and 8.6 was repeated for comparison purposes. Figure 8.13 is very interesting because there is a similar curvature present for both radionuclides. Since the production rate of both ^{22}Na and ^{7}Be are dependent on the incoming GCR and SEP, looking at the trends in these factors may provide some insight into ideal times to model and investigate STE.

Figure 8.14 shows the count rate of neutrons (which are correlated with GCR intensity) observed at a ground-based monitor located in Oulu, Finland, and the SN during the time period of the ^{22}Na study. The curvature present in the top panel of Figure 8.13 looks qualitatively similar to the neutrons observed in Finland and anti-correlated to the SN, as expected from the literature. The maximum neutron count rate and minimum SN occur in 2009, which roughly corresponds to the maximum regression slope obtained for both ^{22}Na and ^{7}Be. In contrast, the smallest neutron count rates and largest SN values are observed in 2005 and 2011. The ^{22}Na and ^{7}Be global activity concentration data, corrected for geomagnetic latitude (represented by R_c), is responding to the neutron and SN influences in a similar fashion to previously published results. Prior illustrations of this effect were restricted to only a few locations, while these new results show the trend on a global basis, with a half-decade of environmental samples from 56 different monitoring sites in both the Northern and Southern hemispheres.

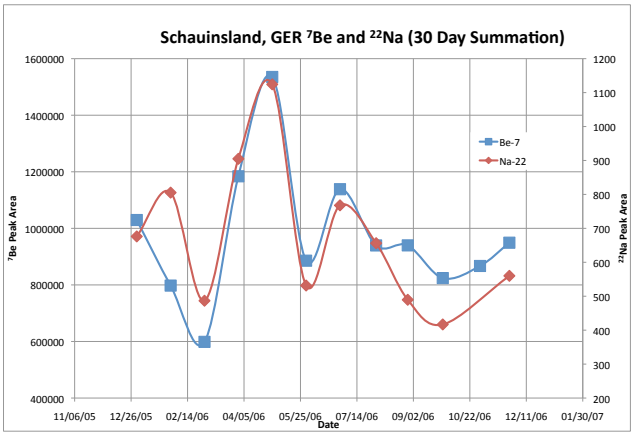

(a) DEP33, Shaunisland, Germany

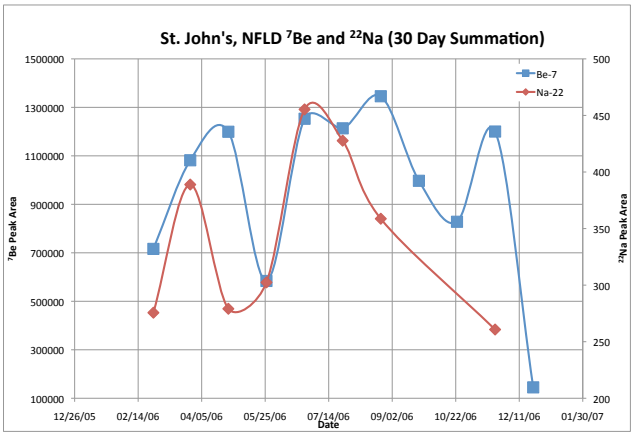

(b) CAP17, St. John's, Newfoundland

Figure 8.1 – Preliminary spectral summation results from the IMS stations DEP33 and CAP17. In the initial phases of *Globalplot* development, the peak areas of ^{7}Be and ^{22}Na were compared and found to be generally well-correlated with an appropriate relative area difference (^{22}Na roughly a factor of 1000x smaller than ^{7}Be), as expected.

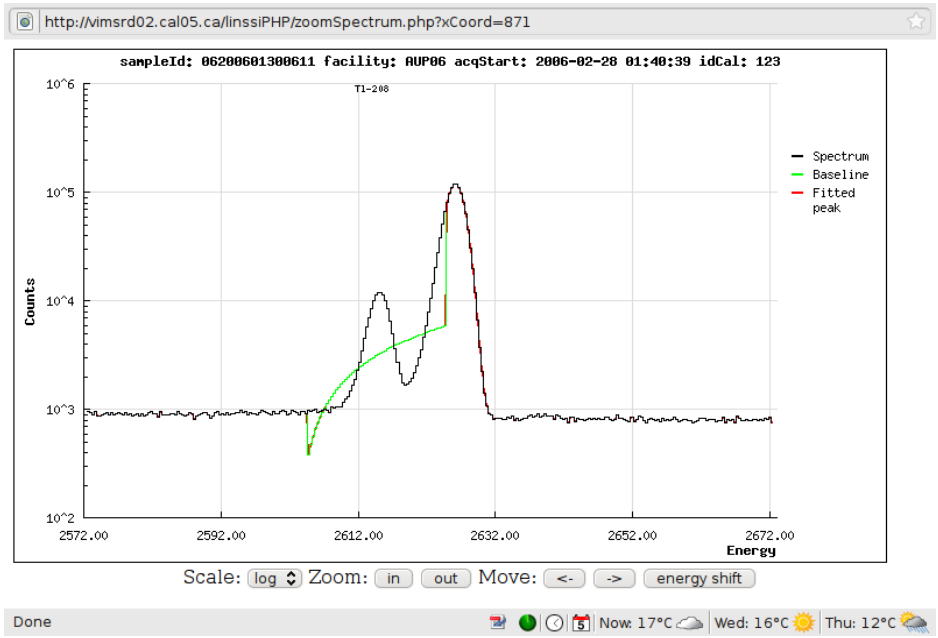

Figure 8.2 – Example of energy calibration drift at the Townsville, Australia (AUP06) IMS site. Normally in this region of the spectra there would only be a single peak at 2614.5 keV. Energy drift during the summation interval has created an artificial doublet.The resulting baseline in green is malformed, since there was only expected to be a single peak in the region.

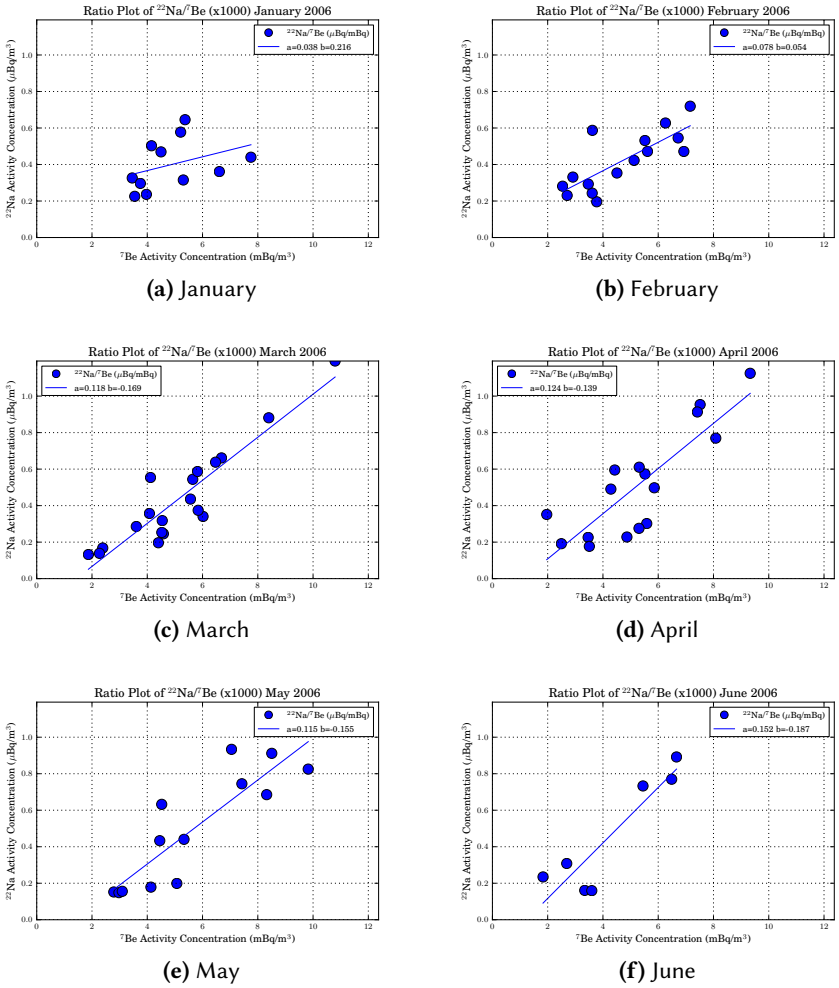

(a) January **(b)** February

(c) March **(d)** April

(e) May **(f)** June

Figure 8.3 – ^{22}Na and ^{7}Be for the first six months of 2006. As the weather warms up, the slope of the regression line increases. March and April are the months with the most data points, which is possibly a sign that atmospheric inversion is stronger during these months.

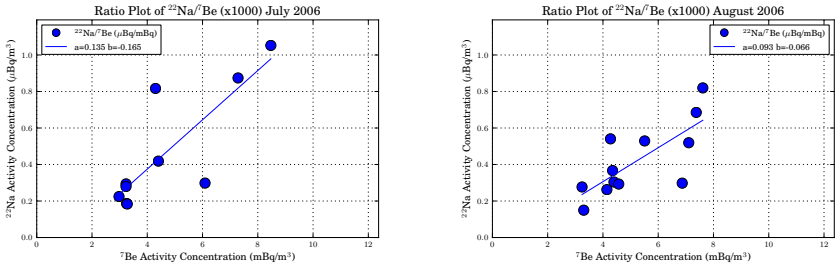

(a) July

(b) August

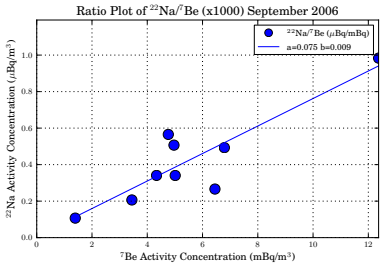

(c) September

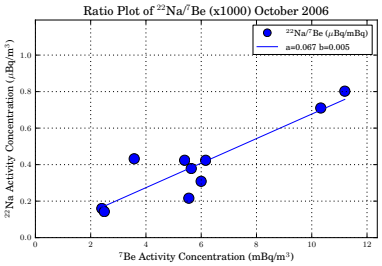

(d) October

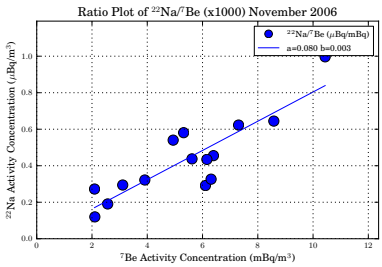

(e) November

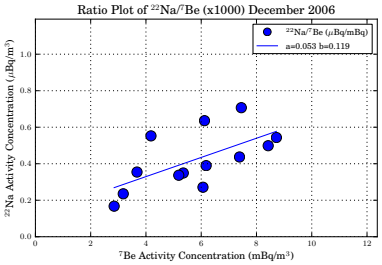

(f) December

Figure 8.4 – ^{22}Na and ^{7}Be for the last six months of 2006. As the weather cools, the slope of the linear regression line decreases. November is the month with the most data points (or most numerous cases of atmospheric inversion.)

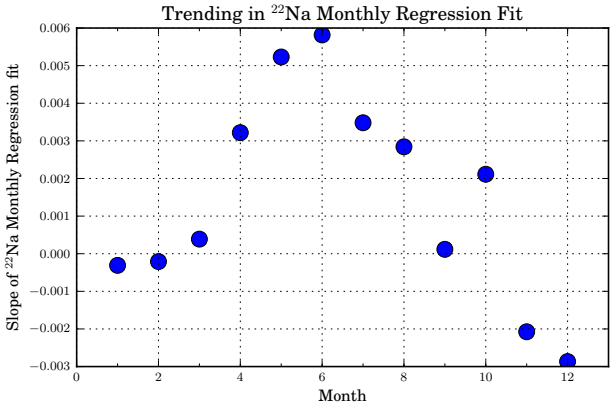

(a) ^{22}Na

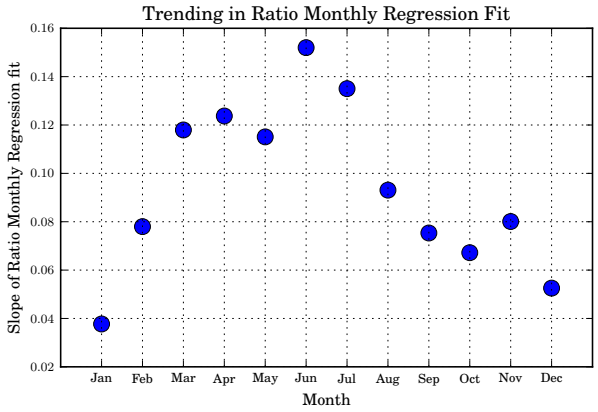

(b) ^{22}Na/^{7}Be

Figure 8.5 – Plot of the slope coefficients from monthly linear regression.

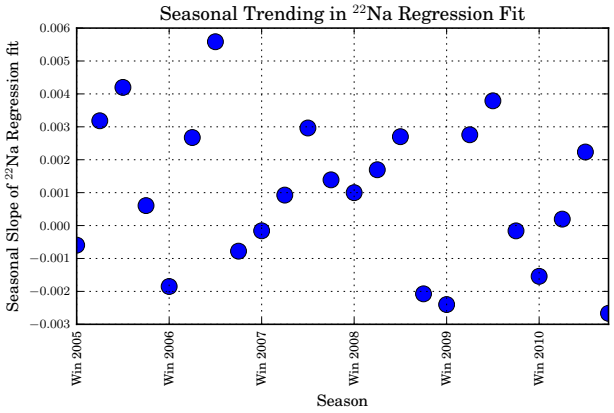

(a) ^{22}Na

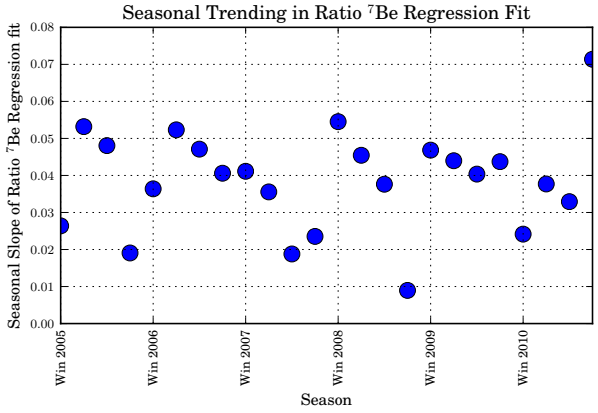

(b) ^{22}Na/^{7}Be

Figure 8.6 – Plot of the slope coefficients from seasonal linear regression over the 2005 to 2011 period.

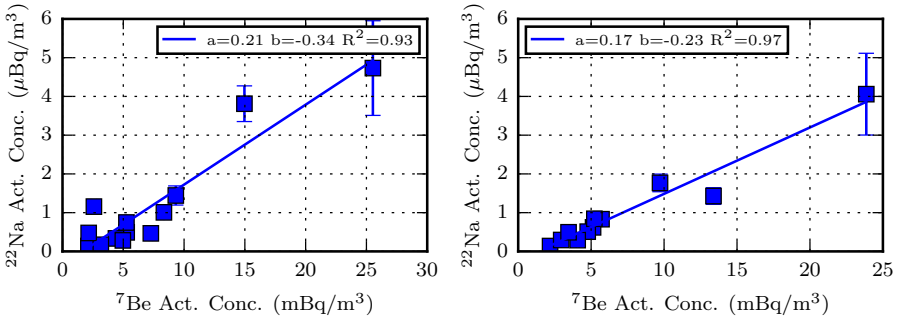

(a) January

(b) February

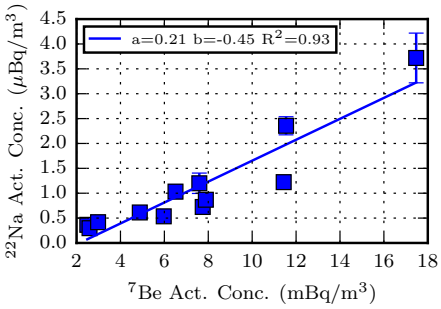

(c) March

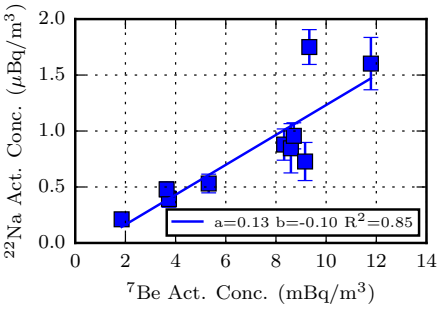

(d) April

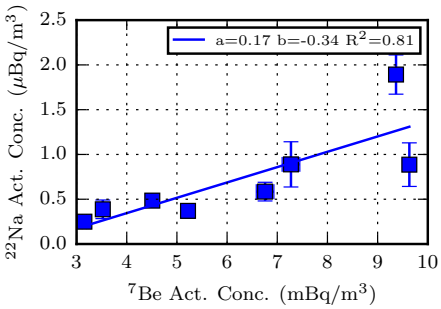

(e) May

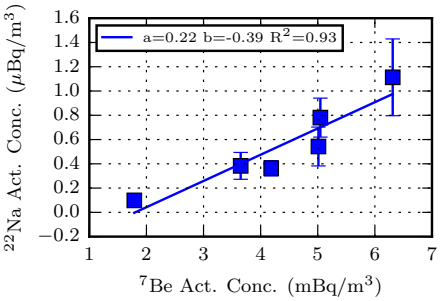

(f) June

Figure 8.7 – Monthly summation with fitting of ^{22}Na and ^{7}Be for the first six months of 2006.

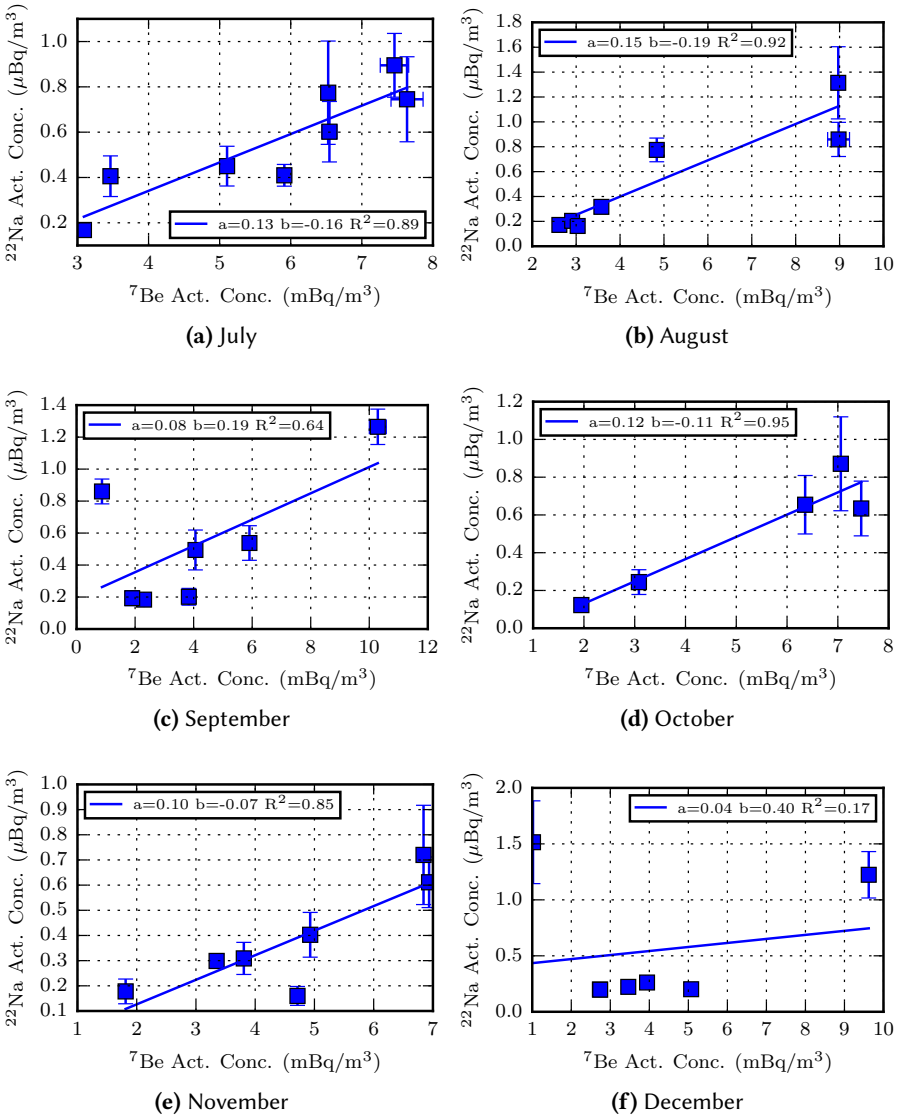

(a) July **(b)** August

(c) September **(d)** October

(e) November **(f)** December

Figure 8.8 – Monthly summation with fitting of ^{22}Na and ^{7}Be for the last six months of 2006.

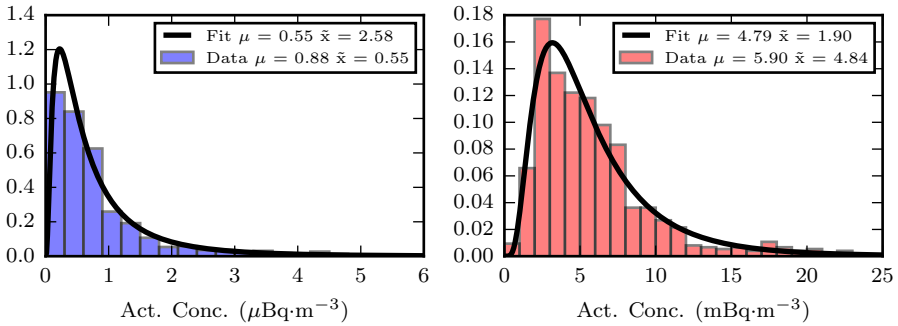

(a) ^{22}Na **(b)** ^{7}Be

Figure 8.9 – Normalized activity concentration histograms for summation spectra from 2005 to 2011. The geometric mean, μ, and geometric median, $\tilde{x}$ of the 749 summation spectra with measurable ^{22}Na, are shown for the PDF and the MLE fit.

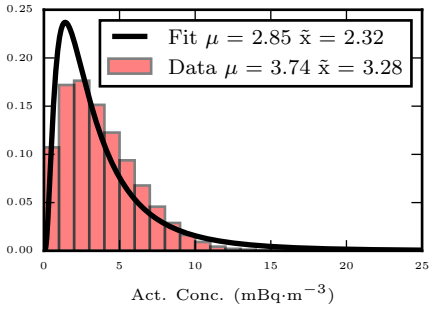

Figure 8.10 – Normalized activity concentration histograms of the entire ^{7}Be set of daily records, from 2005 to 2011. The geometric mean, μ, and the geometric median, $\tilde{x}$, of the 71 782 records in the NDC of HC are shown for the PDF and the MLE fit.

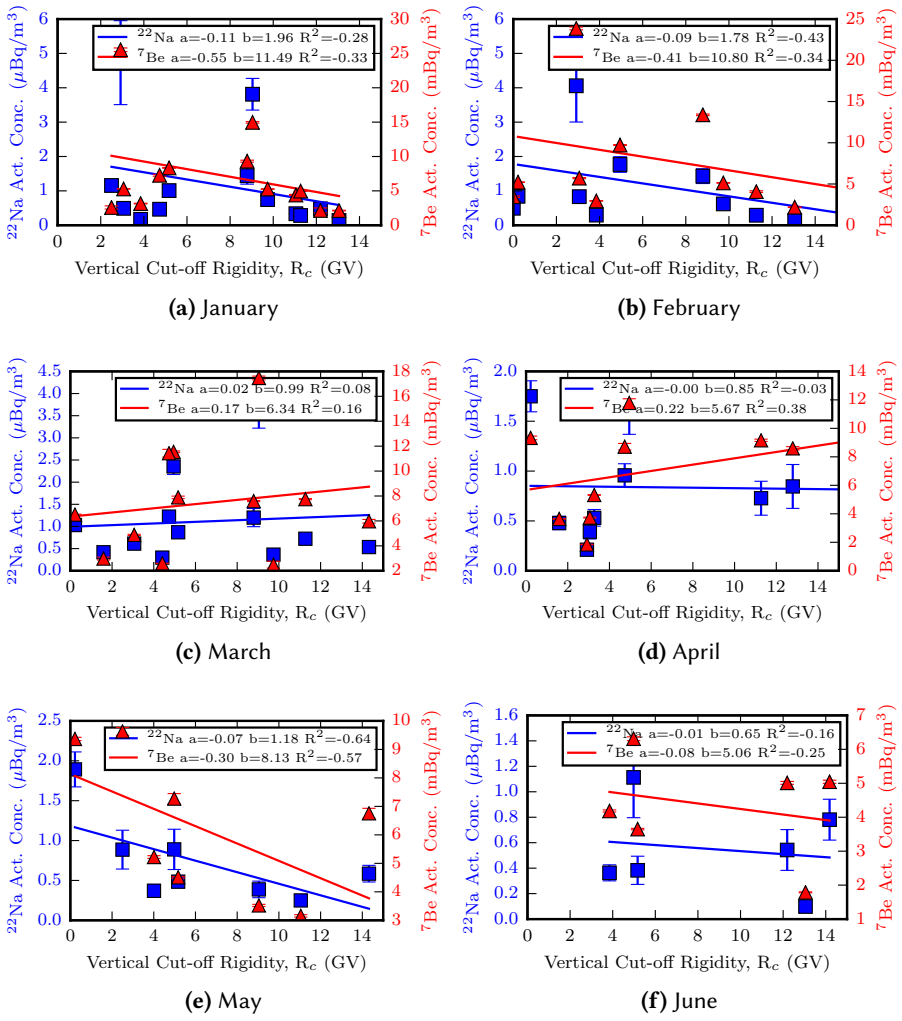

Figure 8.11 – 30 d summation, ^{22}Na (square), ^{7}Be (triangle) as a function of R_c for the first six months of 2006. The linear regression coefficients and correlation coefficient are shown in the legend.

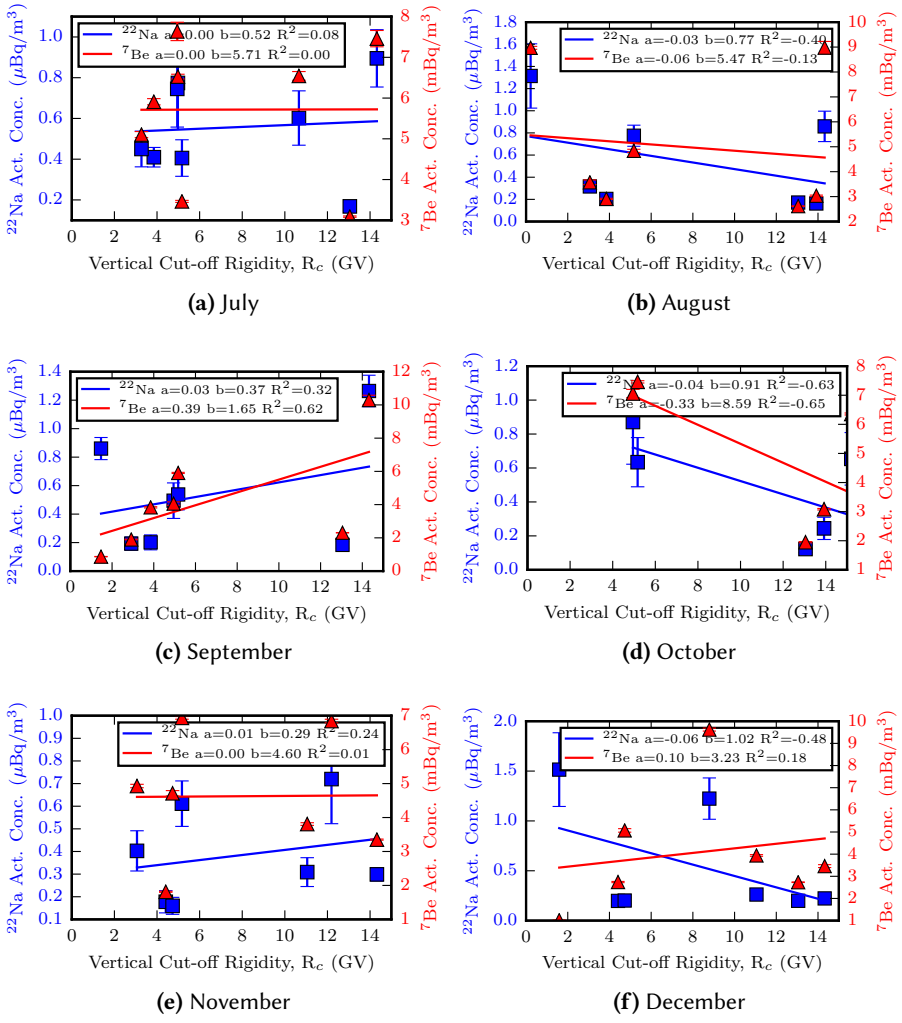

Figure 8.12 – 30 d summation, ^{22}Na (square), ^{7}Be (triangle) as a function of R_c for the last six months of 2006. The linear regression coefficients and correlation coefficient are shown in the legend.

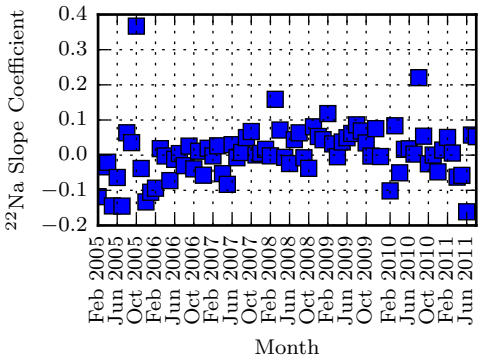

(a) ^{22}Na

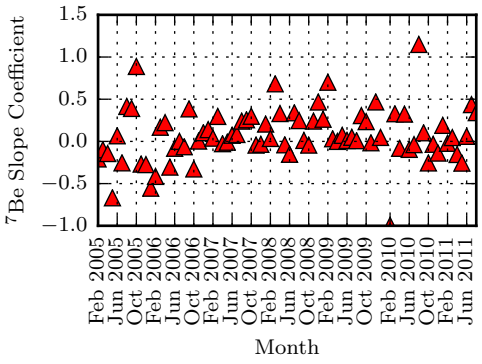

(b) ^{7}Be

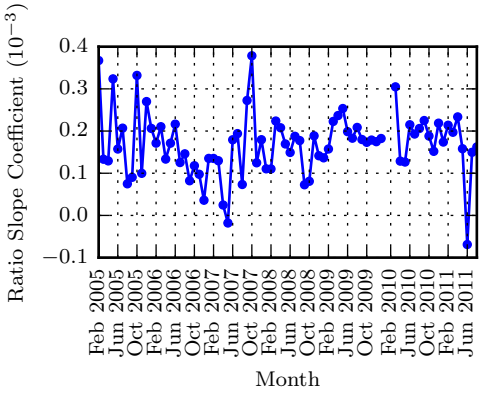

(c) ^{22}Na/^{7}Be

Figure 8.13 – Plot of the monthly slope coefficient of the linear regression of ^{22}Na and ^{7}Be activity concentration as a function of R_c and the ^{22}Na/^{7}Be ratio slope coefficient.

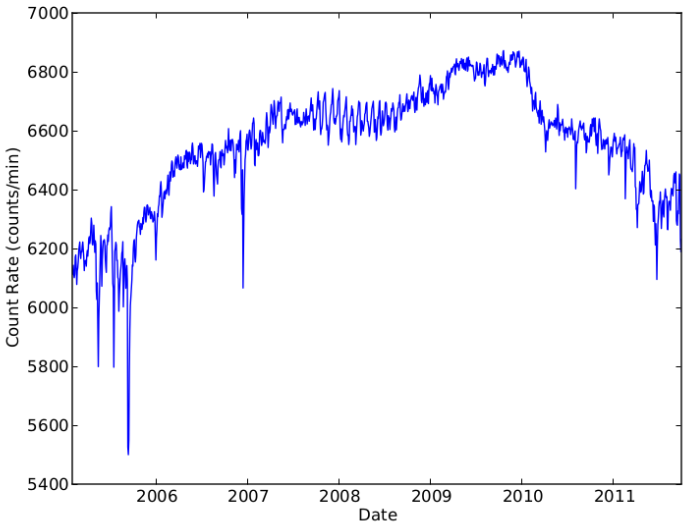

(a) Neutron Count Rate

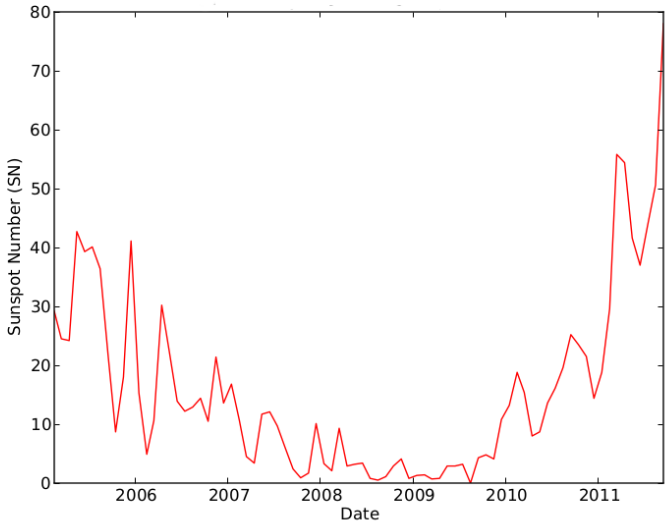

(b) SN

Figure 8.14 – Neutron monitoring in Oulu, Finland and SN. The neutron count rate[75] and SN[76] observed over the summation period.

8.1 Model Discussion

The data derived from spectral summation, discussed in Chapter 7, will now be placed in the framework of a semi-empirical model previously discussed and ultimately described in Equation 7.5. This model is an attempt to unify all the factors that are relevant to the two cosmogenic radionuclides studied in order to provide predictive power on general global trends and behaviour. As this is the first time this has been done for ^{22}Na, the model may benefit from further refinement as new techniques and data become available.

It is important to discuss first uncertainty and environmental interpretation. Although an uncertainty bound can be calculated on the measurement process, it is much more difficult to quantify the uncertainty appropriately in the interpretation of environmental results. Although it is often presented as a relatively straightforward process to quantify the laboratory measurement uncertainty, where most variables are under experimental control, this depends on making simplifying assumptions which are not often fully stated.[1] In environmental studies, where the laboratory is typically not a closed environment, uncertainty is much more difficult to appropriately quantify. In studies such as this, the dominant source of uncertainty is almost always related to the atmospheric transport. Since this work relies only upon geographic domains (Equatorial, Hadley and Ferrell cell boundaries), rather than a full transport model, it is even more difficult to quantify the total uncertainty in the final results. Rather than risk misrepresenting the actual uncertainty by only using a subset of the total uncertainty budget, a different strategy was chosen.

When there is a risk of a few extremely large values dominating a trend, the median is often used as a descriptive statistic for the reasons discussed in Section 7.4. While the median is a suitable non-parametric statistic and there is a technique available to calculate the uncertainty of a median value[77], it is not fully appropriate for this work since the aggregation of data occurs over bands of the Earth's atmosphere rather than as a single point estimate. Essentially, multiple measurement values in each 30 d integration period do not necessarily represent the same parcel of air. A better approach would be to examine both the median and the overall distribution of values to represent the uncertainty, providing a more holistic sense of the data. This approach, while not creating a true uncertainty, gives an idea of the range of values possible and provides a more realistic assessment of the measurement uncertainty and its relationship with the measurement and environment as a whole.

[1] In actuality, the problem can get increasingly complex even in a laboratory. For example, is the sample matrix and aerosol collection during sampling homogeneous? Normally, there is a set of standard assumptions and practices that are followed for convenience and tractability, but these conventions are not necessarily representative of reality.

Before generating any summary statistics and figures, the amount of data in each geographical domain was examined. If the data was presented on a monthly basis, the polar area would be poorly represented statistically. Since there are only a small number of operating stations in the poles, at almost any integration time scale chosen, the amount of data available would still be quite small. To improve the amount of data available in the polar region, while still retaining some temporal sensitivity, a decision was made to use quarterly median values rather than monthly means. For additional clarity, the figures were generated in two different styles. The first style shows just the median values, which allows one to see temporal trends in the data easily and clearly. The second style is a box and whisker plot, plotted by region. The box plot style allows one to examine the distribution of quarterly values to show the overall behaviour of the data. The box plot figures also have the advantage of showing outliers in the data set which has identified interesting individual cases for future study beyond the scope of this work.

There are two important considerations to keep in mind with this analysis. Although the IMS network is global, on a monthly basis, the analysis of the data can be quite regional. This means that the monthly data may not be a good representation of the global average, particularly if there has been strong vertical air movements either locally or regionally. The second consideration is that, since cosmogenic radionuclides circulate around the atmosphere, the sites of production and observation may be significantly different in terms of R_c. Since R_c only accounts for the shielding that is perpendicular to the surface (vertical), it ignores any transport either zonally or meridionally. However, if the stratospheric motion is relatively zonal, the variation in R_c from production to observation site is relatively minimal, as shown in Figure 2.7.

The first generated figures were meant to be used as a reference for comparison with figures generated once other procedures were performed on the data. For example, Figure 8.15 shows the deceleration potential and the quarterly median values in each of the three domains of the atmosphere. Figure 8.16 shows the results when two factors thought to influence the observed surface concentrations are removed from the data set. The two factors are geomagnetic latitude shielding, represented by R_c, and the production rate, represented by the relative ambient dose rate at 10.67 km (from [24]). The compensation by geomagnetic latitude is very specific to each observation location (and includes very small temporal changes), while the grouping into each of the three bands is by standard latitude, as discussed in Chapter 7.

Several features in these two figures are worth further discussion. The first important feature is that, prior to compensation, the data tends to separate into bands, with the polar cell values having both the highest values and most variability, as expected. The Hadley cell equatorial data is the most constant, with the mid-latitude or Ferrell cell typically being between the other two cells. If the mean is

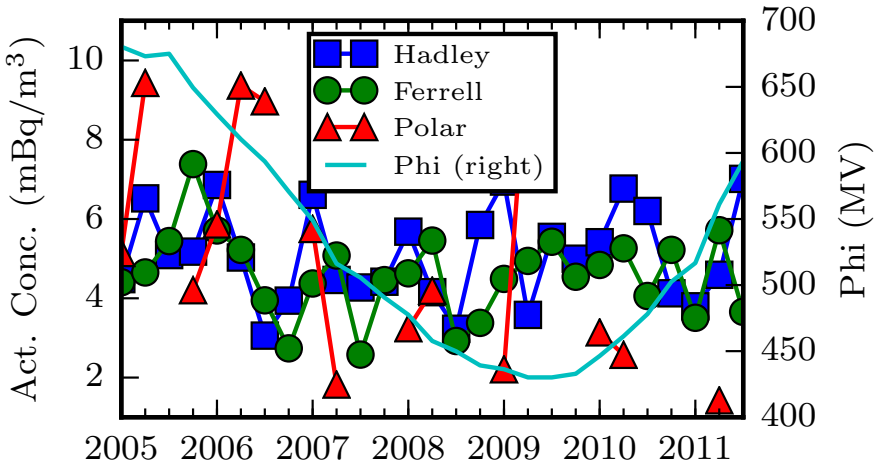

(a) ^{7}Be

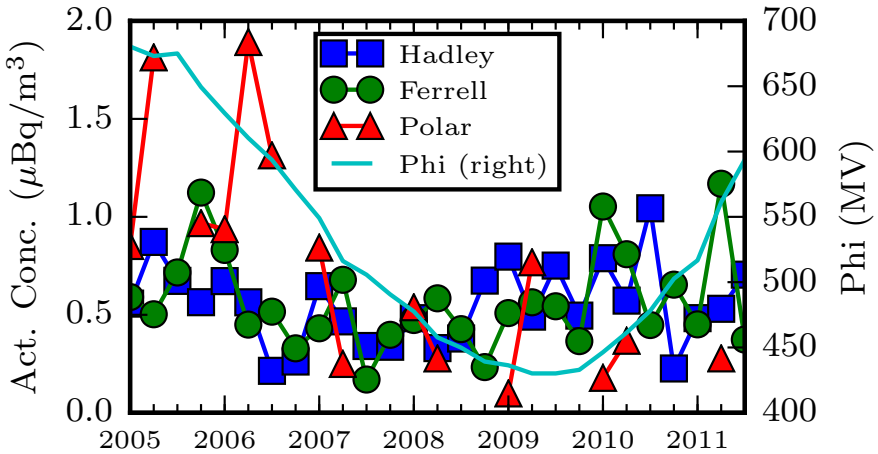

(b) ^{22}Na

Figure 8.15 – Raw quarterly median concentration data using summation spectral data. The square, circle, and triangle markers are for the Hadley, Ferrell and Polar cells respectively.

calculated for each of the medians, the polar region is 5.82 Bq m^{-3}, the mid-latitude regions are 5.04 Bq m^{-3} and the equatorial region is 5.30 Bq m^{-3}.

The next important feature is that the concentrations do not show any obvious immediate or delayed response to changes in the cyan deceleration potential (plotted on the secondary axis). This lack of response to changes in deceleration potential is perhaps unexpected, as it would imply that changes in the production rate (expressed as a variation in potential) do not strongly influence ground-level concentrations.

To confirm that the deceleration potential does not influence the ground-level concentrations much, the full database for ^{7}Be in the NDC was examined. Generating the same plot as Figure 8.16 with the daily NDC records results in Figure 8.17.

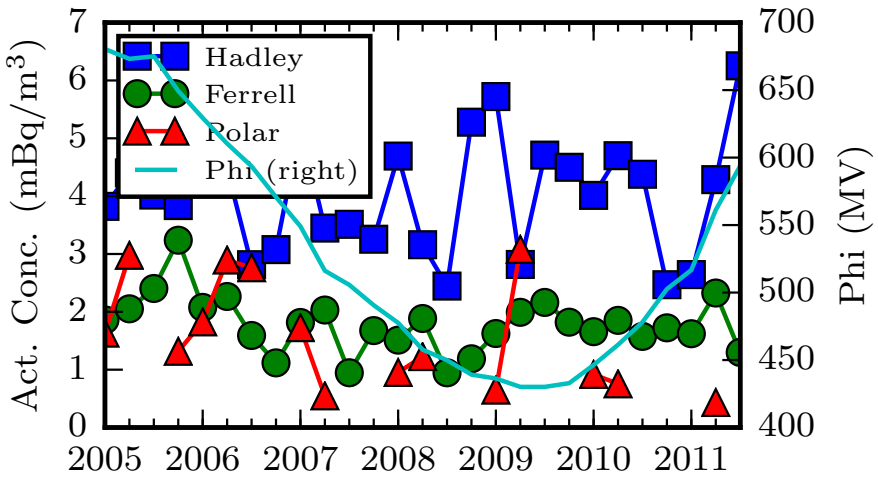

(a) ^{7}Be

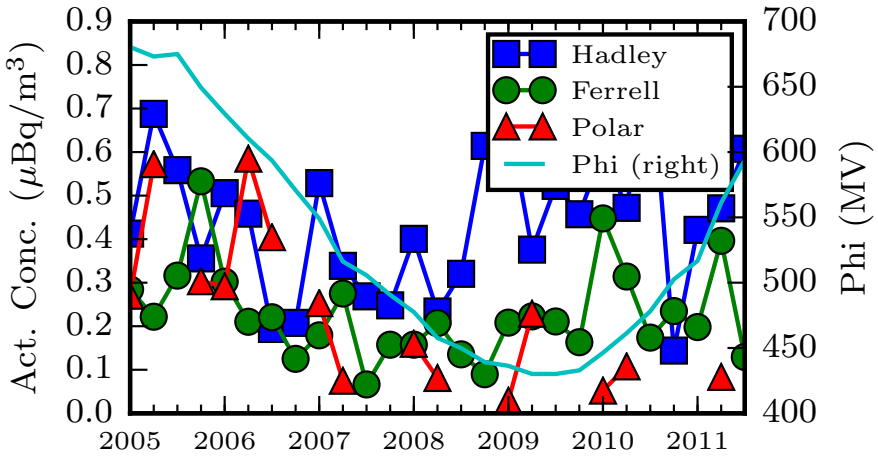

(b) ^{22}Na

Figure 8.16 – Normalized quarterly activity concentrations of ^{7}Be and ^{22}Na. The square, circle, and triangle markers are for the Hadley, Ferrell and Polar cells respectively. Normalizing the quarterly median concentration data by the equatorial dose results in a more constant concentration across all major atmospheric transport cells.

Figure 8.17 is somewhat similar to the previous ^{7}Be summation figure generated

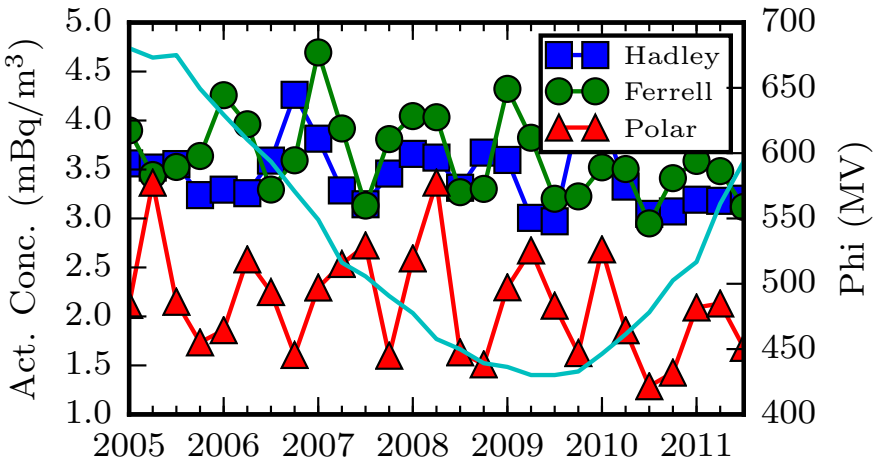

Figure 8.17 – Quarterly concentration data of ^{7}Be using NDC concentrations from HC. The square, circle, and triangle markers are for the Hadley, Ferrell and Polar cells respectively. The NDC ^{7}Be data displays very similar behaviour to the summation results shown in Figure 8.16a.

from spectral summation. However, there are a couple of differences. The data is much less dynamic overall and the polar values are now consistently lower than the Ferrell and Hadley values. As the data set includes the entire set of ^{7}Be measurements, there is no requirement for a simultaneous measurement of ^{22}Na in this dataset. Rather than being only the top 17 % of observations, it includes the entire distribution. This explains both the smaller dynamic range and lower overall median values. However, the increased variability in the polar region is still present, which is encouraging as it manifests similar behaviour to the summation results. Furthermore, there is nothing in these three figures to suggest that the summation spectra are not equally as valid as the individual daily spectra. If the summation-derived ^{7}Be values are sound, then the ^{22}Na values should be equally sound, since they were derived using the same technique.

Examining these figures as a whole, it becomes clear that changes in the production rates are not the dominant factors influencing ground-level concentration observations. This means that the deceleration potential, while an important parameter for the overall production of these cosmogenic radionuclides, is a relatively unimportant factor for the variability in ground-level observations. This conclusion is supported by data collected by the High Altitude Sampling Program of the Environmental Measurements Laboratory in New York[78]. This dataset from 1973 contains over 3200 high-altitude measurements, including 13 samples that reported ^{22}Na activity concentrations. The ^{22}Na subset of samples covered the latitudes from

43°S to 71° N, and the activity concentrations varied by a factor of 2 from the median once the lone outlier was removed.

The next investigation was to examine the overall distribution of data. As mentioned earlier, this was done using box and whisker plots. In a box plot, the median is shown with a horizontal red line and the mean, is plotted by a red diamond. The length of the box shows the extent of the upper and lower quartiles. The whiskers extend by a factor of 1.5 beyond the Interquartile Range (IQR), which is the length of the box (Q3-Q1). The outliers then become defined as values outside the whiskers and are shown as a cross. They most likely represent cases of enhanced stratospheric injections of cosmogenic radionuclides into the troposphere, but an actual ATM would be needed to examine these specific cases. The commissioning of a suite of individual ATM runs to examine these individual cases in detail is recommended for future study.

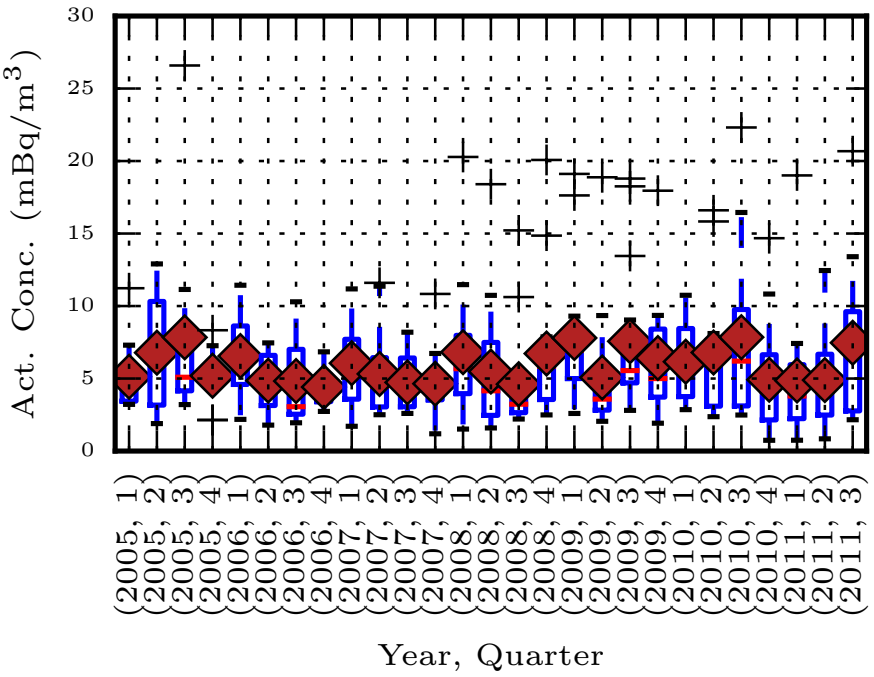

Figure 8.18 – Box and whisker plots of the Hadley region for ^{7}Be activity concentration.

Figures 8.18 and 8.19 show the quarterly activity concentration values are fairly tightly distributed, typically having an IQR of <5 mBq m^{-3}. In Figure 8.20, the scarcity of polar data becomes apparent, as there is only sufficient data to construct a box for 9 quarters over the entire six-year period. This data also has a narrow distribution, with an IQR of less than 5 mBq m^{-3}.

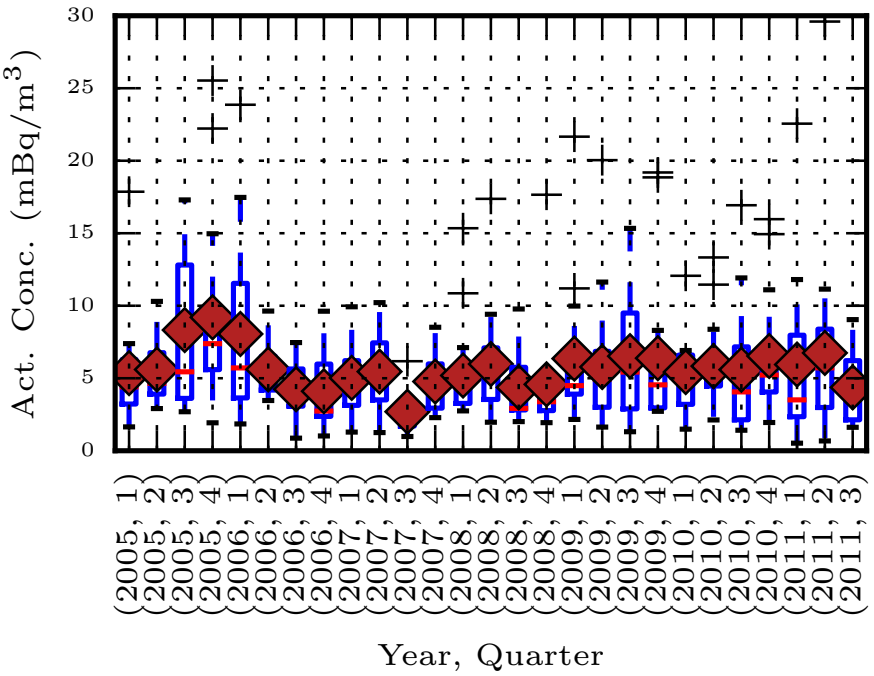

Figure 8.19 – Box and whisker plots of the Ferrell region for ^{7}Be activity concentration.

Repetition of the same process for the ^{22}Na data is shown in Figures 8.21, 8.22, and 8.23. The IQR of ^{22}Na is typically less than 1 µBq m^{-3}. While this may seem to be an overly tight distribution, the variability is roughly commensurate with the relative amounts of beryllium and sodium in the aerosol samples.

8.1.1 The Final Model

To summarize the discussion and results from the preceding section, it is clear that the ground-level activity concentrations are dominated by atmospheric dynamics rather than production influences. Furthermore, the summary statistics presented show that both beryllium and sodium have similar relative variability and that the values presented for ^{7}Be fall within the characteristic range from other studies (see Table 2.2 for a brief summary). The summation spectra data appears to be of high quality, with results very similar to the daily spectra values from the NDC at HC. With a good perspective of both radionuclide distributions, the question remains as to how to represent these figures and their interpretation as a semi-empirical model.

In a paper by Liu et al., a number of meteorological models were run in one GCM to predict the ground-level ^{7}Be concentrations as a function of latitude. The key

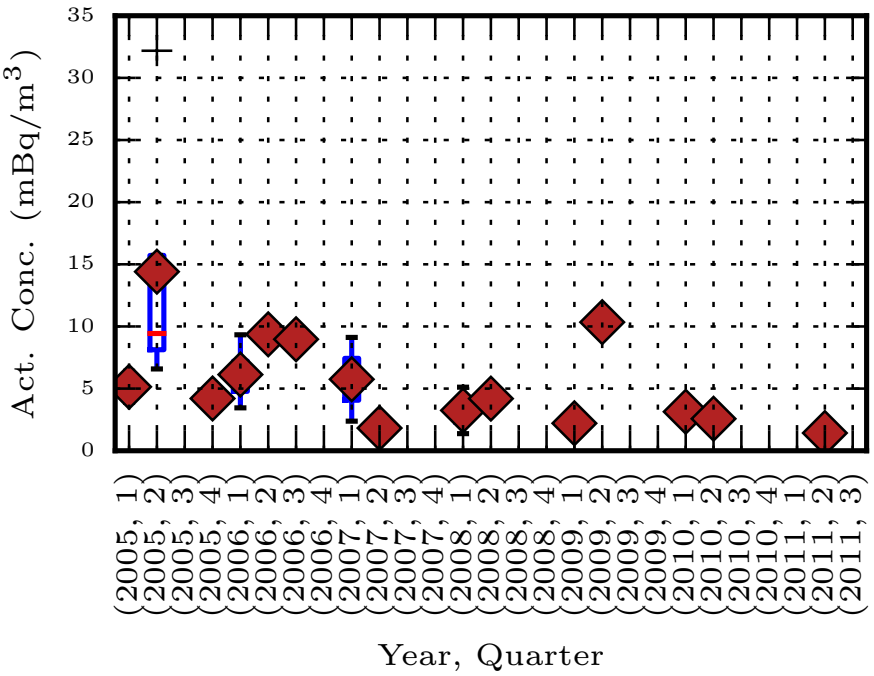

Figure 8.20 – Box and whisker plots of the Polar region for ^{7}Be activity concentration.

figure from this paper is reproduced in Figure 2.9. Although not perfectly aligned, both the modelled data and the observations show a large peak in concentrations near the interface between the Hadley and Ferrell cells (around approximately 30°). The data used for this figure was of lower quality, as the samplers collected weekly samples with approximately 5 % of the daily volume of the IMS samplers used in this study. Furthermore, the 31 sites used by Liu et al. were not as well distributed as those used in this study; therefore, some of the data is quite sparse both temporally (the most records at any one site was 691 and fewest was two with the mean being 215) and geographically (12 countries plus Antarctica).

The summation data was examined in this study in the same manner as Liu et al. The monthly production variations were removed to allow for the entire six-year span of data to be binned into 10° latitude intervals. The results were then plotted for both ^{7}Be and ^{22}Na in Figure 8.24. The same peak at approximately 30° is present, with an additional minor peak at 10°. One possibility to explain the peaks around the equator in this figure is that this region is known as the intertropical convergence zone and is an important feature of Hadley cell circulation. To illustrate the unique characteristics of this region, a map that meteorologists commonly use is a vertical velocity, ω, map. The ECMWF has a historical weather dataset that has been heavily

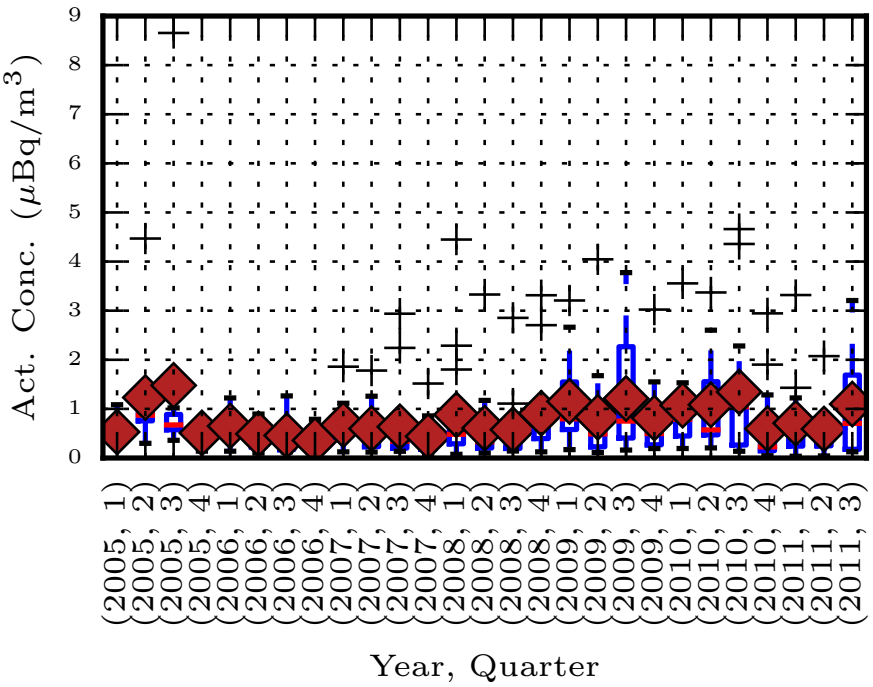

Figure 8.21 – Box and whisker plots of Hadley region for ^{22}Na activity concentration.

validated called ERA-40. This dataset includes various weather data and atlases for over 20 years. An example of a global atlas of annual mean vertical velocity is shown in Figure 8.25[79]. Similar behaviour is observed with the 750 hPa atlas. The vertical velocity shows descending air around the 10° latitude region, while near the equator the air is rising. This could explain the additional peak feature, but, again, a further suite of ATM runs would be necessary to confirm this behaviour and is recommended for future study.

In summary, the proposed semi-empirical model shows limited influence on surface concentrations of cosmogenic radionuclides from changes in the production rate due to solar modulation. A limited set of data from EML also suggests the upper troposphere/lower stratosphere is generally well-mixed and the results from analysis of summation spectra agreed with a well-mixed atmosphere model, at least on a 30 d summation basis. Ground-level observations of ^{22}Na and ^{7}Be were found to depend mostly on atmospheric transport cells and the results obtained from spectral summation compared favourably with a study that used a full GCM to model ^{7}Be and ozone. Finally, the behaviour of the data in the intertropical convergence zone around the equator was discussed using the vertical velocity atlas from the ECMWF.

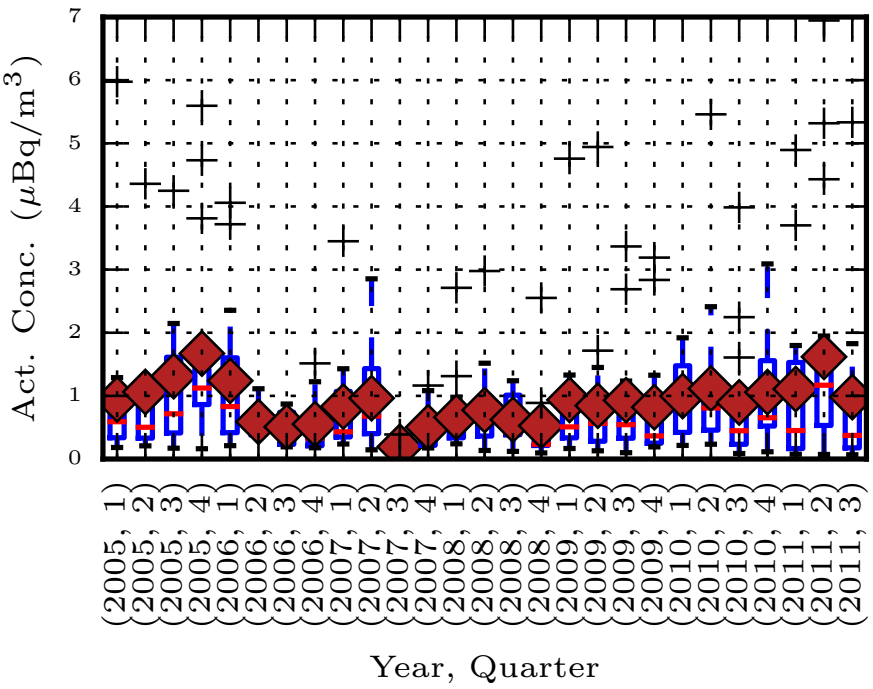

Figure 8.22 – Box and whisker plots of Ferrell region for ^{22}Na activity concentration.

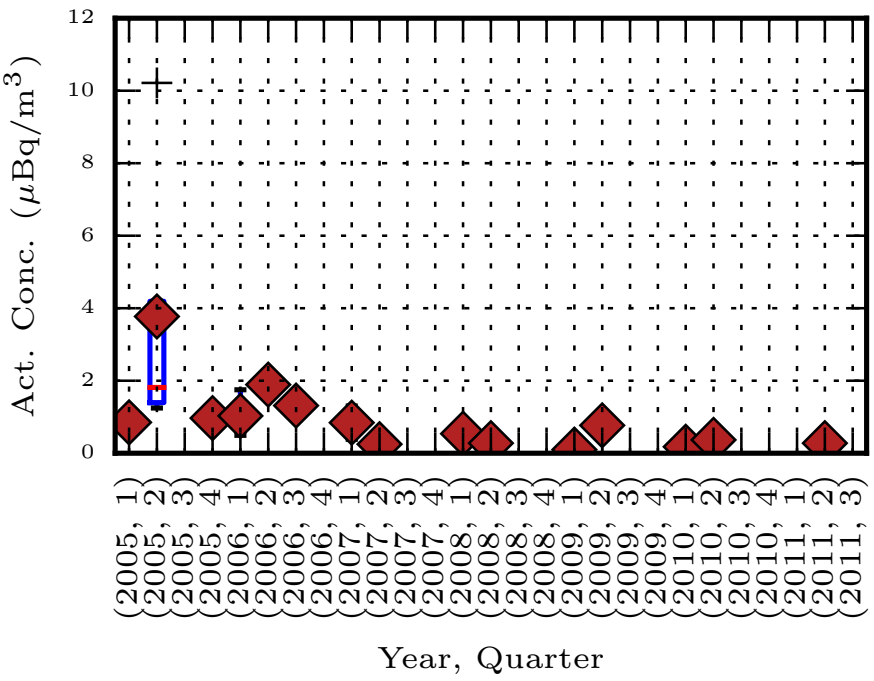

Figure 8.23 – Box and whisker plots of Polar region for ^{22}Na activity concentration.

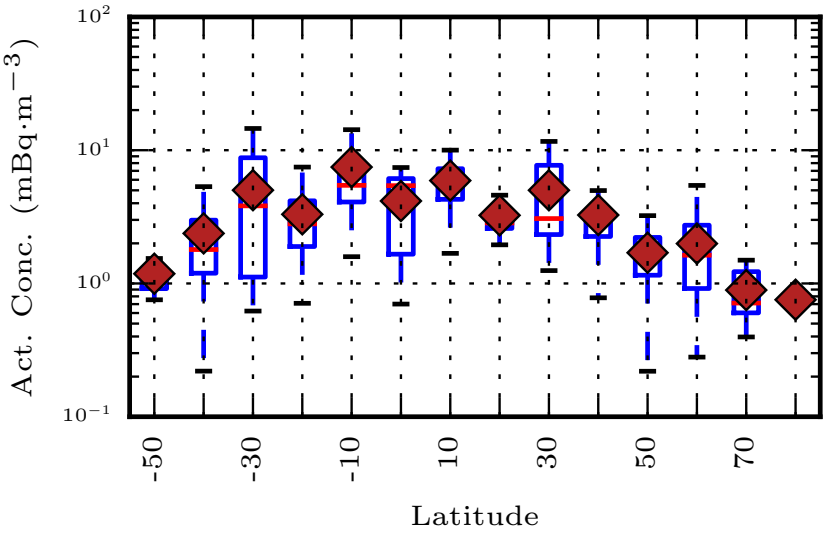

(a) ^{7}Be

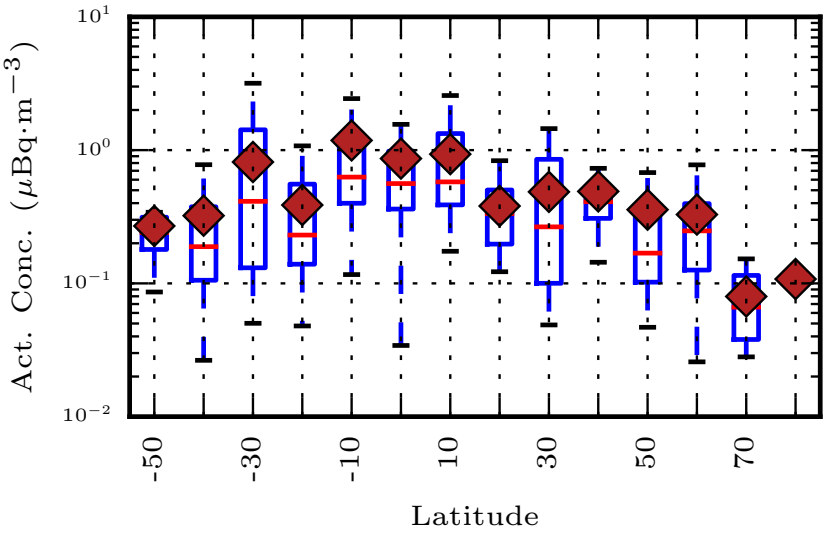

(b) ^{22}Na

Figure 8.24 – Spectral summation concentrations histogram plotted in the same bins as Figure 2.9. A log scale was used to compress the outliers.

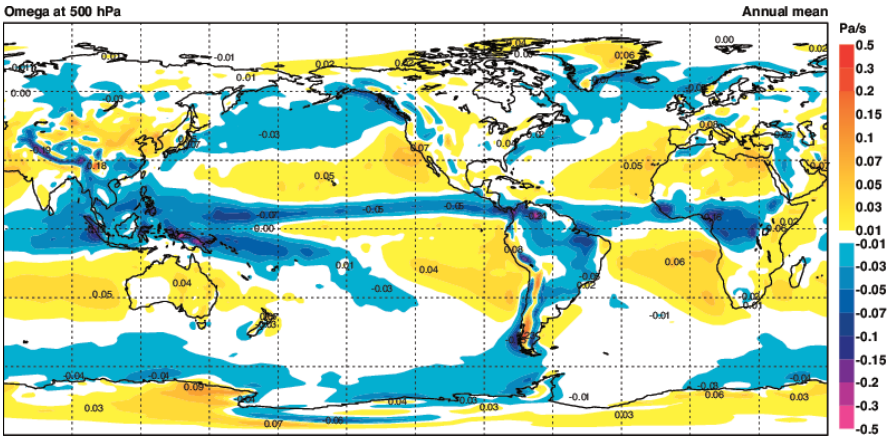

Figure 8.25 – Mean vertical velocity, ω, at 500 hPa (approximately 5 km altitude) for the years 1979–2001. Descending air is positive while ascending air is negative. Figure from [79].

9 Conclusions

The spectral summation technique implemented by the newly developed code *Pysum* successfully created a global data set of ^{22}Na and ^{7}Be activity concentrations from a LINSSI 1.1 database. Various integration periods were tested to find a balance between the number of ^{22}Na observations and temporal resolution, with the goal of finding STE events in the resulting data set. The final summation spectra were generated using a 30 d integration, or summation interval, from 2005 to 2011. The spectra were processed by the AATAMI software package for calibration information and JMUFI performed the peak and baseline fitting, with the results stored in a LINSSI 2.2 database.

The large number (4950) of spectra created required special procedures to ensure the quality and accuracy of the data. Two main techniques were used to ensure high-quality data. The first technique involved careful selection of spectra for summation by validating the biographical data associated with each spectra. The second, more sophisticated technique was to examine the behaviour of several other natural radionuclides present in every spectra. By examining long-term trends of these nuclides, any unusual deviation in nuclide activity concentrations served as a indicator of potential problems with either the energy calibration or the spectra itself.

The peak parameters calculated by JMUFI were converted to airborne activity concentrations by *Globalplot*, which was designed to visualize the results of the spectral summation process. For the first time, a TCS correction was performed for the ^{22}Na data to improve the accuracy of measured concentrations. By plotting the activity concentrations of ^{22}Na versus ^{7}Be, clear correlations between the two isotopes could be seen. Furthermore, monitoring sites that did not follow the general trend were candidates for STE events or slow vertical transport depending on the ratio. Activity concentrations of ^{22}Na were also observed to increase as the geomagnetic rigidity, R_c decreased. These trends were visible in every year, from 2005 to 2011. The ^{22}Na activity concentration values and the ^{22}Na/^{7}Be ratios obtained using the spectral summation technique also agreed very well with previous results obtained in other studies. The activity concentrations of ^{22}Na and ^{7}Be were found to follow a log-normal distribution, but care must be taken to consider the limits of detections

as the data is left censored.

The generated ^{22}Na and ^{7}Be data behaved as expected over the duration of the study. The activity concentrations of both radionuclides appeared to be proportional to the incoming GCR and inversely proportional to SN on a global scale. The geographic and population distribution of the ^{7}Be summation data set were examined and found to agree with previous studies. The behaviour of the ^{22}Na summation data was very similar to the ^{7}Be data, as expected. Overall, this is the first time such a global examination was performed using such a large number (56) of different monitoring locations, located in both hemispheres over an extended time period.

A semi-empirical model was developed incorporating cosmogenic production and atmospheric circulation to examine and explain the observed surface concentrations of these two cosmogenic radionuclides. The cosmogenic production component of the model included the two dominant components in production — incident GCR and production location, represented by R_c, while the atmospheric circulation was examined using the major atmospheric cells — the Hadley, Polar and Farrell cells. The summation results suggest that the atmosphere is well-mixed, as production does not seem to play a significant role in surface concentrations. The major variation in the observed activities of cosmogenic radionuclides appeared to be due to the bulk circulation of the atmosphere. Analysis of the summation data in the context of the model reproduced the characteristics and features of a GCM simulation of ^{7}Be.

With further development, the spectral summation technique could be used to approximate on a relative basis how much air is of stratospheric origin in an aerosol filter. While this approach could be used to understand further STE and circulation in general, it also has a potential CTBT application. Measurements of cosmogenic radionuclides in a filter could be used to detect tampering, as all filters should have a credible quantity of these cosmogenic radionuclides present. Failure to find these cosmogenic radionuclides could mean the sample is not a true environmental aerosol sample.

10 Recommendations

There are many further avenues for extension of this study through the use of other techniques and different data processing algorithms. To improve the utility of ^{22}Na and ^{7}Be as an atmospheric tracer, more data would be helpful. Specifically, density improvements in both a geographic and measurement sense would be beneficial. There are clear trends in the ^{22}Na and ^{7}Be data related to seasonal and solar patterns. Other studies have explored the solar cycle impacts on concentrations of cosmogenic radionuclides, but only on a local scale[80]. A global data set such as this one may be more useful, but it would be better to extend the timeframe of data beyond the 11 year solar cycle. The CTBT network has been operating for around a decade, with more stations to be built and more monitoring data acquired daily. As more stations come online and the monitoring history improves, the geographic density should improve and these types of studies should be possible.

On the measurement side, there is significant room for improvement by using new technology that provides increased measurement sensitivity. While the spectral summation technique has proven successful, there is a large temporal resolution penalty to this approach, so that it is difficult to monitor fine deviations in ^{22}Na concentrations that could be indicative of atmospheric processes such as STE. The examination of fine details in the ^{22}Na/^{7}Be ratio of activity concentrations could indicate more precisely when STE is active.

One of the best means to increase measurement sensitivity is through the use of a $\gamma-\gamma$ coincidence technique. The principle behind the technique is that two nearly simultaneous events are needed for the MCA to register a count, while single gamma events are rejected. It is possible to use coincidence detection on ^{22}Na by using the 511 keV and 1274 keV photons. The end result is that a $\gamma-\gamma$ coincidence system has a very low background, making observations of ^{22}Na far easier with daily observations in a high-volume aerosol sampler being a realistic possibility. Such an approach would greatly increase the sensitivity to small ^{22}Na signals, providing a greater density of data points and allowing measurements of ^{22}Na from sites where the R_c is higher. Since the detection limit is lower, it would also be possible to have a better estimate of the population distribution. However, these coincidence systems are

specialized, as they only function through the use of more sophisticated electronics and data processing systems. A new data source would have to be used, as there are currently no plans to use these systems in the IMS for CTBT verification.

For data processing, there are a couple of improvements that could be made to the summation technique. The first would be to improve *Pysum* so that it adds spectra together by energy, rather than by channel, during summation. This would improve the activity calculation for ^{22}Na as peaks would be better defined and possibly recover a few cases that had to be discarded because the energy calibration had drifted.

Secondly, the integration window used in *Pysum* to create the summation spectra could be optimized through a specific study to find the optimal window, either overall or on a yearly basis, to account for variations in the production rate. With the fine balance between data and temporal density, optimizing the integration period would ensure maximum utility of the data. However, since the activity concentration in each parcel of air is not known, it is only really possible to adjust the summation process empirically. A better approach would be to incorporate an adaptive, moving integration window for the spectral summation process. By adaptively varying the summation interval according to the amount of ^{22}Na signal present, it may be possible to reject periods where there is only noise present. This would increase the accuracy of the quantification and number of available samples, at a cost of a much more complicated algorithm as it would have to evaluate whether a candidate spectra was beneficial for summation.

The interpretation of the results could benefit from a number of different improvements, such as: access to different samples, better production and transport models, and a longer study period. Different samples, such as those collected by specialized aircraft, are important for ATM. These samples would allow a measurement of the cross-sectional ^{22}Na activity concentrations by altitude. With a better model of the production process, and access to both aircraft- and ground-based measurements, it may be possible to improve the modelling of the vertical atmospheric transport through an examination and optimization of the number and thickness of ATM layers. Aircraft data could be particularly valuable to provide precise timing and geographic areas of STE events, for comparison with a theoretical model.

Although involving a great deal of effort, the ^{22}Na activity concentrations could be examined along with either a suite of ATM runs or a full **3D** GCM of the atmosphere. The use of a full production and transport model should allow for the prediction of ground-level ^{22}Na concentrations and comparisons with observed concentrations. Commissioning of ATM runs would allow the exploration of outliers identified by the box plots for evidence of particularly strong STE episodes. ATM may also clarify the circulation behaviour around the equator. The extra feature, or concentration enhancement, at around 10° latitude may clarify if the vertical velocity is an important meteorological phenomenon in observed surface concentrations of cosmogenic

radionuclides. Further benefits may be had if a GCM model is used to assist with the interpretation of results. For example, it would be particularly interesting if the GCM could reproduce the peak in median activity concentrations and validate if the mean vertical velocity is a factor at sites near the equator. A predictive transport model would allow full utilization of these two radionuclides as a radiochronometer.

Bibliography

[1] J. A. Young, C. W. Thomas, and N. A. Wogman. Cosmogenic Radionuclide Production Rates in Argon in the Stratosphere. *Nature*, 227(5254):160–161, 07 1970.

[2] J. Meloen, P. Siegmund, P. van Velthoven, H. Kelder, M. Sprenger, H. Wernli, A. Kentarchos, G. Roelofs, J. Feichter, C. Land, C. Forster, P. James, A. Stohl, W. Collins, and P. Cristofanelli. Stratosphere-troposphere exchange: A model and method intercomparison. *Journal of Geophysical Research: Atmospheres*, 108(D12), 2003. ISSN 2156-2202. doi: 10.1029/2002JD002274. URL http://dx.doi.org/10.1029/2002JD002274.

[3] D. G. Fleishman. Cosmogenic ^{22}Na as an index of the residence time of water in freshwater basins: a review. *Journal of Environmental Radioactivity*, 99(8): 1203–1215, 8 2008.

[4] K. Komura, Y. Kuwahara, T. Abe, K. Tanaka, Y. Murata, and M. Inoue. Measurements of short-lived cosmic-ray-produced radionuclides in rainwater. *Journal of Environmental Radioactivity*, 96(1-3):103–109, 9 2007.

[5] V. Yu. Luyanas, R. Yu. Yasyulyonis, D. A. Shopauskiene, and B. I. Styra. Cosmogenic ^{22}Na, ^{7}Be, ^{32}P, and ^{33}P in atmospheric dynamics research. *Journal of Geophysical Research*, 75(18):3665–3667, 1970.

[6] Dorothy Koch, Gavin A. Schmidt, and Christy V. Field. Sulfur, sea salt, and radionuclide aerosols in GISS ModelE. *Journal of Geophysical Research: Atmospheres*, 111(D6), 2006. ISSN 2156-2202. doi: 10.1029/2004JD005550. URL http://dx.doi.org/10.1029/2004JD005550. D06206.

[7] Christy V. Field, Gavin A. Schmidt, Dorothy Koch, and Colette Salyk. Modeling production and climate-related impacts on ^{10}Be concentration in ice cores.

Journal of Geophysical Research: Atmospheres, 111(D15), 2006. ISSN 2156-2202. doi: 10.1029/2005JD006410. URL http://dx.doi.org/10.1029/2005JD006410.

[8] R. Jasiulionis and H. Wershofen. A study of the vertical diffusion of the cosmogenic radionuclides, ^{7}Be and ^{22}Na in the atmosphere. *Journal of Environmental Radioactivity*, 79(2):157–169, 2005.

[9] James R. Holton, Peter H. Haynes, Michael E. McIntyre, Anne R. Douglass, Richard B. Rood, and Leonhard Pfister. Stratosphere-troposphere exchange. *Reviews of Geophysics*, 33(4):403–439, 1995. ISSN 1944-9208. doi: 10.1029/95RG02097. URL http://dx.doi.org/10.1029/95RG02097.

[10] D. Lal, P. K. Malhotra, and B. Peters. On the production of radioisotopes in the atmosphere by cosmic radiation and their application to meteorology. *Journal of Atmospheric and Terrestrial Physics*, 12(4):306–328, 1958.

[11] C. Papastefanou. Radioactive nuclides as tracers of environmental processes. *Journal of Radioanalytical & Nuclear Chemistry*, 267(2):315–320, 02 2006.

[12] R. C. Reedy, K. Nishiizumi, D. Lal, J. R. Arnold, P. A. J. Englert, J. Klein, R. Middleton, A. J. T. Jull, and D. J. Donahue. Simulations of terrestrial in-situ cosmogenic-nuclide production. *Nuclear Instruments and Methods in Physics Research Section B: Beam Interactions with Materials and Atoms*, 92(1-4): 297–300, 6 1994.

[13] R. C. Reedy. Predicting the production rates of cosmogenic nuclides. *Nuclear Instruments and Methods in Physics Research Section B: Beam Interactions with Materials and Atoms*, 172(1-4):782–785, 10 2000.

[14] Y. Yokoyama, J. L. Reyss, and F. Guichard. Production of radionuclides by cosmic rays at mountain altitudes. *Earth and Planetary Science Letters*, 36(1): 44–50, 1977.

[15] C. Papastefanou. Residence time of tropospheric aerosols in association with radioactive nuclides. *Applied Radiation and Isotopes*, 64(1):93–100, 1 2006. URL http://www.sciencedirect.com/science/article/B6TJ0-4GY88WW-2/2/5b6502726723592c5beb4454080c7e6c.

[16] J. Masarik and J. Beer. Simulation of particle fluxes and cosmogenic nuclide production in the Earth's atmosphere. *J. Geophys. Res.*, 104(D10):12099–12111,

May 1999.

[17] J. L. Reyss, Y. Yokoyama, and F. Guichard. Production cross sections of ^{26}Al, ^{22}Na, ^{7}Be from argon and of ^{10}Be, ^{7}Be from nitrogen: Implications for production rates of ^{26}Al and ^{10}Be in the atmosphere. *Earth and Planetary Science Letters*, 53(2):203–210, 1981.

[18] J. R. Arnold. Beryllium-10 produced by cosmic rays. *Science*, 124(3222): 584–585, September 1956. doi: 10.1126/science.124.3222.584.

[19] L. R. McHargue and P. E. Damon. The global beryllium 10 cycle. *Rev. Geophys.*, 29(2):141–158, 1991. doi: 10.1029/91RG00072.

[20] A. Kulan, A. Aldahan, G. Possnert, and I. Vintersved. Distribution of ^{7}Be in surface air of Europe. *Atmospheric Environment*, 40(21):3855–3868, 7 2006.

[21] A. Kulan, A. Aldahan, G. Possnert, and I. Vintersved. Erratum to"Distribution of ^{7}Be in surface air of Europe" [Atmospheric Environment 40 (2006) 3855-3868]. *Atmospheric Environment*, 40(40):8095–8095, 12 2006.

[22] National Nuclear Data Center. Information extracted from the Nudat 2 database, 09 2011. URL `http://www.nndc.bnl.gov/nudat2/`.

[23] S. Rehfeld and M. Heimann. Three dimensional atmospheric transport simulation of the radioactive tracers ^{210}Pb, ^{7}Be, ^{10}Be, and ^{90}Sr. *J. Geophys. Res.*, 100(D12):26141–26161, 1995.

[24] M. Takada, B. J. Lewis, M. Boudreau, H. Al Anid, and L. G. I. Bennett. Modelling of aircrew radiation exposure from galactic cosmic rays and solar particle events. *Radiation Protection Dosimetry*, 124(4):289–318, 3 2007. doi: 10.1093/rpd/ncm214. URL `http://rpd.oxfordjournals.org/content/124/4/289.abstract`.

[25] Istitituto Nazionale di Geofisica e Vulcanologia. Characteristics of the Earth's magnetic field, 01 2013. URL `http://www.ingv.it/ufficio-stampa/research-areas/the-earth/characteristics-of-the-earth-s-magnetic-field/view?set_language=en`.

[26] H. W. Feely, R. J. Larsen, and C. G. Sanderson. Factors that cause seasonal variations in beryllium-7 concentrations in surface air. *Journal of*

Environmental Radioactivity, 9(3):223–249, 1989.

[27] K. O'Brien. Secular variations in the production of cosmogenic isotopes in the Earth's atmosphere. *Journal of Geophysical Research*, 84(A2):423–431, 1979.

[28] D. Koch and D. Rind. Beryllium 10/beryllium 7 as a tracer of stratospheric transport. *Journal of Geophysical Research-Atmospheres*, 103(D4):3907–3917, Feb 1998. ISSN 0747-7309.

[29] Meteoblue. meteoSchool: Atmosphere. electronic, 02 2016. URL `https://content.meteoblue.com/ro/meteoscool/the-earth/atmosphere`.

[30] Wikipedia. Hadley cell, 11 2010. URL `http://en.wikipedia.org/wiki/Hadley_cell`.

[31] S. Grabowska, J. W. Mietelski, K. Kozak, and P. Gaca. Gamma emitters on micro-becquerel activity level in air at Kraków (Poland). *Journal of Atmospheric Chemistry*, 46(2):103–116, 10 2003.

[32] P. Rulík, H. Malá, V. Bečková, Z. Hölgye, E. Schlesingerová, I. Světlík, and J. Škrkal. Low level air radioactivity measurements in Prague, Czech Republic. *Applied Radiation and Isotopes*, 67(5):969–973, 5 2009.

[33] A. Ioannidou, M. Manolopoulou, and C. Papastefanou. Temporal changes of ^{7}Be and ^{210}Pb concentrations in surface air at temperate latitudes (40°N). *Applied Radiation and Isotopes*, 63(2):277–284, 8 2005.

[34] M. Zähringer, J. Bieringer, and C. Schlosser. Three years of operational experience from Schauinsland CTBT monitoring station. *Journal of Environmental Radioactivity*, 99(4):596–606, 4 2008.

[35] A. P. Leppänen and A. Grinsted. Observations Of Cosmogenic ^{7}Be and ^{22}Na In Aerosol Samples in Northern Finland. *AIP Conference Proceedings*, 1034(1): 112–115, 08 2008.

[36] N. Rastogi and M. M. Sarin. Atmospheric ^{210}Pb and ^{7}Be in ambient aerosols over low- and high-altitude sites in semiarid region: Temporal variability and transport processes. *J. Geophys. Res.*, 113(D11), 06 2008.

[37] A. Baeza, L. Delrío, A. Jiménez, C. Miró, J. Paniagua, and M. Rufo. Analysis of

the temporal evolution of atmospheric ^{7}Be as a vector of the behavior of other radionuclides in the atmosphere. *Journal of Radioanalytical and Nuclear Chemistry*, 207(2):331–344, 1996-07-17.

[38] C. Papastefanou and A. Ioannidou. Beryllium-7 and solar activity. *Applied Radiation and Isotopes*, 61(6):1493–1495, 12 2004. URL http://www.sciencedirect.com/science/article/B6TJ0-4D5XB3W-1/2/904df1a4a248f61e2c14498e4da20674.

[39] W. Viezee and H. B. Singh. The distribution of beryllium-7 in the troposphere: implications on stratospheric/tropospheric air exchange. *Geophys. Res. Lett.*, 7 (10):805–808, October 1980.

[40] I. G. Usoskin, H. Kananen, K. Mursula, P. Tanskanen, and G. A. Kovaltsov. Correlative study of solar activity and cosmic ray intensity. *J. Geophys. Res.*, 103(A5):9567–9574, 1998.

[41] H. Liu, D. B. Considine, L. W. Horowitz, J. H. Crawford, J. M. Rodriguez, S. E. Strahan, M. R. Damon, S. D. Steenrod, X. Xu, J. Kouatchou, C. Carouge, and R. M. Yantosca. Using beryllium-7 to assess cross-tropopause transport in global models. *Atmos. Chem. Phys. Discuss.*, 15(18):26131–26189, 09 2015. doi: 10.5194/acpd-15-26131-2015. URL http://www.atmos-chem-phys-discuss.net/15/26131/2015/.

[42] J. Masarik, K. J. Kim, and R. C. Reedy. Numerical simulations of in situ production of terrestrial cosmogenic nuclides. *Nuclear Instruments and Methods in Physics Research Section B: Beam Interactions with Materials and Atoms*, 259(1):642–645, 6 2007.

[43] G. M. Raisbeck, F. Yiou, M. Fruneau, J. M. Loiseaux, M. Lieuvin, and J. C. Ravel. Cosmogenic ^{10}Be/^{7}Be as a probe of atmospheric transport processes. *Geophys. Res. Lett.*, 8(9):1015–1018, 1981.

[44] A. Aldahan, J. Hedfors, G. Possnert, A. Kulan, A. M. Berggren, and C. Söderström. Atmospheric impact on beryllium isotopes as solar activity proxy. *Geophys. Res. Lett.*, 35(21), 11 2008.

[45] P. Tunved, H.-C. Hansson, M. Kulmala, P. Aalto, Y. Viisanen, H. Karlsson, A. Kristensson, E. Swietlicki, M. Dal Maso, J. Ström, and M. Komppula. One year boundary layer aerosol size distribution data from five nordic background

stations. *Atmospheric Chemistry and Physics*, 3:2183–2205, 2003.

[46] John A. Eddy. The Maunder Minimum. *Science*, 192(4245):1189–1202, 06 1976. URL http://www.sciencemag.org/content/192/4245/1189.short.

[47] U. Heikkilä, J. Beer, and J. Feichter. Modeling cosmogenic radionuclides ^{10}Be and ^{7}Be during the Maunder Minimum using the ECHAM5-HAM general circulation model. *Atmospheric Chemistry and Physics*, 8(10):2797–2809, 2008. doi: 10.5194/acp-8-2797-2008. URL http://www.atmos-chem-phys.net/8/2797/2008/.

[48] U. Heikkilä, J. Beer, and J. Feichter. Meridional transport and deposition of atmospheric ^{10}be. *Atmospheric Chemistry and Physics*, 9(2):515–527, 2009. doi: 10.5194/acp-9-515-2009. URL http://www.atmos-chem-phys.net/9/515/2009/.

[49] J. E. Dibb, L. D. Meeker, R. C. Finkel, J. R. Southon, M. W. Caffee, and L. A. Barrie. Estimation of stratospheric input to the arctic troposphere: ^{7}Be and ^{10}Be in aerosols at Alert, Canada. *J. Geophys. Res.*, 99(D6):12855–12864, 1994.

[50] C. E. Jordan, J. E. Dibb, and R. C. Finkel. ^{10}Be/^{7}Be tracer of atmospheric transport and stratosphere-troposphere exchange. *J. Geophys. Res.*, 108(D8), 04 2003.

[51] A. P. Leppänen, I. G. Usoskin, G. A. Kovaltsov, and J. Paatero. Cosmogenic ^{7}Be and ^{22}Na in Finland: Production, observed periodicities and the connection to climatic phenomena. *Journal of Atmospheric and Solar-Terrestrial Physics*, 74: 164–180, 1 2012. doi: http://dx.doi.org/10.1016/j.jastp.2011.10.017. URL http://www.sciencedirect.com/science/article/pii/S1364682611003002.

[52] F. Arkian, A. H. Meshkatee, and A. Bidokhti. The effects of large-scale atmospheric flows on berylium-7 activity concentration in surface air. *Environmental Monitoring and Assessment*, 168(1):429–439, 2010-09-01.

[53] G. Gilmore and J. Hemingway. *Practical Gamma-Ray Spectrometry.* John Wiley & Sons, 1995.

[54] Nicholas Tsoulfanidis. *Measurement And Detection Of Radiation.* Taylor & Francis, 2nd edition, 3 1995.

[55] L. A. Currie. Limits for Qualitative Detection and Quantative Determination Application to Radiochemistry. *Analytical Chemistry*, 40(3):586–593, 1968.

[56] L. E. De Geer. Currie detection limits in gamma-ray spectroscopy,. *Applied Radiation and Isotopes*, 61(2-3):151–160, 2004/9// 2004.

[57] D. S. Andreev, K. I. Erokhina, V. S. Zvonov, and I. Kh. Lemberg. Consideration of cascade transitions in determining the absolute yield of gamma rays. *Instruments and Experimental Techniques*, 25:1358–1360, 1972.

[58] Marinelli Beaker Dimensions. electronic, 09 2015. URL `http://www.ntsincorg.com/m_beakers_diamensions.htm`.

[59] P. Aarnio, J. Ala-Heikkilä, and T. Hakulinen. *SHAMAN Expert System for Radionuclide Identification.* Baryon Oy, Auringonkatu 2B8, FIN-02210 Espoo, Finland, 1.8.1 edition, 6 2005.

[60] IDC Documentation. *Formats and Protocols for Messages 3.4.1 Revision 6.* Comprehensive Nuclear Test-Ban-Treaty Organization, Vienna, Austria, 2004.

[61] P. Aarnio. *LINSSI SQL Database for Gamma-ray Spectrometry Part I: Database.* Helsinki University of Technology, Espoo, Finland, 2006.

[62] P. Aarnio, J. Ala-Heikkilä, I. Hoffman, T. Ilander, S. Klemola, A. Mattila, A. Kuusi, M. Moring, M. Nikkinen, A. Pelikan, S. Ristkari, T. Salonen, T. Siiskonen, P. Smolander, H. Toivonen, K. Ungar, K. Vesterbacka, and W. Zhang. *LINSSI SQL Database for Gamma-ray Spectrometry Part I: Database.* Helsinki University of Technology, Espoo, Finland, 2011.

[63] M. Moring, H. Toivonen, and A. Pelikan. *User Manual of Radionuclide Analysis and Evaluation Software Aatami - 4.10.* Comprehensive Nuclear Test-Ban-Treaty Organization, Vienna, 3 2007.

[64] A. Pelikan. JMUFI Setup. Technical report, STUK, 6 2008.

[65] H. Toivonen and A. Pelikan. *Reference Manual of Aatami 4.10.* Comprehensive Nuclear Test-Ban-Treaty Organization, March 2007.

[66] J. D. Hunter. Matplotlib: A 2D graphics environment. *Computing In Science & Engineering*, 9(3):90–95, 2007.

[67] Jürg Beer, Ken McCracken, and von Steiger Rudolf. *Cosmogenic Radionuclides Theory and Applications in the Terrestrial and Space Environments*. Springer-Verlag Berlin Heidelberg, 1 edition, 2012. doi: 10.1007/978-3-642-14651-0.

[68] J. Masarik and J. Beer. An updated simulation of particle fluxes and cosmogenic nuclide production in the earth's atmosphere. *Journal of Geophysical Research: Atmospheres*, 114(D11):n/a–n/a, 2009. ISSN 2156-2202. doi: 10.1029/2008JD010557. URL http://dx.doi.org/10.1029/2008JD010557.

[69] G. D. Badhwar and P. M. O'Neill. Long term modulation of galactic cosmic radiation and its model for space exploration. *Adv. Space Res.*, 14:749–757, 1994.

[70] G. D Badhwar and P. M O'Neill. Galactic cosmic radiation model and its applications. *Advances in Space Research*, 17(2):7–17, 1996. doi: http://dx.doi.org/10.1016/0273-1177(95)00507-B. URL http://www.sciencedirect.com/science/article/pii/027311779500507B.

[71] P. M O'Neill. Badhwar-O'Neill 2011 Galactic Cosmic Ray Flux Model Description. Technical report, NASA, June 2013.

[72] T.C. Slaba P. M. O'Neill, S. Golge. *Badhwar-O'Neill 2014 Galactic Cosmic Ray Flux Model Description*. NASA Johnson Space Center, Houston, Texas 77058, USA, 03 2015.

[73] ICRP. Relative Biological Effectiveness, Radiation Weighting and Quality Factore. *ICRP Publication 92. Ann.*, 33(4), 2003.

[74] ICRP. Conversion Coefficients for use in Radiological Protection against External Radiation. *Ann. ICRP Publication 74*, 26(3-4), 1996.

[75] Sodankyla Geophysical Observatory. Neutron Monitor Database, 02 2013. URL http://cosmicrays.oulu.fi/.

[76] National Geophysical Data Center. Sunspot Database, 02 2013. URL http://www.ngdc.noaa.gov/nndc/struts/results?t=102827&s=5&d=8,430,9.

[77] J. Richard Gott III, Michael S. Vogeley, Silviu Podariu, and Bharat Ratra. Median statistics, H(0), and the accelerating universe. *Astrophys.J.*, 549:1–17, 2001. doi: 10.1086/319055.

[78] EML Databases and Sample Archives. electronic, 05 2015. URL http://www.wipp.energy.gov/NAMP/EMLLegacy/databases.htm.

[79] P. Kållberg, P. Berrisford, B. Hoskins, A. Simmmons, S. Uppala, Lamy-Thépaut S., and R. Hine. EPR-40 Atlas. Technical Report 19, ECMWF, June 2005.

[80] A. P. Leppänen, A. A. Pacini, I. G. Usoskin, A. Aldahan, E. Echer, H. Evangelista, S. Klemola, G. A. Kovaltsov, K. Mursula, and G. Possnert. Cosmogenic ^{7}Be in air: A complex mixture of production and transport. *Journal of Atmospheric and Solar-Terrestrial Physics*, 72(13):1036–1043, 8 2010.

A IMS Particulate Specifications

Characteristics	Minimum Requirements
System	Manual or automated
Air flow	500 m^3/h
Collection time	24 h
Decay time	≤24 h
Measurement time	≤20 h
Time before reporting	≤3 d
Reporting frequency	Daily
Filter	Adequate composition for compaction, dissolution and analysis
Particulate collection efficiency	for filter ≥80 % at ⌀=0.2 µm global ≥60 % at ⌀=10 µm
Measurement mode	Hyper pure germanium high-resolution gamma spectrometry
Hyper pure germanium relative efficiency	≥40 %
Hyper pure germanium resolution	<2.5 keV at 1332 keV
Baseline sensitivity	10 µBq m^{-3} to 30 µBq m^{-3} for ^{140}Ba
Calibration range	88 keV to 1836 keV
Data format for gamma spectra and auxiliary data	Radionuclide Monitoring System format
State of health	Status data transmitted to International Data Centre
Communication	Two-way
Auxiliary data	Meteorological data, flow rate measurement every 10 min
Data availability	≥95 %
Down time	≤7 consecutive days ≤15 days annually

B SPHDF File Format

The sample pulse height data file is made up of several required data blocks including a header, collection, acquisition, and processing information, energy, resolution, and efficiency calibration, and the actual spectra itself. The optional data blocks and irrelevant mandatory data blocks are not used in this work and will not be discussed here.

Element	Position	Format	Description
1	1-7	a7	#Header
	9-18	a10	designator
2	1-5	a5	site code
	7-15	a9	detector code
	17	a1	system type: P for particulate
	19-35	a17	sample geometry
	37-40	a4	spectrum qualifier: preliminary (PREL) or full (FULL)
3	1-16	a16	sample reference identification
4	1-31	a31	measurement identification
	33-63	a31	detector background measurement identification
	65-95	a31	gas background measurement identification (memory effect)
5	1-10	i4,a1,i2,a1,i2	transmit date (yyyy/mm/dd)
	12-21	i2,a1,i2,a1,f4.1	transmit time (hh:mm:ss.s)

C Complete Set of Figures

C.1 R_c Plots

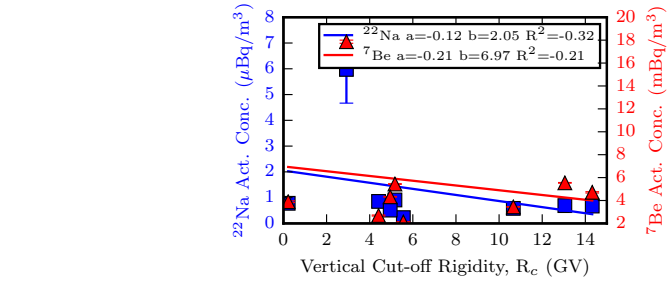

(a) February

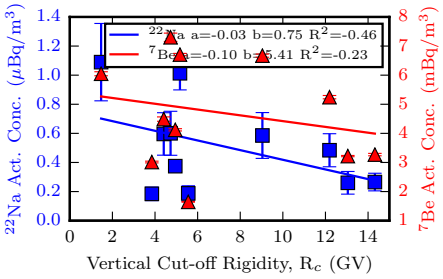

(b) March

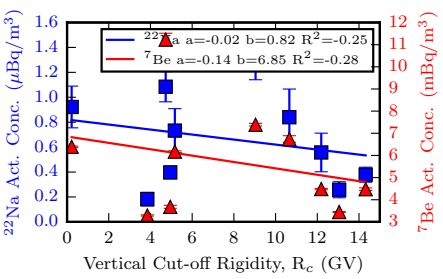

(c) April

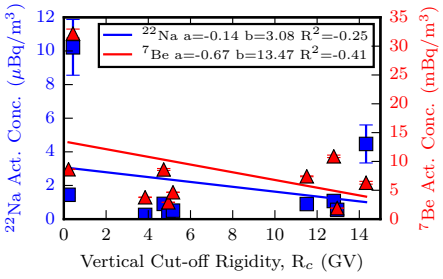

(d) May

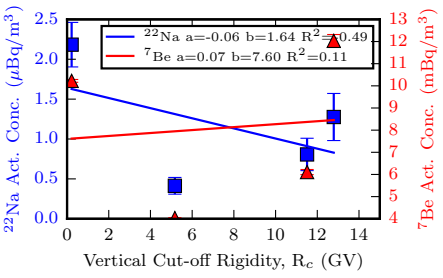

(e) June

Figure C.1 – 30 d summation, ^{22}Na (square), ^{7}Be (triangle) as a function of R_c for the first six months of 2005.

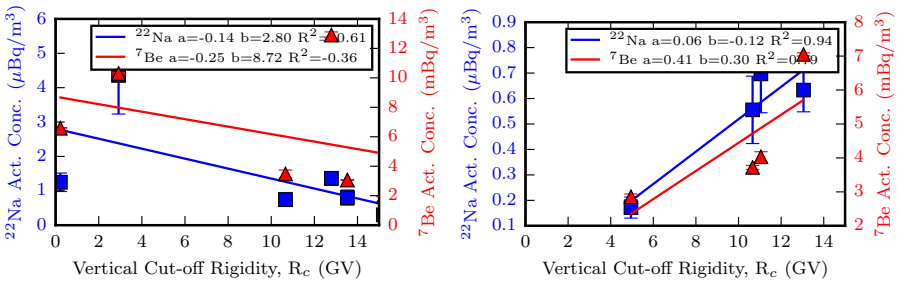

(a) July

(b) August

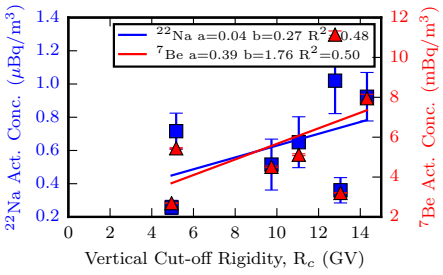

(c) September

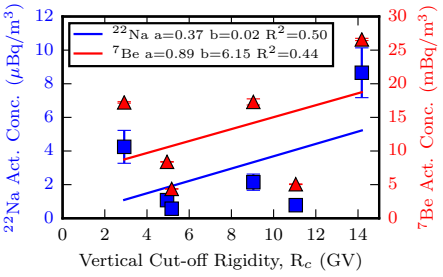

(d) October

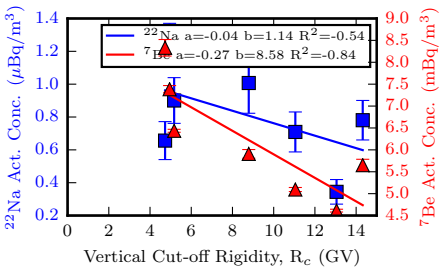

(e) November

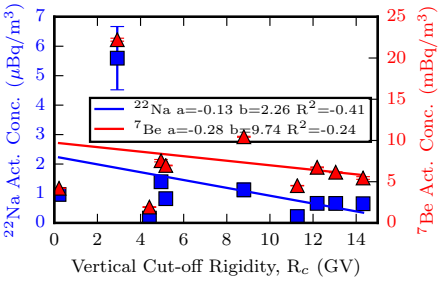

(f) December

Figure C.2 – 30 d summation, ^{22}Na (square), ^{7}Be (triangle) as a function of R_c for the last six months of 2005.

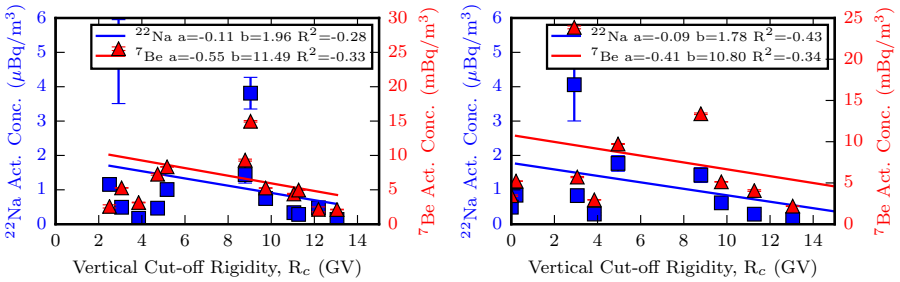

(a) January

(b) February

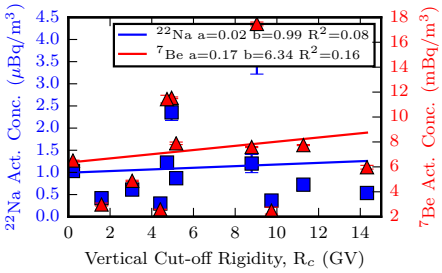

(c) March

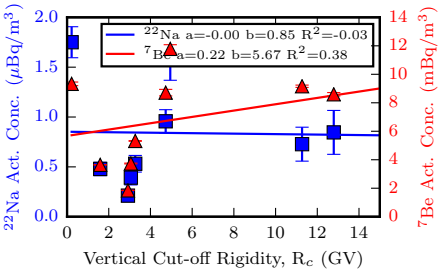

(d) April

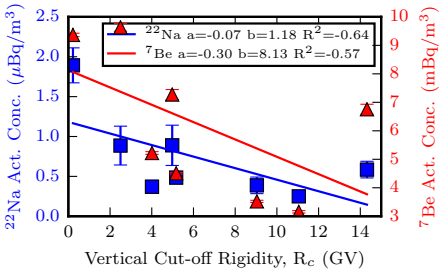

(e) May

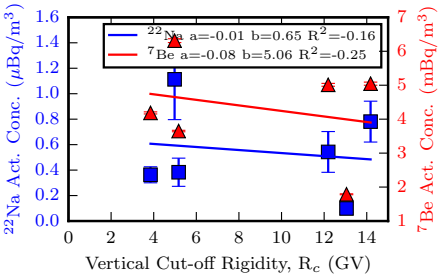

(f) June

Figure C.3 – 30 d summation, ^{22}Na (square), ^{7}Be (triangle) as a function of R_c for the first six months of 2006.

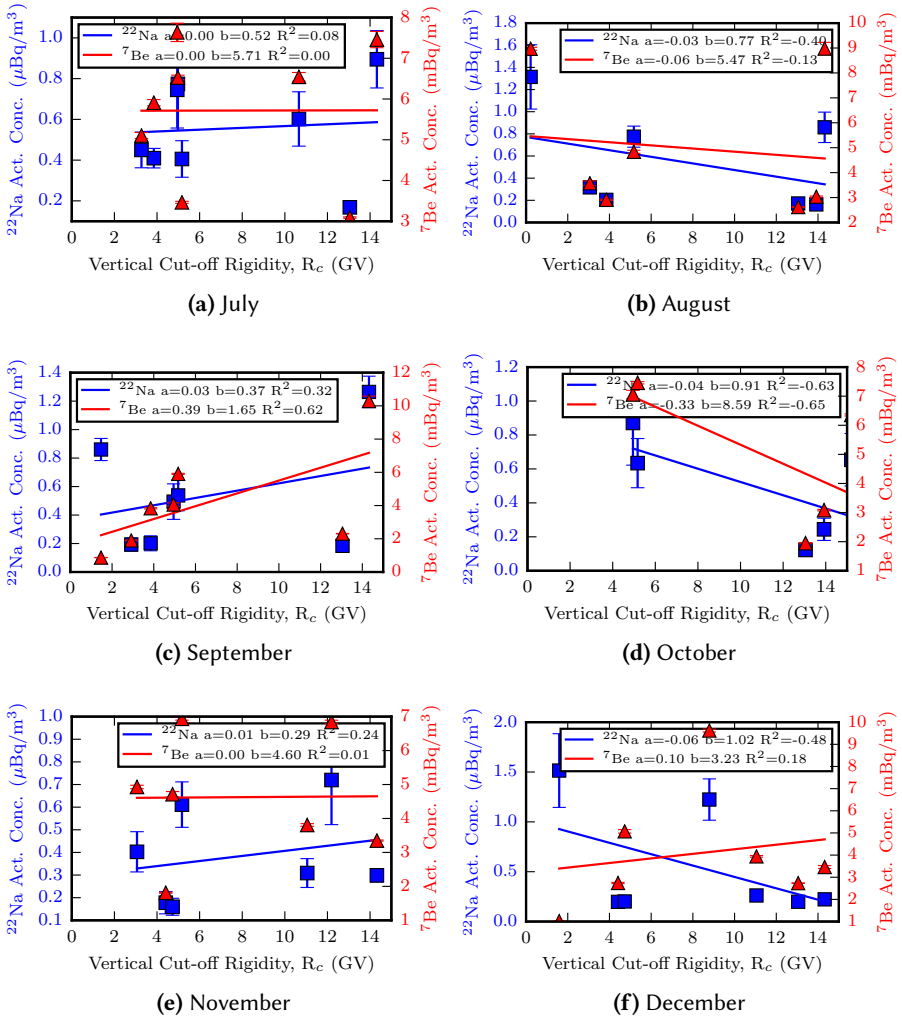

(a) July **(b)** August

(c) September **(d)** October

(e) November **(f)** December

Figure C.4 – 30 d summation, ^{22}Na (square), ^{7}Be (triangle) as a function of R_c for the last six months of 2006.

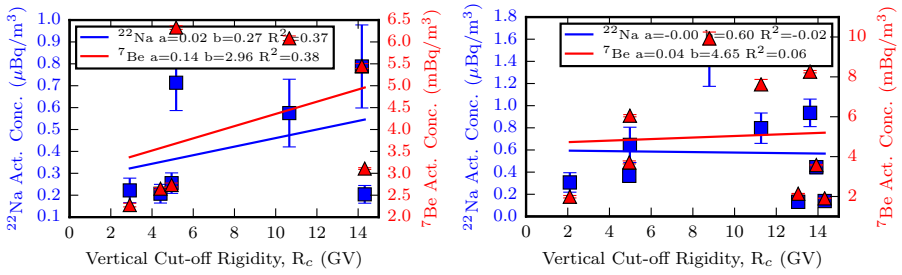

(a) January

(b) February

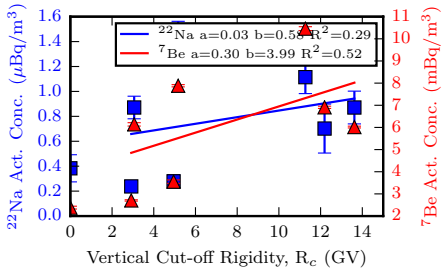

(c) March

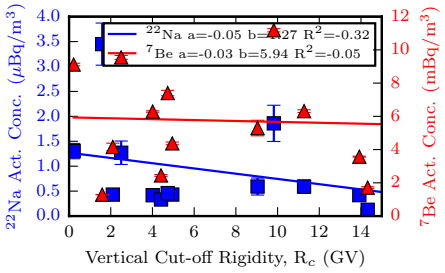

(d) April

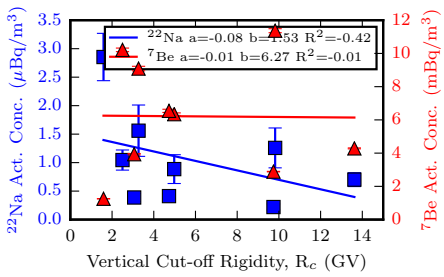

(e) May

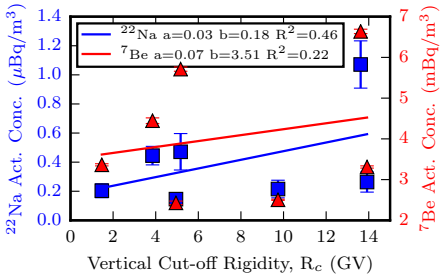

(f) June

Figure C.5 – 30 d summation, ^{22}Na (square), ^{7}Be (triangle) as a function of R_c for the first six months of 2007.

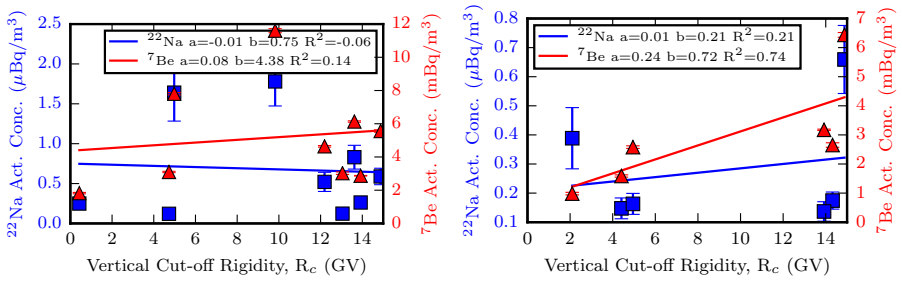

(a) July

(b) August

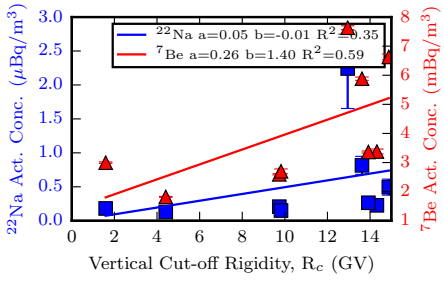

(c) September

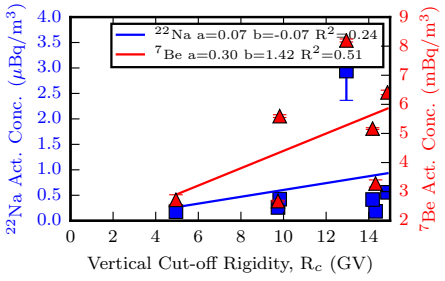

(d) October

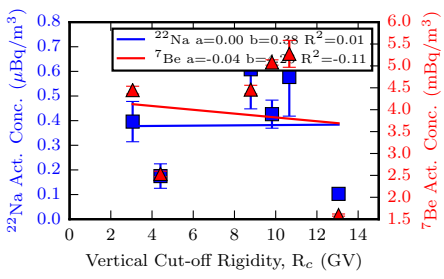

(e) November

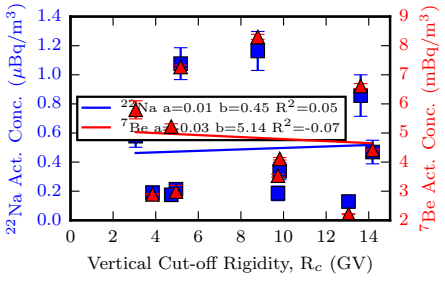

(f) December

Figure C.6 – 30 d summation, ^{22}Na (square), ^{7}Be (triangle) as a function of R_c for the last six months of 2007.

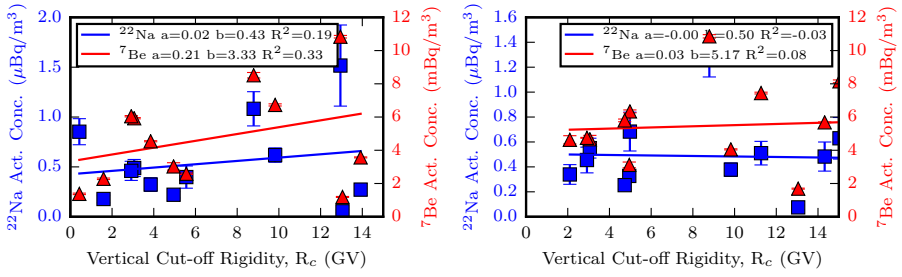

(a) January

(b) February

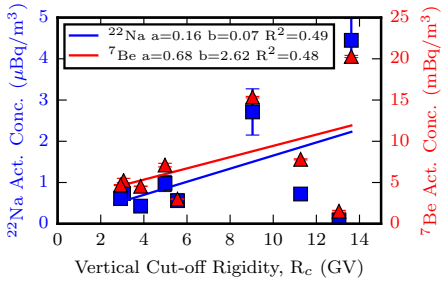

(c) March

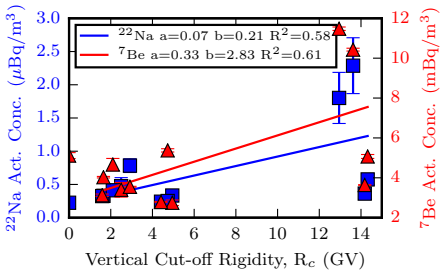

(d) April

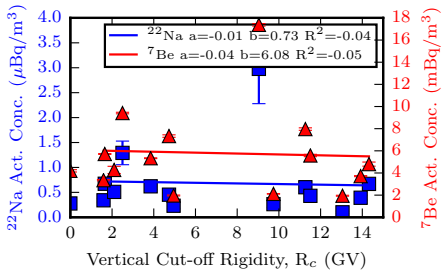

(e) May

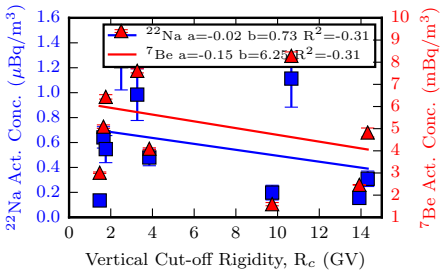

(f) June

Figure C.7 – 30 d summation, ^{22}Na (square), ^{7}Be (triangle) as a function of R_c for the first six months of 2008.

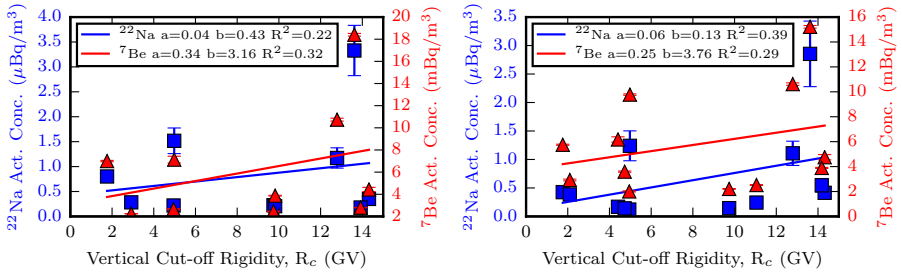

(a) July

(b) August

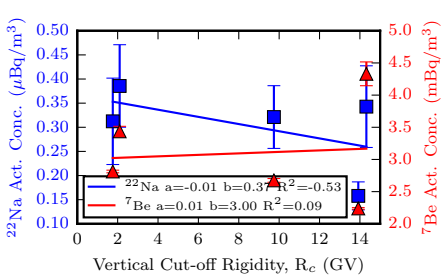

(c) September

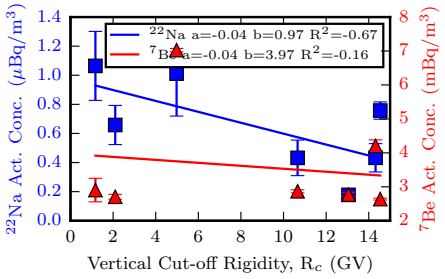

(d) October

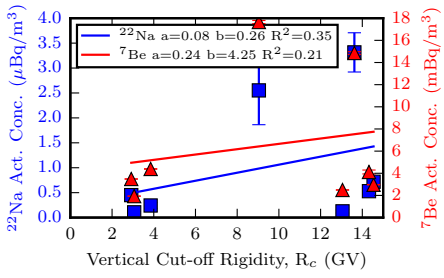

(e) November

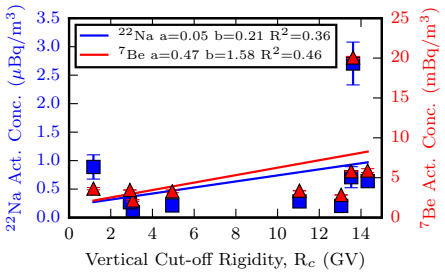

(f) December

Figure C.8 – 30 d summation, ^{22}Na (square), ^{7}Be (triangle) as a function of R_c for the last six months of 2008.

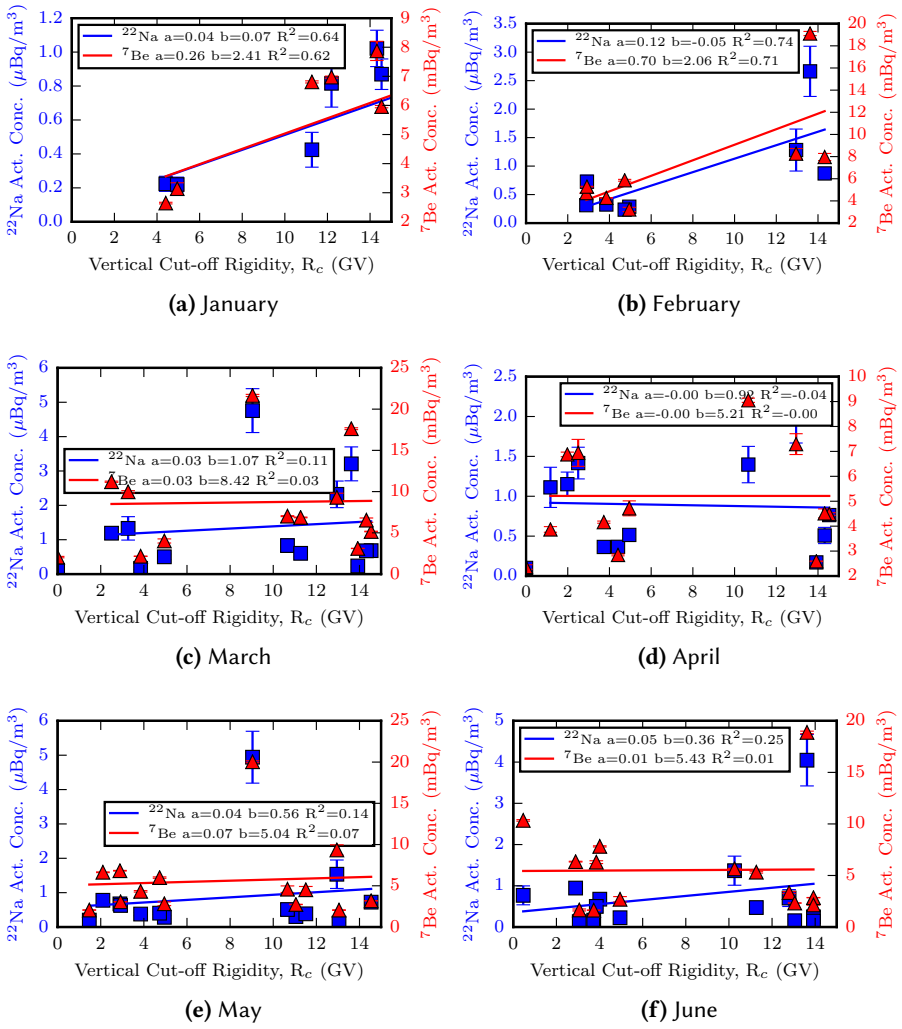

Figure C.9 – 30 d summation, ^{22}Na (square), ^{7}Be (triangle) as a function of R_c for the first six months of 2009.

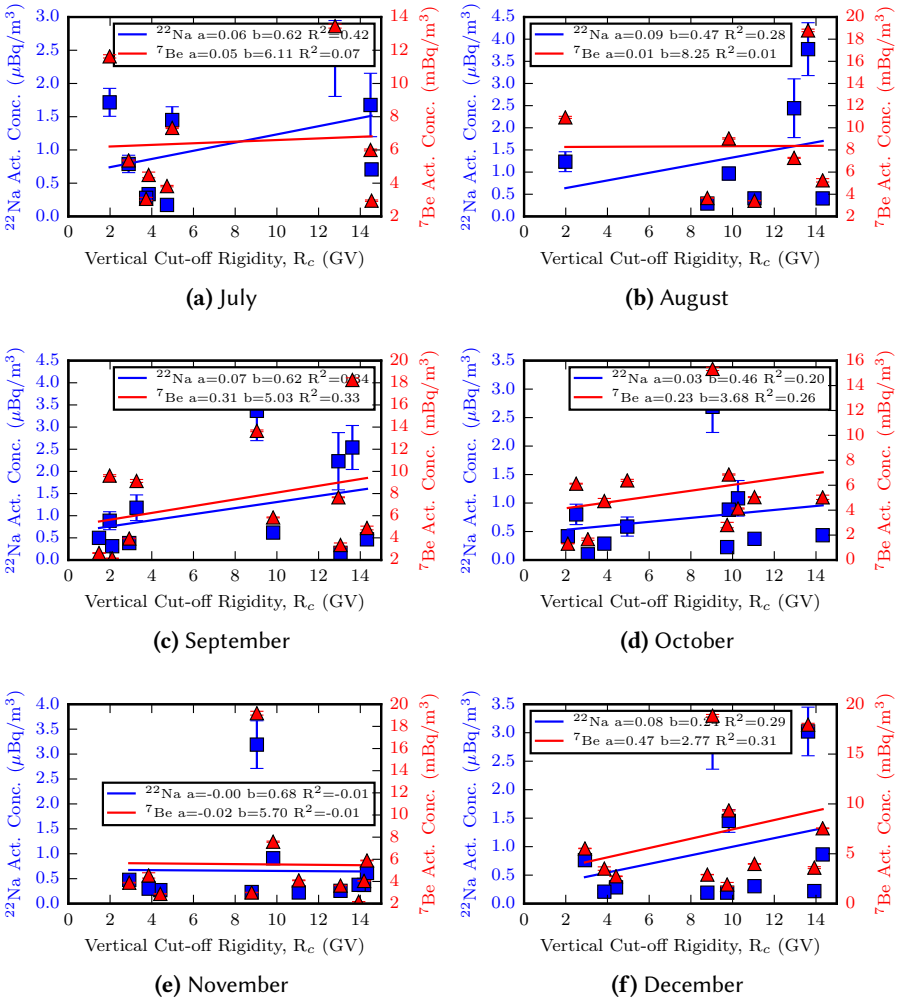

(a) July **(b)** August

(c) September **(d)** October

(e) November **(f)** December

Figure C.10 – 30 d summation, ^{22}Na (square), ^{7}Be (triangle) as a function of R_c for the last six months of 2009.

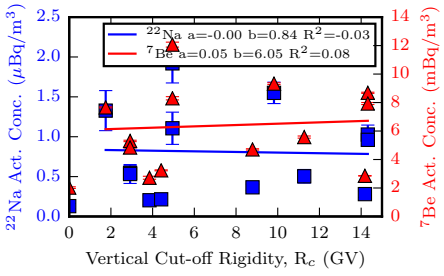

(a) January

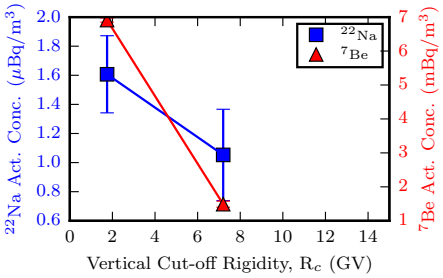

(b) March

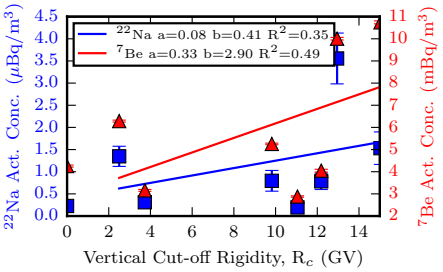

(c) April

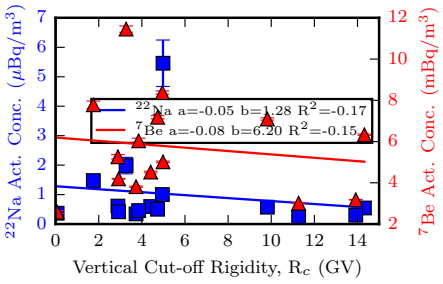

(d) May

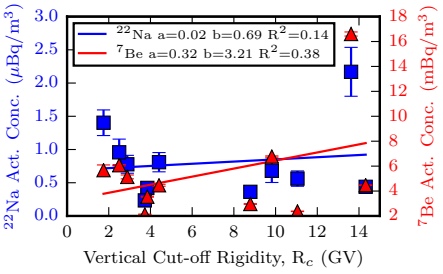

(e) June

Figure C.11 – 30 d summation, ^{22}Na (square), ^{7}Be (triangle) as a function of R_c for the first six months of 2010.

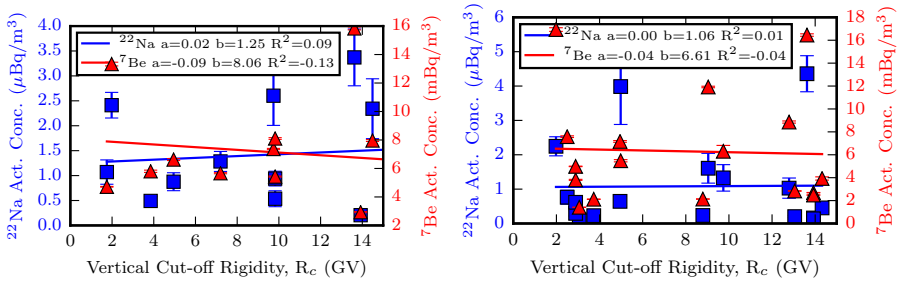

(a) July

(b) August

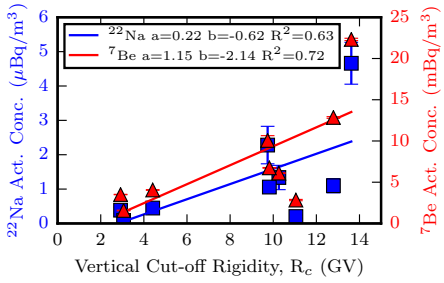

(c) September

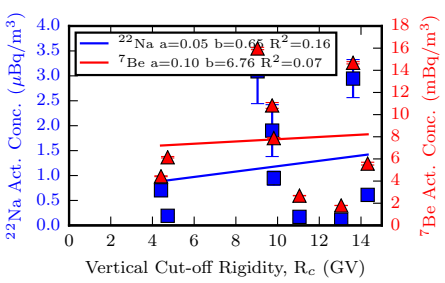

(d) October

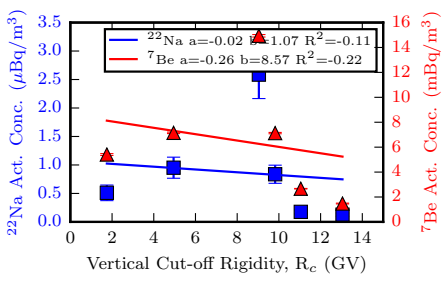

(e) November

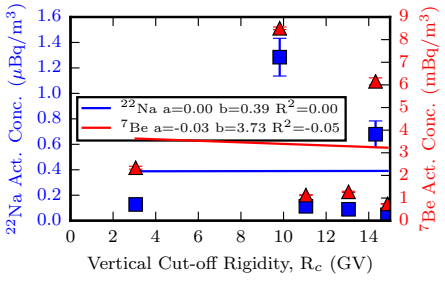

(f) December

Figure C.12 – 30 d summation, ^{22}Na (square), ^{7}Be (triangle) as a function of R_c for the last six months of 2010.

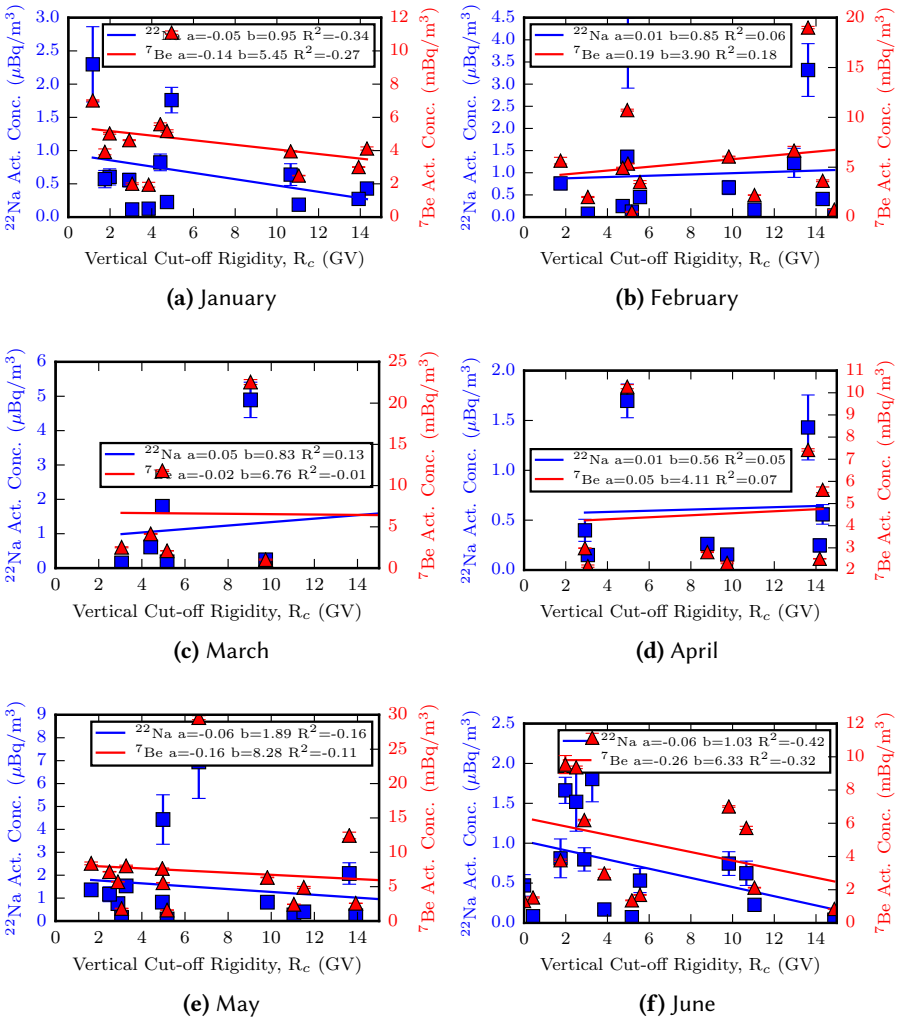

Figure C.13 – 30 d summation, ^{22}Na (square), ^{7}Be (triangle) as a function of R_c for the last six months of 2011.

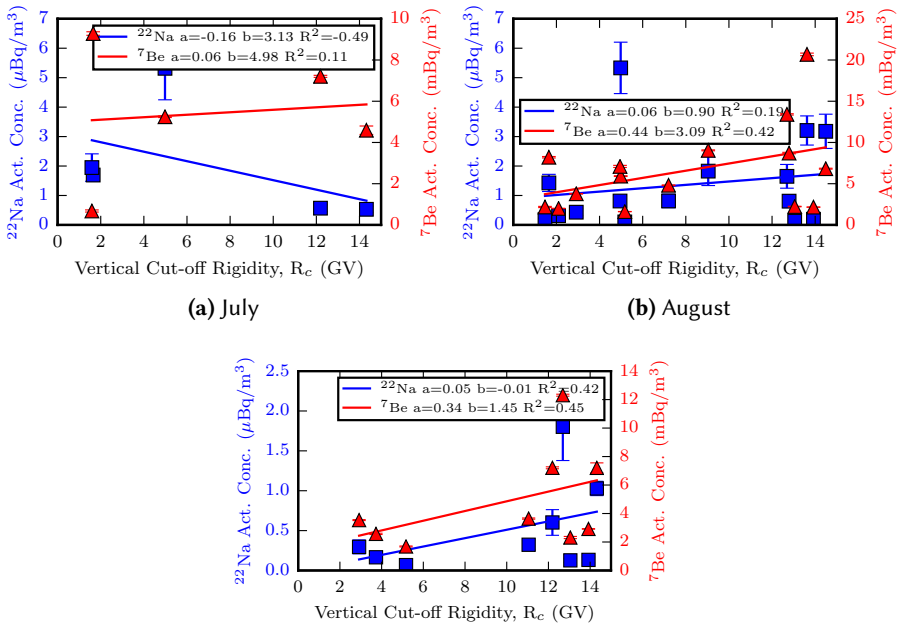

(a) July **(b)** August

(c) September

Figure C.14 – 30 d summation, ^{22}Na (square), ^{7}Be (triangle) as a function of R_c for the last six months of 2011.

C.2 Ratio Plots

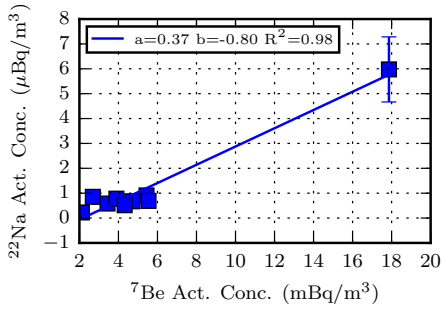

(a) February

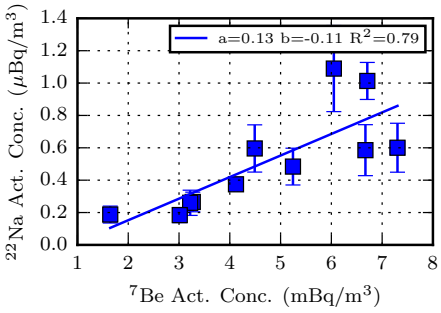

(b) March

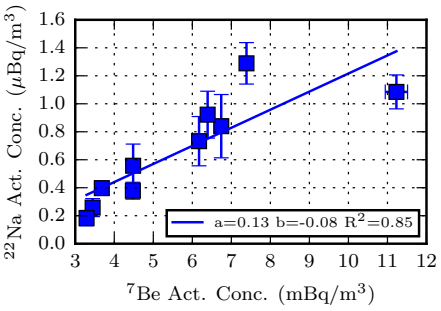

(c) April

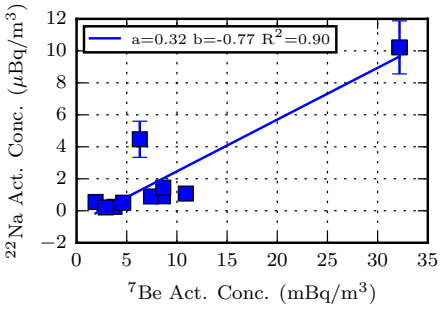

(d) May

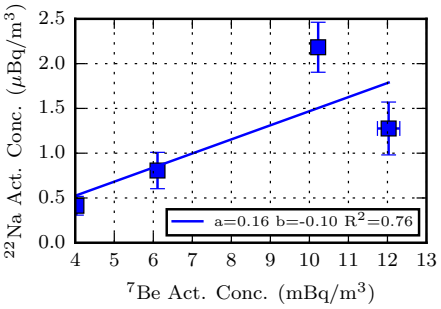

(e) June

Figure C.15 – 30 d summation ^{22}Na/^{7}Be for the first six months of 2005.

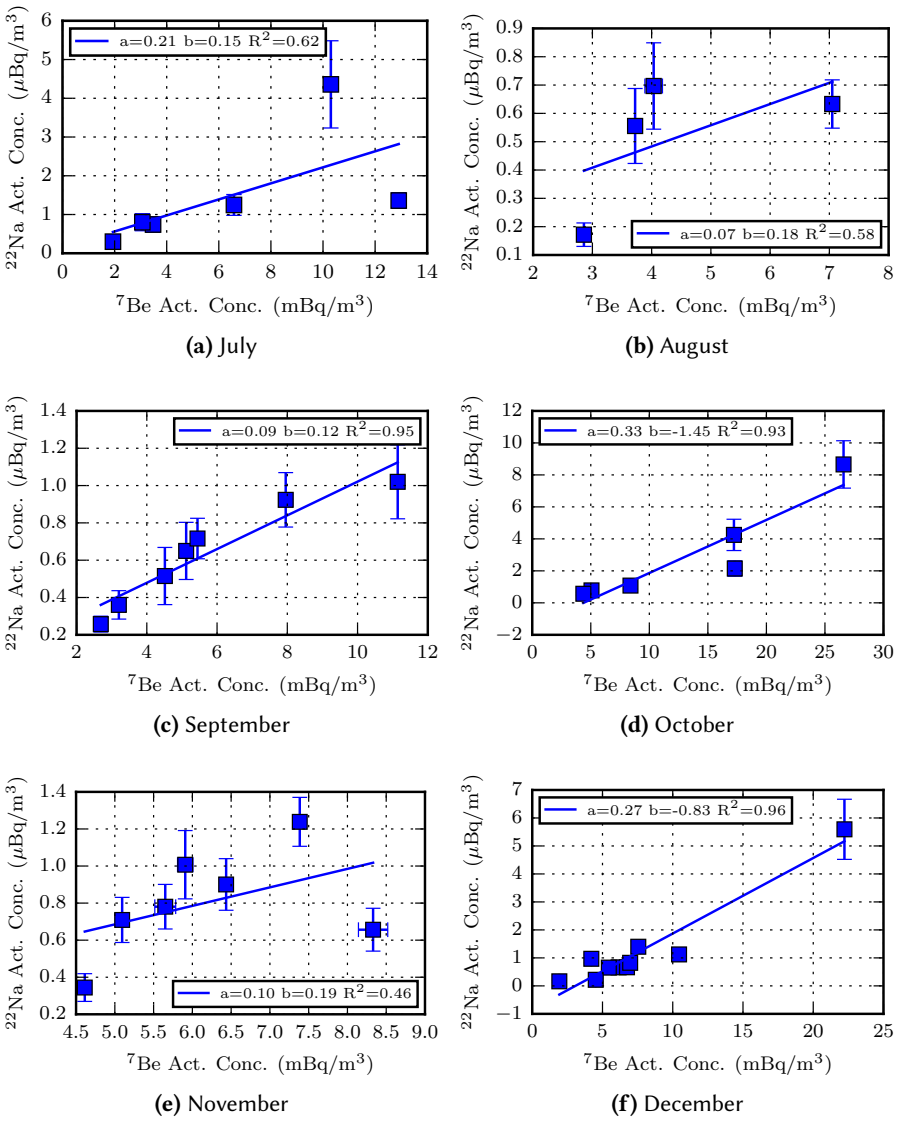

(a) July **(b)** August

(c) September **(d)** October

(e) November **(f)** December

Figure C.16 – 30 d summation $^{22}Na/^{7}Be$ for the last six months of 2005.

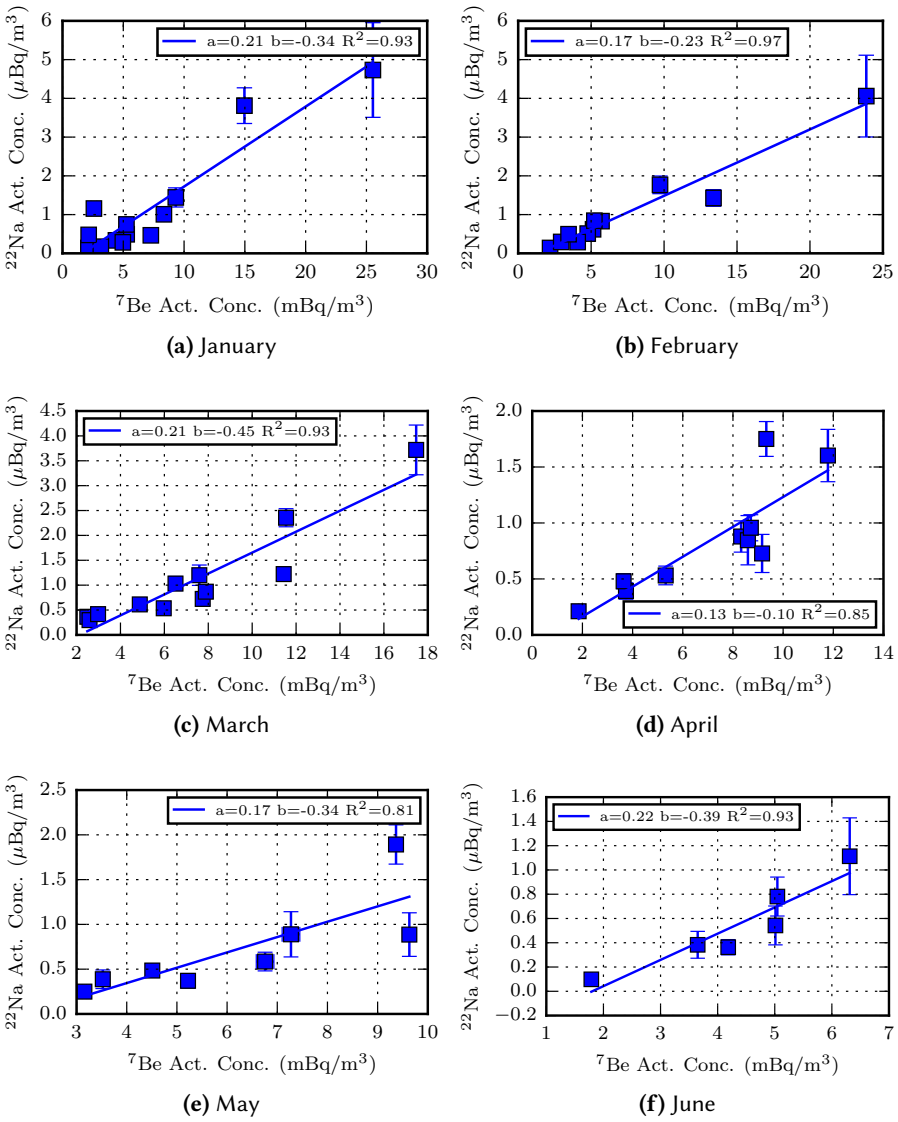

(a) January **(b)** February

(c) March **(d)** April

(e) May **(f)** June

Figure C.17 – 30 d summation ^{22}Na/^{7}Be for the first six months of 2006.

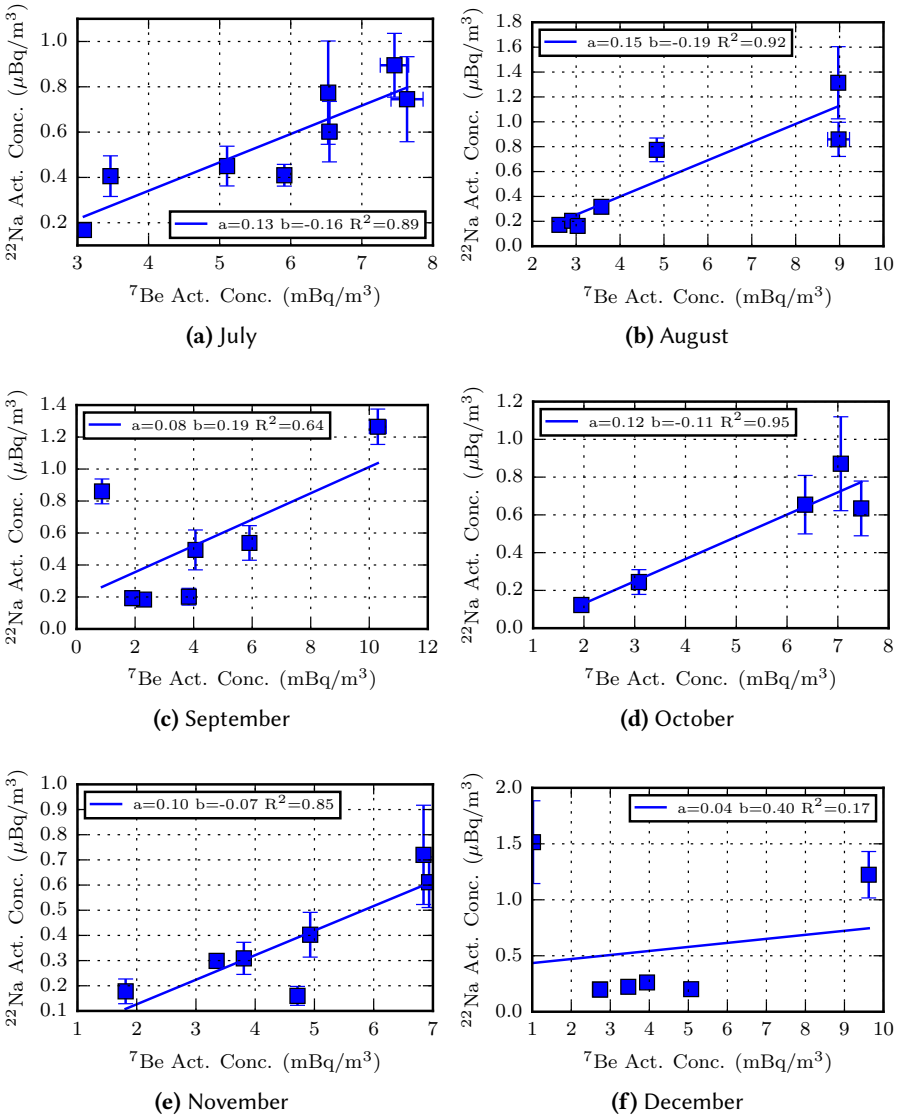

(a) July **(b)** August

(c) September **(d)** October

(e) November **(f)** December

Figure C.18 – 30 d summation ^{22}Na/^{7}Be for the last six months of 2006.

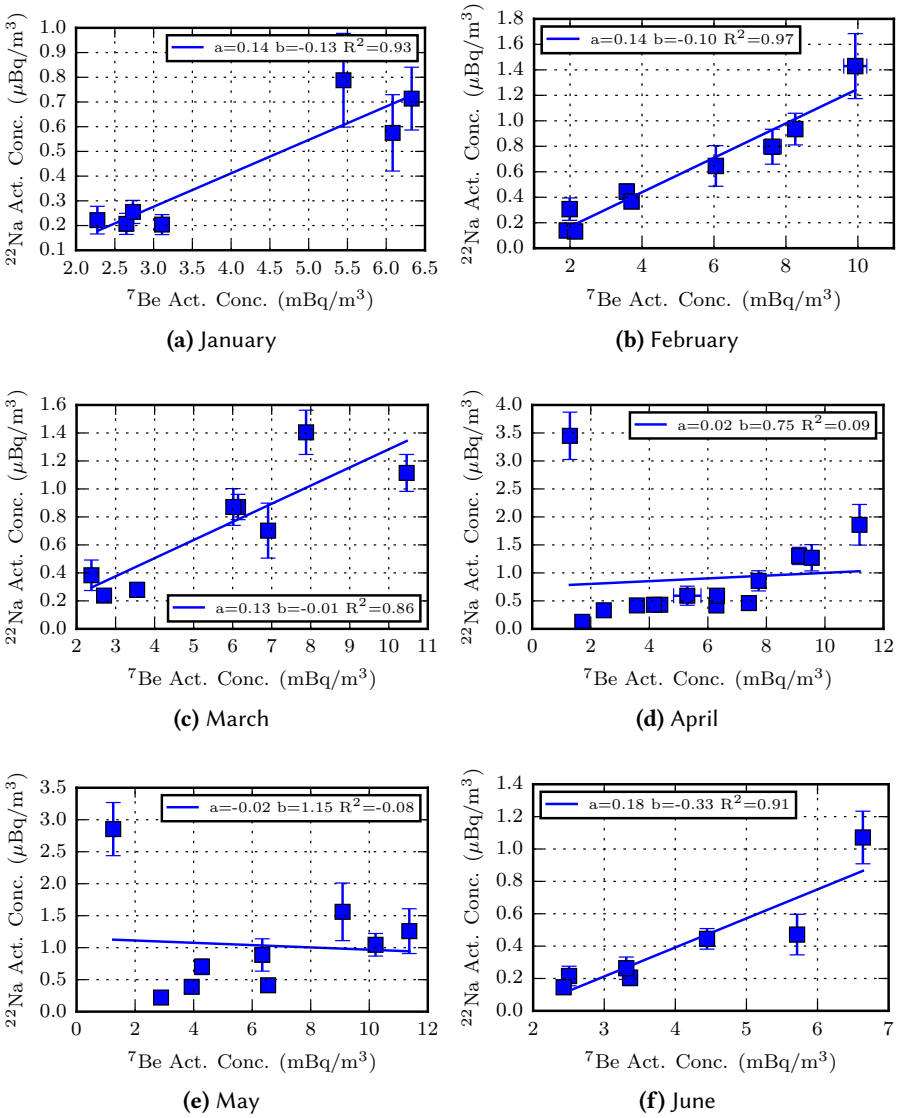

(a) January **(b)** February

(c) March **(d)** April

(e) May **(f)** June

Figure C.19 – 30 d summation ^{22}Na/^{7}Be for the first six months of 2007.

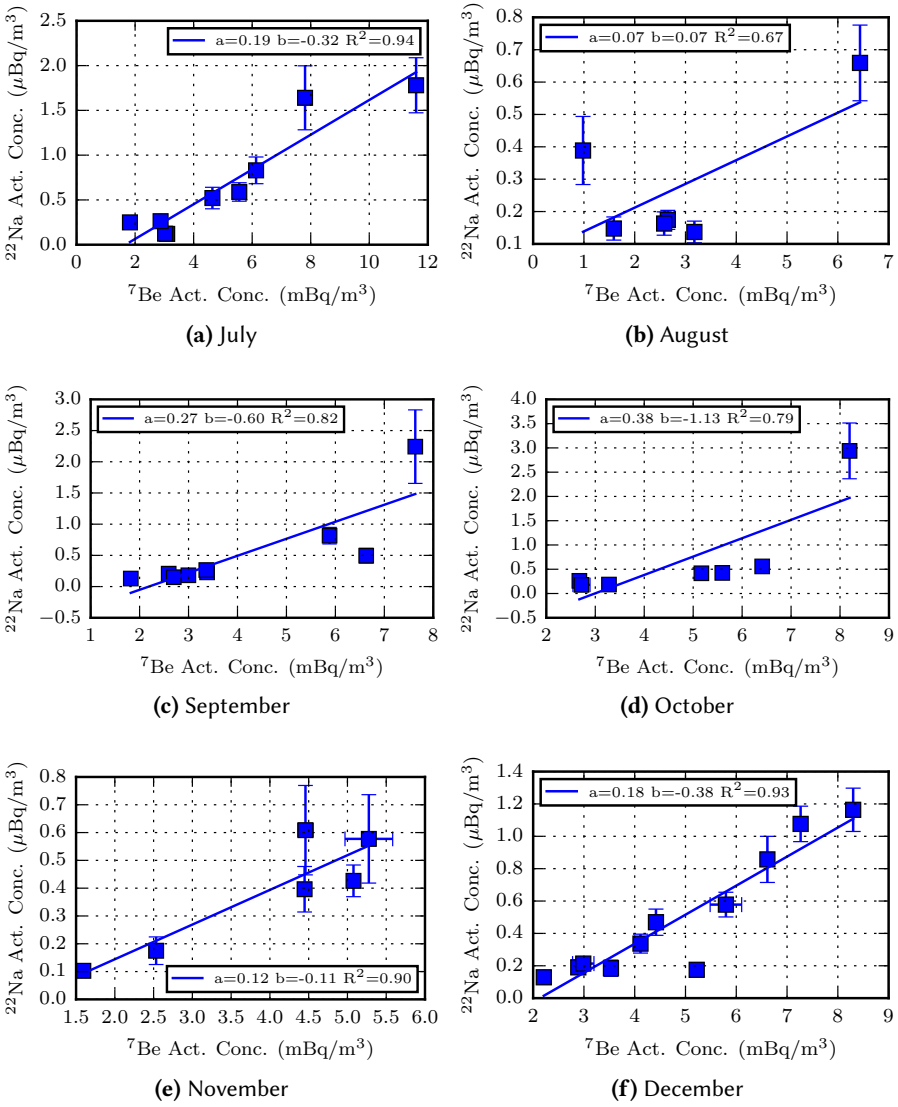

(a) July **(b)** August

(c) September **(d)** October

(e) November **(f)** December

Figure C.20 – 30 d summation $^{22}Na/^{7}Be$ for the last six months of 2007.

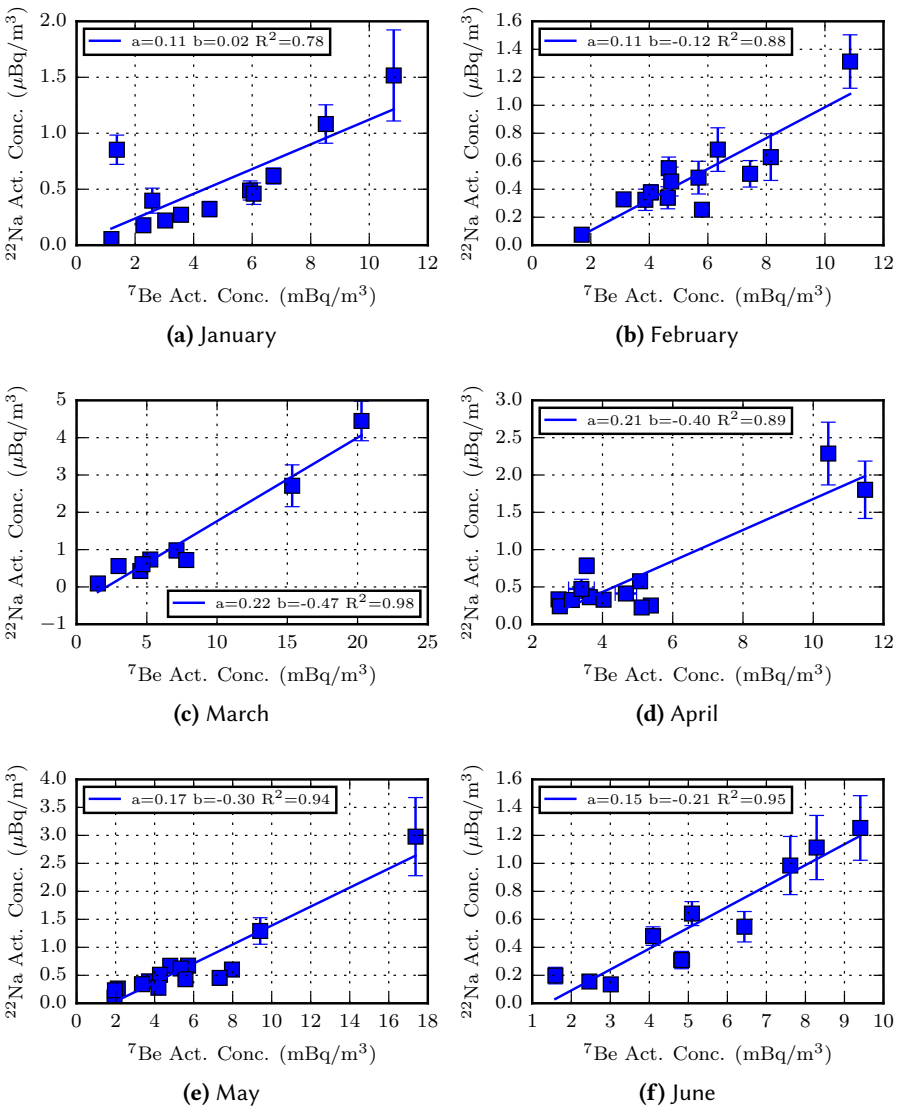

(a) January **(b)** February

(c) March **(d)** April

(e) May **(f)** June

Figure C.21 – 30 d summation ^{22}Na/^{7}Be for the first six months of 2008.

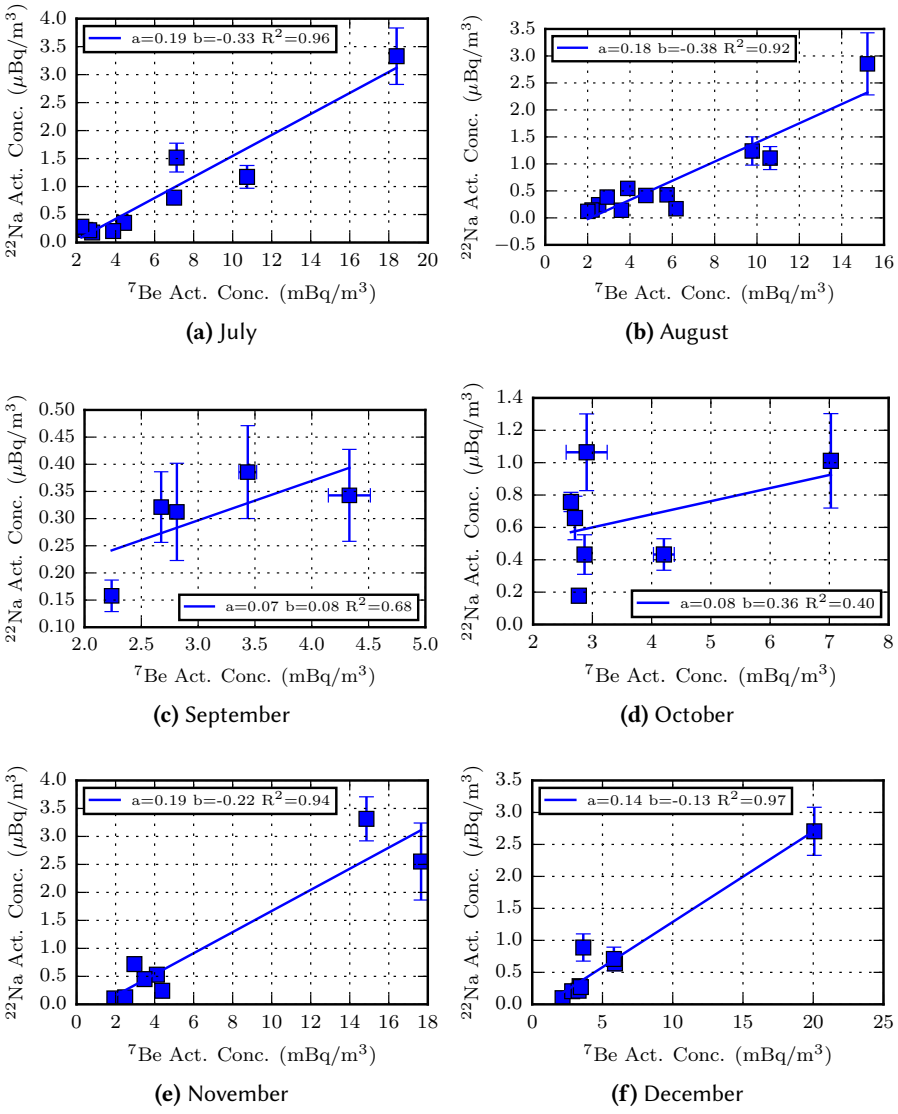

(a) July **(b)** August

(c) September **(d)** October

(e) November **(f)** December

Figure C.22 – 30 d summation $^{22}Na/^{7}Be$ for the last six months of 2008.

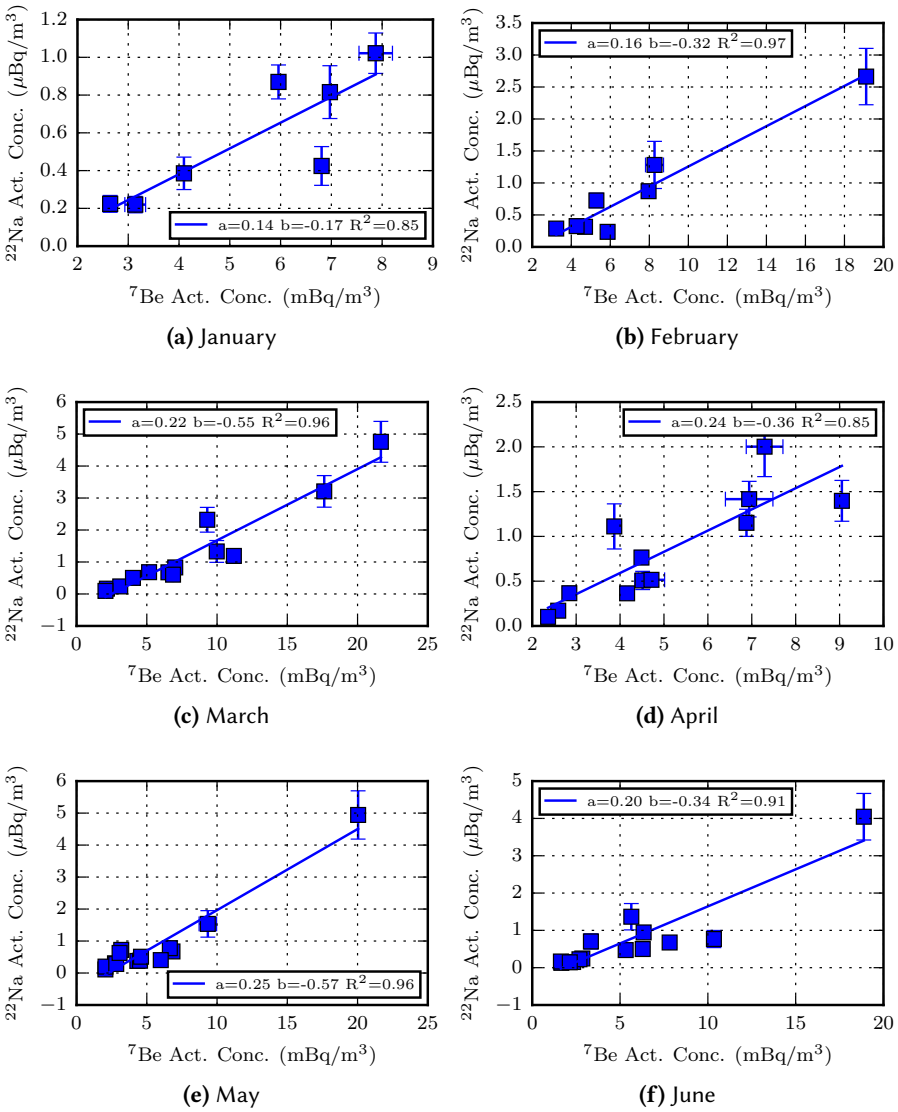

(a) January **(b)** February

(c) March **(d)** April

(e) May **(f)** June

Figure C.23 – 30 d summation $^{22}Na/^{7}Be$ for the first six months of 2009.

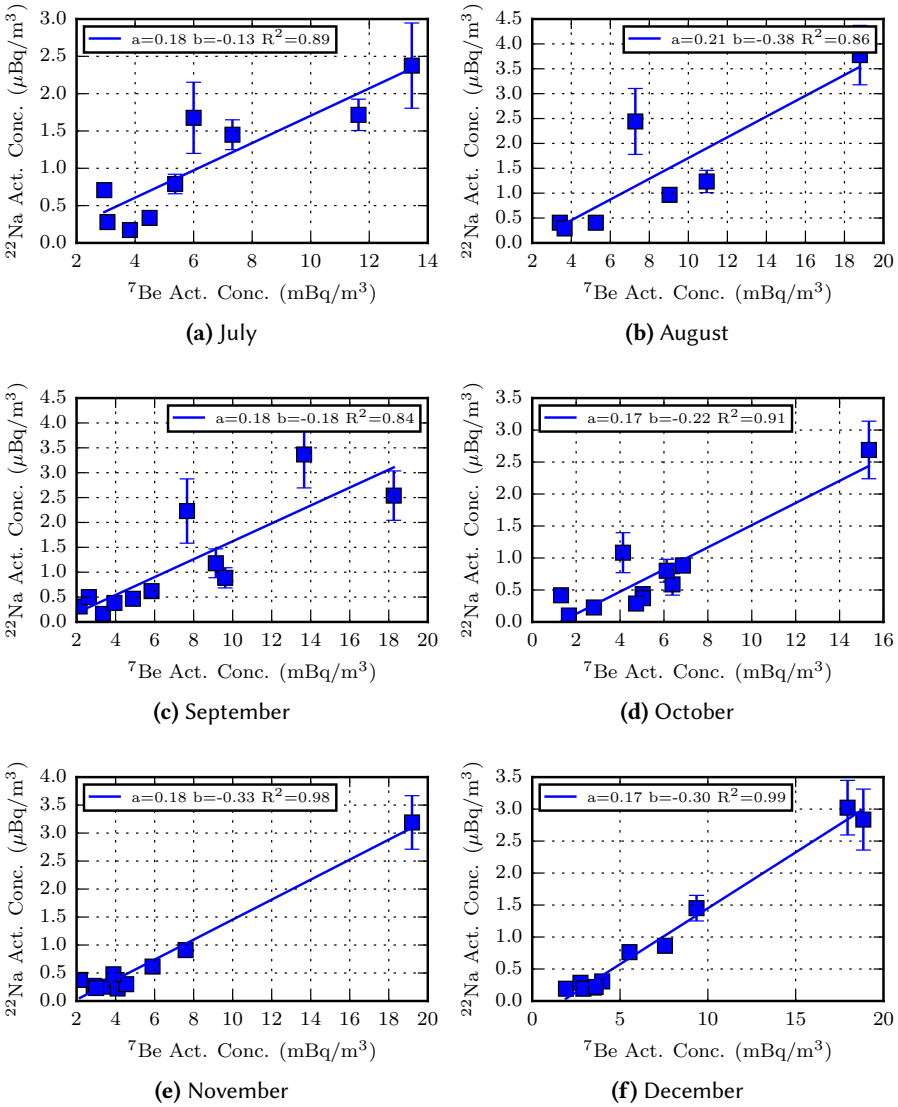

(a) July **(b)** August

(c) September **(d)** October

(e) November **(f)** December

Figure C.24 – 30 d summation ^{22}Na/^{7}Be for the last six months of 2009.

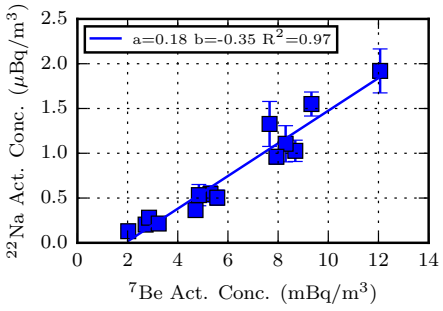

(a) January

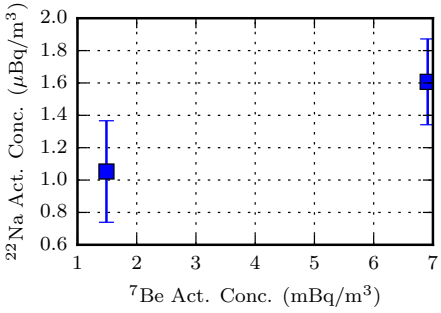

(b) March

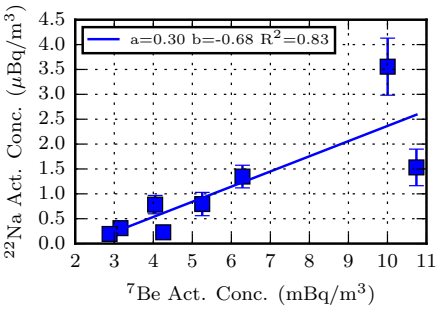

(c) April

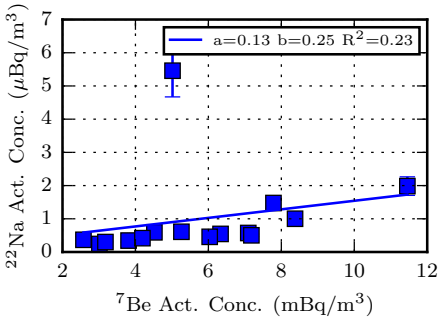

(d) May

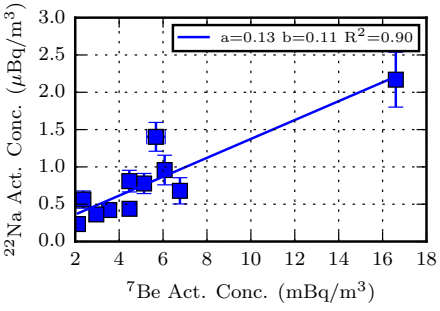

(e) June

Figure C.25 – 30 d summation ^{22}Na/^{7}Be for the first six months of 2010.

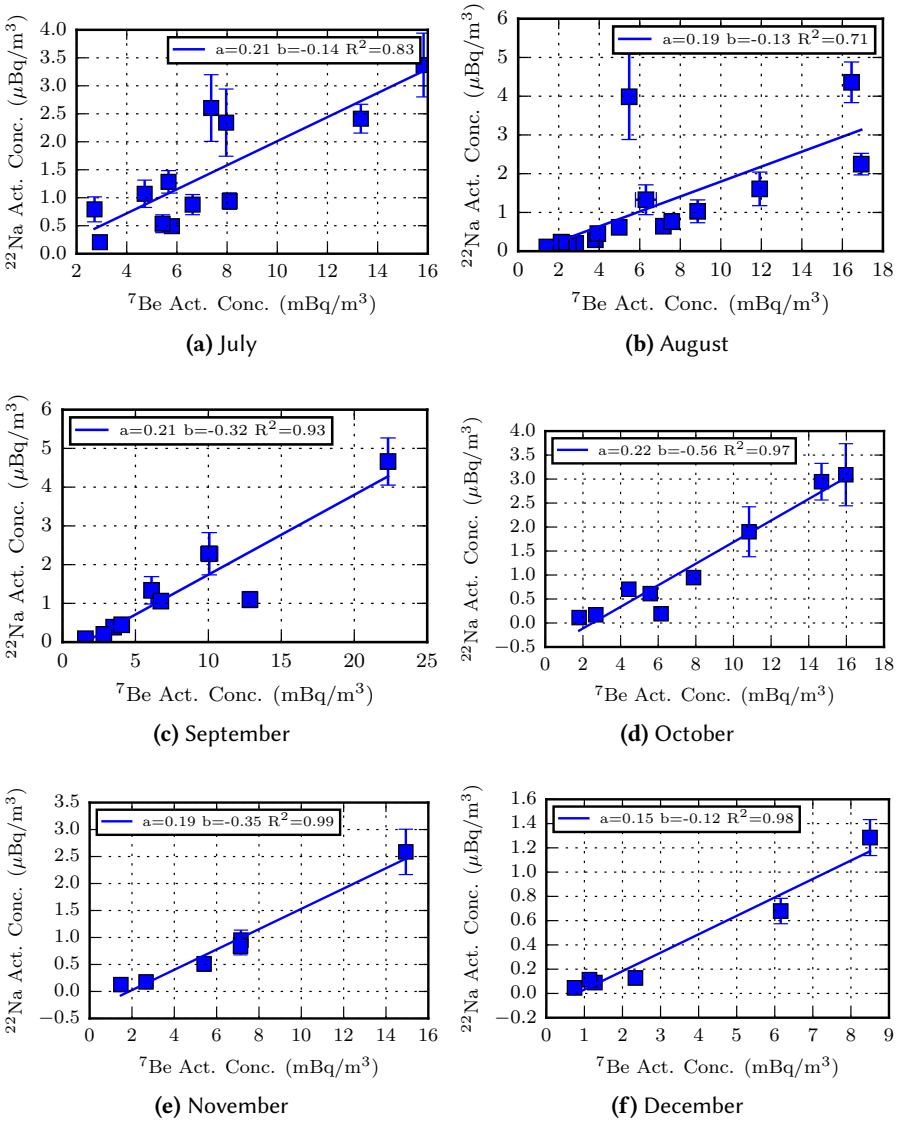

(a) July **(b)** August

(c) September **(d)** October

(e) November **(f)** December

Figure C.26 – 30 d summation ^{22}Na/^{7}Be for the last six months of 2010.

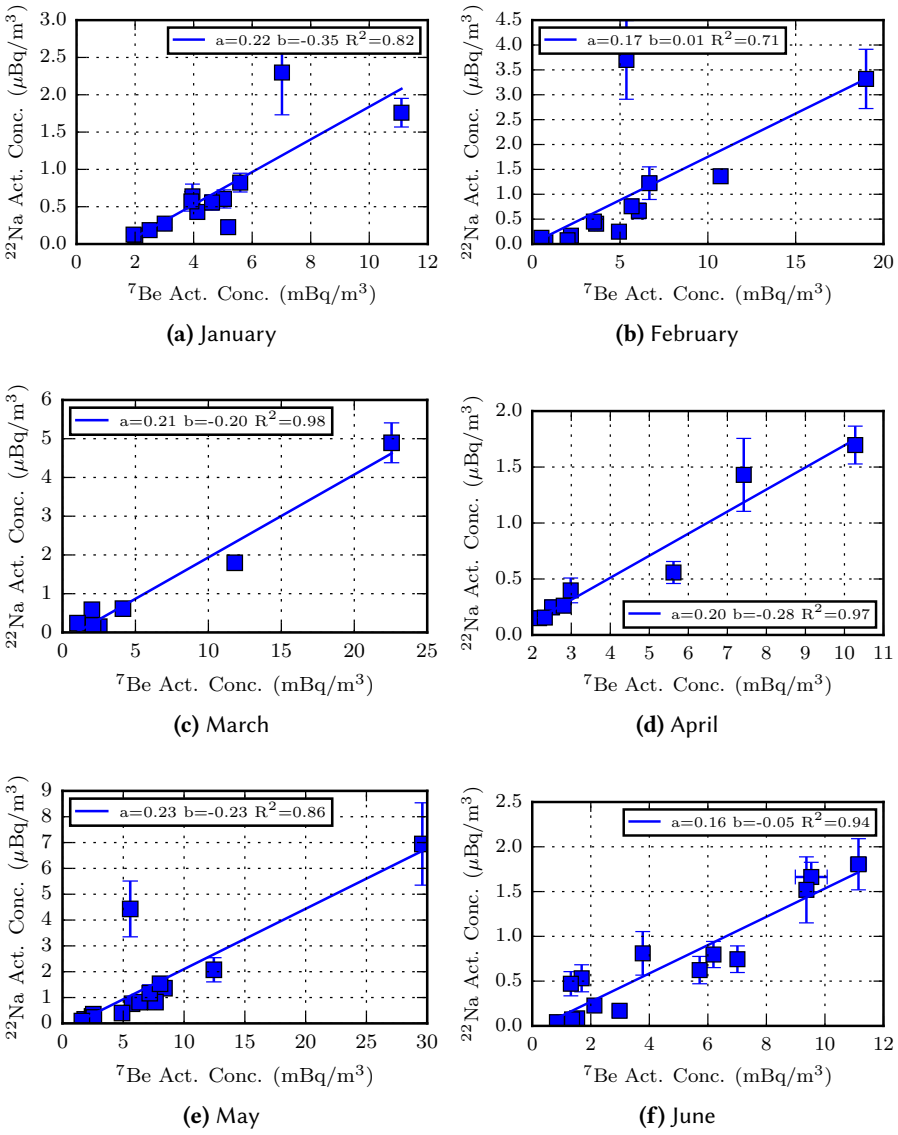

(a) January **(b)** February

(c) March **(d)** April

(e) May **(f)** June

Figure C.27 – 30 d summation $^{22}Na/^{7}Be$ for the last six months of 2011.

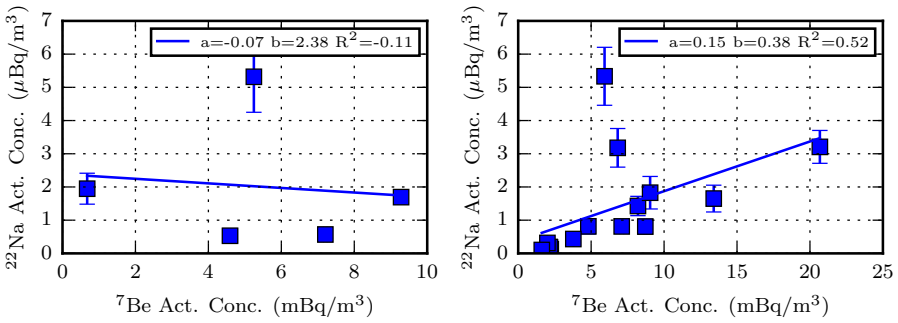

(a) July **(b)** August

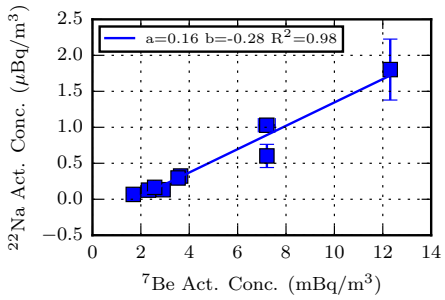

(c) September

Figure C.28 – 30 d summation ^{22}Na/^{7}Be for the last six months of 2011.

C.3 Summary Plots

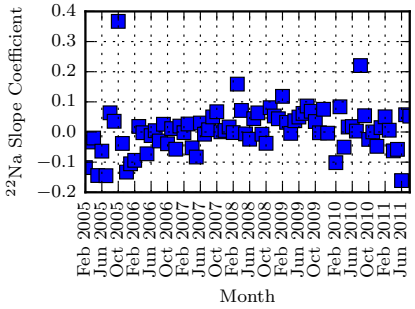

(a) ^{22}Na

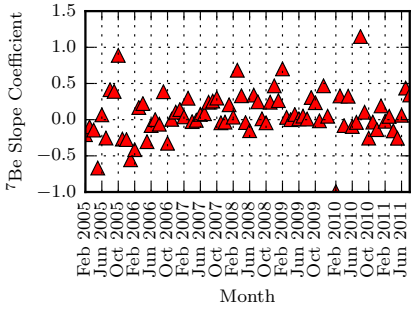

(b) ^{7}Be

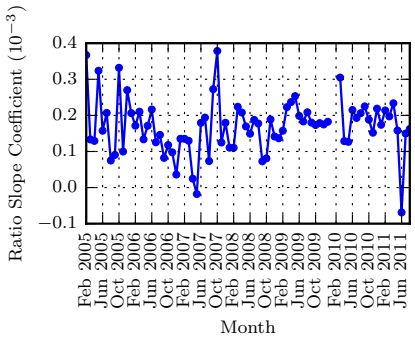

(c) ^{22}Na/^{7}Be

Figure C.29 – Plot of the monthly slope coefficient of the linear regression of ^{22}Na and ^{7}Be activity concentration as a function of R_c and the ^{22}Na/^{7}Be slope coefficient

D Complete Summation Data Table

Station	Collection Start (UTC)	Collection Stop (UTC)	Volume (m^3)	R_c (GV)	^{22}Na ($\mu Bq\,m^{-3}$)	^{7}Be ($mBq\,m^{-3}$)
NZP47	2005-02-12 20:10:43	2005-02-27 20:09:12	307 834	5.2	0.91(22)	5.438(29)
AUP08	2005-02-12 00:44:23	2005-02-28 00:53:38	282 036	14.3	0.67(9)	4.71(6)
FJP26	2005-02-12 01:31:12	2005-02-28 01:13:49	326 576	13.1	0.69(12)	5.542(29)
AUP04	2005-02-12 02:48:05	2005-02-28 03:11:17	344 941	2.9	6.0(13)	17.86(14)
AUP10	2005-02-12 04:32:44	2005-02-28 04:20:24	308 909	4.4	0.85(21)	2.69(4)
FRP28	2005-02-12 11:30:22	2005-02-28 11:21:31	214 803	10.7	0.58(14)	3.441(33)
CLP18	2005-02-11 15:42:42	2005-02-28 15:42:11	362 550	5.6	0.22(6)	2.127(12)
CAP16	2005-02-12 16:02:04	2005-02-28 16:11:06	377 732	0.2	0.78(22)	3.90(8)
GBP68	2005-02-12 17:27:06	2005-02-28 17:30:00	329 341	5.0	0.52(6)	4.320(30)
AUP10	2005-03-02 04:34:48	2005-03-29 04:18:48	549 490	4.4	0.60(15)	4.49(7)
SEP63	2005-03-02 08:58:35	2005-03-29 08:56:11	513 477	1.5	1.09(27)	6.05(7)
NZP47	2005-03-02 20:10:38	2005-03-29 21:09:04	552 084	5.2	1.01(11)	6.71(4)
AUP08	2005-03-02 00:50:42	2005-03-30 00:46:38	489 680	14.3	0.27(6)	3.27(4)
FJP26	2005-03-02 01:26:31	2005-03-30 01:16:41	575 803	13.1	0.26(8)	3.219(21)
DEP33	2005-03-02 06:25:47	2005-03-30 06:25:46	618 958	3.9	0.18(5)	3.014(30)

Station	Collection Start (UTC)	Stop (UTC)	Volume (m^3)	R_c (GV)	^{22}Na ($\mu Bq\,m^{-3}$)	^{7}Be ($mBq\,m^{-3}$)
CLP18	2005-03-02 15:42:24	2005-03-30 15:42:08	642 457	5.6	0.19(5)	1.645(9)
CLP19	2005-03-02 17:25:42	2005-03-30 17:25:42	679 119	12.2	0.48(11)	5.24(6)
GBP68	2005-03-02 17:51:07	2005-03-30 17:48:16	542 044	5.0	0.37(4)	4.12(4)
ARP01	2005-03-02 18:30:00	2005-03-30 18:10:00	353 459	9.0	0.59(16)	6.67(5)
USP72	2005-03-02 21:25:05	2005-03-30 21:25:06	481 014	4.7	0.60(15)	7.30(14)
AUP08	2005-03-31 00:44:22	2005-04-27 00:45:54	461 723	14.3	0.38(6)	4.48(6)
FJP26	2005-03-31 01:13:54	2005-04-29 01:12:23	596 665	13.1	0.26(6)	3.445(19)
DEP33	2005-03-31 06:25:48	2005-04-29 06:25:48	618 802	3.9	0.18(5)	3.290(28)
FRP28	2005-04-02 11:32:04	2005-04-29 11:20:00	171 318	10.7	0.84(23)	6.74(15)
CAP16	2005-03-31 16:26:00	2005-04-29 15:12:41	654 165	0.2	0.92(17)	6.392(32)
CLP19	2005-03-31 17:25:40	2005-04-29 17:25:41	689 699	12.2	0.56(15)	4.483(30)
GBP68	2005-03-31 17:35:41	2005-04-29 17:33:28	529 218	5.0	0.40(5)	3.68(7)
ARP01	2005-03-31 18:20:00	2005-04-29 18:10:00	365 973	9.0	1.29(15)	7.39(6)
NZP47	2005-03-31 21:10:18	2005-04-29 21:09:10	538 364	5.2	0.73(18)	6.17(4)
USP72	2005-03-31 21:25:05	2005-04-29 21:25:06	524 604	4.7	1.08(12)	11.23(29)
USP72	2005-04-30 21:25:04	2005-05-22 21:24:20	363 054	4.7	0.90(17)	8.61(17)
AUP08	2005-05-02 23:52:53	2005-05-29 00:42:11	321 734	14.3	4.5(11)	6.30(24)
DEP33	2005-04-30 06:25:46	2005-05-29 06:25:03	604 032	3.9	0.25(4)	3.78(4)
JPP38	2005-04-30 06:55:31	2005-05-29 06:55:33	681 794	11.5	0.89(17)	7.42(7)
KWP40	2005-04-30 09:25:41	2005-05-29 09:25:41	425 127	12.8	1.08(27)	10.89(21)
ISP34	2005-04-30 11:27:33	2005-05-29 11:23:38	401 297	0.4	10.2(17)	32.2(8)
FRP31	2005-04-30 11:33:05	2005-05-29 11:27:06	415 849	12.9	0.55(15)	1.89(4)
CAP16	2005-04-30 15:27:02	2005-05-29 14:58:36	675 158	0.2	1.45(18)	8.64(4)
GBP68	2005-04-30 17:50:38	2005-05-29 18:01:46	597 992	5.0	0.21(4)	2.909(23)
NZP47	2005-04-30 21:12:00	2005-05-29 21:09:06	570 045	5.2	0.50(11)	4.652(25)
JPP38	2005-05-30 06:55:34	2005-06-28 06:52:39	640 851	11.5	0.81(20)	6.11(12)
KWP40	2005-05-30 09:25:40	2005-06-28 09:25:42	425 963	12.8	1.28(30)	12.03(29)
CAP16	2005-05-30 15:06:46	2005-06-28 15:22:59	624 014	0.2	2.18(28)	10.22(6)

Station	Collection Start (UTC)	Stop (UTC)	Volume (m^3)	R_c (GV)	^{22}Na ($\mu Bq\,m^{-3}$)	^{7}Be ($mBq\,m^{-3}$)
NZP47	2005-05-30 21:10:37	2005-06-28 21:09:06	597 627	5.2	0.41(10)	4.030(21)
GBP66	2005-06-29 05:00:49	2005-07-24 05:00:50	431 878	15.2	0.30(8)	1.937(14)
AUP04	2005-06-29 04:01:56	2005-07-28 03:48:15	663 290	2.9	4.4(11)	10.30(6)
KWP40	2005-06-29 09:25:39	2005-07-28 09:25:42	426 604	12.8	1.36(20)	12.91(21)
FRP28	2005-06-29 11:53:15	2005-07-28 11:22:38	171 346	10.7	0.74(20)	3.48(26)
CAP16	2005-06-29 15:23:11	2005-07-28 15:01:51	640 292	0.2	1.25(27)	6.58(4)
FRP27	2005-06-29 18:51:00	2005-07-28 18:30:00	409 749	13.5	0.80(22)	3.065(25)
FJP26	2005-07-29 01:16:52	2005-08-27 01:19:04	606 769	13.1	0.63(9)	7.05(5)
AUP06	2005-07-29 02:39:23	2005-08-27 02:51:27	531 800	11.1	0.70(15)	4.03(15)
FRP28	2005-07-29 11:31:06	2005-08-27 11:22:43	444 387	10.7	0.56(13)	3.72(6)
GBP68	2005-07-29 17:41:52	2005-08-27 17:38:19	591 706	5.0	0.17(4)	2.86(8)
AUP08	2005-08-28 00:38:40	2005-09-26 00:35:13	520 179	14.3	0.92(15)	7.95(20)
FJP26	2005-08-28 01:39:56	2005-09-26 01:04:48	603 165	13.1	0.36(8)	3.204(17)
AUP06	2005-08-28 02:54:38	2005-09-26 02:53:04	434 207	11.1	0.65(15)	5.12(5)
FRP29	2005-08-28 03:23:51	2005-09-26 03:28:00	378 920	9.7	0.52(15)	4.51(4)
KWP40	2005-08-28 09:25:41	2005-09-26 09:25:40	426 869	12.8	1.02(20)	11.14(18)
GBP68	2005-08-28 17:43:11	2005-09-26 17:51:47	557 398	5.0	0.26(4)	2.690(16)
NZP47	2005-08-28 21:11:19	2005-09-26 21:09:03	577 800	5.2	0.72(11)	5.443(30)
AUP06	2005-09-27 03:08:47	2005-10-26 02:45:40	425 908	11.1	0.78(12)	5.06(5)
AUP04	2005-09-27 03:55:34	2005-10-26 03:48:39	634 926	2.9	4.2(10)	17.23(11)
AUP09	2005-09-27 02:21:13	2005-10-26 03:53:25	380 774	14.2	8.7(15)	26.59(17)
GBP68	2005-09-27 17:58:56	2005-10-26 17:39:28	493 776	5.0	1.08(22)	8.39(4)
ARP01	2005-09-27 18:20:00	2005-10-26 18:00:00	367 006	9.0	2.1(5)	17.3(5)
NZP47	2005-09-28 21:10:25	2005-10-26 20:12:11	568 835	5.2	0.57(9)	4.364(26)
AUP08	2005-10-27 00:45:13	2005-11-25 00:45:22	526 881	14.3	0.78(12)	5.65(13)
FJP26	2005-10-27 01:03:23	2005-11-25 01:11:59	599 378	13.1	0.34(7)	4.612(32)
AUP06	2005-10-27 02:43:54	2005-11-25 02:52:29	516 852	11.1	0.71(12)	5.09(5)
ARP03	2005-10-27 12:50:45	2005-11-25 12:39:02	388 863	8.8	1.01(18)	5.91(10)

Station	Collection Start (UTC)	Collection Stop (UTC)	Volume (m^3)	R_c (GV)	^{22}Na ($\mu Bq\,m^{-3}$)	^{7}Be ($mBq\,m^{-3}$)
GBP68	2005-10-27 17:34:20	2005-11-25 17:36:36	598 266	5.0	1.24(13)	7.39(8)
NZP47	2005-10-27 20:11:04	2005-11-25 20:09:13	595 551	5.2	0.90(14)	6.435(34)
USP72	2005-10-27 21:25:07	2005-11-25 21:25:07	502 475	4.7	0.66(12)	8.33(19)
FJP26	2005-11-26 01:16:26	2005-12-25 01:10:59	595 851	13.1	0.66(10)	6.15(6)
AUP08	2005-11-26 00:54:55	2005-12-25 01:21:01	529 806	14.3	0.65(13)	5.45(16)
AUP04	2005-11-26 02:41:14	2005-12-25 02:38:34	654 063	2.9	5.6(11)	22.22(18)
AUP10	2005-11-26 04:21:03	2005-12-25 04:13:45	642 667	4.4	0.16(4)	1.93(4)
ARP03	2005-11-26 12:36:25	2005-12-25 12:55:44	403 175	8.8	1.12(23)	10.45(6)
PAP50	2005-11-26 12:38:19	2005-12-25 13:05:36	641 034	11.3	0.22(6)	4.521(27)
CAP16	2005-11-26 16:39:22	2005-12-25 16:01:34	753 670	0.2	0.97(15)	4.204(25)
CLP19	2005-11-26 17:25:43	2005-12-25 17:25:43	472 617	12.2	0.66(18)	6.74(5)
GBP68	2005-11-26 17:39:16	2005-12-25 17:34:20	612 359	5.0	1.40(21)	7.55(15)
NZP47	2005-11-26 20:10:34	2005-12-25 20:09:12	581 005	5.2	0.82(13)	6.97(4)
NZP46	2005-12-26 00:10:03	2006-01-24 00:46:39	549 252	3.1	0.49(9)	5.279(35)
FJP26	2005-12-26 01:20:43	2006-01-24 01:07:20	553 573	13.1	0.139(26)	2.13(4)
AUP06	2005-12-26 02:44:08	2006-01-24 02:42:58	512 624	11.1	0.34(9)	4.40(9)
AUP04	2005-12-26 02:45:17	2006-01-24 03:11:03	643 206	2.9	4.7(12)	25.53(26)
FRP29	2005-12-26 03:20:25	2006-01-24 03:28:00	349 010	9.7	0.75(13)	5.260(35)
DEP33	2005-12-26 06:25:08	2006-01-24 06:25:51	647 441	3.9	0.171(31)	3.15(5)
PAP50	2005-12-26 13:42:01	2006-01-24 12:37:15	669 637	11.3	0.28(8)	4.96(4)
ARP03	2005-12-28 12:47:19	2006-01-24 12:44:59	355 454	8.8	1.44(25)	9.32(14)
CLP19	2005-12-26 17:39:48	2006-01-24 17:25:40	432 326	12.2	0.48(13)	2.2(4)
ARP01	2005-12-26 18:20:00	2006-01-24 18:30:00	353 808	9.0	3.8(5)	14.96(11)
USP75	2005-12-26 18:50:52	2006-01-24 18:50:49	744 285	2.5	1.16(17)	2.58(23)
NZP47	2005-12-26 20:10:41	2006-01-24 20:09:03	620 199	5.2	1.01(12)	8.34(5)
USP72	2005-12-26 21:25:10	2006-01-24 21:25:06	549 928	4.7	0.47(13)	7.26(14)
NZP46	2006-01-26 00:02:02	2006-02-23 00:28:54	523 723	3.1	0.83(12)	5.71(7)
FJP26	2006-01-25 01:06:34	2006-02-23 01:13:45	593 184	13.1	0.139(19)	2.18(4)

Station	Collection Start (UTC)	Collection Stop (UTC)	Volume (m^3)	R_c (GV)	^{22}Na ($\mu Bq\,m^{-3}$)	^{7}Be ($mBq\,m^{-3}$)
FRP29	2006-01-25 03:56:31	2006-02-23 03:30:52	372 736	9.7	0.62(11)	5.132(31)
PHP52	2006-01-25 05:45:41	2006-02-23 05:14:38	640 420	16.9	0.51(13)	4.76(6)
DEP33	2006-01-26 06:25:50	2006-02-23 06:25:49	608 450	3.9	0.29(4)	2.949(23)
PAP50	2006-01-25 11:49:36	2006-02-23 12:49:25	530 736	11.3	0.29(6)	4.08(10)
ARP03	2006-01-25 13:02:46	2006-02-23 12:50:36	427 704	8.8	1.43(22)	13.39(9)
CAP16	2006-01-25 16:25:48	2006-02-23 16:22:11	694 181	0.2	0.84(13)	5.221(25)
GBP68	2006-01-25 17:38:55	2006-02-23 17:18:58	607 451	5.0	1.77(23)	9.72(5)
CAP15	2006-01-25 22:55:09	2006-02-23 22:33:01	448 957	0.0	0.49(14)	3.45(9)
AUP04	2006-01-25 02:51:37	2006-02-23 22:43:37	651 331	2.9	4.1(11)	23.86(17)
FRP29	2006-02-24 03:43:07	2006-03-21 03:36:00	341 961	9.7	0.36(10)	2.49(28)
AUP08	2006-02-24 00:34:40	2006-03-25 00:34:10	522 503	14.3	0.54(11)	5.97(15)
NZP46	2006-02-24 00:46:19	2006-03-25 01:05:34	545 256	3.1	0.61(8)	4.88(5)
AUP10	2006-02-24 04:26:40	2006-03-25 04:21:41	643 629	4.4	0.30(6)	2.591(13)
PAP50	2006-02-24 13:42:05	2006-03-25 12:37:09	688 067	11.3	0.72(10)	7.75(4)
ARP03	2006-02-24 12:28:16	2006-03-25 12:47:15	421 033	8.8	1.20(20)	7.59(5)
CAP16	2006-02-24 16:21:35	2006-03-25 16:16:03	685 218	0.2	1.03(14)	6.507(32)
ARP01	2006-02-24 18:40:00	2006-03-25 18:20:00	366 042	9.0	3.7(5)	17.47(15)
GBP68	2006-02-24 17:41:56	2006-03-25 18:32:14	618 928	5.0	2.36(18)	11.54(7)
CAP17	2006-02-24 19:45:26	2006-03-25 19:23:13	689 476	1.6	0.42(7)	2.98(12)
NZP47	2006-02-24 20:10:37	2006-03-25 21:09:15	637 271	5.2	0.87(13)	7.89(10)
USP72	2006-02-23 21:25:06	2006-03-25 21:25:06	605 132	4.7	1.22(13)	11.44(31)
NZP46	2006-03-26 00:54:43	2006-04-24 01:21:11	551 549	3.1	0.39(7)	3.735(29)
PHP52	2006-03-26 06:24:47	2006-04-24 06:10:08	636 802	16.9	0.88(14)	8.33(5)
KWP40	2006-03-26 09:25:42	2006-04-24 09:25:42	426 980	12.8	0.85(22)	8.60(12)
PAP50	2006-03-26 13:05:07	2006-04-24 12:14:03	666 329	11.3	0.73(17)	9.16(8)
CAP16	2006-03-26 16:33:08	2006-04-24 15:12:18	657 351	0.2	1.75(16)	9.33(13)
CAP17	2006-03-26 20:15:53	2006-04-24 16:46:34	730 768	1.6	0.48(7)	3.642(19)
GBP68	2006-03-26 18:35:56	2006-04-24 17:52:41	620 771	5.0	1.60(23)	11.78(29)

Station	Collection Start (UTC)	Collection Stop (UTC)	Volume (m^3)	R_c (GV)	^{22}Na ($\mu Bq\,m^{-3}$)	^{7}Be ($mBq\,m^{-3}$)
USP72	2006-03-26 21:25:06	2006-04-24 21:03:00	578 172	4.7	0.96(12)	8.71(23)
AUP04	2006-03-26 22:31:17	2006-04-24 23:34:52	690 323	2.9	0.21(4)	1.848(12)
USP74	2006-03-26 23:35:05	2006-04-24 23:35:06	616 244	3.3	0.53(8)	5.319(23)
AUP08	2006-04-25 02:34:21	2006-05-24 00:52:51	520 046	14.3	0.58(10)	6.76(18)
AUP06	2006-04-25 01:28:39	2006-05-24 01:25:49	511 365	11.1	0.25(7)	3.16(4)
USP70	2006-04-25 03:05:20	2006-05-24 03:05:22	699 653	4.0	0.37(8)	5.22(5)
MNP45	2006-04-25 03:29:10	2006-05-24 03:29:11	374 731	5.0	0.89(25)	7.27(18)
CAP16	2006-04-25 15:24:30	2006-05-24 15:23:20	658 749	0.2	1.89(22)	9.37(6)
ARP01	2006-04-25 18:30:00	2006-05-24 18:30:00	364 871	9.0	0.39(10)	3.52(4)
USP75	2006-04-25 18:50:42	2006-05-24 18:50:49	705 429	2.5	0.89(24)	9.63(14)
NZP47	2006-04-25 21:09:58	2006-05-24 20:59:17	645 742	5.2	0.48(8)	4.509(29)
USP74	2006-05-25 23:35:06	2006-06-14 23:35:07	368 428	3.3	0.55(11)	2.0(4)
FJP26	2006-05-25 01:13:56	2006-06-15 00:35:50	436 274	13.1	0.099(29)	1.788(14)
AUP09	2006-05-25 02:09:00	2006-06-15 01:52:37	313 400	14.2	0.78(16)	5.05(5)
MNP45	2006-05-25 03:30:58	2006-06-15 03:28:36	258 630	5.0	1.11(32)	6.31(6)
DEP33	2006-05-25 06:04:16	2006-06-15 07:03:10	383 959	3.9	0.36(6)	4.185(31)
CLP19	2006-05-25 17:25:41	2006-06-16 17:25:38	429 657	12.2	0.54(16)	5.01(4)
NZP47	2006-05-26 21:06:31	2006-06-16 21:00:14	438 882	5.2	0.38(11)	3.650(22)
FRP28	2006-06-26 11:45:12	2006-07-21 11:07:52	285 067	10.7	0.60(13)	6.54(11)
FJP26	2006-06-24 01:01:22	2006-07-23 00:57:13	612 265	13.1	0.168(21)	3.090(16)
AUP08	2006-06-24 01:05:47	2006-07-23 02:05:18	519 984	14.3	0.90(14)	7.46(20)
MNP45	2006-06-24 03:28:10	2006-07-23 03:25:13	371 964	5.0	0.77(23)	6.53(6)
DEP33	2006-06-24 06:04:17	2006-07-23 06:04:17	565 970	3.9	0.41(5)	5.91(8)
GBP68	2006-06-24 17:28:05	2006-07-23 16:56:21	608 486	5.0	0.75(19)	7.64(23)
NZP47	2006-06-24 21:01:41	2006-07-23 20:59:40	647 147	5.2	0.41(9)	3.464(25)
USP74	2006-06-25 23:02:59	2006-07-23 23:35:08	679 760	3.3	0.45(9)	5.10(7)
NZP47	2006-07-24 21:01:26	2006-08-21 20:59:06	578 622	5.2	0.77(10)	4.84(6)
AUP08	2006-07-24 01:38:04	2006-08-22 00:40:37	519 860	14.3	0.86(14)	8.98(25)

Station	Collection Start (UTC)	Stop (UTC)	Volume (m^3)	R_c (GV)	^{22}Na ($\mu Bq\,m^{-3}$)	^{7}Be ($mBq\,m^{-3}$)
FJP26	2006-07-24 00:59:34	2006-08-22 01:15:14	610 108	13.1	0.171(26)	2.617(13)
NZP46	2006-07-24 01:03:59	2006-08-22 01:48:36	565 979	3.1	0.32(5)	3.57(9)
DEP33	2006-07-24 06:04:18	2006-08-22 06:04:19	552 019	3.9	0.20(4)	2.908(24)
CAP16	2006-07-24 15:32:33	2006-08-22 15:12:50	620 596	0.2	1.31(29)	8.97(6)
MRP43	2006-07-26 18:17:22	2006-08-22 16:56:57	490 292	13.9	0.163(30)	3.035(26)
GBP68	2006-08-23 17:36:48	2006-09-19 17:40:42	523 972	5.0	0.49(12)	4.06(10)
AUP08	2006-08-23 01:09:14	2006-09-21 00:34:18	521 240	14.3	1.26(11)	10.29(29)
FJP26	2006-08-23 01:03:15	2006-09-21 00:42:16	607 635	13.1	0.184(23)	2.307(13)
DEP33	2006-08-23 06:04:19	2006-09-21 06:04:16	562 514	3.9	0.20(5)	3.84(4)
SEP63	2006-09-15 09:00:23	2006-09-21 08:57:47	106 131	1.5	0.86(8)	0.868(12)
NZP47	2006-08-23 21:00:19	2006-09-21 20:44:11	642 712	5.2	0.54(11)	5.907(35)
AUP04	2006-08-23 22:36:48	2006-09-21 23:10:54	650 158	2.9	0.19(5)	1.900(21)
FJP26	2006-09-22 01:24:27	2006-10-21 00:52:33	585 985	13.1	0.123(21)	1.949(22)
GBP66	2006-09-22 05:25:40	2006-10-21 05:25:41	521 600	15.2	0.65(15)	6.356(34)
MRP43	2006-09-22 17:19:36	2006-10-21 16:55:00	500 475	13.9	0.24(7)	3.082(26)
GBP68	2006-09-23 18:06:13	2006-10-21 17:31:09	529 906	5.0	0.87(25)	7.06(14)
NZP47	2006-09-22 21:01:35	2006-10-21 20:00:15	608 341	5.2	0.63(14)	7.46(4)
NZP46	2006-10-22 00:10:46	2006-11-20 00:10:55	568 223	3.1	0.40(9)	4.93(5)
AUP08	2006-10-22 00:45:29	2006-11-20 00:35:31	518 130	14.3	0.299(29)	3.349(17)
AUP06	2006-10-22 02:16:03	2006-11-20 02:23:29	592 394	11.1	0.31(6)	3.81(4)
AUP10	2006-10-22 04:09:24	2006-11-20 04:09:55	511 004	4.4	0.18(5)	1.813(15)
CLP19	2006-10-22 20:38:10	2006-11-20 17:25:42	502 715	12.2	0.72(20)	6.84(5)
NZP47	2006-10-22 19:47:21	2006-11-20 19:30:32	614 968	5.2	0.61(10)	6.94(4)
USP72	2006-10-22 21:25:07	2006-11-20 21:25:06	645 567	4.7	0.16(4)	4.71(8)
AUP08	2006-11-21 00:37:09	2006-12-20 00:36:27	517 845	14.3	0.223(32)	3.46(7)
FJP26	2006-11-21 01:26:28	2006-12-20 00:56:18	599 395	13.1	0.199(31)	2.733(13)
AUP06	2006-11-22 02:28:04	2006-12-20 01:49:05	569 852	11.1	0.26(4)	3.94(4)
AUP10	2006-11-21 04:22:51	2006-12-20 04:12:43	638 624	4.4	0.20(4)	2.741(28)

Station	Collection Start (UTC)	Collection Stop (UTC)	Volume (m^3)	R_c (GV)	^{22}Na ($\mu Bq\,m^{-3}$)	^{7}Be ($mBq\,m^{-3}$)
ARP03	2006-11-21 12:36:11	2006-12-20 12:57:12	410 823	8.8	1.22(21)	9.62(7)
CAP17	2006-11-21 18:21:34	2006-12-20 17:56:27	740 245	1.6	1.5(4)	1.019(9)
USP72	2006-11-21 21:25:06	2006-12-20 21:25:06	645 542	4.7	0.202(33)	5.07(8)
AUP08	2006-12-21 01:08:48	2007-01-19 00:36:52	517 389	14.3	0.20(4)	3.108(20)
AUP09	2006-12-21 02:09:49	2007-01-19 02:18:39	514 642	14.2	0.79(19)	5.45(6)
AUP10	2006-12-21 04:47:06	2007-01-19 04:13:23	639 604	4.4	0.21(4)	2.649(25)
FRP28	2006-12-21 11:47:34	2007-01-19 11:20:00	385 823	10.7	0.58(15)	6.08(5)
GBP68	2006-12-21 17:49:08	2007-01-19 17:33:34	532 007	5.0	0.26(5)	2.73(4)
NZP47	2006-12-21 19:46:01	2007-01-19 20:00:12	637 069	5.2	0.71(13)	6.33(4)
AUP04	2006-12-21 22:34:33	2007-01-19 22:30:57	637 961	2.9	0.22(6)	2.27(4)
PAP50	2007-01-20 12:50:20	2007-02-10 12:35:20	488 329	11.3	0.80(14)	7.62(25)
AUP08	2007-01-20 00:35:12	2007-02-18 00:50:53	516 485	14.3	0.14(4)	1.909(10)
FJP26	2007-01-20 00:42:55	2007-02-18 01:00:05	595 018	13.1	0.132(23)	2.139(14)
MNP45	2007-01-20 03:28:25	2007-02-18 03:26:24	367 471	5.0	0.65(16)	6.05(6)
ARP03	2007-01-22 12:34:55	2007-02-18 12:32:27	387 672	8.8	1.43(26)	9.93(32)
TZP64	2007-01-20 13:11:20	2007-02-18 12:55:24	555 522	13.6	0.94(12)	8.26(6)
MRP43	2007-01-20 16:35:24	2007-02-18 16:28:57	538 248	13.9	0.44(6)	3.576(33)
GBP68	2007-01-20 17:40:50	2007-02-18 17:34:11	712 035	5.0	0.367(33)	3.71(8)
USP71	2007-01-20 20:11:05	2007-02-18 20:11:05	686 068	2.1	0.31(9)	1.99(6)
NZP47	2007-02-19 20:00:09	2007-03-19 20:59:03	535 750	5.2	1.40(16)	7.88(5)
NZP46	2007-02-19 00:28:19	2007-03-20 01:33:09	579 996	3.1	0.87(9)	6.14(8)
PAP50	2007-02-21 13:18:51	2007-03-20 11:47:10	606 592	11.3	1.11(13)	10.46(9)
TZP64	2007-02-19 13:19:31	2007-03-20 13:08:08	604 323	13.6	0.87(13)	6.02(4)
CLP19	2007-02-19 17:25:41	2007-03-20 17:25:40	503 806	12.2	0.70(20)	6.91(5)
GBP68	2007-02-19 17:33:39	2007-03-20 17:37:54	636 287	5.0	0.28(5)	3.55(8)
AUP04	2007-02-19 22:26:12	2007-03-20 22:15:41	713 722	2.9	0.24(4)	2.704(30)
CAP15	2007-02-19 22:56:09	2007-03-20 22:55:17	507 069	0.0	0.38(11)	2.38(6)
AUP08	2007-03-21 00:40:22	2007-04-19 00:19:34	513 565	14.3	0.125(29)	1.71(6)

Station	Collection Start (UTC)	Collection Stop (UTC)	Volume (m^3)	R_c (GV)	^{22}Na ($\mu Bq\,m^{-3}$)	^{7}Be ($mBq\,m^{-3}$)
USP70	2007-03-21 01:19:01	2007-04-19 01:19:01	700 283	4.0	0.42(11)	6.29(5)
AUP10	2007-03-21 05:07:40	2007-04-19 04:10:24	643 917	4.4	0.33(5)	2.44(6)
PHP52	2007-03-21 05:41:11	2007-04-19 05:32:35	649 807	16.9	0.86(18)	7.73(9)
PAP50	2007-03-21 11:54:55	2007-04-19 12:07:58	751 411	11.3	0.59(13)	6.31(8)
CAP16	2007-03-21 15:27:09	2007-04-19 15:18:39	724 930	0.2	1.30(15)	9.12(8)
CAP17	2007-03-21 17:39:50	2007-04-19 16:40:07	713 966	1.6	3.4(4)	1.287(9)
GBP67	2007-03-21 17:01:29	2007-04-19 17:02:14	678 431	9.8	1.9(4)	11.18(10)
GBP68	2007-03-21 17:36:24	2007-04-19 17:34:31	616 681	5.0	0.43(5)	4.37(8)
ARP01	2007-03-21 18:30:00	2007-04-19 17:40:00	365 832	9.0	0.59(17)	5.3(5)
MRP43	2007-03-21 16:55:15	2007-04-19 17:55:39	536 691	13.9	0.42(5)	3.575(30)
USP75	2007-03-21 18:50:34	2007-04-19 18:50:30	656 875	2.5	1.27(24)	9.55(12)
USP71	2007-03-21 20:11:08	2007-04-19 20:10:46	640 388	2.1	0.43(10)	4.15(23)
USP72	2007-03-21 21:24:46	2007-04-19 21:24:45	643 954	4.7	0.460(31)	7.40(16)
NZP46	2007-04-20 01:29:13	2007-05-19 01:15:21	565 216	3.1	0.39(7)	3.93(4)
FRP29	2007-04-21 03:28:41	2007-05-19 03:04:02	383 750	9.7	0.22(5)	2.886(16)
MNP45	2007-04-20 03:26:28	2007-05-19 03:30:52	305 711	5.0	0.89(25)	6.34(8)
TZP64	2007-04-20 12:51:32	2007-05-19 13:04:09	630 064	13.6	0.70(12)	4.285(29)
GBP67	2007-04-20 16:57:07	2007-05-19 17:01:07	679 675	9.8	1.26(35)	11.37(12)
CAP17	2007-04-20 17:09:12	2007-05-19 17:24:39	706 316	1.6	2.9(4)	1.253(6)
USP74	2007-04-20 18:34:46	2007-05-19 18:34:45	647 385	3.3	1.6(5)	9.09(14)
USP75	2007-04-20 18:50:29	2007-05-19 18:50:28	704 814	2.5	1.05(18)	10.21(11)
USP72	2007-04-20 21:24:45	2007-05-19 21:24:44	620 080	4.7	0.41(4)	6.54(10)
FRP29	2007-05-20 03:19:14	2007-06-17 03:37:51	412 625	9.7	0.22(6)	2.505(14)
DEP33	2007-05-20 06:25:44	2007-06-18 06:25:44	689 200	3.9	0.44(6)	4.45(7)
SEP63	2007-05-20 09:01:58	2007-06-18 09:02:11	400 431	1.5	0.20(5)	3.363(27)
TZP64	2007-05-21 13:12:47	2007-06-18 13:14:42	542 696	13.6	1.07(16)	6.64(5)
MRP43	2007-05-20 16:49:10	2007-06-18 16:19:34	504 823	13.9	0.26(7)	3.310(27)
GBP68	2007-05-20 17:33:27	2007-06-18 17:32:26	642 269	5.0	0.15(4)	2.43(4)

Station	Collection Start (UTC)	Collection Stop (UTC)	Volume (m^3)	R_c (GV)	^{22}Na ($\mu Bq\,m^{-3}$)	^{7}Be ($mBq\,m^{-3}$)
NZP47	2007-05-20 21:00:10	2007-06-18 20:59:04	628 293	5.2	0.47(13)	5.71(5)
MNP45	2007-06-19 03:29:08	2007-07-07 03:26:23	181 056	5.0	1.6(4)	7.81(7)
USP72	2007-06-19 21:24:44	2007-07-17 21:24:43	598 575	4.7	0.121(33)	3.10(4)
FJP26	2007-06-19 01:09:21	2007-07-18 01:01:59	606 432	13.1	0.123(30)	3.02(7)
KIP39	2007-06-19 03:04:20	2007-07-18 03:01:23	580 542	14.9	0.59(10)	5.56(7)
ISP34	2007-06-19 11:22:53	2007-07-18 11:20:13	390 932	0.4	0.25(6)	1.82(4)
TZP64	2007-06-19 13:18:45	2007-07-18 13:09:24	629 363	13.6	0.83(15)	6.13(4)
MRP43	2007-06-19 16:36:21	2007-07-18 16:29:51	535 634	13.9	0.26(4)	2.871(19)
GBP67	2007-06-19 16:58:08	2007-07-18 16:57:34	694 172	9.8	1.78(31)	11.60(12)
CLP19	2007-06-19 17:25:41	2007-07-18 17:25:38	502 162	12.2	0.52(12)	4.64(5)
AUP08	2007-07-19 01:09:48	2007-08-17 01:18:43	517 189	14.3	0.174(29)	2.65(8)
KIP39	2007-07-19 03:05:57	2007-08-17 03:00:50	581 791	14.9	0.66(12)	6.44(8)
AUP10	2007-07-19 04:16:22	2007-08-17 04:09:23	576 566	4.4	0.15(4)	1.59(4)
MRP43	2007-07-19 16:09:59	2007-08-17 16:28:21	569 634	13.9	0.137(34)	3.175(24)
GBP68	2007-07-19 17:34:13	2007-08-17 17:32:40	626 820	5.0	0.16(4)	2.58(5)
USP71	2007-07-19 20:10:46	2007-08-17 20:10:47	690 035	2.1	0.39(11)	0.98(4)
AUP08	2007-08-18 01:14:51	2007-09-16 01:18:11	515 213	14.3	0.227(34)	3.38(8)
FRP29	2007-08-18 03:21:00	2007-09-16 03:01:10	270 523	9.7	0.21(6)	2.594(21)
KIP39	2007-08-18 03:02:25	2007-09-16 03:06:08	585 738	14.9	0.49(12)	6.63(10)
AUP10	2007-08-18 03:57:21	2007-09-16 04:12:34	655 384	4.4	0.13(4)	1.820(15)
FRP31	2007-08-18 11:23:14	2007-09-16 11:32:26	416 218	12.9	2.2(6)	7.63(7)
TZP64	2007-08-18 12:49:52	2007-09-16 12:18:13	678 053	13.6	0.82(13)	5.88(6)
CAP17	2007-08-18 17:19:12	2007-09-16 16:30:11	710 998	1.6	0.18(5)	2.997(25)
MRP43	2007-08-18 16:10:02	2007-09-16 16:38:34	564 734	13.9	0.26(5)	3.362(34)
GBP67	2007-08-18 16:57:50	2007-09-16 17:11:03	773 782	9.8	0.15(4)	2.70(8)
AUP08	2007-09-17 01:45:56	2007-10-15 01:38:21	498 956	14.3	0.185(34)	3.28(12)
KIP39	2007-09-17 03:12:32	2007-10-15 23:38:49	585 700	14.9	0.56(11)	6.41(8)
AUP09	2007-09-17 02:10:10	2007-10-16 02:10:54	571 206	14.2	0.42(9)	5.167(30)

Station	Collection Start (UTC)	Collection Stop (UTC)	Volume (m^3)	R_c (GV)	^{22}Na ($\mu Bq\,m^{-3}$)	^{7}Be ($mBq\,m^{-3}$)
FRP29	2007-09-17 03:18:09	2007-10-16 02:58:27	313 341	9.7	0.26(6)	2.675(29)
FRP31	2007-09-17 11:37:24	2007-10-16 11:21:41	406 627	12.9	2.9(6)	8.20(5)
GBP67	2007-09-17 17:04:03	2007-10-16 17:06:02	631 641	9.8	0.42(6)	5.59(5)
GBP68	2007-09-17 17:32:35	2007-10-16 17:35:12	647 268	5.0	0.18(4)	2.72(17)
NZP46	2007-10-17 00:17:52	2007-11-15 00:24:50	600 005	3.1	0.40(8)	4.45(9)
FJP26	2007-10-17 01:26:28	2007-11-15 01:01:46	601 274	13.1	0.103(23)	1.594(25)
AUP10	2007-10-17 04:09:00	2007-11-15 04:13:02	683 801	4.4	0.18(5)	2.53(6)
FRP28	2007-10-17 11:21:15	2007-11-15 11:24:06	401 569	10.7	0.58(16)	5.28(31)
ARP03	2007-10-24 12:31:49	2007-11-15 12:37:36	260 018	8.8	0.61(16)	4.46(10)
GBP67	2007-10-17 17:16:14	2007-11-15 17:00:10	586 635	9.8	0.43(6)	5.08(6)
ARP03	2007-11-17 12:43:49	2007-12-13 13:14:35	362 864	8.8	1.16(13)	8.30(9)
TZP64	2007-11-16 13:17:07	2007-12-14 13:09:50	529 742	13.6	0.86(14)	6.61(8)
NZP46	2007-11-16 00:48:50	2007-12-15 00:26:03	598 544	3.1	0.58(8)	5.80(31)
FJP26	2007-11-16 01:09:46	2007-12-15 00:46:13	601 752	13.1	0.129(23)	2.210(17)
AUP09	2007-11-16 02:18:19	2007-12-15 02:11:09	557 227	14.2	0.47(8)	4.418(31)
FRP29	2007-11-16 03:25:28	2007-12-15 03:04:37	340 075	9.7	0.18(5)	3.53(5)
DEP33	2007-11-16 06:25:42	2007-12-15 06:25:45	672 268	3.9	0.19(4)	2.889(27)
GBP67	2007-11-16 17:04:03	2007-12-15 16:47:29	587 790	9.8	0.34(6)	4.11(4)
GBP68	2007-11-16 17:42:26	2007-12-15 17:42:42	594 668	5.0	0.214(34)	2.99(21)
NZP47	2007-11-16 19:56:19	2007-12-15 19:59:04	595 816	5.2	1.08(11)	7.27(6)
USP72	2007-11-16 21:24:45	2007-12-15 21:17:54	639 484	4.7	0.175(32)	5.22(10)
CLP18	2007-12-16 23:32:40	2008-01-07 23:31:32	501 540	5.6	0.40(11)	2.59(4)
NZP46	2007-12-16 00:12:03	2008-01-14 00:25:53	601 755	3.1	0.49(9)	5.93(4)
FJP26	2007-12-16 01:18:33	2008-01-14 01:09:23	600 217	13.1	0.055(15)	1.190(30)
DEP33	2007-12-16 06:25:44	2008-01-14 06:04:18	655 311	3.9	0.32(7)	4.543(33)
ISP34	2008-01-02 12:12:43	2008-01-14 11:21:52	157 132	0.4	0.85(13)	1.38(4)
FRP31	2007-12-16 11:29:18	2008-01-14 11:25:53	388 874	12.9	1.5(4)	10.84(8)
ARP03	2007-12-16 11:25:05	2008-01-14 11:36:43	296 206	8.8	1.08(17)	8.52(17)

Station	Collection Start (UTC)	Collection Stop (UTC)	Volume (m^3)	R_c (GV)	^{22}Na ($\mu Bq\,m^{-3}$)	^{7}Be ($mBq\,m^{-3}$)
MRP43	2007-12-16 16:13:12	2008-01-14 16:18:30	538 549	13.9	0.27(6)	3.570(30)
GBP67	2007-12-16 17:07:48	2008-01-14 17:05:25	566 034	9.8	0.62(7)	6.73(6)
GBP68	2007-12-16 17:38:17	2008-01-14 17:33:13	548 105	5.0	0.221(32)	3.03(22)
CAP17	2007-12-16 17:40:47	2008-01-14 18:12:07	748 323	1.6	0.18(4)	2.28(4)
AUP04	2007-12-16 22:36:40	2008-01-14 22:07:00	564 653	2.9	0.46(10)	6.05(4)
GBP68	2008-01-15 17:33:02	2008-02-09 17:31:10	478 844	5.0	0.33(5)	3.12(17)
JPP37	2008-01-15 00:23:53	2008-02-13 00:23:54	634 665	15.0	0.63(17)	8.15(8)
NZP46	2008-01-15 00:29:39	2008-02-13 00:25:43	557 810	3.1	0.55(8)	4.66(23)
FJP26	2008-01-15 01:06:17	2008-02-13 00:54:33	600 234	13.1	0.075(19)	1.690(30)
AUP08	2008-01-15 01:44:13	2008-02-13 01:42:47	474 937	14.3	0.48(12)	5.681(26)
MNP45	2008-01-15 03:28:40	2008-02-13 03:27:20	374 401	5.0	0.68(16)	6.34(9)
PHP52	2008-01-15 05:42:39	2008-02-13 05:27:23	826 403	16.9	0.32(8)	3.864(27)
PAP50	2008-01-18 12:30:58	2008-02-13 12:14:13	613 176	11.3	0.51(9)	7.44(5)
ARP03	2008-01-15 11:16:54	2008-02-13 13:17:38	279 139	8.8	1.31(19)	10.86(10)
GBP67	2008-01-15 16:58:41	2008-02-13 17:09:46	561 703	9.8	0.38(5)	4.054(33)
USP71	2008-01-15 20:10:47	2008-02-13 20:10:49	694 410	2.1	0.34(8)	4.63(25)
USP72	2008-01-15 21:24:45	2008-02-13 21:24:45	622 834	4.7	0.253(35)	5.80(8)
AUP04	2008-01-15 22:34:20	2008-02-13 22:01:45	625 965	2.9	0.46(10)	4.748(27)
NZP46	2008-02-14 00:29:24	2008-03-14 00:55:33	584 088	3.1	0.73(11)	5.25(26)
FJP26	2008-02-14 01:09:52	2008-03-14 01:26:00	603 349	13.1	0.093(25)	1.52(11)
MNP45	2008-02-14 03:30:15	2008-03-14 03:27:52	368 487	5.0	0.98(20)	7.11(22)
DEP33	2008-02-14 06:04:15	2008-03-14 06:04:13	591 701	3.9	0.43(8)	4.538(30)
PAP50	2008-02-14 12:51:13	2008-03-14 11:04:13	658 410	11.3	0.72(11)	7.81(7)
TZP64	2008-02-14 12:33:48	2008-03-14 13:16:58	574 149	13.6	4.4(5)	20.28(13)
ARP01	2008-02-14 17:30:00	2008-03-14 17:20:00	366 736	9.0	2.7(6)	15.35(9)
AUP04	2008-02-14 22:22:41	2008-03-14 22:15:28	645 041	2.9	0.61(11)	4.69(6)
CLP18	2008-01-08 23:32:38	2008-03-14 23:32:26	409 597	5.6	0.56(16)	2.99(4)
GBP68	2008-03-17 17:51:45	2008-04-11 17:35:39	480 465	5.0	0.33(4)	2.75(14)

Station	Collection Start (UTC)	Collection Stop (UTC)	Volume (m^3)	R_c (GV)	^{22}Na ($\mu Bq\,m^{-3}$)	^{7}Be ($mBq\,m^{-3}$)
AUP08	2008-03-15 01:40:07	2008-04-13 01:46:34	511 111	14.3	0.58(8)	5.07(10)
AUP09	2008-03-17 02:10:44	2008-04-13 02:11:37	450 711	14.2	0.36(8)	3.640(16)
AUP10	2008-03-15 04:11:10	2008-04-13 04:06:43	683 009	4.4	0.24(4)	2.784(29)
RUP54	2008-03-15 06:46:01	2008-04-13 05:51:12	646 522	1.6	0.33(7)	4.03(4)
FRP31	2008-03-15 11:34:57	2008-04-13 11:31:21	415 904	12.9	1.8(4)	11.48(9)
TZP64	2008-03-15 12:57:10	2008-04-13 12:32:16	558 316	13.6	2.3(4)	10.43(7)
CAP17	2008-03-15 17:44:34	2008-04-13 16:31:28	744 533	1.6	0.325(33)	3.13(6)
USP75	2008-03-15 18:50:31	2008-04-13 18:50:24	697 822	2.5	0.47(13)	3.4(4)
USP71	2008-03-15 20:10:49	2008-04-13 20:10:49	565 191	2.1	0.41(9)	4.67(31)
USP72	2008-03-15 21:24:46	2008-04-13 21:24:46	644 648	4.7	0.251(30)	5.38(8)
CAP15	2008-03-15 22:55:14	2008-04-13 22:55:08	409 180	0.0	0.22(6)	5.11(15)
AUP04	2008-03-15 22:24:36	2008-04-13 23:13:40	653 101	2.9	0.78(10)	3.550(23)
FRP29	2008-04-14 03:25:32	2008-05-10 03:03:10	370 322	9.7	0.26(7)	2.114(18)
FJP26	2008-04-14 01:06:01	2008-05-13 01:19:27	604 593	13.1	0.100(21)	1.95(4)
AUP08	2008-04-14 01:46:31	2008-05-13 02:00:09	495 680	14.3	0.67(9)	4.80(19)
RUP54	2008-04-14 06:07:28	2008-05-13 05:12:07	593 733	1.6	0.67(9)	5.715(35)
DEP33	2008-04-15 06:04:09	2008-05-13 06:04:11	601 556	3.9	0.62(7)	5.33(4)
PAP50	2008-04-14 10:58:39	2008-05-13 12:32:02	675 817	11.3	0.60(12)	7.96(11)
JPP38	2008-04-14 06:55:37	2008-05-13 12:58:34	580 289	11.5	0.43(9)	5.58(11)
MRP43	2008-04-14 16:14:02	2008-05-13 16:09:21	479 668	13.9	0.39(5)	3.71(5)
ARP01	2008-04-14 17:40:00	2008-05-13 17:00:00	350 272	9.0	3.0(7)	17.37(11)
CAP17	2008-04-14 16:38:41	2008-05-13 17:21:05	685 413	1.6	0.341(34)	3.35(6)
GBP68	2008-04-22 17:42:46	2008-05-13 17:35:17	378 661	5.0	0.23(6)	1.97(4)
USP75	2008-04-14 18:50:24	2008-05-13 18:49:45	672 379	2.5	1.29(24)	9.41(7)
USP71	2008-04-14 20:10:49	2008-05-13 20:10:49	693 985	2.1	0.51(10)	4.28(33)
USP72	2008-04-14 21:24:46	2008-05-13 21:24:46	643 761	4.7	0.45(4)	7.33(11)
CAP15	2008-04-14 22:55:08	2008-05-13 22:55:05	390 775	0.0	0.28(4)	4.19(10)
RUP54	2008-05-14 05:42:33	2008-06-04 06:06:25	399 510	1.6	0.64(9)	5.09(8)

Station	Collection Start (UTC)	Collection Stop (UTC)	Volume (m^3)	R_c (GV)	^{22}Na ($\mu Bq\,m^{-3}$)	^{7}Be ($mBq\,m^{-3}$)
RUP56	2008-05-14 00:05:54	2008-06-12 00:10:23	569 935	1.8	0.55(11)	6.44(10)
USP74	2008-05-15 00:32:39	2008-06-12 01:04:46	643 986	3.3	0.98(21)	7.61(9)
AUP08	2008-05-14 01:54:30	2008-06-12 01:46:30	514 877	14.3	0.31(6)	4.83(20)
FRP29	2008-05-14 04:49:32	2008-06-12 03:05:56	266 039	9.7	0.20(6)	1.59(7)
DEP33	2008-05-14 06:04:11	2008-06-12 06:04:11	552 064	3.9	0.48(7)	4.10(4)
SEP63	2008-05-14 08:46:00	2008-06-12 08:43:37	421 566	1.5	0.14(4)	3.012(33)
MRP43	2008-05-14 17:27:16	2008-06-12 16:21:31	447 925	13.9	0.156(31)	2.464(14)
USP75	2008-05-14 18:49:45	2008-06-12 18:49:45	698 444	2.5	1.25(23)	9.41(6)
FRP28	2008-06-13 11:37:16	2008-06-28 11:31:44	210 596	10.7	1.11(23)	8.29(18)
RUP56	2008-06-13 00:06:12	2008-07-11 23:59:47	480 345	1.8	0.80(10)	7.00(6)
AUP08	2008-06-13 01:56:23	2008-07-12 01:41:34	515 335	14.3	0.35(11)	4.43(19)
FRP29	2008-06-13 03:17:15	2008-07-12 03:02:45	397 517	9.7	0.23(6)	2.446(30)
MNP45	2008-06-13 03:32:55	2008-07-12 03:26:28	370 523	5.0	1.52(26)	7.13(31)
KWP40	2008-06-13 09:22:47	2008-07-12 09:25:43	411 831	12.8	1.17(20)	10.74(13)
TZP64	2008-06-13 12:58:20	2008-07-12 12:45:22	562 075	13.6	3.3(5)	18.40(12)
MRP43	2008-06-13 16:11:28	2008-07-12 16:22:33	543 955	13.9	0.179(20)	2.798(13)
GBP67	2008-06-13 17:22:34	2008-07-12 17:01:29	528 374	9.8	0.21(5)	3.875(32)
GBP68	2008-06-13 17:33:16	2008-07-12 17:32:22	602 849	5.0	0.22(5)	2.65(6)
AUP04	2008-06-13 23:12:24	2008-07-12 23:11:58	668 836	2.9	0.28(8)	2.244(14)
USP77	2008-07-13 03:29:49	2008-08-07 07:15:40	120 622	14.5	0.95(16)	0.57(22)
RUP56	2008-07-13 00:05:37	2008-08-11 00:00:59	506 985	1.8	0.43(11)	5.75(4)
AUP08	2008-07-13 01:48:16	2008-08-11 01:40:09	497 980	14.3	0.42(9)	4.75(21)
AUP09	2008-07-13 02:07:48	2008-08-11 02:20:10	580 225	14.2	0.55(12)	3.89(4)
AUP06	2008-07-13 02:44:04	2008-08-11 02:37:21	632 752	11.1	0.24(7)	2.520(30)
FRP29	2008-07-13 03:17:40	2008-08-11 03:02:54	414 727	9.7	0.15(4)	2.208(31)
MNP45	2008-07-13 03:34:55	2008-08-11 03:27:33	358 641	5.0	1.24(26)	9.78(6)
AUP10	2007-07-28 04:11:55	2008-08-11 04:11:26	653 954	4.4	0.17(5)	6.17(21)
KWP40	2008-07-13 09:25:42	2008-08-11 09:25:46	426 992	12.8	1.11(21)	10.62(10)

Station	Collection Start (UTC)	Collection Stop (UTC)	Volume (m^3)	R_c (GV)	^{22}Na ($\mu Bq\,m^{-3}$)	^{7}Be ($mBq\,m^{-3}$)
TZP64	2008-07-13 12:11:40	2008-08-11 12:39:34	580 478	13.6	2.9(6)	15.22(11)
GBP68	2008-07-13 17:32:06	2008-08-11 17:36:28	630 142	5.0	0.121(32)	2.01(5)
USP71	2008-07-13 20:10:45	2008-08-11 20:10:45	628 593	2.1	0.39(8)	2.92(7)
USP72	2008-07-13 21:24:46	2008-08-11 21:24:45	604 012	4.7	0.142(27)	3.59(5)
RUP56	2008-08-12 00:03:42	2008-09-10 00:00:29	501 006	1.8	0.31(9)	2.813(20)
AUP08	2008-08-12 01:41:02	2008-09-10 01:37:19	480 108	14.3	0.34(8)	4.33(18)
FRP29	2008-08-12 03:16:31	2008-09-10 03:04:31	323 794	9.7	0.32(7)	2.674(29)
MRP43	2008-08-12 16:08:12	2008-09-10 15:52:58	519 794	13.9	0.158(29)	2.239(13)
USP71	2008-08-14 20:10:45	2008-09-10 20:10:45	535 425	2.1	0.39(9)	3.44(8)
FJP26	2008-09-11 01:11:56	2008-10-10 00:50:58	583 992	13.1	0.178(25)	2.77(7)
USP77	2008-09-11 01:34:49	2008-10-10 01:34:51	461 895	14.5	0.76(6)	2.638(28)
AUP08	2008-09-11 01:46:45	2008-10-10 01:37:33	496 981	14.3	0.43(10)	4.21(18)
MNP45	2008-09-11 03:27:23	2008-10-10 03:26:01	359 712	5.0	1.01(29)	7.03(5)
FRP30	2008-09-11 05:11:29	2008-10-10 05:09:24	399 666	1.2	1.06(24)	2.90(35)
FRP28	2008-09-11 11:27:36	2008-10-10 11:25:23	386 650	10.7	0.43(12)	2.87(4)
USP71	2008-09-11 20:10:46	2008-10-10 19:39:24	627 299	2.1	0.66(13)	2.71(7)
NZP46	2008-10-11 00:15:03	2008-11-08 23:39:13	545 207	3.1	0.106(16)	1.937(13)
FJP26	2008-10-11 01:09:32	2008-11-09 01:21:31	549 285	13.1	0.125(33)	2.492(17)
USP77	2008-10-11 01:34:50	2008-11-09 01:34:49	602 518	14.5	0.72(7)	2.965(20)
AUP08	2008-10-11 01:52:49	2008-11-09 01:45:05	478 598	14.3	0.53(6)	4.12(18)
DEP33	2008-10-11 06:04:10	2008-11-09 06:04:11	610 547	3.9	0.24(6)	4.389(26)
TZP64	2008-10-11 12:05:09	2008-11-09 13:04:31	554 297	13.6	3.3(4)	14.86(12)
ARP01	2008-10-11 17:50:00	2008-11-09 16:10:00	353 013	9.0	2.6(7)	17.66(14)
AUP04	2008-10-11 22:11:06	2008-11-09 22:11:06	639 968	2.9	0.45(12)	3.483(20)
NZP46	2008-11-10 00:21:57	2008-12-09 00:09:03	558 250	3.1	0.096(17)	2.16(11)
FJP26	2008-11-10 01:15:08	2008-12-09 01:04:03	599 611	13.1	0.205(22)	2.841(14)
AUP08	2008-11-10 01:40:29	2008-12-09 01:38:32	514 772	14.3	0.64(7)	5.89(24)
AUP06	2008-11-10 02:18:28	2008-12-09 02:53:02	611 349	11.1	0.28(5)	3.372(22)

Station	Collection Start (UTC)	Collection Stop (UTC)	Volume (m^3)	R_c (GV)	^{22}Na ($\mu Bq\,m^{-3}$)	^{7}Be ($mBq\,m^{-3}$)
FRP30	2008-11-10 05:06:58	2008-12-09 05:04:32	415 773	1.2	0.89(21)	3.63(14)
TZP64	2008-11-10 13:14:33	2008-12-09 12:48:37	573 336	13.6	2.7(4)	20.07(13)
GBP68	2008-11-10 17:35:56	2008-12-09 17:36:02	546 507	5.0	0.21(6)	3.30(18)
FRP27	2008-11-10 18:32:00	2008-12-09 18:30:00	417 049	13.5	0.71(18)	5.81(4)
AUP04	2008-11-10 22:15:10	2008-12-09 22:10:27	652 466	2.9	0.27(7)	3.461(20)
USP77	2008-12-10 01:34:47	2009-01-08 01:34:50	660 256	14.5	0.87(9)	5.96(4)
AUP08	2008-12-10 01:39:01	2009-01-08 01:36:49	514 120	14.3	1.02(11)	7.87(33)
AUP10	2008-12-10 04:13:01	2009-01-08 04:13:23	664 854	4.4	0.22(4)	2.644(28)
PHP52	2008-12-10 05:36:47	2009-01-08 05:28:02	797 663	16.9	0.39(9)	4.097(26)
PAP50	2008-12-10 10:31:12	2009-01-08 12:43:38	678 301	11.3	0.42(10)	6.81(4)
CLP19	2008-12-10 15:10:06	2009-01-08 15:10:05	494 774	12.2	0.82(14)	6.97(4)
GBP68	2008-12-10 17:32:00	2009-01-08 17:37:54	520 725	5.0	0.22(4)	3.14(20)
NZP46	2009-01-09 00:29:53	2009-02-06 23:38:43	586 681	3.1	0.057(17)	0.38(7)
AUP08	2009-01-09 01:43:56	2009-02-07 01:45:38	509 773	14.3	0.87(10)	7.96(32)
RUP59	2009-01-09 02:35:04	2009-02-07 02:24:29	696 221	2.9	0.31(6)	4.70(4)
DEP33	2009-01-09 06:04:12	2009-02-07 06:04:11	598 633	3.9	0.33(6)	4.274(24)
FRP31	2009-01-09 11:36:49	2009-02-07 11:22:39	409 058	12.9	1.3(4)	8.3(5)
TZP64	2009-01-09 12:53:02	2009-02-07 12:48:52	552 092	13.6	2.7(4)	19.11(19)
GBP68	2009-01-09 17:34:15	2009-02-07 17:33:41	572 133	5.0	0.29(5)	3.23(19)
AUP04	2009-01-09 22:46:57	2009-02-07 20:37:34	637 100	2.9	0.73(11)	5.288(30)
USP72	2009-01-09 21:24:46	2009-02-07 21:24:47	604 801	4.7	0.24(4)	5.86(8)
USP74	2009-02-08 00:04:47	2009-03-09 00:04:48	712 805	3.3	1.33(34)	9.98(14)
USP77	2009-02-08 01:02:43	2009-03-09 01:34:49	686 789	14.5	0.68(9)	5.161(35)
AUP08	2009-02-08 01:39:32	2009-03-09 01:39:13	507 033	14.3	0.68(12)	6.54(26)
DEP33	2009-02-08 06:04:10	2009-03-09 06:04:18	680 489	3.9	0.17(4)	2.159(12)
FRP28	2009-02-08 11:12:49	2009-03-09 11:01:37	415 266	10.7	0.83(19)	7.02(5)
PAP50	2009-02-08 12:53:32	2009-03-09 11:21:54	675 535	11.3	0.60(10)	6.87(4)
FRP31	2009-02-08 11:44:13	2009-03-09 11:38:21	409 556	12.9	2.3(4)	9.3(5)

Station	Collection Start (UTC)	Collection Stop (UTC)	Volume (m^3)	R_c (GV)	^{22}Na ($\mu Bq\,m^{-3}$)	^{7}Be ($mBq\,m^{-3}$)
TZP64	2009-02-08 12:51:39	2009-03-09 12:57:22	549 390	13.6	3.2(5)	17.63(11)
ARP01	2009-02-08 16:10:00	2009-03-09 16:00:00	353 309	9.0	4.8(6)	21.66(13)
MRP43	2009-02-08 16:41:24	2009-03-09 16:00:06	531 111	13.9	0.24(4)	3.109(17)
GBP68	2009-02-08 17:32:35	2009-03-09 17:31:58	348 050	5.0	0.50(8)	4.01(25)
USP75	2009-02-08 18:49:46	2009-03-09 18:49:45	693 230	2.5	1.19(18)	11.20(7)
CAP15	2009-02-08 22:55:05	2009-03-09 22:55:07	612 281	0.0	0.096(26)	2.06(8)
RUP60	2009-03-09 23:54:49	2009-04-06 00:08:07	636 683	3.7	0.36(5)	4.16(4)
RUP61	2009-03-10 05:12:35	2009-04-06 03:29:15	553 764	2.0	1.15(15)	6.88(9)
AUP10	2009-03-10 03:20:16	2009-04-06 03:45:31	593 199	4.4	0.37(6)	2.844(35)
FRP30	2009-03-10 05:06:30	2009-04-06 05:04:39	373 171	1.2	1.11(25)	3.87(11)
FRP28	2009-03-10 11:15:17	2009-04-06 11:01:08	370 633	10.7	1.40(23)	9.05(9)
FRP31	2009-03-10 11:33:21	2009-04-06 11:29:51	380 133	12.9	2.00(33)	7.3(4)
MRP43	2009-03-10 16:06:07	2009-04-06 16:41:18	552 209	13.9	0.17(4)	2.591(12)
USP77	2009-03-10 01:34:49	2009-04-07 01:34:52	628 095	14.5	0.76(8)	4.49(5)
AUP08	2009-03-10 01:42:40	2009-04-07 01:36:42	473 733	14.3	0.51(10)	4.51(18)
GBP68	2009-03-10 17:40:57	2009-04-07 17:34:34	497 204	5.0	0.52(6)	4.72(30)
CAP15	2009-03-10 22:55:08	2009-04-08 22:55:06	619 326	0.0	0.101(26)	2.36(9)
USP75	2009-04-11 18:49:47	2009-04-25 18:49:48	334 629	2.5	1.42(20)	6.9(5)
FJP26	2009-04-11 01:20:15	2009-05-08 01:00:00	557 277	13.1	0.112(20)	2.051(34)
USP77	2009-04-12 01:34:52	2009-05-08 01:34:53	614 466	14.5	0.72(7)	3.180(22)
AUP06	2009-04-12 02:47:13	2009-05-08 01:40:33	558 966	11.1	0.30(7)	2.734(22)
RUP59	2009-04-12 02:37:39	2009-05-08 01:47:25	564 047	2.9	0.67(13)	6.83(4)
DEP33	2009-04-12 06:04:09	2009-05-08 06:04:10	655 484	3.9	0.38(5)	4.33(9)
JPP38	2009-04-12 06:55:34	2009-05-08 06:55:36	621 316	11.5	0.38(10)	4.5(4)
SEP63	2009-04-14 10:55:59	2009-05-08 08:52:59	325 127	1.5	0.20(5)	2.060(24)
FRP28	2009-04-12 11:15:16	2009-05-08 11:00:52	370 587	10.7	0.51(13)	4.6(4)
FRP31	2009-04-12 11:32:33	2009-05-08 11:27:16	366 412	12.9	1.5(4)	9.3(6)
ARP01	2009-04-11 17:20:00	2009-05-08 17:10:00	322 088	9.0	4.9(8)	20.04(12)

Station	Collection Start (UTC)	Collection Stop (UTC)	Volume (m^3)	R_c (GV)	^{22}Na ($\mu Bq\,m^{-3}$)	^{7}Be ($mBq\,m^{-3}$)
GBP68	2009-04-11 17:42:30	2009-05-08 17:39:22	533 557	5.0	0.28(5)	2.82(23)
USP71	2009-04-07 20:23:11	2009-05-08 20:34:47	510 775	2.1	0.78(9)	6.64(4)
USP72	2009-04-11 21:24:46	2009-05-08 21:24:46	557 837	4.7	0.40(4)	5.99(9)
AUP04	2009-04-11 23:38:19	2009-05-08 23:47:39	590 098	2.9	0.63(14)	3.062(31)
KWP40	2009-05-09 10:33:00	2009-06-05 11:59:57	298 563	12.8	0.70(20)	3.34(10)
NZP46	2009-05-09 01:46:20	2009-06-07 01:08:01	524 125	3.1	0.130(24)	1.65(10)
FJP26	2009-05-09 01:35:00	2009-06-07 01:09:08	564 839	13.1	0.153(25)	2.326(15)
USP76	2009-05-09 01:34:48	2009-06-07 01:34:47	648 004	0.5	0.77(23)	10.34(8)
RUP59	2009-05-09 01:15:47	2009-06-07 01:42:24	563 928	2.9	0.94(14)	6.343(35)
USP70	2009-05-09 03:21:57	2009-06-07 03:21:57	642 399	4.0	0.68(13)	7.82(6)
DEP33	2009-05-09 06:04:15	2009-06-07 06:04:14	643 132	3.9	0.50(5)	6.29(14)
PAP50	2009-05-09 10:35:44	2009-06-07 10:55:00	607 449	11.3	0.47(12)	5.32(9)
TZP64	2009-05-09 12:56:12	2009-06-07 12:36:48	415 592	13.6	4.0(6)	18.88(12)
BRP11	2009-05-09 14:38:07	2009-06-07 14:38:06	651 326	10.3	1.37(35)	5.64(5)
MRP43	2009-05-09 16:09:21	2009-06-07 16:48:06	405 586	13.9	0.25(4)	2.851(14)
GBP68	2009-05-09 17:36:26	2009-06-07 17:32:54	515 058	5.0	0.23(6)	2.69(26)
RUP60	2009-05-09 22:39:40	2009-06-07 23:35:34	623 250	3.7	0.17(4)	1.632(14)
MRP43	2009-06-08 16:25:11	2009-06-29 15:42:29	311 540	13.9	0.14(4)	2.139(12)
USP77	2009-06-09 01:34:53	2009-07-07 01:34:52	613 473	14.5	0.71(8)	2.95(4)
RUP59	2009-06-09 01:45:56	2009-07-07 01:38:45	565 675	2.9	0.79(13)	5.369(29)
MNP45	2009-06-09 03:27:05	2009-07-07 03:29:25	375 281	5.0	1.45(20)	7.33(4)
RUP61	2009-06-09 04:24:57	2009-07-07 04:19:07	557 591	2.0	1.72(21)	11.63(10)
DEP33	2009-06-09 06:04:14	2009-07-07 06:04:14	651 847	3.9	0.34(5)	4.50(17)
CMP13	2009-06-09 07:08:41	2009-07-07 07:15:02	557 114	14.5	1.7(5)	6.00(6)
USP72	2009-06-08 21:24:46	2009-07-07 21:24:47	602 736	4.7	0.17(4)	3.82(4)
RUP60	2009-06-08 23:55:09	2009-07-07 22:57:08	643 398	3.7	0.28(5)	3.06(9)
KWP40	2009-07-09 13:12:17	2009-07-28 14:32:32	62 838	12.8	2.4(6)	13.45(12)
AUP08	2009-07-08 01:40:51	2009-08-06 01:37:43	514 282	14.3	0.41(11)	5.26(15)

Station	Collection Start (UTC)	Collection Stop (UTC)	Volume (m^3)	R_c (GV)	^{22}Na ($\mu Bq\,m^{-3}$)	^{7}Be ($mBq\,m^{-3}$)
AUP06	2009-07-08 02:49:57	2009-08-06 02:44:44	634 281	11.1	0.41(8)	3.412(15)
RUP61	2009-07-08 04:27:41	2009-08-06 04:16:39	588 943	2.0	1.23(22)	10.94(9)
FRP31	2009-07-08 11:35:52	2009-08-06 11:18:12	426 604	12.9	2.4(7)	7.28(5)
TZP64	2009-07-08 13:11:57	2009-08-06 11:49:11	517 999	13.6	3.8(6)	18.79(11)
ARP03	2009-07-08 14:04:28	2009-08-06 13:15:59	570 897	8.8	0.29(6)	3.659(34)
GBP67	2009-07-08 17:05:40	2009-08-06 17:08:37	594 319	9.8	0.97(14)	9.04(6)
USP71	2009-08-07 20:34:47	2009-09-03 20:34:44	627 296	2.1	0.31(7)	2.157(11)
USP74	2009-08-07 00:04:47	2009-09-05 00:04:47	681 888	3.3	1.18(29)	9.14(13)
FJP26	2009-08-07 01:14:01	2009-09-05 01:06:21	590 253	13.1	0.162(23)	3.35(18)
AUP08	2009-08-07 01:42:04	2009-09-05 01:39:13	515 201	14.3	0.47(10)	4.89(17)
RUP61	2009-08-07 04:27:49	2009-09-05 04:50:58	531 910	2.0	0.89(20)	9.62(8)
SEP63	2009-08-07 08:52:02	2009-09-05 08:49:30	371 869	1.5	0.50(8)	2.630(31)
FRP31	2009-08-07 11:30:02	2009-09-05 11:20:57	416 289	12.9	2.2(6)	7.66(4)
TZP64	2009-08-07 12:57:36	2009-09-05 12:50:37	473 430	13.6	2.5(5)	18.25(19)
GBP67	2009-08-07 16:42:10	2009-09-05 16:55:11	597 266	9.8	0.62(11)	5.84(4)
ARP01	2009-08-07 17:20:00	2009-09-05 17:10:00	354 021	9.0	3.4(7)	13.66(8)
AUP04	2009-08-07 23:44:02	2009-09-05 23:33:16	608 916	2.9	0.38(9)	3.941(24)
NZP46	2009-09-06 01:11:09	2009-10-05 00:01:50	623 027	3.1	0.100(24)	1.67(9)
AUP08	2009-09-06 02:14:57	2009-10-05 01:46:35	515 946	14.3	0.44(9)	5.03(17)
AUP06	2009-09-06 02:43:05	2009-10-05 02:53:42	607 210	11.1	0.37(8)	5.05(4)
FRP29	2009-09-06 03:25:55	2009-10-05 03:06:14	408 868	9.7	0.23(6)	2.81(22)
DEP33	2009-09-06 06:04:14	2009-10-05 06:04:15	576 801	3.9	0.29(6)	4.73(21)
BRP11	2009-09-06 14:38:06	2009-10-05 14:38:02	701 429	10.3	1.08(31)	4.13(4)
ARP01	2009-09-06 17:20:00	2009-10-05 17:00:00	343 114	9.0	2.7(5)	15.34(13)
GBP67	2009-09-06 17:10:35	2009-10-05 17:11:15	593 157	9.8	0.88(11)	6.86(5)
GBP68	2009-09-06 17:31:36	2009-10-05 17:32:59	602 649	5.0	0.59(17)	6.39(8)
USP75	2009-09-06 18:49:45	2009-10-05 18:49:45	688 439	2.5	0.80(18)	6.125(34)
USP71	2009-09-21 20:03:56	2009-10-05 20:34:52	295 045	2.1	0.42(10)	1.311(19)

Station	Collection Start (UTC)	Collection Stop (UTC)	Volume (m^3)	R_c (GV)	^{22}Na ($\mu Bq\,m^{-3}$)	^{7}Be ($mBq\,m^{-3}$)
FJP26	2009-10-06 01:13:53	2009-11-04 01:07:06	588 669	13.1	0.256(31)	3.630(18)
AUP09	2009-10-06 02:14:49	2009-11-04 01:44:56	761 151	14.2	0.37(7)	4.05(4)
AUP08	2009-10-07 01:39:03	2009-11-04 01:53:35	496 463	14.3	0.62(8)	5.894(31)
AUP06	2009-10-06 02:41:30	2009-11-04 02:27:26	622 686	11.1	0.22(6)	4.103(33)
AUP10	2009-10-06 04:23:03	2009-11-04 04:37:01	599 123	4.4	0.27(5)	2.878(12)
DEP33	2009-10-06 06:04:15	2009-11-04 06:04:15	563 215	3.9	0.30(5)	4.54(24)
ARP03	2009-10-06 13:01:05	2009-11-04 13:18:39	581 103	8.8	0.23(5)	3.004(17)
MRP43	2009-10-31 15:17:01	2009-11-04 16:04:41	77 957	13.9	0.38(9)	2.174(12)
GBP67	2009-10-06 17:06:54	2009-11-04 17:09:31	592 209	9.8	0.91(12)	7.59(5)
ARP01	2009-10-06 17:10:00	2009-11-04 17:10:00	358 103	9.0	3.2(5)	19.19(17)
AUP04	2009-10-06 22:40:44	2009-11-04 22:12:14	610 135	2.9	0.48(9)	3.889(33)
AUP08	2009-11-05 01:41:42	2009-12-04 01:37:26	509 829	14.3	0.86(9)	7.56(4)
AUP06	2009-11-05 02:27:12	2009-12-04 01:47:09	616 195	11.1	0.31(7)	3.983(30)
FRP29	2009-11-05 03:15:35	2009-12-04 03:02:27	425 158	9.7	0.19(5)	1.92(20)
AUP10	2009-11-05 04:24:54	2009-12-04 04:13:01	577 454	4.4	0.29(5)	2.744(30)
DEP33	2009-11-05 06:04:14	2009-12-04 06:04:17	542 288	3.9	0.21(4)	3.51(17)
TZP64	2009-11-05 13:13:57	2009-12-04 13:28:15	556 760	13.6	3.0(4)	17.95(13)
ARP03	2009-11-05 13:20:46	2009-12-04 14:01:27	572 779	8.8	0.19(5)	2.910(18)
MRP43	2009-11-05 16:32:34	2009-12-04 15:28:57	559 555	13.9	0.22(6)	3.61(10)
ARP01	2009-11-05 17:20:00	2009-12-04 17:00:00	359 597	9.0	2.8(5)	18.85(12)
GBP67	2009-11-05 17:12:52	2009-12-04 17:16:56	508 091	9.8	1.45(20)	9.35(6)
AUP04	2009-11-05 22:19:44	2009-12-04 22:15:06	595 005	2.9	0.76(11)	5.536(24)
AUP08	2009-12-05 01:42:47	2010-01-03 01:50:19	508 547	14.3	1.03(12)	8.68(4)
DEP33	2009-12-05 06:04:17	2010-01-03 06:04:18	584 560	3.9	0.20(5)	2.72(10)
ARP03	2009-12-05 13:44:05	2010-01-03 13:22:09	588 677	8.8	0.37(4)	4.71(5)
GBP67	2009-12-05 16:56:51	2010-01-03 16:53:24	547 350	9.8	1.55(13)	9.33(6)
GBP68	2009-12-05 17:32:11	2010-01-03 17:32:03	586 129	5.0	1.11(20)	8.30(11)
CAP14	2009-12-05 16:48:50	2010-01-03 17:57:41	725 039	1.8	1.33(25)	7.66(4)

Station	Collection Start (UTC)	Collection Stop (UTC)	Volume (m^3)	R_c (GV)	^{22}Na ($\mu Bq\,m^{-3}$)	^{7}Be ($mBq\,m^{-3}$)
AUP04	2009-12-05 22:03:05	2010-01-03 22:46:23	595 801	2.9	0.55(9)	5.30(5)
AUP08	2010-01-04 01:54:35	2010-01-28 01:36:54	316 998	14.3	0.96(8)	7.93(7)
AUP09	2010-01-04 02:13:13	2010-01-28 02:09:31	345 836	14.2	0.28(4)	2.855(13)
AUP10	2010-01-04 03:50:54	2010-01-28 04:50:48	308 214	4.4	0.22(6)	3.240(33)
PAP50	2010-01-04 11:54:21	2010-01-28 11:41:54	398 071	11.3	0.50(9)	5.57(8)
GBP68	2010-01-04 17:39:11	2010-01-28 17:31:11	326 116	5.0	1.92(25)	12.07(17)
AUP04	2010-01-04 22:35:11	2010-01-28 22:22:03	361 518	2.9	0.53(12)	4.84(4)
CAP15	2010-01-04 22:55:07	2010-01-28 22:55:06	618 670	0.0	0.130(33)	2.03(6)
CAP14	2010-02-03 16:41:07	2010-03-04 17:01:28	738 730	1.8	1.61(27)	6.91(6)
RUP58	2010-03-24 02:36:38	2010-03-31 01:47:20	88 059	7.2	1.05(31)	1.49(9)
RUP60	2010-03-23 23:39:29	2010-04-01 23:36:15	221 038	3.7	0.31(7)	3.16(4)
JPP37	2010-03-24 00:23:57	2010-04-03 00:23:57	226 741	15.0	1.5(4)	10.74(7)
AUP06	2010-03-24 02:38:19	2010-04-03 02:40:02	213 322	11.1	0.19(4)	2.880(30)
FRP31	2010-03-24 11:35:01	2010-04-03 11:21:44	143 483	12.9	3.6(6)	10.01(6)
CLP19	2010-03-24 15:09:50	2010-04-03 15:09:52	188 912	12.2	0.78(18)	4.05(6)
GBP67	2010-03-24 16:47:54	2010-04-03 17:06:13	182 342	9.8	0.79(23)	5.25(4)
USP75	2010-03-24 18:49:47	2010-04-03 18:49:47	240 737	2.5	1.35(23)	6.28(4)
CAP15	2010-01-29 22:52:37	2010-04-03 22:55:04	361 362	0.0	0.23(4)	4.25(5)
RUP60	2010-04-03 23:03:30	2010-05-02 23:25:23	698 686	3.7	0.34(5)	3.811(31)
RUP59	2010-04-04 01:57:49	2010-05-03 01:32:54	645 489	2.9	0.61(10)	5.26(10)
AUP08	2010-04-04 01:48:53	2010-05-03 01:41:53	509 492	14.3	0.54(7)	6.333(32)
MNP45	2010-04-04 03:26:05	2010-05-03 03:25:23	358 771	5.0	5.5(8)	5.02(4)
AUP10	2010-04-04 04:15:08	2010-05-03 04:58:19	617 087	4.4	0.59(12)	4.52(4)
DEP33	2010-04-04 06:04:17	2010-05-03 06:04:17	548 620	3.9	0.46(7)	6.04(13)
NOP49	2010-04-04 09:31:47	2010-05-03 09:29:45	435 829	0.1	0.37(10)	2.57(7)
PAP50	2010-04-04 11:21:21	2010-05-03 10:45:46	654 153	11.3	0.24(7)	3.011(25)
CAP14	2010-04-04 15:43:29	2010-05-03 15:44:31	725 530	1.8	1.48(16)	7.78(18)
MRP43	2010-04-04 16:02:21	2010-05-03 15:52:11	577 241	13.9	0.300(24)	3.177(16)

Station	Collection Start (UTC)	Stop (UTC)	Volume (m^3)	R_c (GV)	^{22}Na ($\mu Bq\,m^{-3}$)	^{7}Be ($mBq\,m^{-3}$)
GBP67	2010-04-04 16:45:51	2010-05-03 17:02:23	565 173	9.8	0.57(15)	7.09(5)
GBP68	2010-04-04 17:31:26	2010-05-03 17:33:25	618 445	5.0	1.00(20)	8.38(8)
USP72	2010-04-04 18:54:47	2010-05-03 18:54:46	600 313	4.7	0.50(4)	7.18(8)
USP74	2010-04-04 20:04:47	2010-05-03 20:04:47	686 620	3.3	1.98(28)	11.46(15)
AUP04	2010-04-04 23:17:42	2010-05-03 23:21:25	605 424	2.9	0.42(12)	4.191(18)
AUP08	2010-05-04 01:42:25	2010-06-02 01:38:54	507 000	14.3	0.44(8)	4.472(25)
RUP59	2010-05-04 01:39:31	2010-06-02 01:41:40	619 458	2.9	0.78(13)	5.13(15)
AUP10	2010-05-04 04:45:15	2010-06-02 03:36:21	627 053	4.4	0.81(14)	4.46(8)
DEP33	2010-05-04 06:04:17	2010-06-02 06:04:17	536 400	3.9	0.42(8)	3.55(4)
ARP03	2010-05-04 13:43:01	2010-06-02 13:44:49	612 826	8.8	0.36(6)	2.960(22)
TZP64	2010-05-04 13:46:24	2010-06-02 13:49:00	581 558	13.6	2.2(4)	16.60(16)
CAP14	2010-05-04 15:33:04	2010-06-02 15:56:31	618 281	1.8	1.40(19)	5.7(4)
GBP67	2010-05-04 16:47:17	2010-06-02 16:59:56	580 813	9.8	0.68(18)	6.77(5)
USP75	2010-05-04 18:49:46	2010-06-02 18:49:45	698 071	2.5	0.96(20)	6.07(5)
RUP60	2010-05-04 23:40:09	2010-06-02 22:39:18	688 456	3.7	0.23(6)	2.124(27)
AUP06	2010-06-03 02:48:47	2010-06-16 02:45:41	218 777	11.1	0.56(12)	2.370(20)
RUP58	2010-06-03 01:32:54	2010-07-02 01:32:05	502 071	7.2	1.28(20)	5.67(4)
FRP29	2010-06-03 03:19:45	2010-07-02 03:04:49	365 790	9.7	2.6(6)	7.37(4)
RUP61	2010-06-03 04:27:49	2010-07-02 04:24:40	510 330	2.0	2.41(26)	13.33(13)
DEP33	2010-06-03 06:04:17	2010-07-02 06:04:19	457 720	3.9	0.49(9)	5.80(8)
MYP42	2010-06-03 07:37:53	2010-07-02 07:37:28	428 659	17.4	0.79(22)	2.72(7)
CMP13	2010-06-03 07:16:06	2010-07-02 07:40:13	490 243	14.5	2.3(6)	7.96(6)
TZP64	2010-06-03 14:02:53	2010-07-02 13:04:00	503 401	13.6	3.4(6)	15.83(10)
MRP43	2010-06-03 14:48:12	2010-07-02 15:09:07	491 741	13.9	0.21(5)	2.93(4)
CAP14	2010-06-03 15:51:32	2010-07-02 15:39:33	624 914	1.8	1.07(24)	4.715(24)
GBP67	2010-06-03 16:45:14	2010-07-02 16:50:35	528 893	9.8	0.94(15)	8.10(6)
GBP68	2010-06-03 17:32:01	2010-07-02 17:31:50	552 287	5.0	0.88(18)	6.63(7)
GBP67	2010-07-03 16:47:19	2010-07-31 18:26:19	556 610	9.8	0.54(16)	5.43(4)

Station	Collection Start (UTC)	Collection Stop (UTC)	Volume (m^3)	R_c (GV)	^{22}Na ($\mu Bq\,m^{-3}$)	^{7}Be ($mBq\,m^{-3}$)
NZP46	2010-07-03 00:29:53	2010-08-01 01:09:15	635 299	3.1	0.109(20)	1.414(9)
RUP59	2010-07-03 01:42:05	2010-08-01 01:31:56	579 327	2.9	0.29(8)	3.81(4)
RUP61	2010-07-03 04:13:44	2010-08-01 04:32:08	555 837	2.0	2.25(28)	16.93(16)
KWP40	2010-07-06 13:11:25	2010-08-01 06:25:17	140 962	12.8	1.03(29)	8.86(9)
MRP43	2010-07-03 16:44:29	2010-08-01 15:36:13	537 723	13.9	0.160(33)	2.694(13)
GBP68	2010-07-03 17:33:37	2010-08-01 17:34:25	629 095	5.0	0.64(14)	7.16(8)
USP75	2010-07-03 18:49:45	2010-08-01 18:49:45	698 057	2.5	0.76(20)	7.58(7)
TZP64	2010-08-02 13:50:43	2010-08-30 13:10:16	567 795	13.6	4.4(5)	16.45(11)
FJP26	2010-08-02 01:31:16	2010-08-31 01:07:29	608 486	13.1	0.200(30)	2.838(19)
RUP59	2010-08-02 01:41:31	2010-08-31 01:37:27	609 210	2.9	0.62(16)	4.986(21)
AUP08	2010-08-02 01:40:52	2010-08-31 01:39:19	456 986	14.3	0.45(9)	3.93(14)
FRP29	2010-08-02 03:54:11	2010-08-31 03:09:17	407 392	9.7	1.3(4)	6.3(5)
MNP45	2010-08-02 03:33:46	2010-08-31 03:25:12	374 777	5.0	4.0(11)	5.48(10)
MRP43	2010-08-02 15:13:33	2010-08-31 10:37:39	567 096	13.9	0.137(29)	2.484(12)
ARP03	2010-08-02 13:42:02	2010-08-31 13:06:02	597 717	8.8	0.23(5)	2.134(13)
ARP01	2010-08-02 17:10:00	2010-08-31 17:10:00	365 499	9.0	1.6(4)	11.92(7)
RUP60	2010-08-02 22:42:07	2010-08-31 23:37:50	662 429	3.7	0.23(5)	2.118(15)
AUP04	2010-09-01 23:24:44	2010-09-29 23:40:33	579 300	2.9	0.39(9)	3.505(24)
NZP46	2010-09-01 01:15:45	2010-09-30 00:04:03	500 847	3.1	0.088(23)	1.57(4)
AUP06	2010-09-01 02:44:39	2010-09-30 02:19:20	551 235	11.1	0.20(4)	2.83(8)
AUP10	2010-09-01 04:14:07	2010-09-30 03:45:09	592 606	4.4	0.45(13)	4.06(4)
FRP29	2010-09-01 03:16:08	2010-09-30 03:47:13	414 628	9.7	2.3(5)	10.1(6)
KWP40	2010-09-01 06:25:16	2010-09-30 06:25:17	393 829	12.8	1.10(21)	12.85(10)
BRP11	2010-09-01 13:03:03	2010-09-30 13:03:04	726 404	10.3	1.34(35)	6.10(5)
TZP64	2010-09-01 12:48:54	2010-09-30 13:42:24	464 116	13.6	4.7(6)	22.31(14)
GBP67	2010-09-01 16:38:06	2010-09-30 17:07:53	572 395	9.8	1.06(15)	6.74(4)
FJP26	2010-10-01 01:16:37	2010-10-29 00:14:11	584 643	13.1	0.113(31)	1.797(9)
AUP08	2010-10-01 01:40:38	2010-10-30 01:57:20	514 679	14.3	0.61(10)	5.58(13)

Station	Collection Start (UTC)	Collection Stop (UTC)	Volume (m^3)	R_c (GV)	^{22}Na ($\mu Bq\,m^{-3}$)	^{7}Be ($mBq\,m^{-3}$)
AUP06	2010-10-01 05:54:12	2010-10-30 02:56:02	617 763	11.1	0.17(4)	2.685(18)
FRP29	2010-10-01 03:16:47	2010-10-30 03:03:38	399 318	9.7	1.9(5)	10.83(26)
AUP10	2010-10-01 03:42:52	2010-10-30 03:41:01	608 456	4.4	0.70(12)	4.44(4)
TZP64	2010-10-01 13:30:36	2010-10-30 12:59:03	562 349	13.6	2.9(4)	14.68(10)
ARP01	2010-10-01 17:10:00	2010-10-30 17:00:00	353 632	9.0	3.1(6)	15.97(11)
GBP67	2010-10-01 16:49:07	2010-10-30 17:08:28	554 287	9.8	0.95(14)	7.88(5)
USP72	2010-10-01 18:54:46	2010-10-30 18:54:47	630 270	4.7	0.19(4)	6.15(7)
GBP68	2010-10-31 17:31:58	2010-11-28 17:33:32	603 520	5.0	0.95(19)	7.15(6)
FJP26	2010-10-30 23:59:19	2010-11-29 00:12:36	606 162	13.1	0.127(29)	1.476(32)
AUP06	2010-10-31 02:24:21	2010-11-29 03:05:59	611 401	11.1	0.177(35)	2.665(22)
GBP67	2010-10-31 17:12:21	2010-11-29 16:42:35	571 429	9.8	0.84(16)	7.13(5)
CAP14	2010-10-31 15:41:58	2010-11-29 16:44:04	731 647	1.8	0.51(14)	5.41(7)
ARP01	2010-10-31 17:10:00	2010-11-29 16:50:00	366 452	9.0	2.6(4)	14.94(10)
FJP26	2010-11-30 00:27:47	2010-12-29 00:09:38	607 808	13.1	0.090(22)	1.275(27)
NZP46	2010-11-30 00:16:48	2010-12-29 00:16:33	621 374	3.1	0.128(25)	2.34(6)
AUP08	2010-11-30 01:42:56	2010-12-29 01:43:55	515 009	14.3	0.68(10)	6.16(15)
KIP39	2010-12-14 02:24:05	2010-12-29 02:43:50	307 353	14.9	0.046(14)	0.742(5)
AUP06	2010-11-30 02:46:09	2010-12-29 02:54:48	595 709	11.1	0.113(31)	1.133(8)
GBP67	2010-11-30 16:47:24	2010-12-29 17:00:18	590 790	9.8	1.28(15)	8.50(6)
NZP46	2010-12-30 00:20:24	2011-01-28 00:17:59	645 874	3.1	0.115(23)	2.01(5)
AUP08	2010-12-30 01:43:34	2011-01-28 01:57:44	513 544	14.3	0.43(8)	4.13(10)
AUP06	2010-12-30 02:46:57	2011-01-28 02:16:18	606 930	11.1	0.19(4)	2.496(16)
AUP10	2010-12-30 03:39:35	2011-01-28 04:02:53	604 225	4.4	0.82(13)	5.59(8)
FRP30	2010-12-30 05:09:19	2011-01-28 05:04:43	415 823	1.2	2.3(6)	7.018(34)
RUP61	2010-12-30 05:37:21	2011-01-28 05:19:59	666 723	2.0	0.60(12)	5.04(5)
DEP33	2010-12-30 06:04:18	2011-01-28 06:04:22	612 309	3.9	0.13(4)	1.95(14)
MRP43	2010-12-30 11:05:08	2011-01-28 09:02:41	571 092	13.9	0.27(5)	3.011(20)
FRP28	2011-01-15 11:29:09	2011-01-28 11:29:04	200 900	10.7	0.64(16)	3.958(30)

Station	Collection Start (UTC)	Collection Stop (UTC)	Volume (m^3)	R_c (GV)	^{22}Na ($\mu Bq\,m^{-3}$)	^{7}Be ($mBq\,m^{-3}$)
CAP14	2010-12-30 16:46:02	2011-01-28 16:47:46	736 134	1.8	0.57(13)	3.92(18)
GBP68	2010-12-30 17:32:47	2011-01-28 17:31:22	617 830	5.0	1.76(19)	11.10(10)
USP72	2010-12-30 18:54:47	2011-01-28 18:54:47	608 304	4.7	0.23(4)	5.18(7)
AUP04	2010-12-30 22:46:13	2011-01-28 22:34:00	593 630	2.9	0.56(10)	4.629(29)
AUP06	2011-01-29 01:48:42	2011-02-26 02:10:03	402 293	11.1	0.17(4)	2.203(21)
NZP46	2011-01-29 00:31:25	2011-02-27 00:32:21	602 327	3.1	0.076(22)	2.01(5)
AUP08	2011-01-29 01:37:09	2011-02-27 02:08:31	489 096	14.3	0.41(8)	3.64(9)
KIP39	2011-01-29 03:19:42	2011-02-27 02:58:47	588 567	14.9	0.036(8)	0.746(5)
MNP45	2011-01-29 03:26:15	2011-02-27 03:25:28	375 111	5.0	3.7(8)	5.362(34)
TZP64	2011-01-29 12:42:10	2011-02-27 09:30:00	390 299	13.6	3.3(6)	19.01(12)
FRP31	2011-01-29 10:04:32	2011-02-27 10:01:22	402 483	12.9	1.22(33)	6.7(4)
GBP67	2011-01-29 17:20:24	2011-02-27 16:56:48	537 391	9.8	0.67(16)	6.07(4)
CAP14	2011-01-29 16:53:44	2011-02-27 17:15:37	720 502	1.8	0.76(14)	5.66(33)
GBP68	2011-01-29 17:31:41	2011-02-27 17:31:02	612 963	5.0	1.36(14)	10.73(9)
USP72	2011-01-29 18:54:47	2011-02-27 18:54:48	608 627	4.7	0.25(4)	4.94(6)
CLP18	2011-01-29 19:05:37	2011-02-27 19:05:36	449 347	5.6	0.45(14)	3.51(15)
NZP47	2011-01-29 20:01:17	2011-02-27 19:59:21	374 970	5.2	0.125(27)	0.52(5)
NZP46	2011-02-28 00:39:00	2011-03-29 00:23:31	626 807	3.1	0.149(18)	2.52(6)
PGP51	2011-02-28 01:27:25	2011-03-29 00:49:41	641 868	15.7	0.59(17)	2.013(12)
FRP29	2011-02-28 03:17:29	2011-03-29 03:05:22	224 294	9.7	0.24(7)	1.03(6)
AUP10	2011-02-28 04:14:22	2011-03-29 03:32:35	456 801	4.4	0.61(16)	4.14(5)
ARP01	2011-02-28 17:20:00	2011-03-29 16:50:00	366 482	9.0	4.9(5)	22.56(30)
GBP68	2011-02-28 17:32:11	2011-03-29 17:31:07	620 236	5.0	1.80(19)	11.81(10)
NZP47	2011-02-28 20:00:49	2011-03-29 19:59:17	609 421	5.2	0.182(19)	2.095(12)
AUP08	2011-03-30 02:04:03	2011-04-28 01:37:20	514 726	14.3	0.56(10)	5.62(13)
NZP46	2011-03-30 00:13:38	2011-04-28 01:59:38	632 527	3.1	0.150(24)	2.17(5)
AUP09	2011-03-30 02:08:24	2011-04-28 02:12:17	557 939	14.2	0.25(7)	2.507(11)
FRP29	2011-03-30 03:17:10	2011-04-28 03:08:25	413 855	9.7	0.16(5)	2.32(4)

Station	Collection Start (UTC)	Collection Stop (UTC)	Volume (m^3)	R_c (GV)	^{22}Na ($\mu Bq\,m^{-3}$)	^{7}Be ($mBq\,m^{-3}$)
TZP64	2011-03-29 14:21:57	2011-04-28 12:55:52	492 035	13.6	1.43(33)	7.42(5)
ARP03	2011-03-30 13:24:06	2011-04-28 13:18:09	512 618	8.8	0.26(5)	2.807(20)
GBP68	2011-03-30 17:31:10	2011-04-28 17:31:32	621 757	5.0	1.70(17)	10.28(9)
AUP04	2011-03-30 22:17:37	2011-04-28 23:20:12	614 297	2.9	0.40(11)	2.985(14)
NZP46	2011-04-29 02:20:44	2011-05-14 01:41:47	322 152	3.1	0.154(29)	1.82(4)
RUP59	2011-04-29 01:42:31	2011-05-28 01:33:00	623 819	2.9	0.76(16)	5.72(5)
AUP06	2011-04-29 03:00:43	2011-05-28 02:28:53	632 455	11.1	0.27(6)	2.431(22)
MNP45	2011-04-29 03:25:44	2011-05-28 03:25:24	374 766	5.0	4.4(11)	5.571(33)
RUP54	2011-04-29 05:40:58	2011-05-28 05:07:14	558 648	1.6	1.36(20)	8.39(20)
PHP52	2011-04-29 05:39:53	2011-05-28 06:23:04	798 273	16.9	0.36(11)	2.533(13)
JPP38	2011-04-29 06:55:17	2011-05-28 06:55:17	678 563	11.5	0.40(9)	4.90(13)
MRP43	2011-04-29 09:55:32	2011-05-28 09:32:24	570 934	13.9	0.229(28)	2.578(16)
PTP53	2011-04-29 11:29:31	2011-05-28 11:26:19	407 933	6.6	6.9(16)	29.60(28)
TZP64	2011-04-29 12:51:43	2011-05-28 12:40:21	580 886	13.6	2.1(5)	12.4(5)
GBP67	2011-04-29 17:09:10	2011-05-28 17:03:32	515 306	9.8	0.82(16)	6.34(4)
GBP68	2011-04-29 17:31:56	2011-05-28 17:31:01	612 595	5.0	0.82(19)	7.65(7)
USP75	2011-04-29 18:49:47	2011-05-28 18:46:59	724 856	2.5	1.17(32)	7.18(4)
USP74	2011-04-29 20:04:58	2011-05-28 20:04:48	700 145	3.3	1.53(27)	8.02(10)
NZP47	2011-04-29 21:01:57	2011-05-28 20:56:24	607 643	5.2	0.089(11)	1.593(23)
RUP59	2011-05-29 01:40:53	2011-06-27 01:36:44	579 711	2.9	0.80(15)	6.19(4)
KIP39	2011-05-29 02:35:09	2011-06-27 02:29:10	584 767	14.9	0.042(7)	0.843(6)
AUP06	2011-05-29 02:46:27	2011-06-27 02:50:57	640 591	11.1	0.23(6)	2.123(22)
RUP61	2011-05-29 04:38:29	2011-06-27 03:40:36	640 576	2.0	1.66(16)	9.5(5)
DEP33	2011-05-24 13:18:48	2011-06-27 06:25:25	688 248	3.9	0.17(5)	2.98(25)
FRP28	2011-05-29 11:19:00	2011-06-27 11:22:00	413 550	10.7	0.62(15)	5.72(10)
ISP34	2011-05-29 13:26:05	2011-06-27 13:22:38	434 490	0.4	0.084(22)	1.534(35)
CAP14	2011-05-29 15:39:15	2011-06-27 15:48:55	720 067	1.8	0.81(24)	3.78(7)
GBP67	2011-05-29 16:59:53	2011-06-27 16:42:57	574 792	9.8	0.74(15)	7.01(5)

Station	Collection Start (UTC)	Collection Stop (UTC)	Volume (m^3)	R_c (GV)	^{22}Na ($\mu Bq\,m^{-3}$)	^{7}Be ($mBq\,m^{-3}$)
USP75	2011-05-29 18:49:37	2011-06-27 18:46:59	628 406	2.5	1.5(4)	9.37(8)
CLP18	2011-06-06 21:42:56	2011-06-27 19:05:36	330 090	5.6	0.53(15)	1.688(24)
USP74	2011-05-29 20:04:47	2011-06-27 20:04:46	601 122	3.3	1.80(29)	11.15(27)
NZP47	2011-05-29 21:00:04	2011-06-27 20:59:01	638 022	5.2	0.072(12)	1.360(23)
CAP15	2011-05-29 22:55:07	2011-06-27 22:55:06	476 079	0.0	0.47(14)	1.32(10)
AUP08	2011-06-28 01:33:58	2011-07-27 01:36:09	373 434	14.3	0.53(10)	4.59(21)
MNP45	2011-06-28 03:28:04	2011-07-27 03:39:55	358 835	5.0	5.3(11)	5.25(4)
RUP54	2011-06-28 05:58:33	2011-07-27 05:41:46	541 536	1.6	1.69(20)	9.28(9)
CLP19	2011-06-28 16:38:56	2011-07-27 16:38:56	602 225	12.2	0.57(11)	7.21(5)
CAP17	2011-06-28 16:33:10	2011-07-27 17:06:22	701 791	1.6	1.9(5)	0.68(5)
KWP40	2011-07-28 06:25:15	2011-08-24 06:25:16	182 508	12.8	0.81(22)	8.71(9)
FJP26	2011-07-27 00:55:58	2011-08-26 01:13:40	634 531	13.1	0.126(21)	2.232(29)
RUP58	2011-07-28 01:33:37	2011-08-26 01:31:34	565 368	7.2	0.81(23)	4.81(4)
MNP45	2011-07-28 03:27:37	2011-08-26 03:25:34	374 809	5.0	5.3(9)	5.92(4)
RUP54	2011-07-28 05:41:54	2011-08-26 05:38:14	549 549	1.6	1.43(29)	8.21(9)
CMP13	2011-07-28 07:17:40	2011-08-26 07:19:55	560 093	14.5	3.2(6)	6.82(6)
SEP63	2011-07-29 09:25:16	2011-08-26 08:48:13	323 947	1.5	0.18(5)	2.18(7)
MRP43	2011-07-29 09:36:51	2011-08-26 09:31:23	536 295	13.9	0.193(27)	2.159(13)
TZP64	2011-07-28 13:35:07	2011-08-26 13:29:41	509 720	13.6	3.2(5)	20.68(16)
ARP01	2011-07-28 17:20:00	2011-08-26 17:10:00	353 031	9.0	1.8(5)	9.04(5)
GBP68	2011-07-28 17:28:25	2011-08-26 17:34:17	496 369	5.0	0.81(18)	7.10(13)
USP71	2011-07-28 20:34:49	2011-08-26 20:34:46	614 969	2.1	0.31(8)	2.003(14)
NZP47	2011-07-28 20:58:45	2011-08-26 21:00:14	626 570	5.2	0.102(12)	1.617(12)
CKP23	2011-07-28 22:19:21	2011-08-26 22:19:21	617 195	12.7	1.7(4)	13.40(8)
AUP04	2011-07-28 23:26:30	2011-08-26 23:24:58	618 502	2.9	0.43(11)	3.78(4)
FJP26	2011-08-27 01:19:02	2011-09-25 01:10:06	605 614	13.1	0.127(25)	2.31(8)
AUP08	2011-08-27 01:43:16	2011-09-25 01:38:06	512 842	14.3	1.03(9)	7.21(35)
AUP06	2011-08-27 02:51:19	2011-09-25 02:55:37	632 317	11.1	0.32(6)	3.64(4)

Station	Collection Start (UTC)	Stop (UTC)	Volume (m^3)	R_c (GV)	^{22}Na ($\mu Bq\,m^{-3}$)	^{7}Be ($mBq\,m^{-3}$)
MRP43	2011-08-27 09:33:28	2011-09-25 09:23:56	574 157	13.9	0.13(4)	2.919(18)
CLP19	2011-08-27 17:00:45	2011-09-25 17:00:17	556 481	12.2	0.60(16)	7.21(7)
NZP47	2011-08-27 21:03:17	2011-09-25 19:57:30	621 603	5.2	0.067(13)	1.686(33)
CKP23	2011-08-27 22:20:29	2011-09-25 22:21:08	611 519	12.7	1.8(4)	12.31(7)
RUP60	2011-08-27 22:31:45	2011-09-25 22:35:00	668 910	3.7	0.17(4)	2.57(5)
AUP04	2011-08-27 23:26:51	2011-09-25 23:14:59	612 801	2.9	0.30(9)	3.538(34)